

# **A Haptic Feedback System for Lower Limb Amputees Based on Gait Event Detection**

**Muhammad Afif Bin Husman**

**Submitted in accordance with the requirements for the degree of  
Doctor of Philosophy**

**The University of Leeds  
School of Mechanical Engineering**

**December 2017**

The candidate confirms that the work submitted is his own, except where the work that has formed part of jointly-authored publications has been included. The contribution of the candidate and the other authors to this work has been explicitly indicated. The candidate confirms that appropriate credit has been given within the thesis where reference has been made to the work of others.

This copy has been supplied on the understanding that it is a copyright material and that no quotation from the thesis may be published without proper acknowledgement.

The right of Muhammad Afif Bin Husman to be identified as Author of this work has been asserted by him in accordance with the Copyright, Designs and Patents Act 1988.

---

## Abstract

Lower limb amputation has significant effects on a person's quality of life and ability to perform activities of daily living. Prescription of prosthetic device post amputation aims to help restore some degrees of mobility function, however studies have shown evidence of low balance confidence and higher risk of falling among amputee community, especially those suffering from above knee amputation. While advanced prostheses offer better control, they often lack a form of feedback that delivers the awareness of the limb position to the prosthetic user while walking.

This research presents the development and evaluation of a wearable skin-stretch haptic feedback system intended to deliver cues of two crucial gait events, namely the Initial Contact (IC) and Toe-off (TO) to its wearer. The system comprises a haptic module that applies lateral skin-stretch on the upper leg or the trunk, corresponding to the gait event detection module based on Inertial Measurement Unit (IMU) attached at the shank. The design and development iterations of the haptic module is presented, and characterization of the feedback parameters is discussed. The validation of the gait event detection module is carried out and finally the integration of the haptic feedback system is described.

Experimental work with healthy subjects and an amputee indicated good perceptibility of the feedback during static and dynamic (walking) condition, although higher magnitude of stretch was required to perceive the feedback during dynamic condition. User response time during dynamic activity showed that the haptic feedback system is suitable for delivering cues of IC and TO within the duration of the stance phase. In addition, feedback delivered in discernible patterns can be learned and adapted by the subjects.

Finally, a case study was carried out with an above-knee amputee to assess the effects of the haptic feedback on spatio-temporal gait parameters and on the vertical ground reaction force during treadmill and overground walking.

The research presented in this report introduces a novel design of a haptic feedback device. As such, the outcome includes a well-controlled skin-stretch effect which contributes to the research by investigating skin-stretch feedback for conveying discrete event information rather than conveying direction information as presented

in other studies. In addition, it is found that stretch magnitude as small as 3 mm could be perceived in short duration of 150 ms during dynamic condition, making it a suitable alternative to other widely investigated haptic modality such as vibration for ambulatory feedback application. With continuous training, the haptic feedback system could possibly benefit lower limb amputees by creating awareness of the limb placement during ambulation, potentially reducing visual dependency and increasing walking confidence.

*To Mak and Bapak, for their unconditional love. To my wife, Afifah Hanum Mohd Jamal, who has been the backbone of my whole PhD journey. To my source of joy, 'Umair and Ahmad, who grow fast before my eyes.*

## Acknowledgements

My PhD has been an amazing experience. As this thesis can only describe a portion of this experience, I would like to take this opportunity to acknowledge the people who have provided support directly and indirectly towards the completion of my PhD study.

My deepest appreciation goes to my supervisor, Professor Abbas Dehghani for his time and support throughout my entire study. Under his supervision, not only did I obtain valuable suggestions and ideas, but I was also given the chance to acquire valuable skills which will be beneficial for the many years to come.

My sincere thanks go to my fellow colleagues, Dr. Mohammed Ibrahim Awad, Dr. Hafiz Farhan Maqbool, and Dr. Alireza Abouhossein for the stimulating discussions, and for sharing with me valuable knowledge in the field. Special thanks go to the Mechanical Engineering laboratory staff, particularly Mr. Tony Wiese, Mr. David Readman, and Mr. Abbas Ishamel who spent a lot of time assisting me in using the laboratory tools and machines. Thanks to my fellow postgraduate friends at the Institute of Design, Robotics and Optimization (iDRO), for the wonderful time we had in the past few years.

I cannot express enough gratitude to my parents, who have been providing me with moral support, kind words and prayers while being thousands of miles away. I am forever indebted to them for their unconditional love and sacrifice. Also, I would have never been able to complete my PhD without the utmost support from my wife, Afifah, and my two inquisitive kids ‘Umair and Ahmad. They have been cherishing every moment with me throughout my journey, and supported me when I needed it most.

Finally, I would like to thank my sponsors, the Ministry of Higher Education Malaysia and International Islamic University Malaysia for providing financial assistance and support throughout my study.

---

## List of Contents

<b>Abstract .....</b>	<b>iii</b>
<b>Acknowledgements.....</b>	<b>vi</b>
<b>List of Contents.....</b>	<b>vii</b>
<b>List of Figures .....</b>	<b>xii</b>
<b>List of Tables.....</b>	<b>xviii</b>
<b>List of Abbreviations.....</b>	<b>xx</b>
<b>List of Publications.....</b>	<b>xxii</b>
<b>Chapter 1: Introduction.....</b>	<b>1</b>
1.1 Background .....	1
1.2 Motivation .....	3
1.3 Aim and Objectives.....	4
1.3.1 Aim.....	4
1.3.2 Objectives.....	4
1.4 Scope of this Research .....	4
1.5 Contributions of this research .....	5
1.6 Organization of the Thesis .....	5
<b>Chapter 2: Literature Review .....</b>	<b>7</b>
2.1 Introduction .....	7
2.2 Human Lower Limb .....	7
2.2.1 Lower Limb Physiology.....	7
2.2.2 Lower Limb Biomechanics .....	9
2.2.2.1 Movement Terminologies .....	9

---

2.2.2.2	Gait Analysis .....	11
2.3	Gait Measurement and Event Detection .....	14
2.3.1	Gait Measurement .....	14
2.3.1.1	State of the art .....	14
2.3.1.2	Alternative Gait Measurement Methods .....	16
2.3.2	Gait Event Detection and Classification .....	18
2.4	Lower Limb Amputation.....	22
2.4.1	Lower Limb Prostheses .....	22
2.4.2	Amputation Effects .....	23
2.4.2.1	Gait Deviations.....	24
2.4.2.2	Increased Energy Expenditure .....	25
2.4.2.3	Effects to Sensory System.....	26
2.4.2.4	Reduced Balance Control and Risk of Falling.....	26
2.5	Haptic Feedback.....	27
2.5.1	Somatosensory System.....	28
2.5.2	Haptic Feedback Modality .....	29
2.5.3	Lower Limb Haptic Feedback Literature .....	34
2.6	Gap of Knowledge .....	39
2.7	Summary .....	40

### **Chapter 3: Haptic Feedback Module Development and Design**

<b>Iterations .....</b>	<b>41</b>	
3.1	Introduction .....	41
3.2	Preliminary Design.....	41
3.2.1	Design Consideration .....	41
3.2.2	Initial Design Concept.....	42
3.2.3	Skin-stretch Mechanism.....	43
3.2.4	Actuators and assembly.....	44
3.3	Preliminary Trials.....	46
3.3.1	Methods.....	46
3.3.2	Analysis.....	48
3.3.3	Results .....	48
3.3.4	Discussion and Recommendation .....	50
3.4	First Iterative Design.....	52



---

3.4.1	Actuation Mechanism .....	52
3.4.2	Haptic Module Design .....	56
3.4.2.1	Design Description.....	56
3.4.2.2	Calculation of Movement Parameters.....	57
3.4.2.3	Design Details .....	59
3.4.3	Characterization .....	63
3.4.3.1	Movement Profile.....	63
3.4.3.2	Force Profile.....	68
3.5	Revised Design.....	70
3.5.1	Design Justification.....	70
3.5.2	CAD Design and Prototyping .....	71
3.6	Control and Power Unit .....	75
3.7	Summary .....	78
<b>Chapter 4: Gait Event Detection and Analysis Modules.....</b>		<b>79</b>
4.1	Introduction .....	79
4.2	Gait Event Detection .....	79
4.2.1	Background .....	80
4.2.2	Hardware setup.....	81
4.2.3	Detection Method.....	84
4.2.4	Experimental Validation .....	87
4.2.5	Predictive Algorithm for Feedback.....	94
4.3	Plantar Force Insole.....	95
4.3.1	Sensor Placement .....	96
4.3.2	Hardware .....	98
4.3.2.1	Sensor.....	98
4.3.2.2	Insole Fabrication.....	98
4.3.2.3	Electronics.....	99
4.3.3	Calibration.....	101
4.3.4	Experimental Validation .....	103
4.4	System Integration .....	108
4.4.1	Graphical User Interface .....	108
4.5	Summary .....	111

---

## **Chapter 5: Haptic Feedback: Static and Dynamic Evaluation .....112**

5.1	Introduction .....	112
5.2	Experimental Setup .....	113
5.2.1	Walking Platform .....	113
5.2.2	Determining Normal Force .....	114
5.3	Single Module-Perceptibility Test .....	115
5.3.1	Methods.....	116
5.3.2	Data Collection and Analysis.....	119
5.3.3	Results and Discussion.....	120
5.4	Gait-Event-Based Feedback.....	125
5.4.1	Feedback Strategy .....	126
5.4.2	Feedback mode.....	127
5.4.3	Experimental Setup .....	129
5.4.4	Data Analysis .....	131
5.4.5	Results .....	134
5.4.5.1	Perceptibility (PE).....	134
5.4.5.2	Response Time (RT) .....	135
5.4.6	Discussion and Key Findings.....	139
5.5	System Evaluation with Amputee.....	141
5.6	Summary .....	141

## **Chapter 6: Summary, Conclusion, and Future Works .....143**

6.1	Summary and Assessment of the Research Aim and Objectives.....	143
6.2	Conclusions .....	145
6.3	Future Works.....	148

## **References .....150**

## **APPENDIX A: Evaluation of Haptic Feedback System Effects on Amputee Gait.....160**

A.1	Introduction .....	161
A.1.1	Subject Background .....	161
A.1.2	Amputation History.....	161
A.1.3	Mobility.....	161

---

A.1.4	Prosthesis Use .....	162
A.1.5	Gait Challenge.....	162
A.2	Experimental Work .....	163
A.2.1	Method .....	163
A.2.2	Data Collection and Analysis.....	165
A.2.3	Results .....	168
A.2.4	Discussion and Key Findings.....	178
A.3	Summary .....	180
<b>APPENDIX B: Additional Literature Review.....</b>		<b>181</b>
B.1	Prosthetic Components.....	182
B.2	Advancements in Lower Limb Prosthetics .....	186
<b>APPENDIX C: PCB Drawings .....</b>		<b>188</b>
<b>APPENDIX D: Ethical Approval .....</b>		<b>192</b>

## List of Figures

Figure 2.1(a) bones and joints at pelvis and legs and (b) major muscle groups, adapted from [49] .....	8
Figure 2.2 Anatomical position and associated planes and directions [37] .....	9
Figure 2.3 Feet placement while walking [37].....	11
Figure 2.4 Normal gait cycle [29] .....	12
Figure 2.5 (a) Joints angle (b) muscle activities and (c) ground reaction forces for one complete gait cycle. IC = initial contact; OT = opposite toe off; HR = heel rise; OI = opposite initial contact; TO = toe off; FA = feet adjacent; TV = tibia vertical. Compiled from [37].....	13
Figure 2.6 Activities of major muscle groups during gait. Edited from [167].....	13
Figure 2.7 A force platform indicating force and moment vectors in Cartesian coordinate system [39] .....	14
Figure 2.8 Normal gait shown by (a) Components of GRF [37] and (b) Butterfly diagram [40] .....	15
Figure 2.9 Independent photos showing markers fitted on the body and detected markers viewed in the software [168] .....	16
Figure 2.10 Levels of lower limb amputation [72] .....	22
Figure 2.11 Prosthetic leg components .....	23
Figure 2.12 Sketch of several gait abnormalities for transfemoral amputees [79] ..	25
Figure 2.13 Mechanoreceptors' location and structure from [104] .....	28
Figure 2.14 C2 and Tactaid vibrotactors from [68] .....	31
Figure 2.15 Experimental setup in (a) [113] and (b) [17] .....	31
Figure 2.16 Embodiment illusion via vibrotactile feedback on reinnervated skin in [100] .....	32
Figure 2.17 1 cm <sup>2</sup> piezoelectric sensors for giving stretch feedback at fingertip mentioned in [115] .....	33

---

Figure 2.18 (a) TeslaTouch surface allows user to feel different textures via friction manipulation [119] and (b) HyVE interface [123].....	34
Figure 2.19 Subject wearing a vibrotactile feedback system standing on a wobble board [125] .....	35
Figure 2.20 Pneumatic tactile feedback for PN subjects. Adapted from [128].....	36
Figure 2.21 Rutgers' Ankle Force Feedback System. Modified from [129] .....	36
Figure 2.22 Feedback system strategy used in [102] .....	37
Figure 2.23 Neoprene cuff fitted with pneumatic driven silicone balloon actuator [16] .....	38
Figure 3.1 Mechanisms for skin-stretch haptic. $F_s$ = stretch force, $F_N$ = Normal force, $v$ = velocity direction .....	42
Figure 3.2 Modular-multiple-contacts design concept.....	43
Figure 3.3 Working principle of the mechanism. (a) the module in inactive state, the belt contacts the skin. (b) Rotation of the motor causes the belt to extend and stretches the skin. ....	44
Figure 3.4 CAD illustration of a single feedback module.....	45
Figure 3.5 Assembled four quadrants haptic feedback modules.....	45
Figure 3.6 Experimental setup .....	47
Figure 3.7 Possible actuation methods to create skin-stretch stimuli .....	53
Figure 3.8 Examples of: (a-b) linearized stepper and DC motor (c) solenoid (d) pneumatic actuator (e) servo motors .....	54
Figure 3.9 The top and side view of the haptic plate .....	56
Figure 3.10 Rack and pinion parameters.....	57
Figure 3.11 Haptic module – frame assembly.....	59
Figure 3.12 Haptic module – drive assembly.....	60
Figure 3.13 Haptic module – linker frame .....	60
Figure 3.14 Haptic module – haptic plate .....	61
Figure 3.15 Haptic module – adjustable limb contact.....	61
Figure 3.16 Haptic module – full assembly .....	62
Figure 3.17 The haptic feedback module on an anatomical leg model.....	62
Figure 3.18 Setup for validating distance and speed profile of the haptic module .	63
Figure 3.19 An overshoot when returning to baseline position as observed with target distance of 2-5 mm.....	64

---

Figure 3.20 Movement profile for 1 mm target distance with 200 ms duration. (a) distance profile for 15 trials. (b) Average movement profile with shaded area indicating standard deviation. (c) velocity profile of the mean data and (d) acceleration profile.....	65
Figure 3.21 Movement profile for 5 mm target distance with 200 ms duration. (a) distance profile for 15 trials. (b) Average movement profile with shaded area indicating standard deviation. (c) velocity profile of the mean data and (d) acceleration profile.....	66
Figure 3.22 Drive mechanism, showing the tangential force $F_p$ .....	68
Figure 3.23 Experimental setup for measuring current-torque relationship .....	69
Figure 3.24 Torque and force acting on the servo arm .....	69
Figure 3.25 Torque vs current graph for various loads .....	70
Figure 3.26 Configuration of the new haptic plate.....	72
Figure 3.27 Haptic frame assembly.....	72
Figure 3.28 Drive assembly .....	73
Figure 3.29 Linker frame .....	73
Figure 3.30 The haptic plate.....	74
Figure 3.31 Assembled haptic module.....	74
Figure 3.32 Moteino microcontroller .....	76
Figure 3.33 Left: battery unit. right: voltage regulator .....	76
Figure 3.34 Handheld response switch used in (a) first design (b) revised design..	77
Figure 3.35 Revisions of circuit board.....	77
Figure 3.36 Control unit scheme .....	78
Figure 4.1 Proposed scheme for haptic feedback system.....	80
Figure 4.2 (a) MEMS gyroscope structure and (b) its working principle [169] .....	81
Figure 4.3 (a) IMU attachment for obtaining gait event information (b) GY-521 IMU breakout board.....	82
Figure 4.4 Connection schematics. ....	83
Figure 4.5 Event detection modules (a) old modules with two attachments. (b) revised module single attachment and reduced footprint .....	84
Figure 4.6 Sample of shank angular velocity during walking.....	85
Figure 4.7 Placement of IMU and motion capture markers on shank and foot .....	87
Figure 4.8 Calcaneus and toe marker positions in anterior-posterior direction .....	88
Figure 4.9 Marker placement on the x-y coordinate system.....	89

---

Figure 4.10 (a) Shank angular velocity from motion capture data and IMU from CS1. (b) Correlation plot between the signals. ....	90
Figure 4.11 (a) Shank angular velocity from motion capture data and IMU from CS2. (b) Correlation plot between the signals. ....	91
Figure 4.12 Sample of detected events from (a) motion capture and (b) IMU. ....	92
Figure 4.13 (a) Sensor attachment sites suggested by Soames [139] and (b) sensor placement location adopted in the insole design. ....	96
Figure 4.14 Design of the 3D printed insole .....	99
Figure 4.15 FlexiForce recommended circuit from [151]. ....	99
Figure 4.16 data acquisition schematics for the force insole .....	101
Figure 4.17 The setup for force sensor calibration. (inset) Signal conditioning circuit .....	102
Figure 4.18 Calibration plot for individual FlexiForce sensors .....	104
Figure 4.19 Experimental setup for investigation of force profile generated by the insole .....	105
Figure 4.20 GRF data generated from the insole compared against the force plate for all three subjects. Three samples are shown for each subjects. ....	107
Figure 4.21 Workflow of the integrated system. ....	109
Figure 4.22 Example of the GUI window, with description of the functions .....	109
Figure 4.23 Database management child window .....	110
Figure 4.24 Experiment control and data analysis window .....	110
Figure 5.1 Treadmill setup, with fall safe rigid frame .....	113
Figure 5.2 Setup for determining force range for haptic-skin interface. ....	114
Figure 5.3 Feedback scheme for the perceptibility experimental work .....	117
Figure 5.4 Experimental setup, showing placement of haptic module on the amputee for (a) static and (b) dynamic experiment. ....	119
Figure 5.5 Result of the subjects' perception to the stimuli in both static and dynamic mode. ....	120
Figure 5.6 Muscle activities during gait. Darker shade indicates more intense activity. Adapted from [158] .....	124
Figure 5.7 Haptic feedback strategy, showing the placement of corresponding feedback modules. Images modified from [158]. ....	126
Figure 5.8 SD feedback mode .....	127
Figure 5.9 SA feedback mode .....	128

---

Figure 5.10 SC feedback mode .....	128
Figure 5.11 Experimental apparatus.....	129
Figure 5.12 Experimental setup, showing the placement of the (a) haptic module and (b) event detection modules and response button .....	130
Figure 5.13 An example of visualization of data analysis from the data collected during SD feedback mode. ....	131
Figure 5.14 Possible irregular data scenarios (a) double response and (b) early response.....	133
Figure 5.15 PE across walking speed.....	134
Figure 5.16 $RT_{IC}$ and $RT_{TO}$ for all subjects. Error bar shows the standard deviation value .....	136
Figure 5.17 $RT_{IC}$ and $RT_{TO}$ across different feedback modes.....	137
Figure 5.18 $RT_{IC}$ and $RT_{TO}$ across different walking speeds.....	138
Figure A.1 Experimental setup. (a) treadmill walk and (b) overground walk. (inset) placement of the haptic module on the lower trunk. ....	164
Figure A.2 Calculation of temporal gait parameters from angular velocity signal. I= intact and P= prosthetic. ....	165
Figure A.3 Sample of a vertical GRF data, with important features marked.....	166
Figure A.4 Spatio-temporal parameters during TM baseline walking. I= Intact. P=Prosthetic .....	169
Figure A.5 Stance and swing duration during baseline treadmill walk .....	170
Figure A.6 TMW Spatio-temporal parameters during BL, SA and SC condition-slow walk .....	170
Figure A.7 TMW Spatio-temporal parameters during BL vs SA and SC condition-normal walk.....	171
Figure A.8 TMW Spatio-temporal parameters during BL, SA and SC condition-fast walk .....	171
Figure A.9 Average stance and swing percentage during all treadmill walking conditions .....	172
Figure A.10 Mean FZ1, TZ1, and LR recorded on the prosthetic leg during all treadmill walking conditions. Error bar shows the standard deviation. ....	173
Figure A.11 OGW Spatio-temporal parameters during BL, SA and SC condition-slow walk.....	174



---

Figure A.12 OGW Spatio-temporal parameters during BL, SA and SC condition-normal walk.....	175
Figure A.13 OGW Spatio-temporal parameters during BL, SA and SC condition-fast walk .....	175
Figure A.14 Gait cycle percentage throughout experimental conditions.....	176
Figure A.15 Mean FZ1, TZ1, and LR recorded on the prosthetic leg during all overground walking conditions. Error bar shows the standard deviation. ....	177
Figure B.1 PTB socket (left) and TSB socket (right) for below knee amputee [76] .....	183
Figure B.2 (a) Manual lock (b) single axis constant friction and (c) weight activated and (d) Polycentric prosthetic knee joints. All models from Ottobock [76] .....	184
Figure B.3 Example of commercially available non-energy storing foot (left) and energy storing foot (right) .....	185
Figure B.4 (left) Reinnervation strategy and (right) the patient ascending stairs [58] .....	187
Figure C.1 (top) schematics for final haptic feedback system. (bottom) PCB layout for board fabrication.....	189
Figure C.2 (top) schematics for earlier revision of the haptic feedback system, which allows testing different actuators. (bottom) PCB layout for board fabrication .....	190
Figure C.3 (top) schematics the force insole. (bottom) PCB layout for board fabrication.....	191

---

## List of Tables

Table 2.1 Movements of the limbs with associated motion of range. Adapted and modified from [37] .....	10
Table 2.2 Examples of Alternative Wearable Gait Measurement System.GRF= Ground Reaction Force, CoP = Center of Pressure.....	17
Table 2.3 Examples of Gait Event Detection Applications in literature.....	19
Table 2.4 Classification of mechanoreceptors and associated features, adapted from [102] and [105].....	29
Table 3.1 Summary of accuracy of location detection for the two experiments.....	48
Table 3.2 Results of responses from the subjects for single quadrant assessment...	49
Table 3.3 Results of responses from the subjects for simultaneous quadrants assessment. ....	49
Table 3.4 Comparison of actuator properties .....	55
Table 3.5 Servo motor specification .....	55
Table 3.6 Actual movement distance achieved for various target positions and movement duration. Values indicate Mean $\pm$ SD .....	67
Table 3.7 Error in positioning of the haptic assembly (mm). Shaded area indicates range of error.....	67
Table 3.8 Comparison of design parameters .....	75
Table 4.1 Mean $\pm$ SD difference in timing of detected events using the IMU algorithm in comparison to motion capture data. Positive value indicates delayed detection while negative values indicates early detection. ....	93
Table 4.2 Force sensing methods and sensor locations described in literatures. Adapted from [142].....	97
Table 4.3 Pearson's correlation coefficient for signal samples shown in Figure 4.20 .....	105
Table 5.1 Demographic data of Control Subjects (CS) .....	116
Table 5.2 Details on the Above-knee (AK).....	116
Table 5.3 Summary of perceptibility (%). Darker shades indicate higher perceptibility.....	120

---

Table 5.4 Instances of false perceptions (indicating stimuli when none was given)	122
Table 5.5 Evaluation of alternative placement for haptic feedback module	125
Table 5.6 Perceptibility distribution across experimental parameters	134
Table 5.7 Mean difference in RT (ms) between SA, SD and SC mode	139
Table 5.8 Response time distribution across experimental parameters	139
Table A.1 Details of the AKS prosthetic components	163
Table A.2 Walking speed across experimental conditions	168
Table A.3 p-value for comparison between BL and feedback condition. * indicates significance difference	176
Table A.4 CoV (%) of temporal parameters during TMW and OGW	178

---

## List of Abbreviations

3D	3-Dimension
AK	Above-knee
AKS	Above-knee Subject
ANOVA	Analysis of Variance
BL	Baseline
CAD	Computer Aided Design
CoP	Centre of Pressure
CS	Control Subjects
CoV	Coefficient of Variation
DAQ	Data Acquisition
EMG	Electromyography
FES	Functional Electrical Stimulation
FSR	Force Sensitive Resistor
GRF	Ground Reaction Force
GUI	Graphical User Interface
IC	Initial Contact
I <sup>2</sup> C	Inter-integrated Circuit
IMU	Inertial Measurement Unit
LR	Loading Rate
LLA	Lower Limb Amputation
MEMS	Micro Electro Mechanical Systems
MSW	Mid-Swing
OGW	Overground Walk
PC	Personal Computer
PCB	Printed Circuit Board
PE	Perceptibility
PR	Push-off Rate
RT	Response Time
SA	Sequential-alternate
SACH	Solid Ankle Cushioned Heel
SC	Sequential-continuous
SD	Sparsely Distributed

SL	Stride Length
TFA	Transfemoral Amputee
TMW	Treadmill Walk
TO	Toe-Off
TTA	Transtibial Amputee

---

## List of Publications

Section 3.2 and Section 3.3 of this thesis are based following jointly-authored publication:

Husman, M. A. B., H. F. Maqbool, M. I. Awad, A. Abouhossein, and A. A. Dehghani-Sanij. "A wearable skin-stretch haptic feedback device: Towards improving balance control in lower limb amputees." In *Engineering in Medicine and Biology Society (EMBC), 2016 IEEE 38th Annual International Conference of the*, pp. 2120-2123. IEEE, 2016.

Section 3.4 and Section 5.3 are based on the following jointly-authored publication:

Husman, M. A. B., H. F. Maqbool, M. I. Awad, and A. A. Dehghani-Sanij. "Portable Haptic Device for Lower Limb Amputee Gait Feedback: Assessing Static and Dynamic Perceptibility" *IEEE International Conference on Rehabilitation Robotics (ICORR), 2017 IEEE, 2017*.

The candidate performed the major tasks of the work presented in these published papers, such as development of the hardware and electronics, experimental work, data analysis and preparation of the manuscript. The co-authors were involved in experimental design and preparation of the manuscript.

Section 4.2 includes references to the following publications:

1. H. F. Maqbool, M. A. B. Husman, M. I. Awad, A. Abouhossein, N. Iqbal, and A. A. Dehghani-Sanij, "A Real-Time Gait Event Detection for Lower Limb Prosthesis Control and Evaluation," *IEEE Transactions on Neural Systems and Rehabilitation Engineering*, vol. 25, pp. 1500-1509, 2017.
2. Maqbool, H. F., M. A. B. Husman, M. I. Awad, A. Abouhossein, P. Mehryar, N. Iqbal, and A. A. Dehghani-Sanij. "Real-time gait event detection for lower limb amputees using a single wearable sensor." In *Engineering in Medicine and Biology Society (EMBC), 2016 IEEE 38th Annual International Conference of the*, pp. 5067-5070. IEEE, 2016.

The candidate aided in developing the data collection hardware and electronics and was involved during the experimental work.

# CHAPTER 1: INTRODUCTION

## 1.1 Background

One of the major challenges in today's healthcare is the occurrence of lower limb amputation (LLA). It is estimated that lower limb amputees account for over 75% of the 32 million amputees' population worldwide [1]. More worryingly, year by year, the prevalence of LLA across the world has been shown to be steady, if not increasing. In England alone, between 2003 and 2013, there were 95449 LLA amputations were carried out, with 50.2% of them were major amputations (above ankle) [2]. In 2009/10, 530 deaths were recorded following LLA episodes [3]. The cause of amputation differs geographically, with peripheral arterial disease being the major cause of amputation in developed countries, and trauma and uncontrolled infections causing most amputation in developing countries [4]. In addition, involvement in war has resulted in surviving service members with amputations caused by explosion and other lethal weaponry.

LLA has significant effects on a person's quality of life and ability to perform activities of daily living. Prescription of prosthetic device post amputation is intended to help restore some degrees of mobility function, however, the physiological change after amputation have shown to cause suboptimal walking performance. For example, in comparison to able-bodied person, the energy expenditure for amputees could increase between 25% to 100% depending on the cause and level of amputation [5]. Amputation also causes changes in biomechanics of walking, most common being the amputees favouring the intact limb during walking. As a result, amputees often develop secondary complications such as back pain and osteoarthritis on the intact limb, and osteopenia and osteoporosis on the amputated limb [6]. This is in addition to the phenomenon known as phantom limb pain, resulting from the change in

---

peripheral and central nervous system, which affects 60% to 80% of patients following amputation [7].

Of particular concern is the loss of sensorimotor due to severed nerve post amputation, which has been associated with lack of response to external perturbation during walking [8]. Moreover, studies have shown evidence of low balance confidence among amputee populations [9] which has been shown to cause reduction in prosthetic mobility and engagement in social activities [10]. In addition, higher risk of falling was indicated among amputee community, especially those suffering from above knee amputation [11]. Improving amputees' gait often takes form in the most fundamental ways, for example by ensuring optimal prosthetic alignment [12] and fit [6]. However, technologically advanced prosthetic components have also contributed to the improvement in gait performance. For above-knee amputees, the use of variable damping knee has been shown to enhance gait in comparison to the mechanically passive knees [13]. Similarly, in comparison to conventional knee, microprocessor controlled knee such as C-leg (Ottobock, Germany) was shown to significantly reduce energy expenditure and improve walking agility [14]. Powered prostheses offer even better control and allow amputees to navigate more challenging terrain such as upslope and stairs, however, they are expensive and therefore not available for wider amputee population.

While advanced prostheses offer improvement in gait, they often lack a form of feedback which replaces the loss of sensory pathway post amputation. Lack of meaningful sensation can limit the use of lower limb prosthesis by the amputee [15] and prolongs rehabilitation [16], which leads to suboptimal use of the prosthetic device. To tackle this problem, non-invasive tactile or haptic feedback has been suggested as a measure to recreate the sensory pathway severed due to amputation. The use of haptic feedback in upper limb powered prostheses, which has been studied earlier and more extensively, has shown the possibility of improving their functional capability [17, 18]. Although lower limb bears biologically different functionality from upper limb, equivalent effect from haptic feedback in terms of functional improvement can be expected. Despite existence of a wide variety of lower limb prostheses in the market, only a few of them provide sensory feedback [19]. Nevertheless, the use of non-invasive haptic feedback has been shown to provide functional improvement for lower limb amputees such as improvement in gait



parameters [20], improved static balance [21] and reduction in response time to perturbation [22].

## 1.2 Motivation

Very few studies in the literature investigated the use of haptic feedback to improve the outcome of lower limb amputee's functionality such as balance control and gait pattern. Among the studies that did so or proposed conceptual ideas for this application, different haptic modalities were presented including vibration [22-25], pneumatic balloon [16, 26], and electrical stimulation [20, 21]. The use of pneumatic actuation requires bulky apparatus and sizable power unit, making it less usable outside the laboratory environment without adding weight to the feedback system. Vibration actuators, although finding its way in many haptic feedback application, are known to show adaptation effect, especially for long-term use [27]. Recent studies have shown the advantages of skin-stretch feedback in providing stimuli on the hairy skin [28-32]. Apart from the fact that skin-stretch can be perceived at relatively low magnitude, [31], this type of stimuli activates the slow adapting receptors of the skin, possibly preventing adaptation and desensitization effect in the long-term use. [33] However, the use of skin-stretch feedback in literature was very limited, and has been used so far for conveying geometry information [34], positional cues [28, 29], and directional cues [30-32].

The study is motivated on the fact that no device describing a lateral skin-stretch feedback can be found in the literature for conveying gait event information concerning the placement of the foot on the ground, namely the initial contact and toe-off to its wearer. Conveying this specific gait information is anticipated to improve amputee's awareness of the limb placement on the ground during walking, thus improving the gait pattern. In addition, investigation into user's perception towards skin-stretch feedback during walking has not been described before. Developing such device presents its own challenge since the skin-stretch stimuli must be delivered within the time constraint of gait events. In addition, such feedback system will require mechanism for identifying gait events, and utilizing it to control the activation of the skin-stretch feedback. This motivation serves as the basis of this research.

## **1.3 Aim and Objectives**

### **1.3.1 Aim**

The aim of this research is defined as follows:

- To develop a wearable lateral skin-stretch haptic feedback system intended to create awareness of limb placement during walking for lower limb amputees.

### **1.3.2 Objectives**

To meet the aim mentioned above, the following objectives are defined for this research:

- To carry out an iterative design of a skin-stretch module that can be worn around the lower limb or on the body.
- To characterize the skin-stretch module to obtain its performance and working parameters.
- To evaluate users' perception to the skin-stretch module in static and dynamic conditions.
- To integrate an event detection module for controlling the activation of the skin-stretch device during gait.
- To assess users' perception and performance of the complete haptic feedback system
- To evaluate the system on lower limb amputee and assess its effects on the gait parameters.

## **1.4 Scope of this Research**

This research presents the development and evaluation of skin-stretch haptic feedback system for creating awareness of the limb placement for lower limb amputee. The scope of the research includes:

- Development of a wearable and portable skin-stretch device.
- Integration with an event detection and designing a feedback strategy to create a complete haptic feedback system.
- Evaluation with healthy subjects and unilateral amputee subjects who are free from sensory deficit that can affect perception to stimuli.

## 1.5 Contributions of this research

The research contributes to the body of knowledge in the field of haptic feedback with specific application in gait intervention.

Contributions of this research work are summarised as follows:

1. Presenting a novel design of a non-directional wearable lateral skin-stretch haptic device.
2. Integrating a non-plantar based gait event detection module to form a real-time gait events based haptic feedback system.
3. Evaluating the user perception to the lateral skin-stretch stimuli in static and dynamic condition.
4. Evaluating the practicality of the proposed haptic feedback system in providing real-time gait event information by investigating different feedback strategies during robust walking task.
5. Evaluating the effect of skin-stretch haptic feedback system on the gait parameters of an above-knee amputee.

## 1.6 Organization of the Thesis

The thesis is organized and divided into six chapters. The summary of each chapter is presented as follows.

**Chapter 1** introduces the background, motivation, aims and objectives for the development of a skin-stretch haptic feedback system for lower limb amputee. The contributions of the research are described, and the research scope is defined.

**Chapter 2** begins with the introduction to relevant literature concerning human lower limb physiology, including the human gait. The methodology for gait event detection and gait measurement was reviewed to understand the underlying principles. The review then continues with description of lower limb amputation, and the challenges caused by amputation in terms of gait deficiency were highlighted. Afterwards, literature regarding haptic feedback as a possible method for improving amputee's gait was reviewed and haptic modalities used across the literature are presented. The

last section of this chapter presents the gap of knowledge which serves as a foundation of the research.

**Chapter 3** presents the development of the skin-stretch haptic feedback module. A preliminary non-portable design and experimental work with a focus group is initially described. Afterwards, an iterative design of a skin-stretch module is presented, detailing the actuator selection, stimuli delivery mechanism and the device fabrication. Characterization of the device to quantify its characteristics and performance is then described. Lastly, the design of revised version of the skin-stretch module for the use in the final haptic feedback system is presented.

**Chapter 4** describes additions necessary to complete the haptic feedback system. First, an event detection module designed in previous work is described. Modification was made to the module to reduce its footprint and provide better attachment. Validation of the angular velocity signal was carried out using a motion capture system, and an additional adaptive algorithm was designed to improve the module's capability. Next, the design of a force insole for measuring ground reaction force parameters is presented. The force insole will serve as a measurement tool for evaluating gait parameters for the evaluation of the system with the amputee. The output from the insole was validated against force plate and its limitations are described. The chapter finishes with the description of the complete haptic feedback system integration and its underlying design scheme.

**Chapter 5** describes two experimental works carried out to evaluate the skin-stretches device and the haptic feedback system. The first experimental work assessed the effect of stretch magnitude towards the perceptibility of the skin-stretch stimuli in static and dynamic conditions. The second experiment evaluated the complete haptic feedback system during robust walking task, and assessed subject's perceptibility and response time across various feedback strategies and walking speed. The key findings are summarized at the end of this chapter.

**Chapter 6** summarizes the research work, analyses the achievement of research objectives and put forward the recommendations for future works.

A case study with an above knee amputee is presented in Appendix A to evaluate the effects of the skin-stretch haptic feedback in improving the amputee's gait. Spatio-temporal gait parameters obtained using inertial sensors and vertical ground reaction force parameters obtained via the force insole with and without the feedback was evaluated. Key findings are discussed at the end of the chapter.

## **CHAPTER 2: LITERATURE REVIEW**

### **2.1 Introduction**

This chapter focuses on the literatures relevant to the research carried out in this thesis. The early section gives a background and an introduction to human lower limb and its biomechanical aspects and relevant terminologies. The discussion is then followed by a review of lower limb amputation, covering its characteristics and associated effects to gait. To facilitate towards the development of the haptic feedback system, an introduction and review of current research in haptic feedback system for sensory augmentation is presented, particularly in the application of lower limb rehabilitation. Different feedback modalities and their use in the literature is also described. As the haptic feedback system will incorporate gait event detection for conveying gait information, relevant literatures concerning the gait event detection methods and gait measurements devices are also discussed. In these sections, apart from the state-of-the-art methods, emphasis is given to wearable and portable devices. The chapter concludes with the gap of knowledge found in the literature that served as a basis for this research.

### **2.2 Human Lower Limb**

#### **2.2.1 Lower Limb Physiology**

Lower limb or lower extremity is defined as the part of body extending between the hip and toes. It is the body region that is responsible for locomotion, weight-bearing and gravitational adaptation. Lower limb includes three major joints responsible for locomotion, namely the hip, knee, and ankle joints. The extension and flexion of the joints and the muscles attached to the bone facilitate the movements of the leg throughout the gait.

For gait analysis, the discussion will focus on the bones and muscles of the pelvis and legs and the hip, knee, ankle joints. The pelvis is formed from the sacrum, the coccyx and the two innominate bones. Since only small movement of pelvis occurs during locomotion, the pelvis is normally regarded as single rigid structure. Femur is the longest bone in the body. The spherical femoral head articulates with the pelvic acetabulum to form ball-and-socket hip joint. Hip joint is a three degree of freedom joint capable of flexion, extension, abduction, adduction, and internal and external rotation [35]. The tibia condyles meet with the femoral condyles to form the knee joint. Knee joint has single degree of freedom, and are capable of flexion and extension, with a small amount of internal and external rotation. The gap between the condyles is filled with meniscus or cartilage which functions to spread the load and reduce pressure at the contact point. The ankle joint has three surfaces. Tibia and talus bone forms the upper surface, inner medial malleolus of tibia and talus forms the medial side, and inner lateral malleolus of fibula and talus forms the lateral side. Ankle joint allows for dorsiflexion and plantar flexion motion. Figure 2.1(a) shows the structure of the bones and joints in the lower limb.

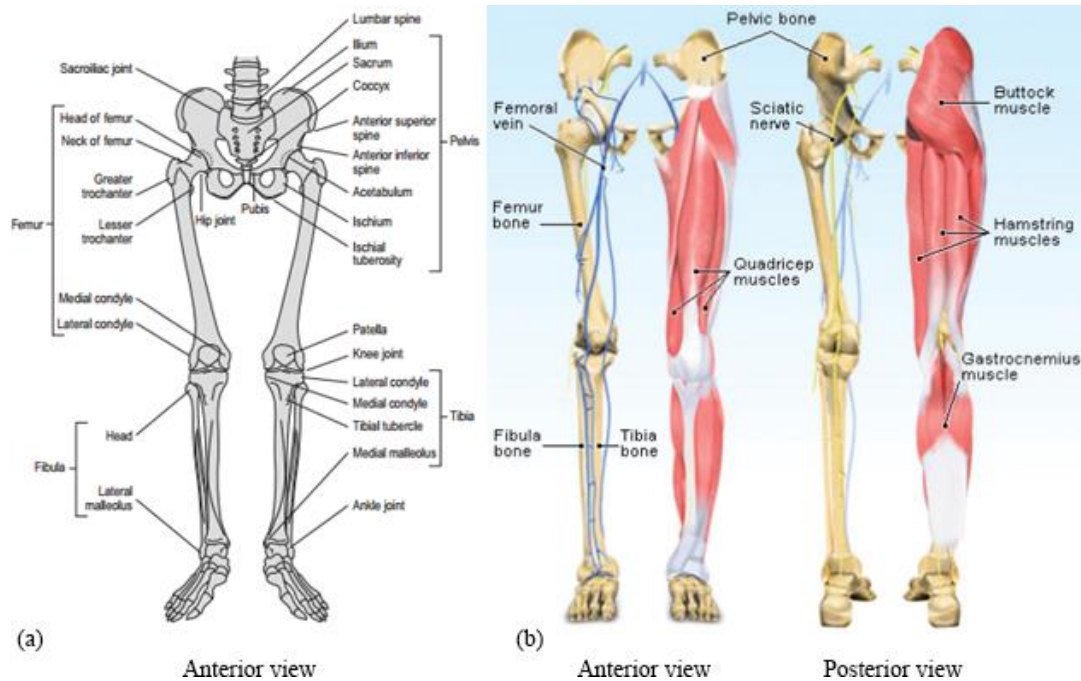


**Figure 2.1(a) bones and joints at pelvis and legs and (b) major muscle groups, adapted from [49]**

The movements of the lower limb are impossible without the function of muscles. Figure 2.1(b) shows the major muscle groups in human leg, which include

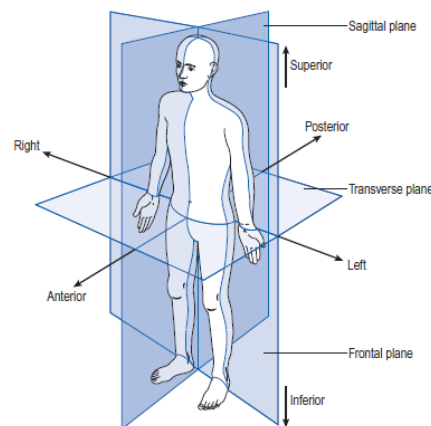
hamstrings, quadriceps and gluteus muscles. Hamstrings comprise three muscles at the back of the thigh and are responsible for knee flexion and hip extension. Quadriceps, a four-muscle group in front of the thigh, acts as knee and lower leg extensors [36]. The gluteus muscle groups are responsible for hip extension and abduction. The gastrocnemius and soleus are responsible for plantar flexion and knee flexion and assist forward propulsion during walking. The Achilles tendon connects plantaris, soleus and calf muscle to the heel bone. It functions to store the elastic energy during walking.

## 2.2.2 Lower Limb Biomechanics

Biomechanics, or the study of human movement holds the key to understanding performance, injury and disease related to lower limb. This section will discuss the movement terminologies related to the study of biomechanics, followed by fundamental gait analysis. The discussion is significant to help understand the impact of lower limb amputation which are discussed later in this chapter.

### 2.2.2.1 Movement Terminologies

Association of various terminologies related to the limb movement are made when the body is in the anatomical position. A body is said to be in the anatomical position when it is standing upright with arms to the side and head and eyes and palms of the hands facing forward. Figure 2.2 shows the anatomical position and the associated direction and planes with respect to the centre of body. The motions of the lower limb take place in one of these planes.

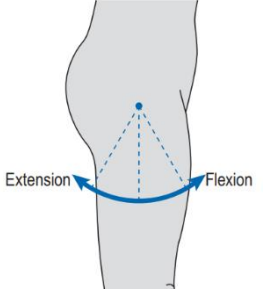
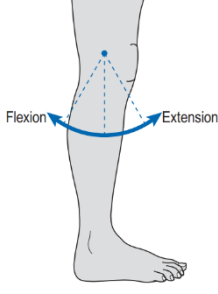
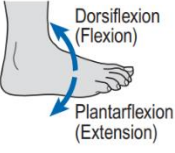
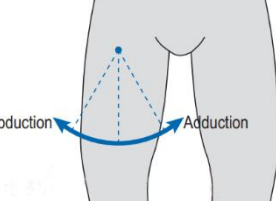
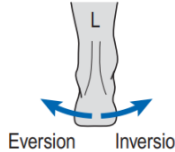


**Figure 2.2 Anatomical position and associated planes and directions [37]**

Flexion and extension takes place in the sagittal plane. Flexion reduces the angle between limbs while extension increases the angle and lead to straightening of the limb. The movement of the ankle joint in the sagittal plane is called plantar flexion and dorsiflexion respectively. The terms abduction and adduction refer to the movement of limbs away or towards the midline of the body and they take place in the frontal plane. External and internal rotations take place in the transverse plane and are significant only in hip joint.

The musculoskeletal system has limited range of motion due to the attachment of the muscle, ligaments and tendons to the bone as well as due to the type of joints at hip, knee and ankle. Disease and injuries in a limb can cause change in the range of motion (increase or decrease) and affects the locomotion. Table 2.1 summarizes the movement terminologies associated with the lower limb in all planes, with respect to the hip, knee and ankle joints.

**Table 2.1 Movements of the limbs with associated motion of range. Adapted and modified from [37]**

		Motions [range]		
		Hip	Knee	Ankle
Plane	Sagittal			
		Flexion [+120°] Extension [-30°]	Flexion [+150°] Extension [0°]	Plantarflexion [-40°] Dorsiflexion [+20°]
	Frontal		-	
	Abduction [-20°] Adduction [+45°]		Inversion [-35°] Eversion [+20°]	
	Transverse	External rotation [-50°] Internal rotation [+40°]	-	-



### 2.2.2.2 Gait Analysis

Before analysing amputation and its effects towards locomotion, it is necessary to study human normal walking gait. Gait is generally described as the manner in which the limbs move. Gait analysis is the systematic study of human locomotion, using observation and aided by instrumentation for measuring body movements, mechanics and muscle activity [37].

The placement and positioning of the feet while walking defines the different stages of the gait cycle. A step is the length when one foot moves forward in front of the other one. Stride, which consist of two steps, is the length between successive placements of a same foot. The side to side width between the lines of two feet is called walking base. Figure 2.3 depicts the terminologies referring to feet position during walking.

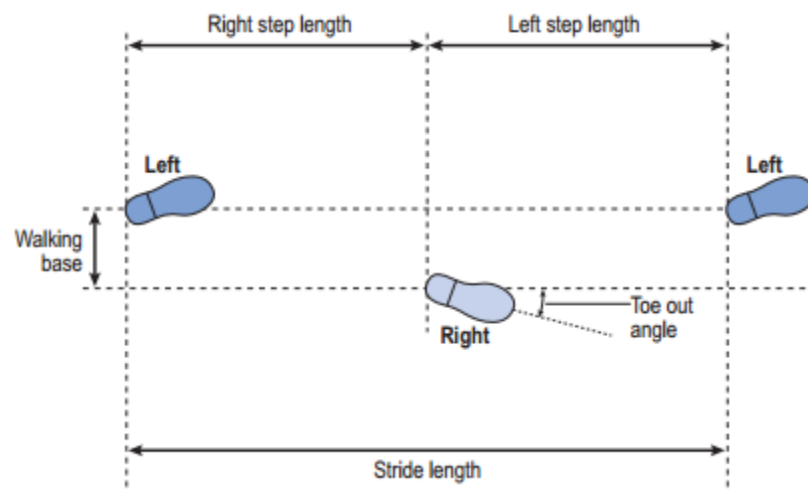


**Figure 2.3 Feet placement while walking [37]**

A gait cycle can be divided into stance and swing periods, which executes three tasks; weight acceptance, single limb support, and limb movement. Stance is the period in which the foot is in contact with the ground. Stance is followed by swing period, where the foot is in the air for limb advancement. Since gait cycle occurs in sequences that are independent of time, it is preferable to express the complete gait cycle in terms of percentage rather than time. The stance phase normally lasts for 60% of the gait while the swing phase last for 40%. However, as the walking speed increases, the duration of swing phase will increase [37]. Figure 2.4 shows a diagram of a normal gait cycle.

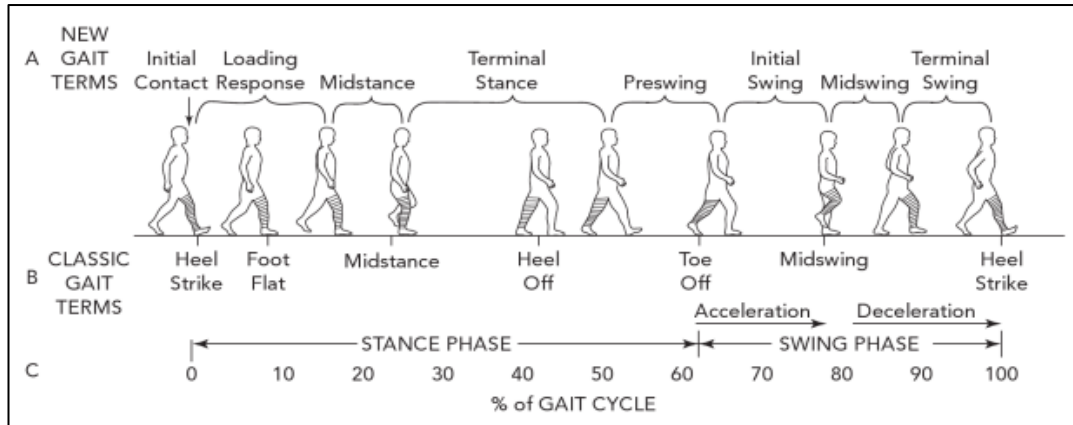


**Figure 2.4 Normal gait cycle [29]**

A discussion of both the stance and the swing phase throughout the gait cycle will follow. The rocker theory of the gait cycle as discussed by Perry [38] are used as reference while diagrams of the joint angles and ground reaction force are adapted from [37].

**Stance Phase** Loading response begins with heel strike or initial contact where hip flexion occurs at about  $30^\circ$  and knee is close to full extension and ankle at neutral position (Figure 2.5 (a)). This generates optimum ‘heel rocker’, in which the heel acts as a fulcrum and rolls the limb forward. Loading response ends when the contralateral limb leaves the ground, ankle plantar flexion lowers the foot flat on the ground and full body weight is assumed by the foot. Mid-stance denotes the beginning of single support period. At mid-stance, the ‘ankle rocker’ motion takes place, in which the tibia is rotated forward about the ankle joint, allowing forward progression. The body weight aligns over the supporting foot and the hip moves to extension while the knee reaches maximum extension. An observation of the fore-aft force indicates that at the end of mid-stance, the body changes from braking motion to propulsion. The terminal stance phase follows, beginning with the heel rise of the stance foot caused by ankle dorsiflexion and mark the beginning of knee flexion. During the opposite limb initial contact, the third rocker which is ‘forefoot rocker’ allows the foot to rotate forward about the forefoot. The last phase in stance period is pre-swing, in which the ankle rapidly changes from dorsiflexion to about  $20^\circ$  of plantar flexion. The pre-swing ends when the stance foot experiences to-off in which the limb is rapidly unloaded.

**Swing Phase** As soon as the stance toe leave the ground, the initial swing phase begins. Sufficient knee flexion allows clearance of the foot from the ground while rapid hip flexion contributes to significant propulsion force. During mid-swing, the foot is maintained on air by active ankle dorsiflexion. The hip continues to flex, advancing the limb ahead of the body until the tibia becomes vertical. At terminal swing phase, knee returns to full extension and ankle dorsiflexes to neutral position to allow placement of the foot on the ground. The muscle activity is intense, particularly the hamstrings, tibialis anterior and the quadriceps muscles (Figure 2.6)

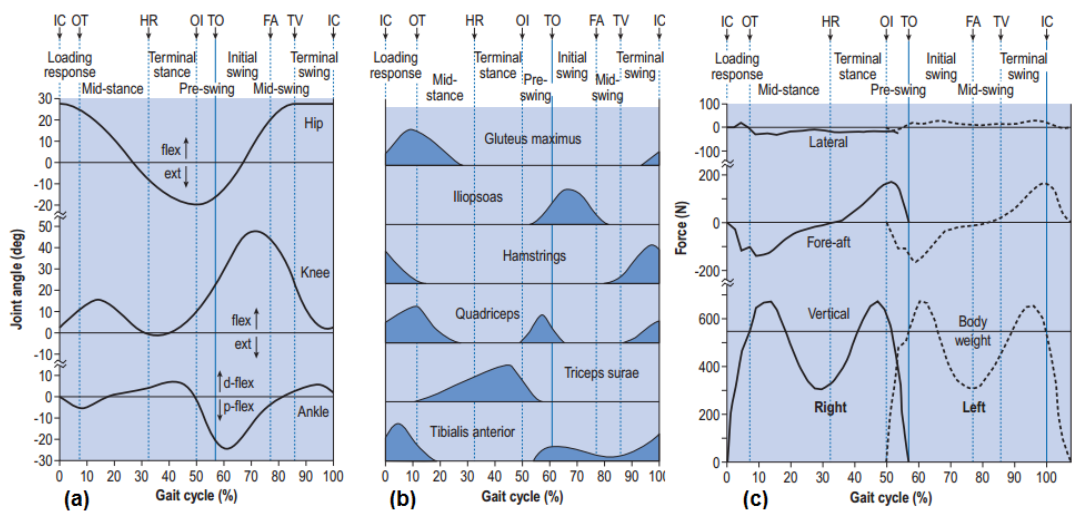


**Figure 2.5 (a) Joints angle (b) muscle activities and (c) ground reaction forces for one complete gait cycle. IC = initial contact; OT = opposite toe off; HR = heel rise; OI = opposite initial contact; TO = toe off; FA = feet adjacent; TV = tibia vertical. Compiled from [37]**

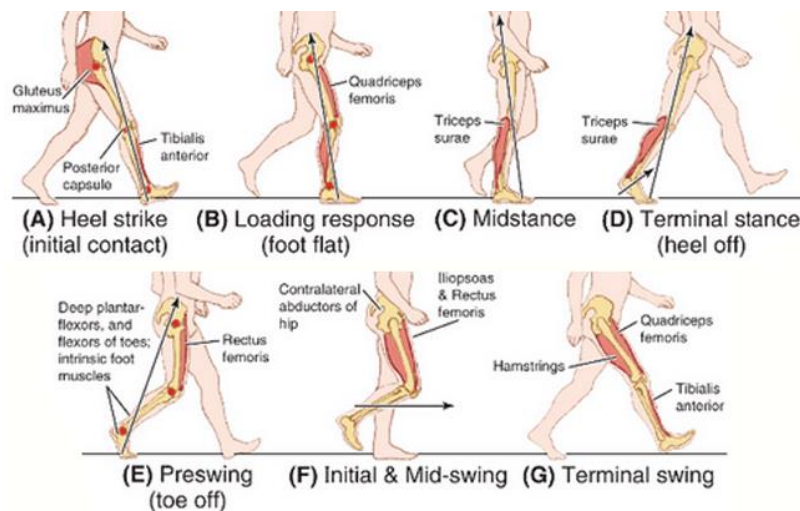


**Figure 2.6 Activities of major muscle groups during gait. Edited from [167]**

## 2.3 Gait Measurement and Event Detection

Typical gait analysis includes obtaining kinematic parameters (gait velocity, joint angles, angular velocity, and angular acceleration), and kinetics parameters (ground reaction force, centre of pressure, joints moment and torque). Several measurement tools commonly used to obtain these parameters are briefly discussed.

### 2.3.1 Gait Measurement

#### 2.3.1.1 State of the art

##### 1. Force Platform

Force platform is an instrument which measures moments and the total force applied by a body in contact with it. It has been widely used in car crash test, clinical gait analysis and analysis of sports technique [39]. In gait analysis, this total force is referred to as Ground Reaction Force (GRF) i.e. the force exerted by the ground on the body in contact with the platform. The location in which this total force appears to be exerted is called the Centre of Pressure (CoP). GRF is a three-dimensional vector consisting of a vertical force and two shear forces. Figure 2.7 shows an example of a commercial force platform and the force and moment components acting on the platform.  $F_x$ ,  $F_y$  and  $F_z$  refers the anterior-posterior, medio-lateral and vertical components of the GRF, while  $M_x$ ,  $M_y$ , and  $M_z$  signifies the moments around the axes.

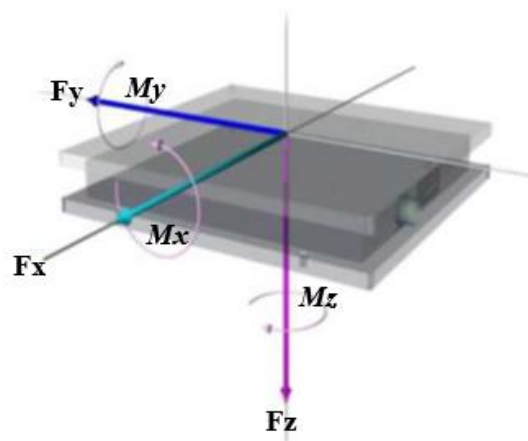


**Figure 2.7** A force platform indicating force and moment vectors in Cartesian coordinate system [39]

The ground reaction forces are typically represented in two ways, either as the magnitude of force components over gait percentage graph or the butterfly or Pedotti diagram which shows combined vertical and horizontal force with respect to the position of the CoP. The former representation is useful in studying the force acting at the foot in three dimensions during walking while the latter has the advantage of showing the direction of the force vector and its point of application through the whole cycle gait. Figure 2.8 shows both representation obtained by force platform measurement.

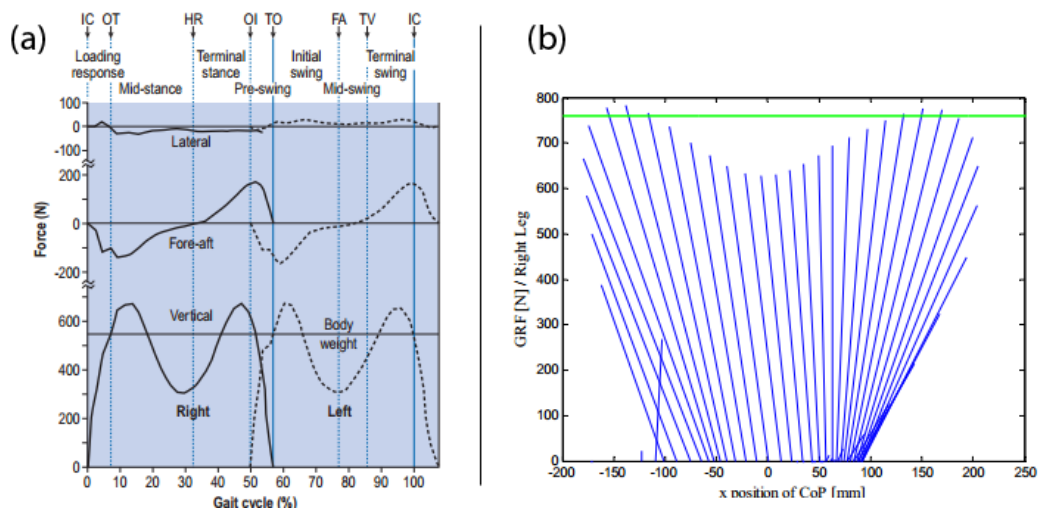


**Figure 2.8 Normal gait shown by (a) Components of GRF [37] and (b) Butterfly diagram [40]**

## 2. Marker Based Motion Capture

In combination with force platform and anthropometric data, marker based motion capture can give valuable information on walking kinematics and kinetics parameters, as well as modelling various human activities. The system normally consists of motion cameras mounted around a calibrated volumetric space, which captures the movement of passive or active reflective markers within the space. Typical motion cameras have infrared LEDs which emit an infrared pulse which are reflected by the marker. Infrared filters are used in the camera lens to pick up these reflections and suppress other background below the specified threshold [41]. The captured data can be viewed in real-time using computer software which maps the marker location and save the data for offline calculation and analysis. Some commercial motion camera analysis vendors are Vicon™ and Qualisys™ which comes with their own proprietary software. However, due to the high cost of

purchasing the software, attempts have been made to develop open source software such as the Biomechanical Toolkit [42]. Figure 2.9 shows an example marker placement on the body for motion capturing and an example of the marker view in the software.



**Figure 2.9 Independent photos showing markers fitted on the body and detected markers viewed in the software [168]**

Challenges with motion camera capture include restricted recording volume and accidental obscuring of the markers, which can result in incomplete data [43].

### **2.3.1.2 Alternative Gait Measurement Methods**

Apart from state-of-the-art gait measurement devices, alternative methods have been presented to allow gait to be studied outside laboratory environment or in the absence of commercial gait measurement technology, by using wearable sensors. Main motivations of using alternative methods for measurement would include lower cost [43, 44], greater measurement volume [43], portability [45] and the ability to have unrestricted movement compared to the conventional system [44]. Inertial Measurement Unit (IMU) was the most commonly found sensors in literature for measurement of kinematics parameters due to its low cost and small size [43, 46-49]. For GRF and CoP measurement, the use of both flexible [46, 50] and rigid [51] force sensors were present in the literature. Table 2.2 summarizes some of the alternative gait measurement methods found in the literature based on commonly used sensor types.

**Table 2.2 Examples of Alternative Wearable Gait Measurement System. GRF= Ground Reaction Force, CoP = Center of Pressure**

<b>Sensor Type</b>	<b>Sensors</b>	<b>No of Sensors</b>	<b>Reference</b>	<b>Location</b>	<b>Parameters Measured</b>	<b>Target</b>	<b>Realtime?</b>
<b>Inertial Sensors</b>	Accelerometer	2	[43]	Frontal and medial shank and thigh	Shank, thigh and knee angle	10 Healthy	No
	Gyroscope	2			Shank, thigh angular velocity and acceleration Knee linear acceleration		
	Accelerometer	1	[46]	Foot	Foot acceleration and rotation	10 Healthy	Yes
	Gyroscope	1				5 Parkinson	
	Accelerometer	1	[47]	Foot, Thigh, Shank	Shank, thigh, foot angular velocity	10 Healthy	Yes
Gyroscope	3			Shank, thigh, foot angular acceleration			
	Gyroscope		[48]	Posterior Shank	Shank angular velocity	7 healthy	No
	Gyroscope	1	[49]		Shank angular velocity	8 Healthy 2 Amputees	Yes
<b>Plantar Force Sensor</b>	Force Sensitive Resistor	4	[46]	Foot	Force distribution under foot	10 Healthy 5 Parkinson	Yes
	Optoelectronics	64	[50]	Foot Insole	GRF, CoP	2 Healthy	Yes
	6 DoF Force Sensor	2	[51]	Foot Insole	GRF, CoP		
<b>Optical</b>	Plastic optical Fibre	1	[52]	Knee	Knee angle	4 Healthy	Yes
	Plastic optical Fibre	1	[53]	Knee	Knee angle	1 Healthy	Yes
<b>Soft Sensor</b>	Elastic Strain Sensor	6	[54]	Hip, knee, ankle joints	Hip, knee, and ankle angle	3 healthy	Yes
	Resistive bend sensor	2	[46]	Back of heel	Ankle angle	10 Healthy 5 Parkinson	
	Flexible Goniometer	1	[55]	Lateral knee	Knee angle	6 Healthy	No

### **2.3.2 Gait Event Detection and Classification**

Gait event detection refers to identification of gait events from the measured gait parameters (kinematics, kinetic or both). Event detection can be useful in two applications. Firstly, the ability to identify gait events and phases allows analysis of gait parameters and assessment of pathological gait. Secondly, identifying the gait events could enable feedback to be delivered to the user in response to the identified gait events and parameters. Table 2.3 shows compilation of studies in gait event detection in the literature that reflects both applications. Gait detection were carried out mainly using IMU [49, 56-63] and plantar force sensing [25, 26, 60, 64-67]. However, some studies also investigated the use of EMG [68] and ultrasonic sensors for event detection [69]. Apart from obtaining gait parameters from event detection [49, 56, 57, 61, 62, 65, 66, 68, 69], some studies also utilized event detection to control stimulations or provide feedback to its wearer [25, 26, 59, 60, 62-64, 67] .



**Table 2.3 Examples of Gait Event Detection Applications in literature.**  
**TFA = Transfemoral Amputee, TTA = Transtibial Amputee**

Reference	Application	Study Population	Detection Method	Detected Gait Events/Phase	Activities	Parameters Used for Detection	Detection Algorithm
[58]	Spinal cord injury (SCI) gait assessment	Healthy SCI	IMU	Toe-off Heel-strike	Level ground walk	Shank angular velocity Foot linear velocity and accelerations	Rule-based
[62]	Navigation system	Healthy	Gyroscope Force Resistive Sensor	Pre-swing, Swing Mid-stance Loading response Terminal stance	Level ground walk	Plantar force Foot angular velocity	Hidden Markov Model
[69]	Gait parameters assessment	Healthy Ankle Impairment	Ultrasonic Sensors	Heel-strike Heel-off Toe-off Mid-swing	Level ground walk	Ultrasonic signal	Local spherical positioning technique
[57]	Gait parameters assessment	Healthy	Accelerometer	Heel-strike	Level ground walk	Foot angular acceleration	Rule-based
[65]	Gait parameters assessment	Healthy Ankle Impairment	Air pressure sensor	Pre-swing Swing Mid-stance Loading response Terminal stance	Level ground walk	Plantar force	Fuzzy logic

**Table 2.3 Examples of Gait Event Detection Applications in literature.**  
**TFA = Transfemoral Amputee, TTA = Transtibial Amputee (Cont.)**

Reference	Application	Study Population	Detection Method	Detected Gait Events/Phase	Activities	Parameters Used for Detection	Detection Algorithm
[49]	Gait parameters assessment	Healthy TTA TFA	Gyroscope	Toe-off heel-strike	Level ground walk Ramp ascend and descend	Shank angular acceleration	Rule-based
[66]	Gait parameters assessment	Healthy	Force Platform	Heel-strike toe-off	Treadmill walking	Centre of Pressure	Rule-based
[68]	Gait Prediction	Cerebral Palsy	Electromyography	Heel-strike Mid, terminal stance Pre, initial, mid and terminal swing	Level ground walk	EMG from leg muscle	Fuzzy neural-networks
[56]	Spatio-temporal gait parameters	Healthy Osteoarthritis	Gyroscope	Toe-off heel-strike	Level ground walk	Shank and thigh angular velocity	Wavelet analysis
[26]	Sensory feedback	TTA	Force sensitive resistors	All stance events	Level ground walk	Plantar force	Threshold-based
[25]	Sensory feedback	Healthy	Optoelectronics sensors	Toe-off, foot-flat, heel-strike	Treadmill walking	Ground reaction force	Threshold-based
[64]	FES control	Healthy	Force sensitive resistors	Custom gait phases	Level ground walk	Plantar force	Machine Learning

**Table 2.3 Examples of Gait Event Detection Applications in literature.**  
**TFA = Transfemoral Amputee, TTA = Transtibial Amputee (Cont.)**

Reference	Application	Study Population	Detection Method	Detected Gait Events/Phase	Activities	Parameters Used for Detection	Detection Algorithm
[67]	Functional Electrical Stimulation (FES) control	Paraplegic	Force sensitive resistors	Toe-off foot-flat heel-strike heel-off	Level ground walk	Plantar force	Fuzzy Logic Rule-Based
[63]	FES control	Healthy	Accelerometer	Pre-swing Swing Mid-stance Loading response Terminal stance	Level ground walk in figure-8 path	Shank angular acceleration	Rule-based Rough Sets and Adaptive Logic Networks
[60]	Neuro-prostheses control	Healthy Impaired gait (multiple cause)	Gyroscope Force sensitive resistors	Stance heel-off swing heel-strike	Walking on flat, irregular, inclined surface Stair ascend and descend	Foot angular velocity	Rule-based state-machine
[59]	Control of drop foot stimulator	Stroke	IMU	heel-off heel-down	Multiple surface walking, stairs ascend and descend	shank angular velocity and acceleration	Rule-based

## 2.4 Lower Limb Amputation

Between 1 April 2007 and 31 March 2010, 34,109 lower limb amputations (major and minor) took place in 151 hospitals across England [70]. The common causes to amputation are peripheral vascular disease, trauma, tumors, infections, and congenital limb deficiency. Figure 2.10 shows various levels of amputation for lower limb. Major lower limb amputations are those performed above ankle while minor amputation refers to amputation below the ankle [70]. Major amputation can be either transtibial which refers to below the knee amputation or transfemoral which is the above the knee amputation. National Amputee Statistical Database UK (NASDAB) indicated in a report in 2002 that 9 out of 10 lower limb amputation were either transtibial (50%) or transfemoral (40%) [71].

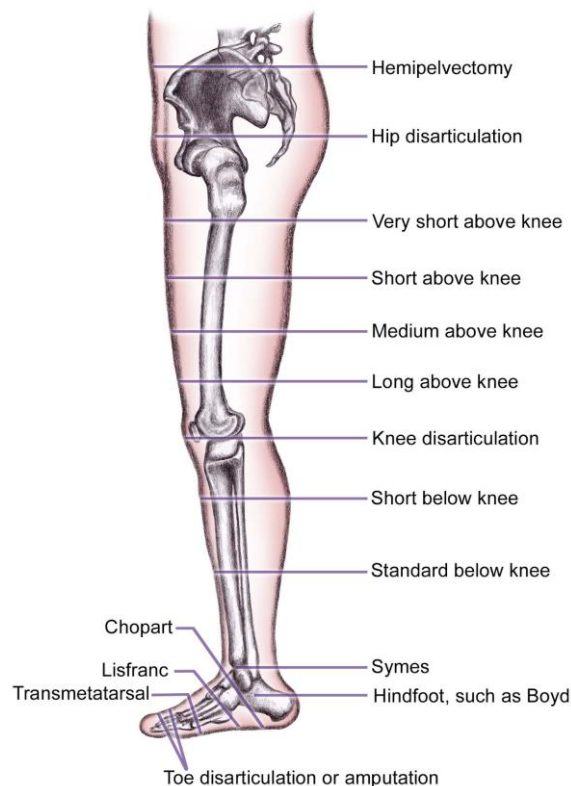


**Figure 2.10 Levels of lower limb amputation [72]**

### 2.4.1 Lower Limb Prostheses

Post amputation, amputees will undergo series of rehabilitation procedures. One of the biggest milestones in the rehabilitation process is the prescription of prosthetic legs. A prosthetic leg acts as the interface between the residual limb and the ground

and is ideally expected to emulate the behaviour of an anatomical foot. However, this emulation means having perfect integration of anatomical qualities such as shock absorption, balancing, and cosmetic appearance. Apart from mechanically sound and reasonable maintenance requirement, an ideal prosthesis must provide comfort, easy fitting and removal, portability, durability and acceptable appearance. These facts however, do not necessarily guarantee successful prosthesis training, as it highly depends on the motivation of the amputees themselves [72]. Lower limb prosthesis typically consists of socket and its interface, suspension system, necessary joint components, a shank (pylon) and a prosthetic foot. Figure 2.11 shows typical components of a prosthetic leg. Additional details regarding the prosthetic components can be referred to Appendix B.1.



**Figure 2.11 Prosthetic leg components**

### 2.4.2 Amputation Effects

Although prosthesis helps in restoring ambulation function, amputees commonly exhibit suboptimal gait performance due to the spatiotemporal gait asymmetries [78]. These effects include gait deviations, increased energy expenditure, impairment to the sensory system, as well as decrease in balance control.

### **2.4.2.1 Gait Deviations**

Figure 2.12 shows some of the most common gait abnormalities. This section will describe common pathological gait for amputees in both stance and swing phases.

#### **1. Lateral Trunk Bending**

Most prevalent gait abnormality in transfemoral amputees is lateral trunk bending towards the amputated side while in stance phase [79]. This can be caused by weak hip abductors or excessively short prosthesis.

#### **2. Abducted gait**

An amputee tends to abduct his prosthesis during the double support period if discomfort is experienced in the crotch area or if the prosthetic brim is causing pain. This results in abducted gait in which wider walking base is observed compared to normal gait. Similarly, if the prosthesis is too long, widening base is adopted to increase area of support. Apart from prosthesis problem, wider base can also be caused by fear of pain or insecurity such that an amputee tries to compensate them by widening his walking base [79].

#### **3. Vaulting**

While swinging the prosthetic limb, an amputee can vault by going up on the toe of the sound limb to raise his hip. Vaulting increases energy expenditure and can be the result of excessive length of prosthesis, since the amputee needs additional time to maintain ground clearance while swinging the prosthetic limb. Vaulting can also happen as a result of insecurity, since reduced proprioception forces an amputee to vault to ensure prosthesis clearance [79].

#### **4. Circumduction**

In normal gait, the limbs swing linear to body midline. However, if a prosthesis travels laterally in a curve line instead of linear during swing period, this is known as circumduction. This is basically caused by excessive prosthetic length due to improper fitting, excessive knee friction, or insecurity [79].

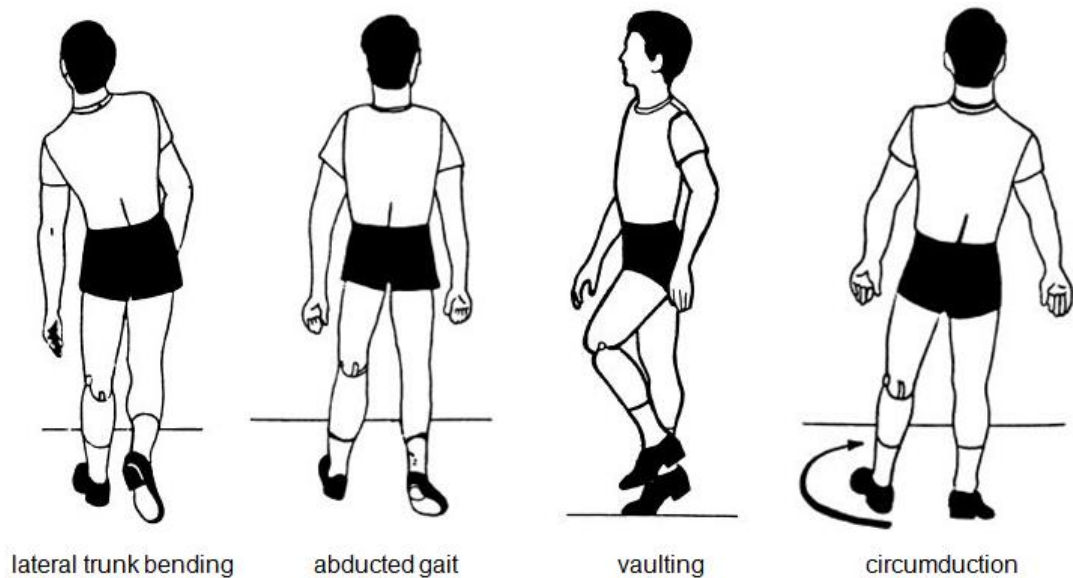


**Figure 2.12 Sketch of several gait abnormalities for transfemoral amputees [79]**

Abducted gait, vaulting and circumduction are common deviations for transfemoral amputees (TFA), although sometimes occurs for transtibial amputees (TTA). In a study carried out with TFA, Jaegers et al. [80] summarized these following gait characteristics observed from the amputee gait:

- Lower comfortable walking speed compared to normal subjects
- Larger stride width compared to normal subjects.
- Longer time spent on intact leg than prosthetic side. Also, the double limb support phase for intact and sound leg is not the same.
- The intact knee remained at flexion throughout stance phase.

#### **2.4.2.2 Increased Energy Expenditure**

It is generally agreed that the metabolic cost or energy expenditure of the amputees during walking is higher than non-amputees [81]. Kishner [5] reported that compared to normal person, amputee can exhibit at least the following increase in energy expenditure:

- 25% for traumatic TTA
- 40% for vascular TTA
- 68% for traumatic TFA
- 100% for vascular TFA

The increase in the energy expenditure can be attributed to a number of factors. Amputation level was shown to directly correlate with the energy expenditure, with

higher level of amputation resulting higher energy expenditure [82, 83]. Schmalz et al. [84] reported significant increase in energy expenditure for TFA (~13%) when prosthetic knee alignment was not optimized. In addition, the author stated that using mechanical knee increases energy expenditure in comparison to using microprocessor knee which allows automated control of resistance and damping parameters. Similar finding was noted by Taylor et al. [85] where using mechanically damped knee showed significantly higher energy expenditure at faster walking speed (> 3.2 km/h). It is clear from the literature that amputees suffer from increased energy expenditure despite the optimization of the prosthesis device, especially with the TFA.

#### **2.4.2.3 Effects to Sensory System**

Among the most common pain after lower limb amputation is the result of a phenomenon called phantom limb pain which is defined as pain perceived to be emanating from the missing part of the limb. The phantom limb pain is considered to be neuropathic (pain resulting from problems with the signal from the nerve) and assumed to be connected to damage of central and peripheral neurons [86]. It was estimated that around 85% of persons undergoing limb amputation will experience this effect [87] and that the pain has been proven to have effect on the health-related quality of life [88]. In addition, amputation has also been shown to cause sensory deficit not only in the amputated leg, but also in the non-amputated leg, especially for amputations caused by trauma [89]. Partial limb loss due to amputation also cause loss of proprioception, or the sense of awareness of the limb position in space. Isakov et al. [90] described an experiment where below-knee amputees' upright stability was measured in eyes open and eyes closed condition and demonstrated that in comparison to control (healthy) group, the amputees exhibited less stability. The authors concluded that this was due to the proprioceptive deficit caused by loss of limb post amputation.

#### **2.4.2.4 Reduced Balance Control and Risk of Falling**

A study by Miller et al. [9] indicated that persons with lower limb amputation have low balance confidence, especially those suffering from vascular amputation. Following lower limb amputation, an amputee develops compensatory strategies for balance control. For example, TTAs compensate the loss of ankle joint by increasing



movements and loading in the non-affected limb. However, the ability to cope with balance perturbations are still limited [91]. The lack of balance for amputee is a serious functional deterioration because it can increase the risk of falling. In another study by Miller et al. [11], it was found that among the people with lower limb amputation living in the community, 52.4% reported falling in the past 12 months, whereas 49.2% reported fear of falling. The authors reported that transfemoral amputation was identified as the highest risk factors for falling, followed by back and joint pain. The loss of sensorimotor also increases the risk of falling due to lack of response from the amputated limb following external perturbation [92]. Barnett et al. [93] conducted balance assessment of amputee's balance within 6 months after being discharged from inpatient rehabilitation and found out that although balance strategy improved over time, the amputees were still heavily reliant on vision to maintain balance. This is in line with findings by Fernie et al. [94], which noted increased dependence on vision for both below knee and above knee amputees post amputation.

Advancements in the field of prosthetics have seen the emergence of advanced prosthetic components and cutting-edge surgical technologies which attempts to improve the outcome of the prosthetics use (details in Appendix B.2). Despite this fact, an amputee may still experience lack of confidence during locomotion due to the fact that the sensory system that provides feedback and proprioception information was lost. Ku et al. [99] in their review mentioned several studies establishing the fact that loss of somatosensory as one of the main factors for reduced static balance control ability of lower limb amputees. One proposed solution to this problem is to enable the amputee to experience feedback from the worn prostheses to compensate their sensory loss [16]. In addition, providing feedback can also increase the sense of embodiment of the prosthesis to the user [100]. Sensory feedback can be delivered via mechanical feedback such as tactile, vibration, or force feedback. These feedbacks which apply direct sense of touch or contact with the limb, are also referred to as haptic feedback and are discussed in the next section.

## **2.5 Haptic Feedback**

The word haptic or haptics refers to sensing natural or synthetic mechanical environment through touch. Haptic feedback is the recreation of the sense of touch by applying forces, vibrations, or motions to the user [101]. Human haptic combines

the perception of touch from somatosensory system with proprioception (perception of limb position in space). To further discuss on the haptic feedback system, an introduction to human sensory system is discussed as follows.

### 2.5.1 Somatosensory System

Haptic system works based on the sensory information derived from mechanoreceptors and thermal receptors embedded in the skin (cutaneous input) together with mechanoreceptors embedded in muscle and joints (kinaesthetic input) [102]. These receptors work by translating environmental stimulus into an electrical signal that is transmitted to the central nervous system. Cutaneous receptors can be found throughout body surface, beneath hairy and hairless (glabrous) skin. All cutaneous receptors are stimulated by physical deformation of the receptor itself or its surrounding area. Main cutaneous receptors are the Ruffini ending, Pacinian corpuscles, Meissner corpuscles, and Merkel disks (Figure 2.13). The distribution of these receptors in the body depends on the level of sensation needed in the respective parts of the body. Mechanoreceptors are classified according to the size of the receptive field and its adaptation rate. Small receptive field is classified as type I, while large receptive field as type II. Fast adapting (FA) receptors has no response to sustained pressure, only to changes in pressure (either an increase or a decrease) while slow adapting (SA) receptors respond continuously to sustained stimuli [103].

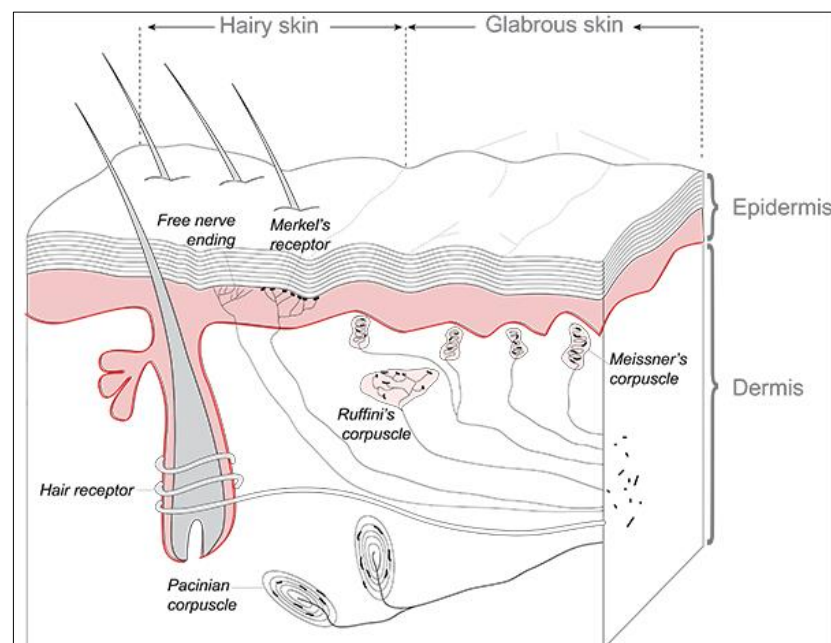


**Figure 2.13** Mechanoreceptors' location and structure from [104]

It was established that FA I is associated with Meissner corpuscles, SA I with the Merkel disks, SA II with Ruffini organs and the FA II with Pacinian corpuscles. In addition to these receptors, hairy skin has hair follicle that detects movement on skin surface [103]. Table 2.4 shows the classification of mechanoreceptor types and their associated features.

**Table 2.4 Classification of mechanoreceptors and associated features, adapted from [102] and [105]**

Features	Meissner Corpuscles	Pacinian Corpuscles	Merkel's Disks	Ruffini Endings
Adaption Rate	Fast	Fast	Slow	Slow
Type	FA I	FA II	SA I	SA II
Distribution	43%	13%	25%	19%
Receptive field	Small	Large	Small	Large
Location	Superficial	Deep	Superficial	Deep
Innervation density	High, variable	Low, constant	High, variable	Low, constant
Sensed parameters	Skin-stretch, local shape, flutter, slip	vibration, acceleration	Skin curvature,	Directional skin-stretch, force
Response frequency range	100-200 Hz	50-1000 HZ	0-100 Hz	0-15 Hz

## 2.5.2 Haptic Feedback Modality

Haptic feedback can be presented in various modalities to the user, the most common being mechano-tactile (in the form of force or pressure), vibrotactile (vibration) and skin-stretch. In addition, non-mechanical feedback such as electro-tactile was also present in the literature for conveying haptic feedback to the user.

### 1. Force and pressure feedback

This type of feedback, commonly found in entertainment and rehabilitation devices, relays haptic feedback to the user in the form of physical force or pressure. Typical mechanical actuation for mechano-tactile feedback are DC motor and pneumatic devices. However, apparent sense of force feedback can also be created by using electrical stimulation. Electrical stimulation delivered at skin surface induces involuntary muscle contraction and in effect creates force feedback perception when

the user tries to counter this motion [106]. Kim et al. [18] described the incorporation of haptic feedback system comprising touch, pressure, shear, and temperature sensation in upper limb targeted reinnervation (TR) amputees. Although the authors mentioned that delivery of simultaneous haptic sensation (i.e shear and pressure) reduces grip control performance, significant enhancement of grip control force was recorded for single haptic sensation (either shear or pressure). Force feedback has been suggested as a mean to improve efficiency in tele-operated surgery since it can help reduce force applied by the robotic hand [107], and lowering the risk of tissue damages [108]. Force feedback is especially useful in active haptic exploration, since it enhances realization of an environment to an active user.

## **2. Electrotactile feedback**

Electrotactile feedback induces touch sensation by passing current through the skin by means of surface or subcutaneous electrodes [27]. The stimulation can trigger tingle, itch, vibration, buzz, touch, pressure, pinch, and sharp and burning pain sensation, depending on the electrode properties and location and condition of the skin [27]. Altinsoy et al. [109] developed an electrotactile display for handheld devices that can give perception of texture (i.e roughness) at user's fingertip by varying the current and the pulse frequency. The use of electrotactile feedback, however, may cause some irritation to the user. The electrode contacts on the skin may cause burns and discomfort to the user in long term use while the use of cutaneous electrodes require invasive surgery which further limits its application for wider population target [27].

## **3. Vibrotactile feedback**

The most commonly used feedback modality found in literature was the vibrotactile feedback. In common application, a vibrotactile actuators (vibrotactors) is fixed such that it vibrates in the plane normal to the skin. Figure 2.14 shows two types of vibrotactors commonly used in the literatures. The C2 tactor is a voice-coil-type linear actuator while the Tactaid VBW32 tactor is an electromagnetic inertial transducer.

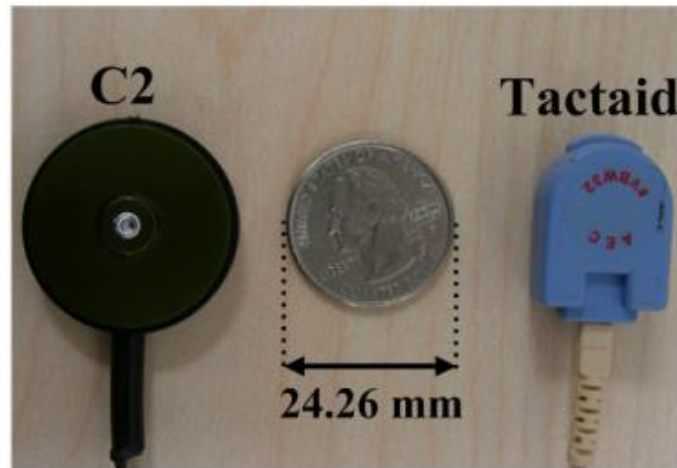


**Figure 2.14 C2 and Tactaid vibrotactors from [68]**

Vibrotactile actuators have been determined to work best at 250 Hz spatial resolution [110], which is ideal vibration sensing range for human somatosensory system [111]. Vibration at this frequency stimulates the Fast Adapting Type II Pacinian corpuscle receptors [112]. Brown et al. [113] studied the effect of adding force feedback and vibrotactile feedback to an EMG controlled hand gripper (Figure 2.15(a)). The authors mentioned significant improvement for grasp and lift task with feedback compared to without feedback, suggesting potential utility of haptic feedback for amputees wearing active prostheses. Walker et al. [17] carried out a study of grasp and hold task using virtual environment setup. They reported that adding vibrotactile feedback allowed the participants to reduce slipping of the virtual object in the absence of visual feedback from the virtual environment (Figure 2.15(b)).

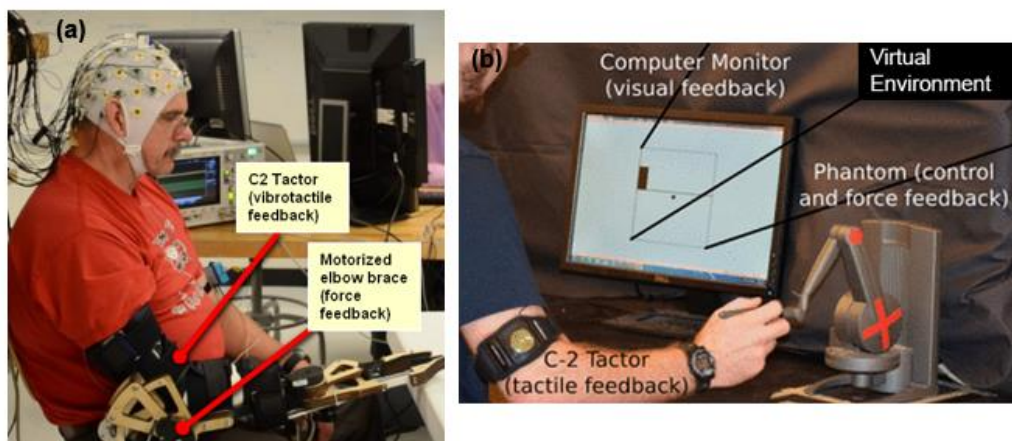


**Figure 2.15 Experimental setup in (a) [113] and (b) [17]**

Marasco et al. [100] described an experiment where a load cell was fixed on a prosthetic hand and a vibrotactile sensor placed at the reinnervated skin of the amputee's hand. Upon touching the load cell, the vibrotactor will press into the reinnervated skin (Figure 2.16) to give an illusion of touching the amputee's own hand. The authors mentioned that the haptic feedback managed to establish sense of embodiment of the prosthesis to the user.

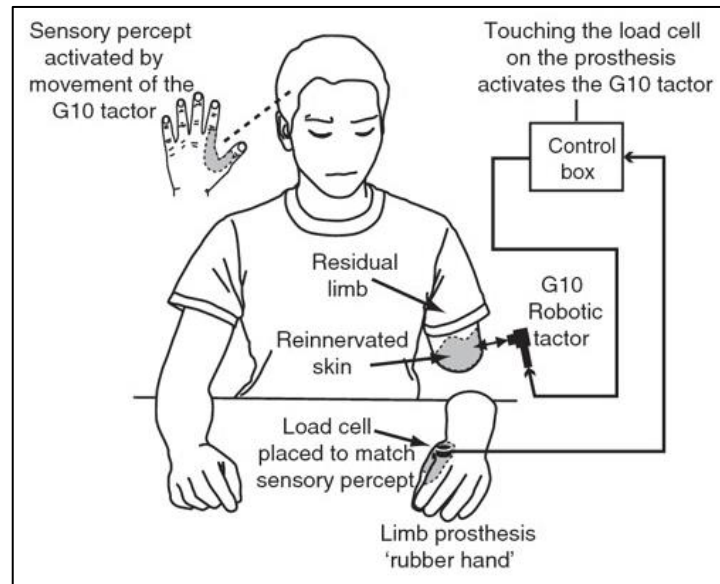


**Figure 2.16 Embodiment illusion via vibrotactile feedback on reinnervated skin in [100]**

Despite being used in many applications, vibrotactile feedback may be subject to habituation or adaptation. A study carried out by Chelette et al. [114] reported that vibrotactile haptic feedback fixed at knee joint for learning task positioning were effectively ignored by the subjects during movement, possibly down weighted by motor sensory system. Adaptation effect reduces viability for long period use of the haptic system.

#### **4. Skin-stretch Feedback**

A search of the literature showed that skin-stretch was used initially as a feedback for glabrous (non-hairy) skin, especially the fingertip. Pasquero et al. [115] reported development of such system dubbed STRESS, which consists of 100 ( $10 \times 10$ ) laterally moving piezoelectric skin contactors packed in  $1 \text{ cm}^2$  area used to give meaningful sensation to the skin (Figure 2.17).

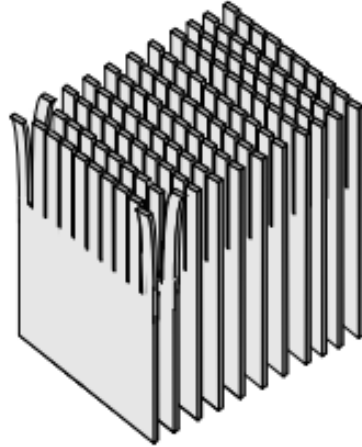


**Figure 2.17 1 cm<sup>2</sup> piezoelectric sensors for giving stretch feedback at fingertip mentioned in [115]**

Similar studies have shown that applying skin-stretch feedback at fingertip was able to give perception of friction [116], create illusion of surface geometry [117], and give directional cue for navigational aid [118]. Apart from glabrous skin, several studies were carried out to apply skin-stretch feedback at hairy skin. Ion et al. [34] designed a wearable skin-stretch device intended to convey geometric shapes or characters and compared it to a vibration based device for similar purpose. The authors reported that the users could identify conveyed information significantly better using skin-stretch modality. Bark et al. [28] conducted an experiment to compare effectiveness of vibrotactile and skin-stretch feedback in providing proprioceptive information. The authors reported that skin-stretch provided superior results to vibratory feedback in conveying the proprioceptive information. Similar study was conducted by Wheeler et al. [29], using a wearable rotational skin-stretch device. The authors fixed a rotational skin-stretch feedback on able-bodied subjects' arm. The outcome of the experimental trial with able-bodied subjects indicated feasibility of rotational skin-stretch to provide proprioceptive feedback in prosthesis limbs. In addition, they mentioned that skin-stretch feedback has the advantage of higher analog resolution compared to vibrotactile feedback, and since it stimulates the superficial small receptive field mechanoreceptors, it can be placed closely to each other in case multiple feedback devices need to be used. In another work, Caswell et al. [31] conducted a study using skin-stretch device for conveying directional cues (north, east, south, west) on the hairy part of the forearm and reported 95% accuracy responses from the participants for a skin displacement of 2.0 mm.

The authors noted that although more skin displacement was needed on the hairy skin compared to the palm, the placement on hairy skin allows greater flexibility and allows the hand to be used freely without any hindrance.

## 5. Multimodal Feedback

In extension to single haptic modality, attempts have been made to combine haptic modalities for haptic feedback improvement. Bau et al. [119] demonstrated an electrovibration touch surface named TeslaTouch (Figure 2.18(a)) that can give wide range of tactile feedback to fingers moving across the surface by controlling the electrostatic friction between the surface and the user's fingers. Combined with an interactive display, the user could feel virtual elements via touch. D'alonzo et al. [120, 121] presented a hybrid vibro-electrotactile interface named HyVE (Figure 2.18(b)) which provides simultaneous electrical and vibrational tactile sensation, creating dual modality sensory feedback at the contact site. The preliminary tests suggested the interface is feasible to be integrated into prosthetic devices for the purpose of relaying haptic feedback to prosthetic users. Gwilliam et al. [122] developed a joystick combining force feedback and fingertip skin-stretch feedback and reported improved accuracy and precision in directional matching task.

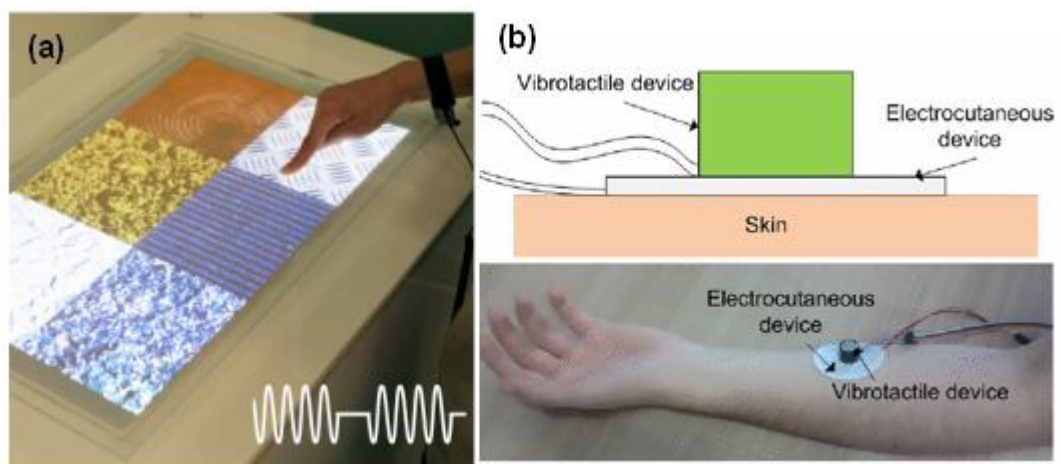


**Figure 2.18 (a) TeslaTouch surface allows user to feel different textures via friction manipulation [119] and (b) HyVE interface [123]**

### 2.5.3 Lower Limb Haptic Feedback Literature

While research in sensory feedback for upper limb is well developed, similar progress is not achieved for lower limb. For example, intuitive prosthesis control such as targeted innervation has been achieved for upper limb amputees while the same



procedure is still at early phases for lower limb amputees [124]. This section will review the applications of haptic feedback in lower limb rehabilitation, with attention to lower limb amputation.

### **1. Postural stability and balance control**

Several studies proved the viability of haptic feedback to improve postural control. Gopalai et al. [125] used vibrotactile feedback fixed at subject's waist while the subject was standing on a wobble board (Figure 2.19), a platform used to create uneven standing surface. Subjects were to respond to the perturbation and maintain the balance on the board. The result indicated improvement in postural control with vibrotactile feedback compared to the absence of feedback. At least three studies described the effect of vibrotactile feedback in improving postural and balance control for patients having vestibular disease. Honegger et al. [111] reported reduction in patients' sway during stance phase. Sienko et al. [126] reported significant decrease in medial lateral trunk sway during locomotion activities while Horak et al. [127] reported immediate improvement in patients' postural stability during tandem gait.

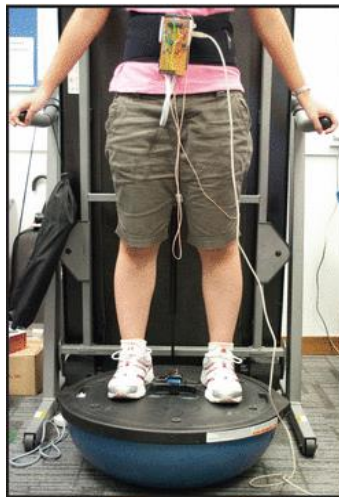


**Figure 2.19 Subject wearing a vibrotactile feedback system standing on a wobble board [125]**

## 2. Rehabilitation

McKinney et al. [128] conducted a pilot test using pneumatic controlled tactile feedback system for peripheral neuropathy (PN) patients (Figure 2.20). The authors reported that improvement of gait in real time was observed especially increase in walking speed, step cadence, step length, and peak joint powers.

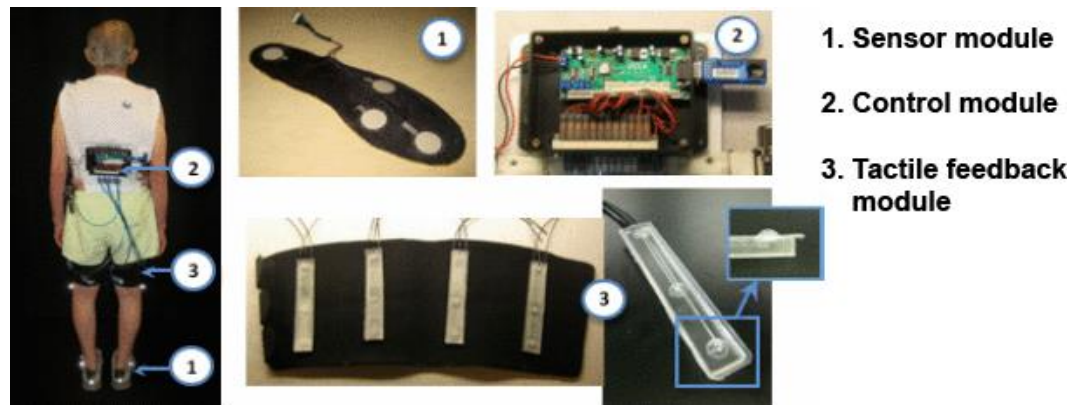


**Figure 2.20** Pneumatic tactile feedback for PN subjects. Adapted from [128]

Several force feedback haptic devices have been developed to improve medical rehabilitation. One of them was the Rutgers's Ankle, developed from a six degree of freedom robotic platform called Stewart Platform (Figure 2.21). The Rutgers's ankle incorporates force feedback haptic interface on top of the platform to be used in ankle tele-rehabilitation [129].

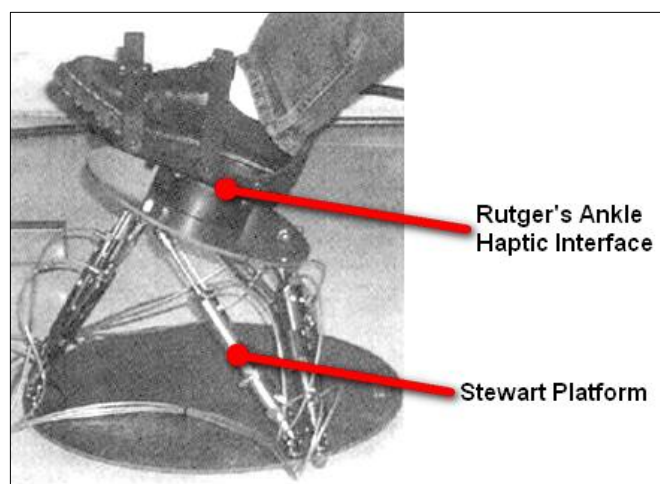


**Figure 2.21** Rutgers's Ankle Force Feedback System. Modified from [129]

### 3. Lower Limb Prosthetic Wearer

Among the earliest work in this field was by Sabolich and Giovani [20], which studied the effect of transcutaneous electrical stimulation on amputees' gait. The electrodes were placed on the stump and electrical stimulation was provided in response to the pressure distribution measured at the plantar surface of the prosthetic foot. The outcome of the study which was conducted with 12 transfemoral and 12 transtibial amputees suggested an improvement in gait parameters such as weight distribution symmetry, standing balance and step length. Lee et al. [21] demonstrated the effect of sub-sensory electrical stimulation in combination with auditory-visual feedback in enhancing balance control for trans-tibial amputees. The subjects were tested for static single leg quiet standing and dynamic ambulation on treadmill while continuously being subjected to sub-sensory electrical stimulation and auditory-visual cues. The authors mentioned that sub-sensory electrical feedback was shown to increase the static balance performance while the auditory-visual increased dynamic balance performance of the amputee subjects.

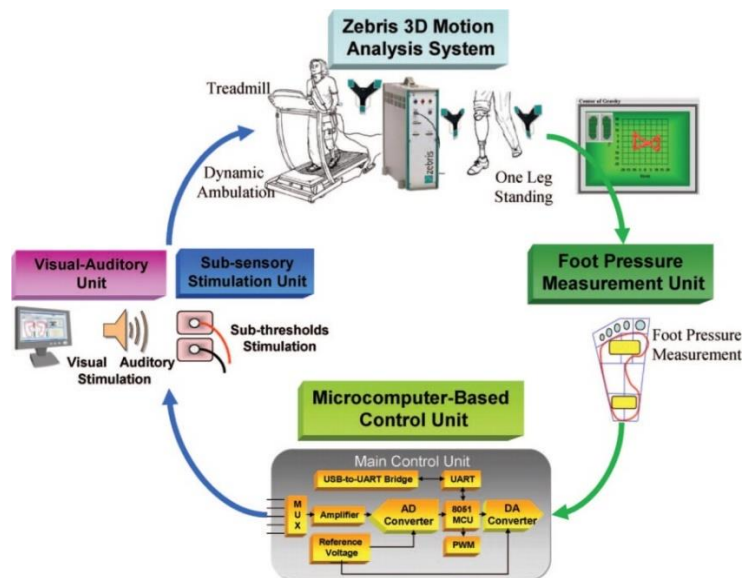


**Figure 2.22 Feedback system strategy used in [102]**

Rusaw et al. [22] reported improvement of postural stability and response time to perturbation for 24 TTA subjected to vibratory feedback while standing on a moveable platform. Marayong et al. [24] investigated feasibility of providing vibrotactile feedback during swing phase with a TTA. Rather than placing the feedback on the skin, a solenoid and a vibration motor were fitted at the prosthetic

pylon to transfer vibration to the stump during swing phase. The authors mentioned that the participant can identify different types of vibration created by the two actuators, which can be useful in rehabilitation post prosthetic fitting. Crea et al. [25] investigated the use of vibrotactile actuators at thigh intended to convey gait phase transition information for lower limb prosthetic wearers. Rather than continuously stimulating the thigh, a time-discrete feedback method was used and experiment with healthy subject indicated high ability to perceive the feedback during walking. The experiment, however, was carried out on a controlled walking speed of 2 km/h, which is a slow walking speed for an average person. Another study concerned with conveying gait information to lower limb amputees via haptic feedback was of Fan et al. [16, 26, 130] which proposed a wearable pneumatic actuated balloon based tactile haptic feedback system. The actuators were cast out of a PDMS base material with a thin-film silicone membrane, fitted into neoprene cuff, to be worn on residual limb of TTAs (Figure 2.23).



**Figure 2.23 Neoprene cuff fitted with pneumatic driven silicone balloon actuator [16]**

Fan in [16] argued that the tactile feedback provided by the balloon inflation stimulates the Slow Adapting Type II (SA II) receptors which are more preferable in the lower limb since SA II receptors dominate in the hairy skin. The system is complemented by an insole fitted with piezoresistive force sensor aimed to provide a cue for gait events, acting like a pseudo ‘sensory path’ to the amputee. Trials were carried out with healthy subjects [16] and one amputee [26]. In trials with both groups, subjects were asked to determine different inflation levels, determine sequence of inflation pattern (sequential), and localize single or combined stimuli (directional). The results showed slightly lower accuracy for sequential and

directional test for amputee than to healthy subjects. However, in both groups (healthy and amputee), an overall accuracy of  $> 90\%$  of the tactile stimulation perceived demonstrated viability for improving gait rehabilitation outcome such as gait and balance performance. The authors mentioned possible error from cuff fitting that was not customized for stump shape which may reduce optimal skin contact. Also, the trial was conducted only with TTA possibly to eliminate the effect of various possible knee types in transfemoral prostheses.

## 2.6 Gap of Knowledge

Although severed nerve of an amputated limb has shown reduction in the nerve action potential, impulse speed and impulse conducting ability, the reflex pathway is well maintained [131]. Despite existence of a wide variety of lower limb prostheses in the market, only a few provide sensory feedback [19]. However, it was established that loss of sensory feedback contributes to impaired gait, balance problem and prolonged rehabilitation [19]. Apart from very limited studies to convey gait information to lower limb prosthetic wearers [20, 23, 25, 26], haptic feedback for lower limb has only been employed to assist stroke, vestibular disease and peripheral neuropathy patients. Skin-stretch feedback has been suggested as an effective method for providing stimuli on the hairy skin, specifically skin-stretch applied in tangential/lateral direction [132]. One advantage is that skin-stretch as small as 2.0 mm can be perceived on the hairy skin [31], making it a preferable choice for designing wearable devices. In addition, since skin-stretch targets slow adapting receptors, continuous stimulus is not required, and the desensitization effect shown by stimuli like vibration can be prevented [33]. However, the use of skin-stretch feedback in literature was very limited, and has been studied so far for conveying geometry and shape information [34], positional cues [28, 29], and directional cues [30-32]. Despite the advantage of this haptic modality, no description of a wearable lateral skin-stretch device can be found in the literature for conveying gait event information to its user. Therefore, investigation into user's perception to skin-stretch feedback in a robust and dynamic environment such as walking has never been investigated before. One potential reason for this is that in comparison to providing directional and positional cues, a skin-stretch device for use in gait application is time dependent, and therefore needs to be able to deliver feedback in short period of time.

---

The design of such system is absent in the literature and will serve as the basis of this research.

## **2.7 Summary**

This chapter reviewed literatures regarding human lower limb and locomotion and the effects of amputation to the walking gait. Since feedback is a common item that is lacking in current prostheses, the topic of haptic feedback was reviewed to gather information on the work done in this field, especially concerning the rehabilitation or gait improvement of lower limb amputees. The survey of literature indicated very little research in haptic feedback for lower limb amputees, and revealed skin-stretch as a potential haptic modality that can be manipulated as a feedback mechanism. The review of gait event detection methods served as a complement to the feedback system, allowing design of a feedback scheme comprising gait event detection and haptic feedback. The gaps of knowledge in the literatures were summarized to obtain insights on possible new contributions of this research.

## **CHAPTER 3:**

# **Haptic Feedback Module Development and Design Iterations**

### **3.1 Introduction**

This chapter presents the development of the skin-stretch haptic feedback module. A preliminary design and experimental work with a focus group will initially be presented. The chapter then proceeds with the description of an iterative design process, including actuator selection, mechanism and electronics design. To assess the design performance, characterization of the design parameters are described. The experimental work to assess the haptic module design, in combination with the event detection system is discussed in Chapter 5 of the thesis, while the system evaluation with an above-knee amputee is presented in Appendix A.

### **3.2 Preliminary Design**

The initial design considers the design of a wearable module with elementary mechanism to provide skin-stretch stimuli.

#### **3.2.1 Design Consideration**

Several design criteria and restrictions considered for the preliminary system design as follows:

- **Mobility**

Ideally the system must be completely mobile and untethered. This can be achieved by using wireless communication system such as Radio Frequency (RF) and Bluetooth.

- **Weight and Size**

The system should not add significant weight that can cause fatigue or modification of gait during locomotion. A weight of around 300g is considered for the system [133]. Since the haptic device should be wrapped around the limb or body, it should allow flexibility to accommodate different sizes of the attachment site.

- **Speed**

For a quasi-real-time stimulation of the feedback device to the skin, a responsive system is needed. According to the data from work carried out by Öberg et al. [102], normal walking stride frequency is about 1 Hz which means that the stance phase (60% of gait cycle) last for only about 600 ms and swing phase lasts for 400 ms. The system must then be able to give multiple feedback sensation within the stance duration during the gait cycle.

- **Comfort**

To ensure safety and comfort, the device must be safe when wrapped around the limb, and does not have pressure points which will irritate the skin. Also, it should be comfortable for long-time use, considering amputees who are wearing the prosthetics all day.

### 3.2.2 Initial Design Concept

The skin-stretch stimuli works by manipulating the elastic properties of the skin. In non-glabrous (hairy) skin, three types of stretch can be conveyed as described in the literature. A lateral or tangential skin-stretch works by applying normal and shear force to the skin, a rotational skin-stretch applies a combination of tensile and shear [30] on the skin surface, and spatio-temporal stretch stretches the skin whilst moving along the skin surface. Figure 3.1 shows the depiction of the different possible stretch mechanisms.

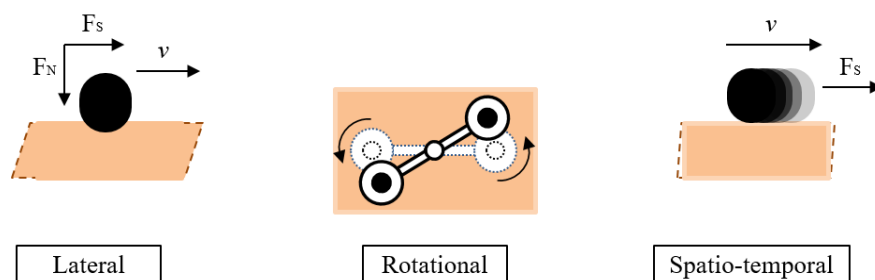


**Figure 3.1 Mechanisms for skin-stretch haptic.  $F_s$ = stretch force,  $F_N$  = Normal force,  $v$  = velocity direction**



The initial design focused on the haptic module around the lower limb, specifically around the thigh area. To apply lateral skin-stretch, a combination of methodology presented in [16] where modules were separated into anterior, posterior, medial and lateral quadrants of the limb, and methodology in [115], where multiple contact points exists in single modules, were adopted. Figure 3.2 shows the intended design scheme.

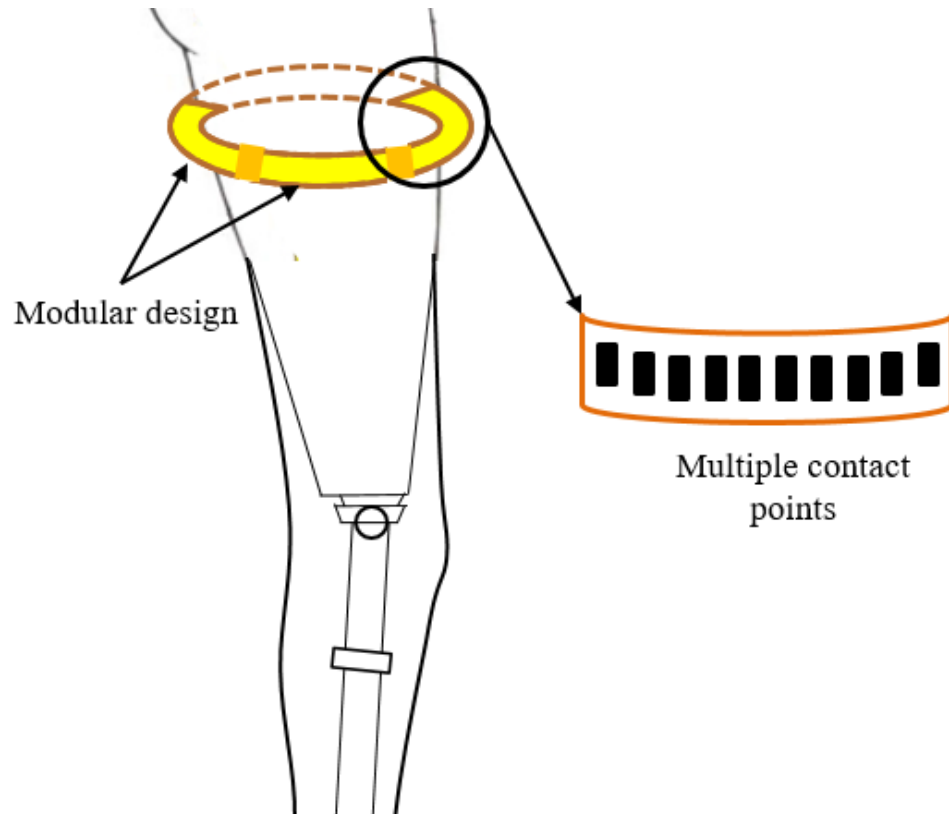


**Figure 3.2 Modular-multiple-contacts design concept**

### 3.2.3 Skin-stretch Mechanism

An elementary mechanism using a DC motor and a timing belt were designed for the preliminary system. To simulate multiple contact points, a small cogged V-belt, which has grooved shape was used as the haptic contact. The belt was flexed into a curvature and attached on its two ends to two pulleys, with the grooved side facing outward. On one end, the pulley was connected to a DC motor, which allows limited rotation. On the other end, the pulley was fixed such that the rotation of the motor will extend the belt which was already in contact with the skin, hence stretching it. Figure 3.3 shows the working principle of the mechanism.

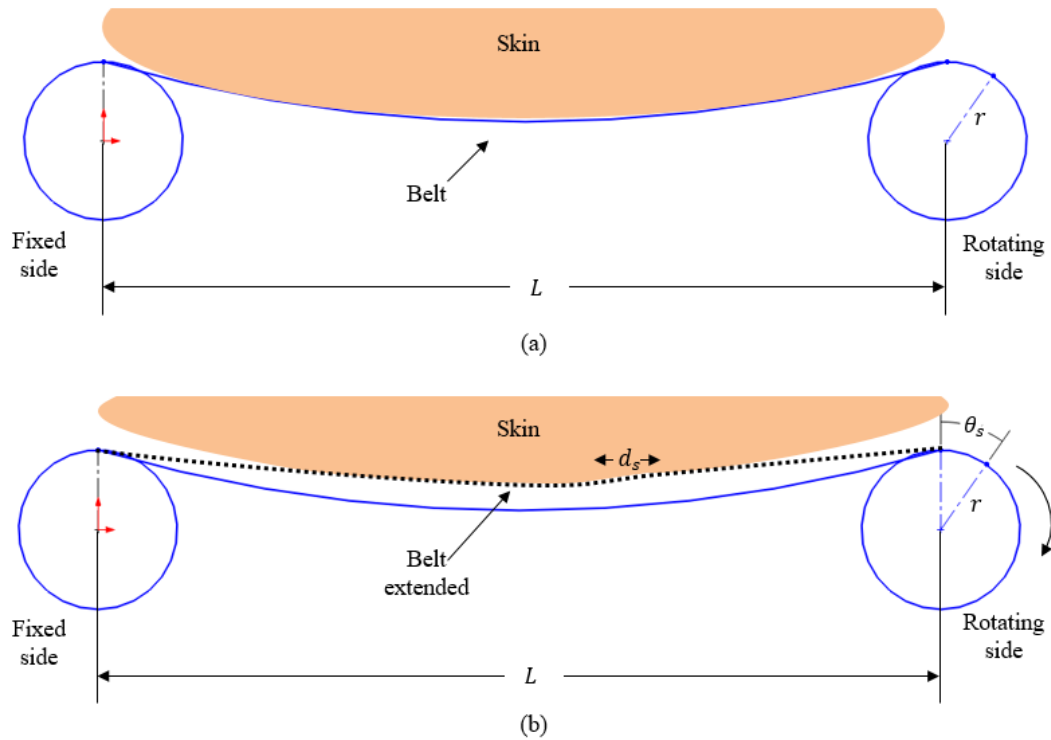


**Figure 3.3 Working principle of the mechanism. (a) the module in inactive state, the belt contacts the skin. (b) Rotation of the motor causes the belt to extend and stretches the skin.**

Let  $r$  equals the radius of the rotating pulley and  $L$  is the fixed distance between the two pulleys. At any rotation angle of  $\theta_s$ , the extension of the belt,  $d_s$ , can be described as

$$d_s = \theta_s \times r \quad (3.1)$$

### 3.2.4 Actuators and assembly

A Maxon (Maxon Motor AG) brushed DC Motor with 16:1 gearbox was used as the actuator. The combination of the gearbox and motor constitute a diameter of 10 mm and length of 53.4 mm, making it an acceptable size for the system.

Figure 3.4 shows the design of single haptic module. A cogged V-belt with a pitch length of 4.5 mm was chosen as the haptic contact. To allow flexibility when wrapping the module around the limb, a flexible plastic sheet was used to hold the motors and the belt assembly. The motor and the fixed shaft were hold onto the plastic sheet using a shaft holder. A flexible strap was passed through the slit at the end of each module to allow adding multiple modules together. Figure 3.5 shows the

assembly of 4 haptic modules to form a cuff shape, hold together by a lever cam buckle.

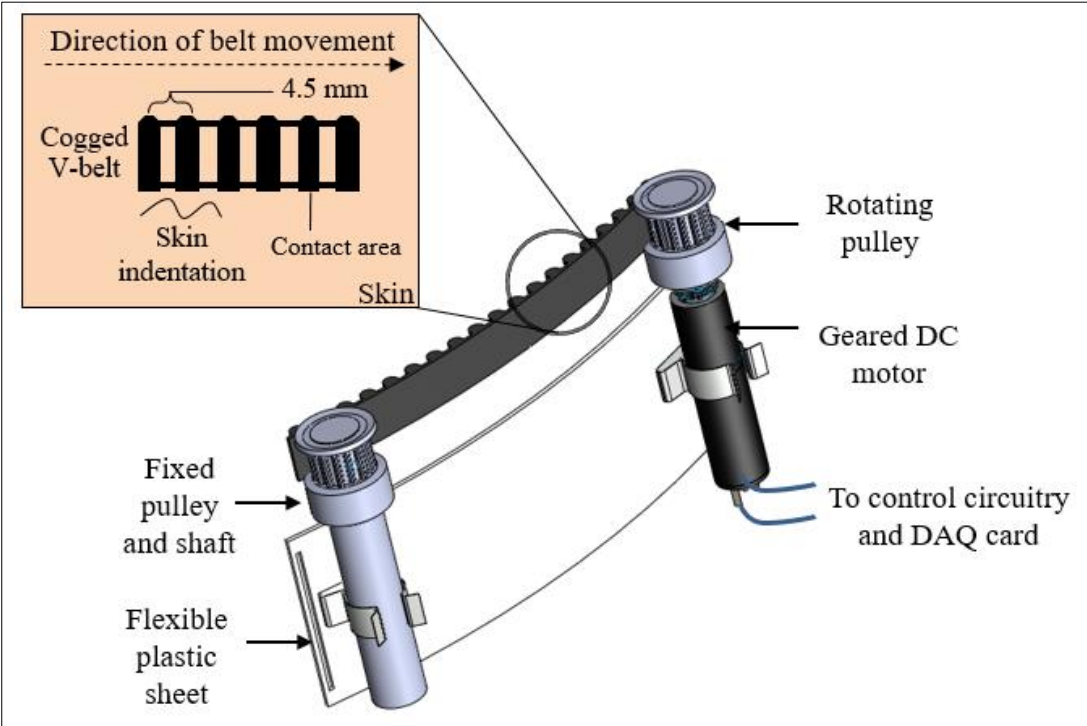


Figure 3.4 CAD illustration of a single feedback module

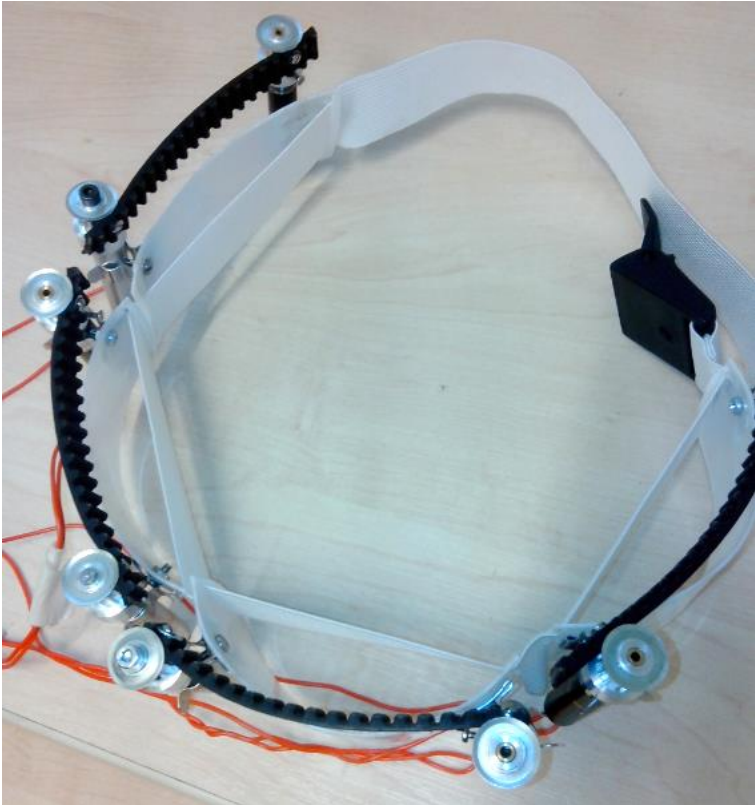


Figure 3.5 Assembled four quadrants haptic feedback modules

### 3.3 Preliminary Trials

Since the investigation did not require the subjects to perform dynamic activities, only the haptic feedback cuff was assessed in this initial experiment and only healthy subjects were involved. Objectives of this experiment are as follows:

- To determine the ability of a user to discriminate the location of the feedback in single point feedback configuration.
- To determine the ability of a user to discriminate the location of the feedbacks in simultaneous feedback configuration.
- To obtain feedback from the user on the design of the haptic cuff system.

#### 3.3.1 Methods

Three adult male subjects (H1, H2, and H3) aged 22-30 years old participated in this trial. Subjects were provided with the information sheet and briefed about the experiments. Consent were obtained from the subjects and the protocols have been approved by MaPS and Engineering Joint Faculty Research Ethics Committee (MEEC FREC, Ethical Reference MEEC 14-012) University of Leeds.

Subjects were seated in comfortable position on a chair, with the response sheet placed on a desk. The haptic cuff was wrapped around middle thigh of the right leg at anterior, posterior, medial and lateral sides. For convenience, these quadrants were labelled as front, back, right and left respectively in the response sheet. The subjects were seated close to the table such that the apparatus is not visible to them, to avoid visual identification of the haptic cuff movement. White noise was played throughout the session to prevent influence of auditory stimuli caused by the noise coming from the haptic module. Figure 3.6 shows the experimental setup.

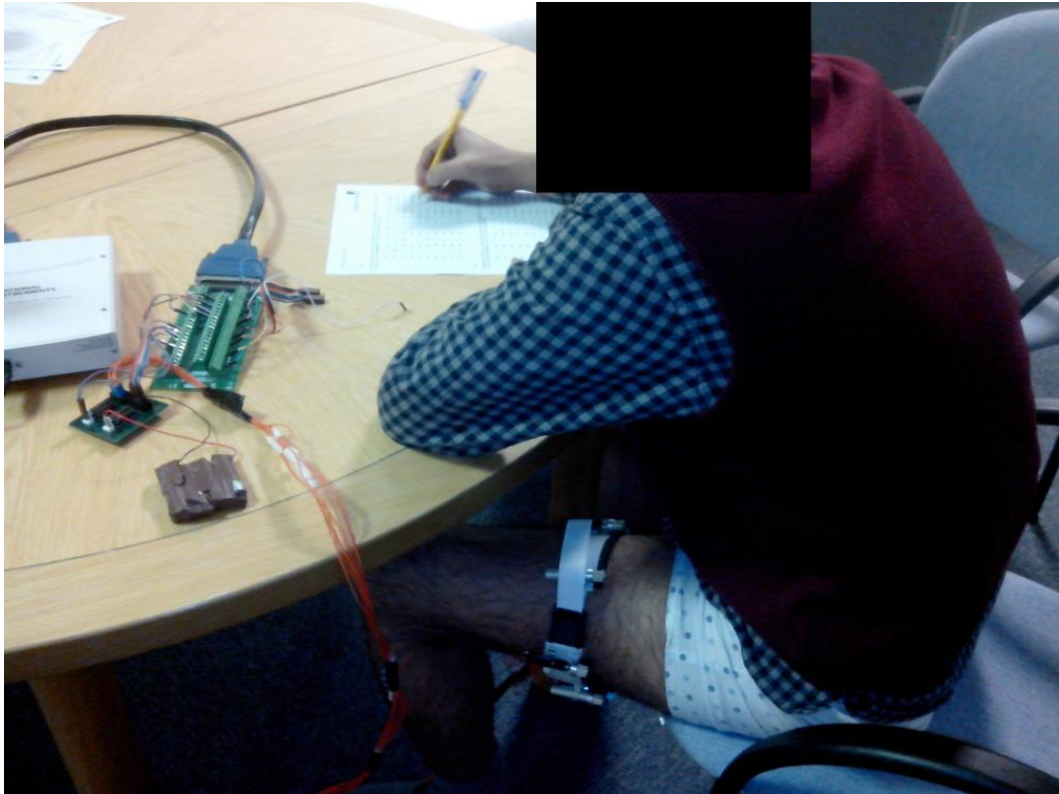


**Figure 3.6 Experimental setup**

### **1. Single quadrant feedback perception (varied contact time)**

A LabView (National Instruments, Austin) program was designed to send 10 signals activating a random haptic quadrant each time in which the belt on the haptic device would make 50 ms stretch of the skin. There was 5 s pause between the signals to allow recording the response in the datasheet. Subjects were instructed to indicate in the response sheet, at which of these four quadrants (front, back, left, or right) they felt the skin-stretch occurred or if the location cannot be determined or if no sensation was felt at all. The test was repeated with 150 ms, 300 ms and 450 ms belt contact period.

### **2. Simultaneous two quadrants feedback perception**

The LabView sent 10 signals activating two haptic quadrants simultaneously in the following standardized pattern:

<b>Signal</b>	<b>Activated Quadrants</b>
1	Front + Back
2	Front + Left
3	Right + Left
4	Right+ Back

5	Front+ Left
6	Front + Right
7	Front + Left
8	Right + Back
9	Front + Back
10	Front + Back

Each time, the belt on the haptic device will make 450 ms contact with the skin. There was 5 s pause between the signals to allow recording the response in the datasheet. The subjects were instructed to indicate in the response sheet, at which two of these four quadrants (front, back, left, or right) they felt the skin indentation occurred or if the location cannot be determined or if no sensation was felt at all. The test was carried out two times for each subject.

### 3.3.2 Analysis

The ability to discriminate the location of contact for both single quadrant and two quadrants feedback were calculated using the following formula:

$$\text{Percentage of Detection Accuracy} = \frac{\text{(number of correct responses)}}{\text{number of trials}} \times 100$$

### 3.3.3 Results

Table 3.1,

Table 3.2, and Table 3.3 shows the summary of detection accuracy for each subject H1, H2 and H3.

**Table 3.1 Summary of accuracy of location detection for the two experiments**

Assessment	% Detection Accuracy (Subject Average)			% Detection Accuracy (Assessment Average)
	H1	H2	H3	
Single Quadrant Feedback	100	100	96	<b>98.33</b>
Simultaneous Feedback	50	40	60	<b>51.67</b>

**Table 3.2 Results of responses from the subjects for single quadrant assessment.**

Stimuli	50ms			150ms			300ms			450ms		
	H1	H2	H3	H1	H2	H3	H1	H2	H3	H1	H2	H3
1	1	1	1	1	1	1	1	1	1	1	1	1
2	1	1	1	1	1	1	1	1	1	1	1	1
3	1	1	1	1	1	0	1	1	1	1	1	1
4	1	1	1	1	1	1	1	1	1	1	1	1
5	1	1	1	1	1	0	1	1	1	1	1	1
6	1	1	1	1	1	1	1	1	1	1	1	1
7	1	1	1	1	1	1	1	1	1	1	1	1
8	1	1	1	1	1	1	1	1	1	1	1	1
9	1	1	1	1	1	1	1	1	1	1	1	1
10	1	1	1	1	1	1	1	1	1	1	1	1
Subject average (%)	100	100	100	100	100	80	100	100	100	100	100	100
Stretch period Average (%)	100			93.33			100			100		
Assessment average (%)	98.33											

**Table 3.3 Results of responses from the subjects for simultaneous quadrants assessment.**

Activated Quadrants	Simultaneous (450 ms contact period)						% Detection Accuracy
	Trial 1			Trial 2			
	H1	H2	H3	H1	H2	H3	
Front + Back	0	0	1	1	1	1	66.67
Front + Left	1	0	1	0	0	1	50.00
Right + Left	0	1	0	0	0	0	16.67
Right + Back	0	0	0	1	0	0	16.67
Front + Left	1	0	1	0	1	0	50.00
Front + Right	1	0	1	1	0	0	50.00
Front + Left	1	1	0	1	1	0	66.67
Right + Back	0	1	1	1	1	1	83.33
Front + Back	0	0	0	0	1	1	33.33
Front + Back	1	1	1	0	1	1	83.33
Subject Average (% Detection Accuracy)	50	40	60	50	60	50	
Trial Average (% Detection Accuracy)	50			53.33			
Assessment Average (% Detection Accuracy)	51.67						

Table 3.1 shows that great accuracy was achieved with single location feedback with a mean of 98.67% detection accuracy. On the other hand, when subjected to feedback simultaneously at two different quadrants, the subjects scored poorly, with a mean of only 51.67% detection accuracy. These observations and other related analysis are discussed on the next section.

### 3.3.4 Discussion and Recommendation

The experimental results show that the feedback from the haptic cuff can be perceived, suggesting that the feedback modality chosen was appropriate for giving feedback to lower limb in static mode. This is evident from the response by the subjects, where in both assessments, feedback on the thigh was perceived, although in simultaneous two quadrants assessment, the feedback location might not be identified correctly. The single quadrant feedback test indicated accuracy of 98.76%, suggesting that the activated quadrant can be identified accurately even when making very short contact period of the belt on the skin. While the single quadrant test yielded positive results, the same cannot be said for multiple quadrants test. Although the subjects did feel stimulation inflicted by the belt, they were not able to accurately identify the correct quadrants at which the two feedbacks occurred. The mean for the detection accuracy was only 50%. In contrary, Fan et al. [16, 26] reported >87.5% accuracy for balloon tactile feedback and Wentink et al. [134] reported negligible difference in detection ability between sequential and simultaneous vibration feedback. The observation could be caused by one of these factors:

1. The magnitude of skin-stretch applied on the skin was not enough to allow easy identification of combined stimuli.
2. The cuff was not optimally fitted around the limb.
3. Slippage occurs during the movement of the belt, making the delivered stimuli less perceptible.

An increase of 3.33% in detection accuracy for the second trial as indicated in Table 3.3 cannot be used to indicate learning effect as the increase was observed in only two of the subjects, H1 and H2, while subject H3 showed decline in detection accuracy in the second trial. The combination of the locations of the activated quadrants (adjacent or opposite) also showed to have no effect in the detection ability of the subjects. For



example, the lowest detection accuracy of 16.67% was shown for both Right + Left (adjacent quadrants) and Right + Back (opposing quadrants). When asked for feedback from the experiment, subject H2 indicated that after the cuff was removed, it was felt as if the cuff was still attached to the thigh. This ‘phantom’ sensation could be due to the cuff being fixed too tight during the experiment. Subject H3 was concerned with the design that “looks like sharp edges”, which suggests for the device’s cosmetic improvement. Based on this experimental work, the following recommendation were made for the next haptic module design iteration:

1. A mechanism with more predictable output should be considered. Although the behaviour of the belt mechanism can be observed, there were very little control over the movement path and the properties of the stimuli delivered. Also, characterization should be carried out to assess the parameters of the design.
2. Custom design of the parts will allow flexibility in the design. In this regard, 3D printing was suggested as the methods for developing parts for rapid prototyping of the next follow-up design and mechanisms.
3. The direction of the stretch in the previous design was not in line with movement of the leg in the sagittal plane. The cyclic movement of the legs during walking means the leg were ‘down’ on the ground during Initial Contact (IC) and brought ‘up’ off the ground during Toe-off (TO). Therefore, it makes most sense to deliver the stretch up and down the skin rather than left-to-right manner as presented in the preliminary design.
4. An untethered/portable haptic module should be considered as this allows dynamic activities to be carried out with little or no constraint. In addition, incorporation of wireless communication will allow real-time control of the module as well as data gathering.
5. The module should incorporate a digitized user response mechanism such as touch screen or push button to allow subjects to record their response. Apart from the fact that this enables the trials to be carried out in dynamic mode, response can be automatically stored in the computer for future analysis.

### 3.4 First Iterative Design

This section will describe the first iterative design of a stretch module based on the outcome and findings from the preliminary design. The focus of the design was still fitting the module on the lower leg, rather than universal fitting to the whole body. Appropriate actuators were selected for the proposed mechanism and characterization was carried out to assess the design parameters. Experimental works to assess the module described in this section are presented in Chapter 5.

#### 3.4.1 Actuation Mechanism

To deliver skin-stretch along the proximal-distal line of the limb, several actuation methods were considered. The methods can either employ motorised or non-motorised linear actuation. As every actuation method will have their own advantages and disadvantages, ultimately, the selection of the most suitable actuator will depend on the following parameters:

1. **Speed** – Since two feedbacks are to be delivered in real-time during stance phase of the gait cycle (one during IC and one during TO), it is important that a single feedback is delivered within 200 ms, to cater for different walking speed.
2. **Weight and Size** – The weight and size of the actuator must be within the constraint of a portable modules, to allow untethered attachment to the limb. A range of 200 g to 1 kg was deemed acceptable for lower leg [133].
3. **Control Circuitry** – Some actuators such as pneumatic actuators require complex circuitry for actuation control, or external sensors for measuring parameters such as speed and position. Actuator with the least complexity is desirable because it allows easy troubleshooting, and provides high degree of programmability.
4. **Cost** – A low cost actuator is desirable parameter for rapid prototyping, in case replacement of actuators are needed or different actuator specification is required.
5. **Power requirement** – For a wearable module, it is desirable to have actuators that can be powered from batteries. Therefore, an operating voltage of less than 6V is desirable.

Figure 3.7 shows possible actuation methods considered for iterative design of the skin-stretch module.

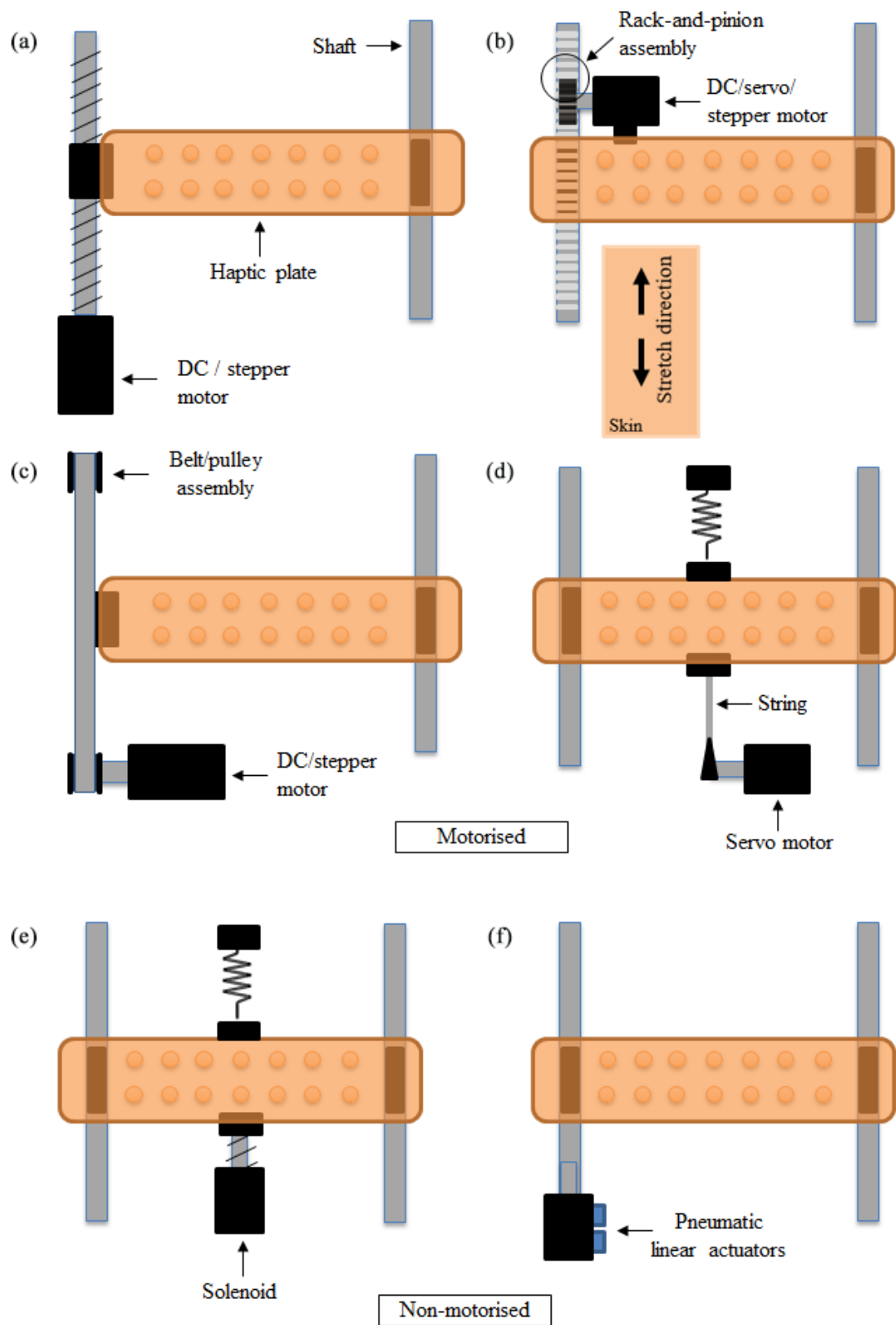
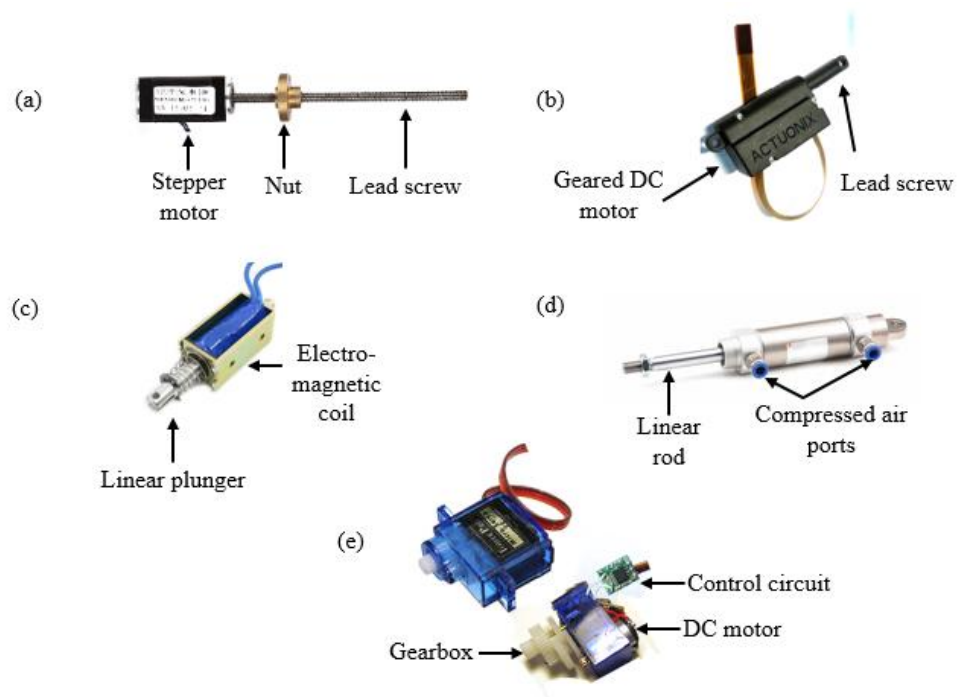


Figure 3.7 Possible actuation methods to create skin-stretch stimuli

A motorised linear actuator typically consists of a stepper motor or a Direct Current (DC) motor with a built-in leadscrew in place of the output shaft. The working principle of a stepper motor makes it possible to achieve high movement resolution, allowing for precise position control. A DC motor on the other hand, can output high rotational speed and high torque can be achieved with gearing. For linear application, DC motors are normally geared for high force output. Servo motors are a special kind of motor which combines a Geared DC motor and control circuitry, which results in the advantage of having high speed and force output while allowing position control. Servo motors are generally used in discrete positioning as they typically allow limited rotation, unlike continuous rotation with normal DC motor. Direct-drive configuration can possibly be designed for delivering skin-stretch stimuli using DC, stepper or servo motor as shown in Figure 3.7(a-b). Alternatively, an indirect drive configuration could also possibly deliver the stimuli by using belt drive (Figure 3.7(c)) or string attached to spring mounted haptic plate (Figure 3.7(d)). Non-motorised options include the use of solenoid and pneumatic linear actuators such as those shown in Figure 3.7(e-f).

Table 3.4 summarizes the advantages and disadvantages of each actuators, focusing especially for this design requirement.



**Figure 3.8** Examples of: (a-b) linearized stepper and DC motor (c) solenoid (d) pneumatic actuator (e) servo motors

**Table 3.4 Comparison of actuator properties**

	Speed	Force/ Torque	Size	Control	Power requirement
<b>DC motor</b>	High	High with gearing	Small - large	<ul style="list-style-type: none"> <li>• Simple speed control using Pulse Width Modulation (PWM)</li> <li>• Direction control requires additional circuit</li> <li>• Position control requires an encoder</li> </ul>	Low-high, depending on the motor size (typically 3-12 V)
<b>Stepper motor</b>	Medium-High	High holding torque	Small - large	<ul style="list-style-type: none"> <li>• Open loop position control</li> </ul>	Medium to high (6-12V)
<b>Servo Motor</b>	High	High	Small- large	<ul style="list-style-type: none"> <li>• Embedded control circuitry</li> <li>• Simple closes-loop position control</li> </ul>	Low-high, depending on the motor size (typically 3-12 V)
<b>Solenoid</b>	High	Very high	Small- large	<ul style="list-style-type: none"> <li>• Typically on/off configuration with no control</li> </ul>	Medium to high (6-12V)
<b>Pneumatic</b>	High	Very high	Medium - large	<ul style="list-style-type: none"> <li>• Complex position control</li> </ul>	Medium to high (6-12V)

Comparing the features of the actuators, motorised actuation presented as the most viable choice for designing the haptic module. Servo motors was decided as the most suitable actuator for the revised haptic module because it is available in miniature sizes, has a built-in position control capability, and is very economical in cost. The servo motor used to realize the drive mechanism was a TowerPro SG90 micro servo motor. This servo motor is available off the shelf from many electronics outlets and has small footprint and reasonable price. Table 3.5 shows the servo motor specification.

**Table 3.5 Servo motor specification**

Specification	Value	
Dimension	Length: 23.0 mm Width: 12.2 mm Height: 29.0 mm	
Weight	9.0 g	
Speed	0.12 s/60°	
Torque	176.5 N.mm	
Dead bandwidth	10 μs	
Voltage	4.8 – 6V	
Cost	~ £2.50 / unit	

### 3.4.2 Haptic Module Design

This section will provide a detailed description on the design and prototyping of the haptic module. All 3D printed parts were fabricated from Polylactic Acid (PLA) material using Fixed Deposition Manufacturing (FDM) 3D printers. Parts requiring specific attention to strength such as the drive assembly were printed using PolyMax™ (Polymaker LLC, Shanghai) material, which was a specialized PLA with improved mechanical properties compared to the normal PLA.

#### 3.4.2.1 Design Description

The haptic module is a combination of 5 parts:

1. The frame assembly
2. The drive assembly
3. The linker
4. The haptic plate
5. The adjustable limb contacts

The haptic plate (Figure 3.9) consists of a grid of 24 cylindrical pins with 4 mm diameter, arranged in cross-grid formation (3 rows  $\times$  8 columns). The pins were spaced 5 mm (vertically) and 1 mm (horizontally) from each other. The surface on which the pins are placed was curved to match the curvature present in human upper leg.

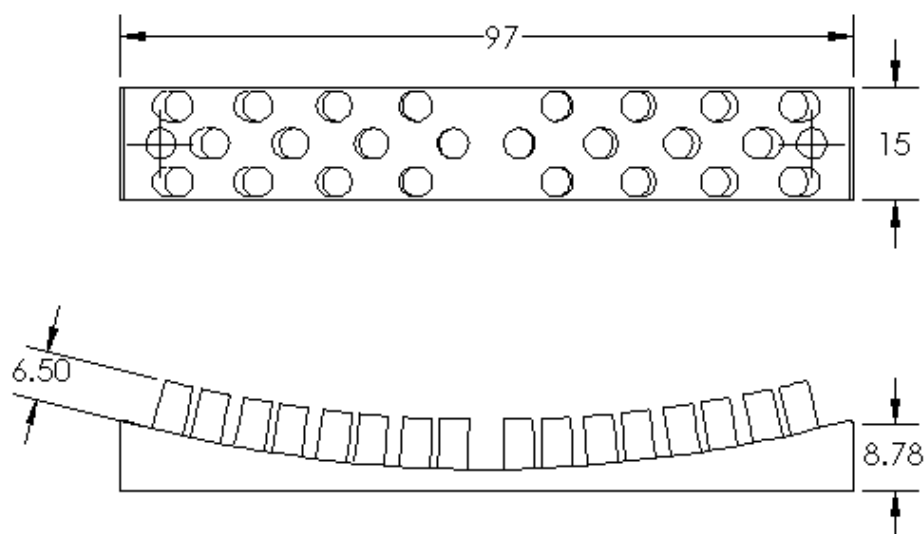


**Figure 3.9** The top and side view of the haptic plate

An array of stimuli pins was chosen rather than a single stimulus points to increase the area covered by the stimuli on the skin while having the advantage of eliciting additional sensation via movement of the hair follicle during the stretching motion. In addition, an array of pins allows better grip of the haptic plate on the skin and reduces chance of slipping during its movement.

A rack-and-pinion mechanism was chosen as the haptic module drive mechanism. Two micro servo motors arranged back-to-back were each connected to a 16-tooth 0.6 module pinion gear. This gear size was selected because it allowed good approximation of the relation between the servo motor rotation angle to the linear stretch distance, and was a reasonable size for prototyping using desktop 3D printing. Figure 3.10 shows the profile of the pinion and rack mechanism.

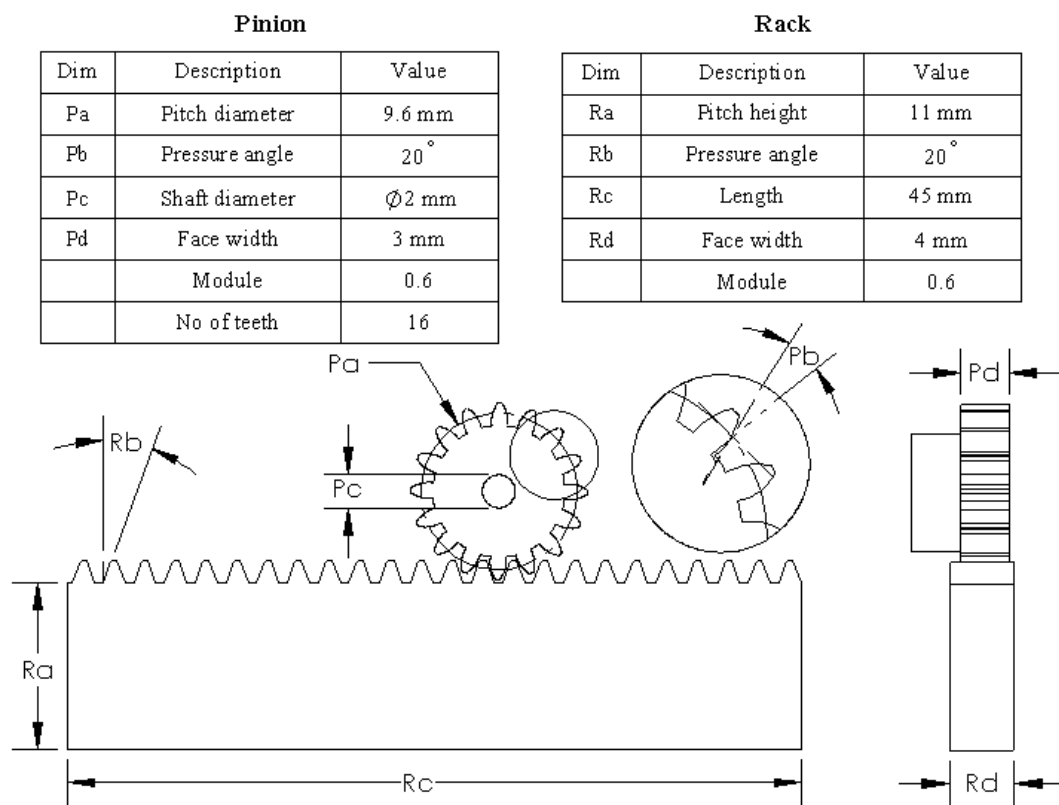


**Figure 3.10 Rack and pinion parameters**

### 3.4.2.2 Calculation of Movement Parameters

To obtain the operating parameters of the haptic module, following calculations based on the known drive parameters were carried out. In Section 3.4.3, these parameters are characterized experimentally to evaluate the design.

### 1. Relationship between servo angle and linear travel

Number of tooth,  $N_p = 16$  and

Gear module,  $M_p = 0.6$

The pitch diameter of the gear,

$$\begin{aligned} P_d &= M_p \times N_p & (3.2) \\ &= 0.6 \times 16 \\ &= 9.6 \text{ mm} \end{aligned}$$

For a full revolution of the pinion gear, linear travel of the pinion,  $d_p$  is

$$\begin{aligned} d_p &= \pi \times P_d & (3.3) \\ &= \pi \times 9.6 \\ &= 30.2 \text{ mm} \end{aligned}$$

Therefore, 1 mm of travel requires

$$\frac{360}{30.2} = 11.92 \sim 12^\circ$$

of servo motor rotation.

### 2. Linear velocity

From motor specification, angular velocity of the motor,  $\omega_m$  can be calculated as follows,

$$\begin{aligned} \omega_m &= \frac{60 \text{ deg}}{0.12 \text{ s}} & (3.4) \\ &= 500 \text{ deg/s} \\ &= 8.73 \text{ rad/s} \end{aligned}$$

The maximum linear velocity of the pinion movement,  $v_p$  can be described as,

$$\begin{aligned} v_p &= \omega_m \times \frac{P_d}{2} & (3.5) \\ &= 8.73 \times 9.60/2 \\ &= 41.90 \text{ mm/s} \end{aligned}$$



### 3. Tangential force

As only the stall torque information was available from the data sheet (176.5 N.mm) the maximum force exerted by the drive assembly can be found as follows

$$\begin{aligned}
 F_p &= 2 \frac{T_s}{P_d} & (3.6) \\
 &= \frac{2(176.5)}{9.6} \\
 &= 36.77 \text{ N}
 \end{aligned}$$

#### 3.4.2.3 Design Details

The haptic module frame consists of a base plate cut from acrylic (subsequently from plywood to reduce the weight) which houses 3D printed shaft holders, and were arranged symmetrically to each other. 3 mm precision shaft were fixed on the shaft holders to allow linear movement of the haptic plate assembly. Figure 3.11 - Figure 3.16 show the CAD illustration for the components of the haptic module and the full assembly.

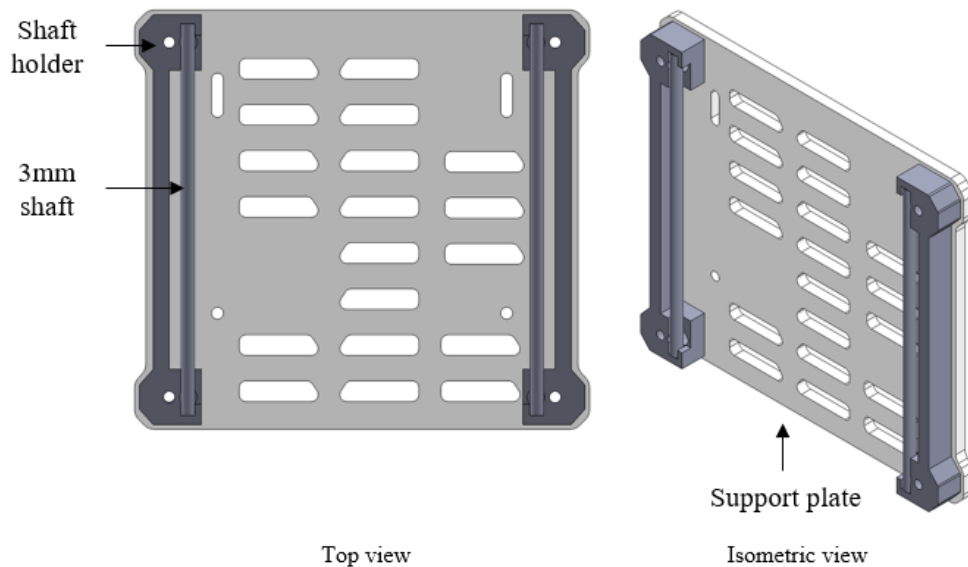


**Figure 3.11 Haptic module – frame assembly**

The drive assembly consists of two servo motors which translates rotational to linear movement via the rack-and-pinion mechanism. Since the rack was fixed to the haptic frame, simultaneous rotation of the servo motors drives the whole motor assembly upwards and downwards as shown in Figure 3.12.

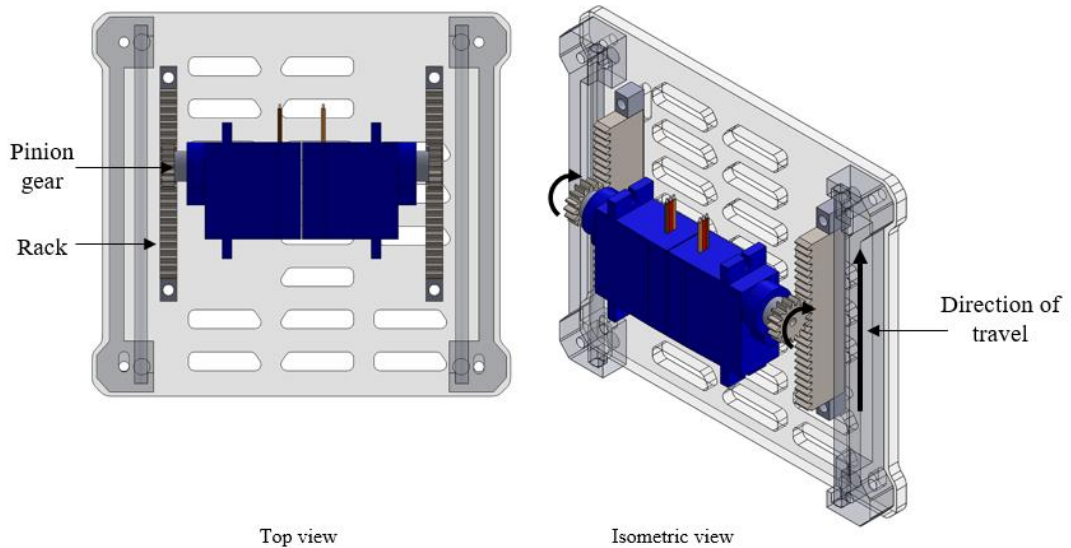


**Figure 3.12 Haptic module – drive assembly**

To take advantage of this behaviour, the haptic plate was linked to the motor assembly, such that it follows the linear movement of the motor assembly. This was achieved by using a ‘linker’ frame, which holds the motor and the haptic plate together (Figure 3.13). The linker frame was also connected to the shaft using bronze bushing to ensure smooth movement.

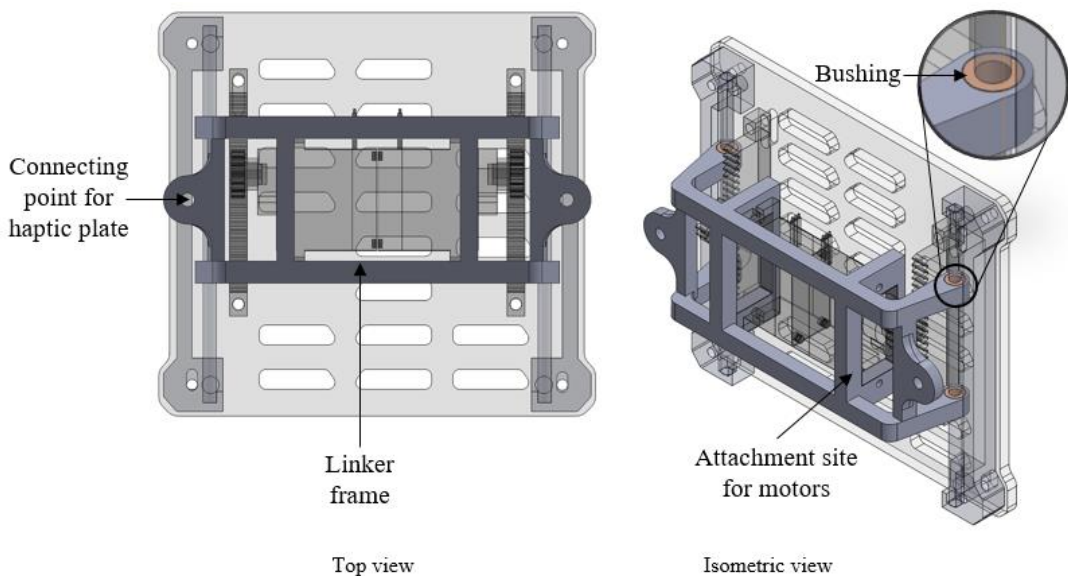


**Figure 3.13 Haptic module – linker frame**

The haptic plate was connected to the linker frame via two spacers (Figure 3.14). This arrangement made it easier to change or replace the haptic plate without disassembling the whole haptic module.

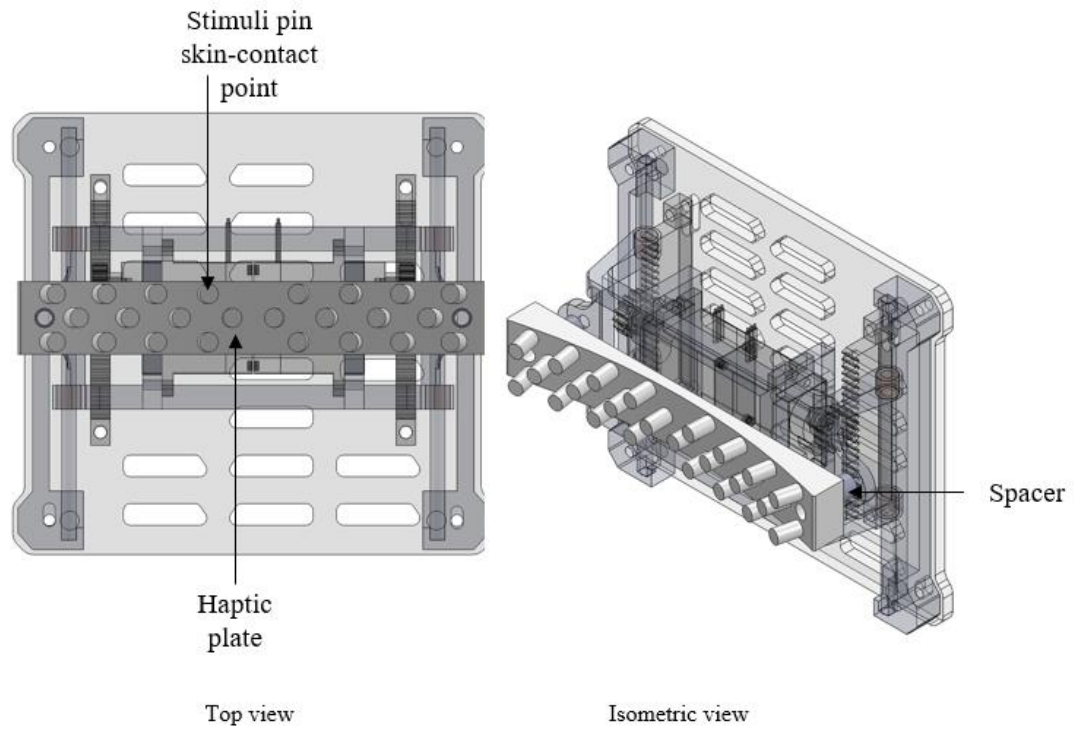


**Figure 3.14 Haptic module – haptic plate**

For attachment to the leg, especially around the thigh region, it was necessary to equip the module with a limb contact parts. This allowed the module to rest on the limb, and the adjustable feature made it possible for the haptic plate to be positioned flush on the skin (Figure 3.15).

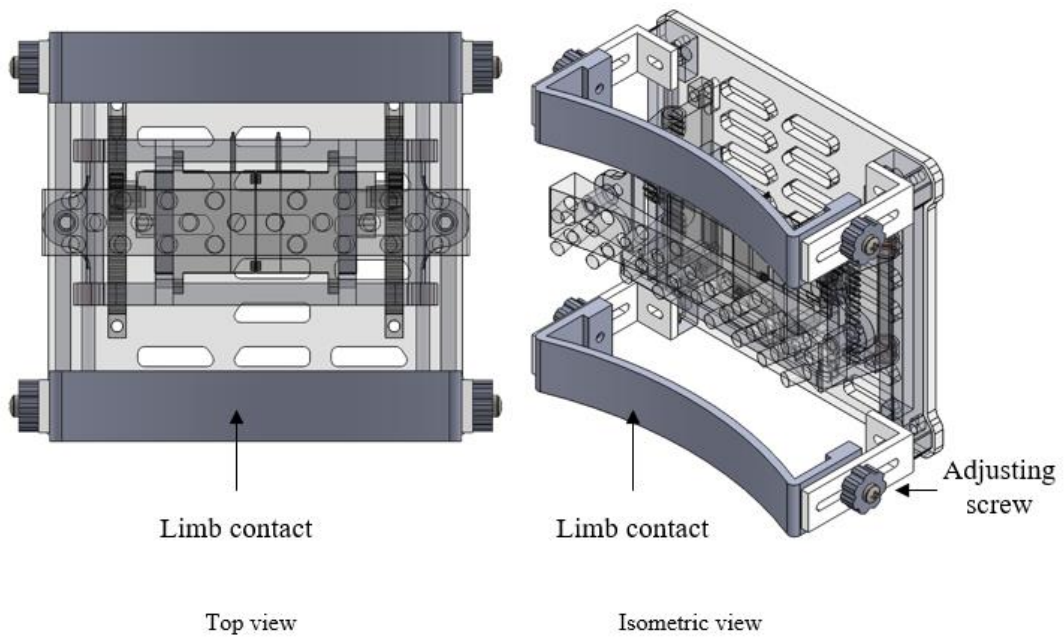


**Figure 3.15 Haptic module – adjustable limb contact**

Figure 3.16 shows the full assembly of the haptic module, and Figure 3.17 shows the assembled haptic module donned on an anatomical leg model.

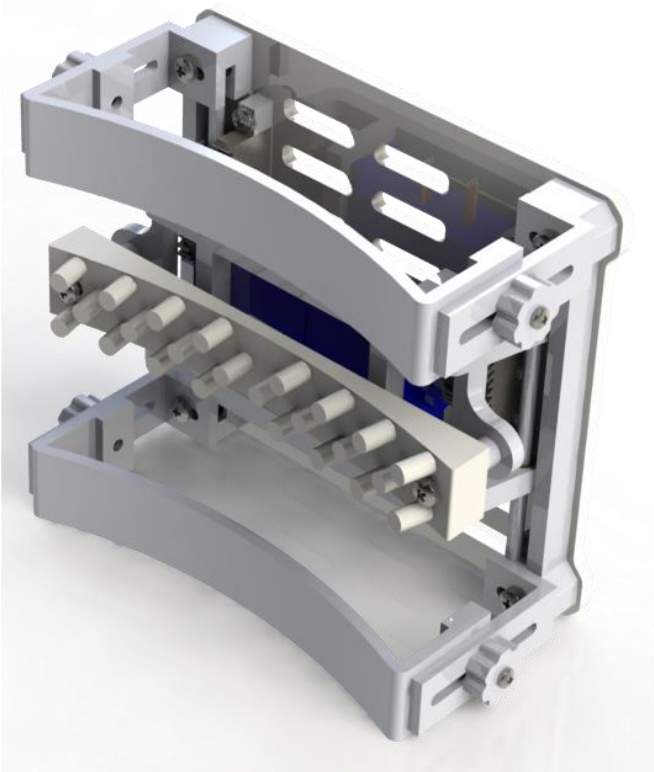


**Figure 3.16 Haptic module – full assembly**

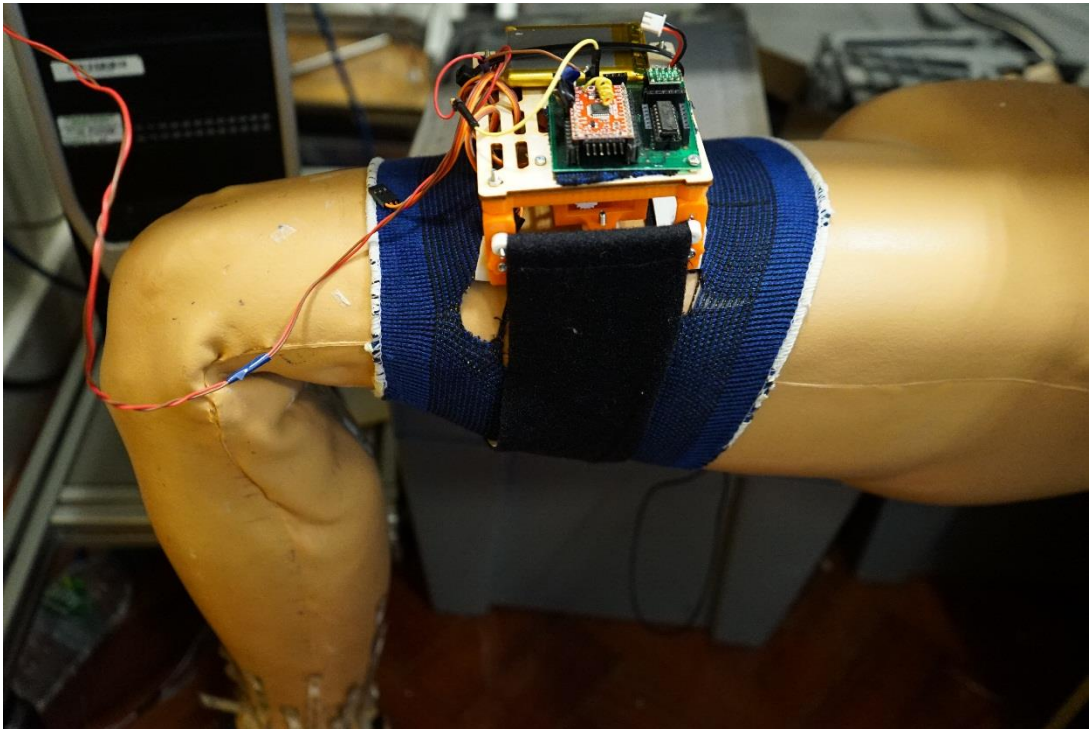


**Figure 3.17 The haptic feedback module on an anatomical leg model**

### 3.4.3 Characterization

The characterization of the design mechanism is described here. First, the movement profile of the haptic assembly was experimentally validated against the theoretical calculation carried out in the previous section. The experiment allowed determining the accuracy of the angle-linear distance relationship. Additionally, for each stretch position the duration in which the stimuli took place was varied, to identify the minimum amount of time required for the delivery of the stimuli. This investigation was important in deciding whether the designed mechanism can provide the stimuli within reasonable time as per design requirement. The second experiment investigated the motor force profile by obtaining the relationship between the motor torque and the motor current.

#### 3.4.3.1 Movement Profile

**Method** To validate the movement profile, an optical laser distance sensor (Leuze Electronics, Germany) was positioned opposite to the body of the haptic frame, along the axis of the movement as shown in Figure 3.18. The output from the distance sensor was sampled at 2 kHz using a NI USB-6225 Data Acquisition Card (National Instruments, Austin, Texas). Initial distance reading was recorded as the baseline position. Subsequently, the haptic frame was programmed to move 1 mm (12-degree servo rotation) within a duration of 200 ms towards the distance sensor, and return to the baseline position. The output from the optical sensor were recorded throughout each movement. The task was repeated 15 times, with 1s pause between each movement. The same procedure was repeated with a combination of 1-5 mm travel (in 1 mm steps) and with 100-200 ms movement duration (in 10 ms steps), resulting in 55 sets of experimental data.

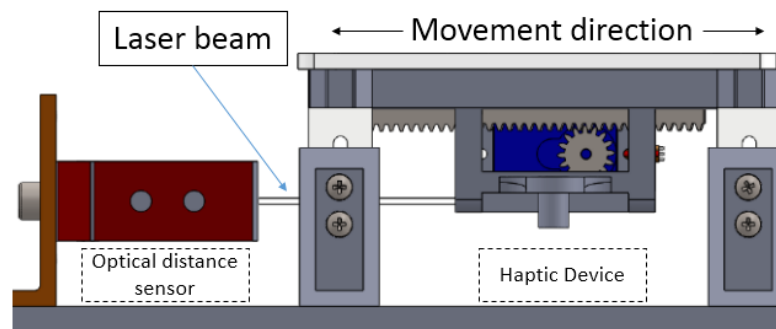


**Figure 3.18 Setup for validating distance and speed profile of the haptic module**

**Analysis** For each combination of distance (stretch distance) and duration (stretch duration), the mean  $\pm$  SD value from the 15 trials were plotted. The positioning error for a particular stretch duration was obtained by using the following calculation:

$$\text{target distance} = X_t$$

$$\text{actual distance} = X_a$$

$$\text{Positioning error} = |X_t - X_a|$$

The velocity profile was obtained by differentiating the distance over time

$$v_a = \frac{dX_a}{dt} \quad (3.7)$$

Subsequently, the acceleration profile could be obtained as,

$$a_a = \frac{dv_a}{dt} \quad (3.8)$$

**Results** Figure 3.19, Figure 3.20 and Figure 3.21 shows sample of the data collected during the experimental work for the movement of the haptic frame to target distance of 1 mm and 5 mm (200 ms duration) respectively. For both target distance, the distance vs time curve follows an s-curve movement profile, due to the tuning made by the built-in control circuitry in the servo motor. However, it can be observed that for 5 mm distance, there was an overshoot when the haptic frame returns to baseline position (Figure 3.19). The same overshoot was observed in all target distances apart from 1 mm. However, the frame could return to the baseline position after the overshoot period in reliable manner.

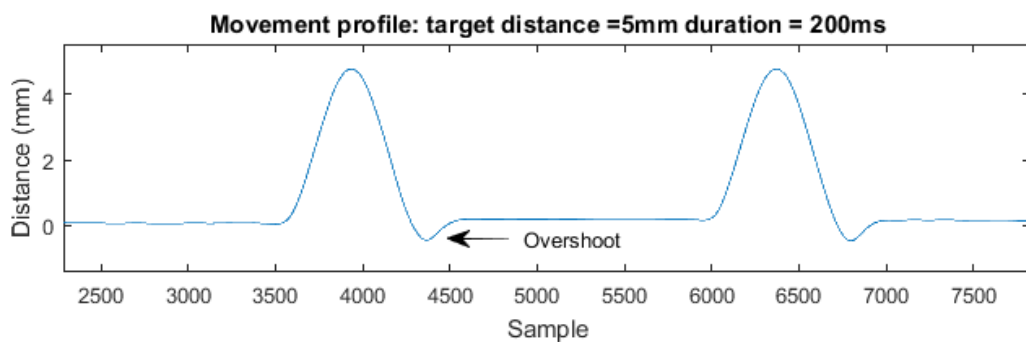


**Figure 3.19** An overshoot when returning to baseline position as observed with target distance of 2-5 mm

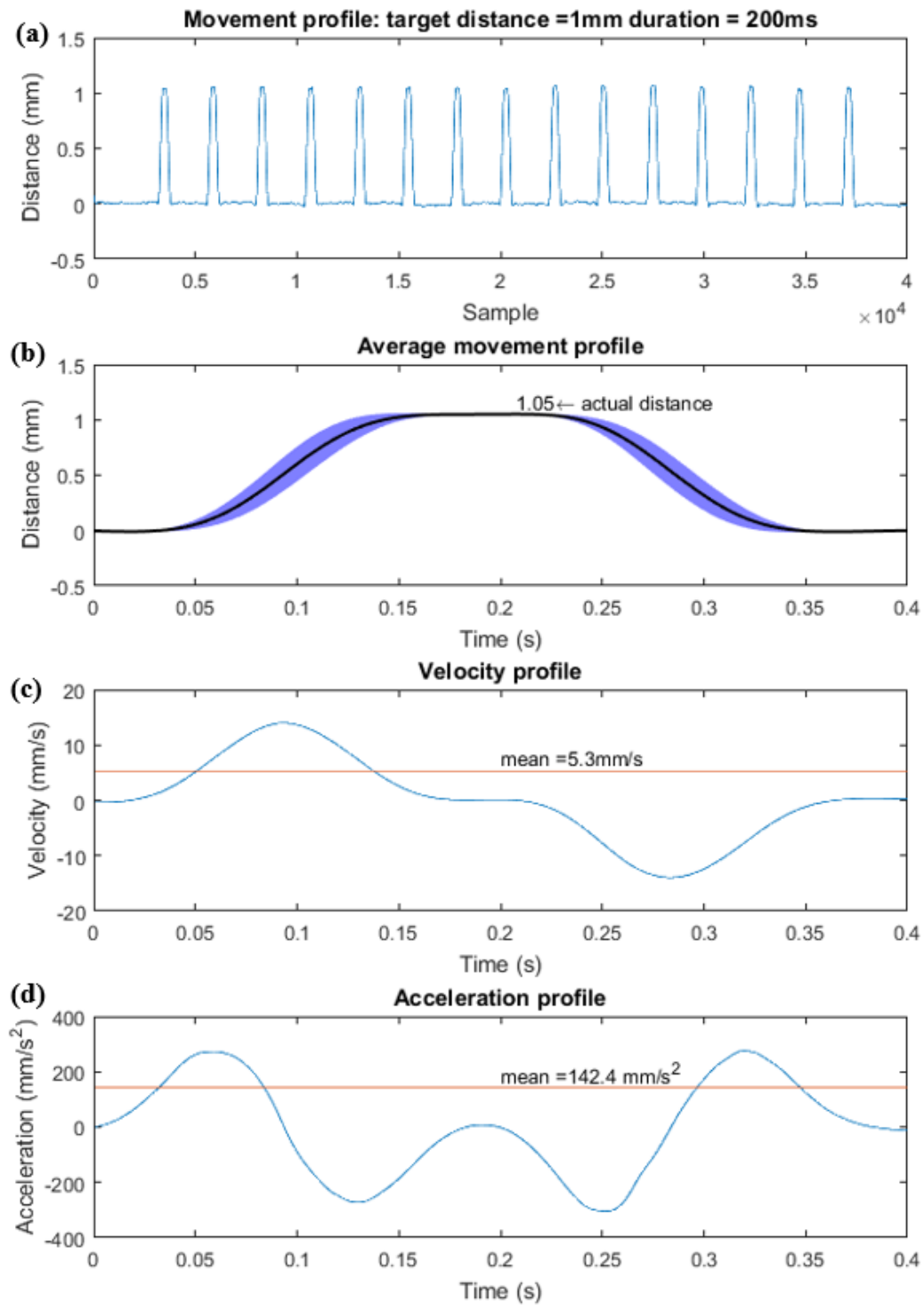


**Figure 3.20** Movement profile for 1 mm target distance with 200 ms duration. (a) distance profile for 15 trials. (b) Average movement profile with shaded area indicating standard deviation. (c) velocity profile of the mean data and (d) acceleration profile

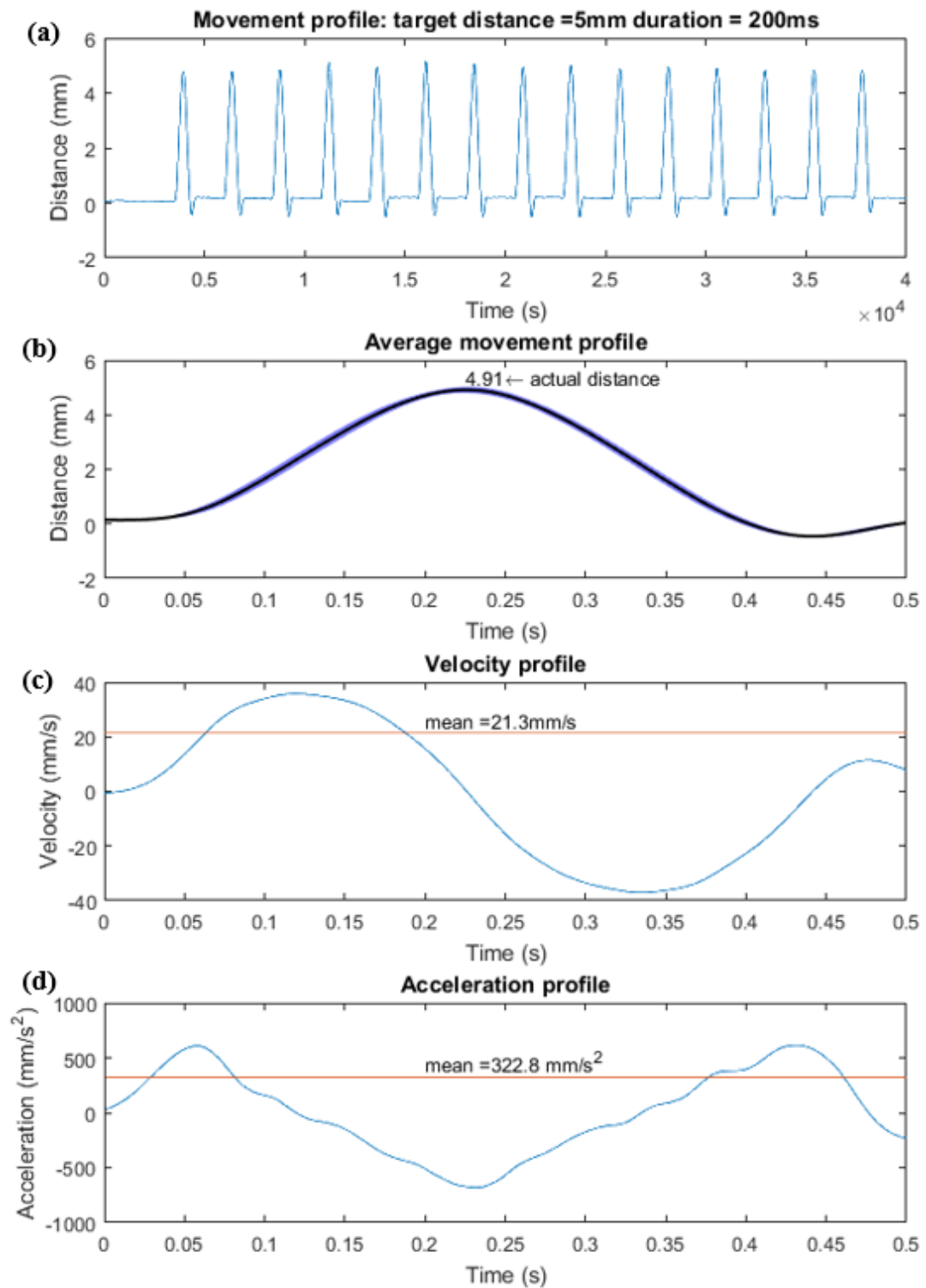


**Figure 3.21** Movement profile for 5 mm target distance with 200 ms duration. (a) distance profile for 15 trials. (b) Average movement profile with shaded area indicating standard deviation. (c) velocity profile of the mean data and (d) acceleration profile



It was important to understand the influence of the movement duration to the positioning of the haptic assembly. Table 3.6 shows the actual distance travelled by the haptic frame as recorded during the experimental work, as compared to the intended position target. In general, reducing the movement duration caused an increase in the position error. Table 3.7 made this assertion clearer. It can be noted that for a stretch magnitude to be delivered with the lowest error possible, a longer movement duration is preferred. For stretch up to 4 mm, a movement duration as low as 140 ms can be employed to deliver the stimuli. However, for 5 mm stimuli, 200 ms duration yielded the lowest error, with the error rapidly increasing with the decrease in movement time. 150 ms movement duration showed lowest error in all 1-4 mm target position ( $< 0.1$  mm), making this the appropriate movement duration for future experimental purpose.

**Table 3.6 Actual movement distance achieved for various target positions and movement duration. Values indicate Mean  $\pm$  SD**

		Movement Duration (s)										
		200	190	180	170	160	150	140	130	120	110	100
Intended Position Target (mm)	1	0.97 $\pm$ 0.04	0.98 $\pm$ 0.05	0.99 $\pm$ 0.06	1.03 $\pm$ 0.04	1.00 $\pm$ 0.06	1.02 $\pm$ 0.04	0.96 $\pm$ 0.06	0.97 $\pm$ 0.04	1.07 $\pm$ 0.06	0.92 $\pm$ 0.04	0.86 $\pm$ 0.06
	2	2.03 $\pm$ 0.07	1.91 $\pm$ 0.14	2.06 $\pm$ 0.08	1.90 $\pm$ 0.11	1.99 $\pm$ 0.08	2.02 $\pm$ 0.06	1.96 $\pm$ 0.08	1.92 $\pm$ 0.08	1.83 $\pm$ 0.08	1.90 $\pm$ 0.07	1.80 $\pm$ 0.09
	3	3.17 $\pm$ 0.09	3.15 $\pm$ 0.09	3.17 $\pm$ 0.10	3.22 $\pm$ 0.09	3.10 $\pm$ 0.10	2.94 $\pm$ 0.13	2.98 $\pm$ 0.10	2.90 $\pm$ 0.08	2.89 $\pm$ 0.12	2.70 $\pm$ 0.13	2.73 $\pm$ 0.12
	4	4.10 $\pm$ 0.13	3.95 $\pm$ 0.11	4.03 $\pm$ 0.12	3.92 $\pm$ 0.14	3.98 $\pm$ 0.11	3.92 $\pm$ 0.15	3.84 $\pm$ 0.13	3.68 $\pm$ 0.16	3.36 $\pm$ 0.18	3.03 $\pm$ 0.27	2.53 $\pm$ 0.12
	5	4.83 $\pm$ 0.15	4.76 $\pm$ 0.11	4.79 $\pm$ 0.08	4.62 $\pm$ 0.06	4.51 $\pm$ 0.11	4.54 $\pm$ 0.06	4.33 $\pm$ 0.15	4.21 $\pm$ 0.05	3.76 $\pm$ 0.12	3.71 $\pm$ 0.05	3.31 $\pm$ 0.21

**Table 3.7 Error in positioning of the haptic assembly (mm). Shaded area indicates range of error.**

		Movement Duration (s)										
		200	190	180	170	160	150	140	130	120	110	100
Intended Position Target (mm)	1	0.03	0.02	0.01	0.03	0	0.02	0.04	0.03	0.07	0.08	0.14
	2	0.03	0.09	0.06	0.1	0.01	0.02	0.04	0.08	0.17	0.10	0.20
	3	0.17	0.15	0.17	0.22	0.10	0.06	0.02	0.10	0.11	0.30	0.27
	4	0.10	0.05	0.03	0.08	0.02	0.08	0.16	0.32	0.64	0.97	1.47
	5	0.17	0.24	0.21	0.38	0.49	0.46	0.67	0.79	1.24	1.29	1.69

The results showed that the haptic module can deliver stimuli in the range of 1-4 mm within a duration of 150 ms.

### 3.4.3.2 Force Profile

Figure 3.22 shows the rack-and-pinion mechanism used to drive the haptic module.

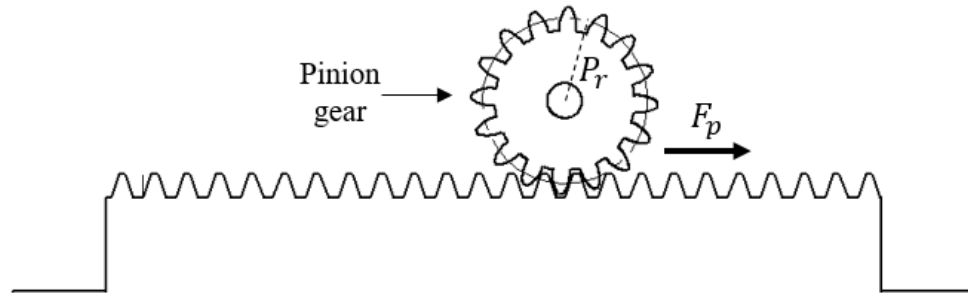


**Figure 3.22 Drive mechanism, showing the tangential force  $F_p$**

To obtain the force profile, it was necessary to first identify a relationship between the motor parameters under load condition. It is known that for DC motor, the torque,  $T_m$  is proportional to the current,  $I_m$  such that

$$T_m = K_t I_m \quad (3.9)$$

Where  $K_t$  is known as the motor constant. By finding the torque-current relationship, the force generated by the rack pinion drive assembly  $F_p$  can be obtained using the following equation

$$F_p = \frac{T_m}{P_r} \quad (3.10)$$

where  $P_r$  is the radius of the pinion gear.

**Method** To obtain the torque current relationship, an experimental setup shown in Figure 3.23 was arranged. An arm was connected to the servo motor. A weight holder, acting as the platform for adding load to the servo motor was hung on a string fixed 10 mm away from the centre of the servo rotation. A current sensor (ACS715, Allegro Microsystems) was connected in between the ground connection of the servo motor. Varying load between 250 g to 1050 g were added to the weight holder and the resulting current measurement when the arm was moved upwards to lift the load was recorded. The output from the distance sensor was sampled at 2 kHz using a NI USB-6225 (National Instruments, Texas) DAQ card.

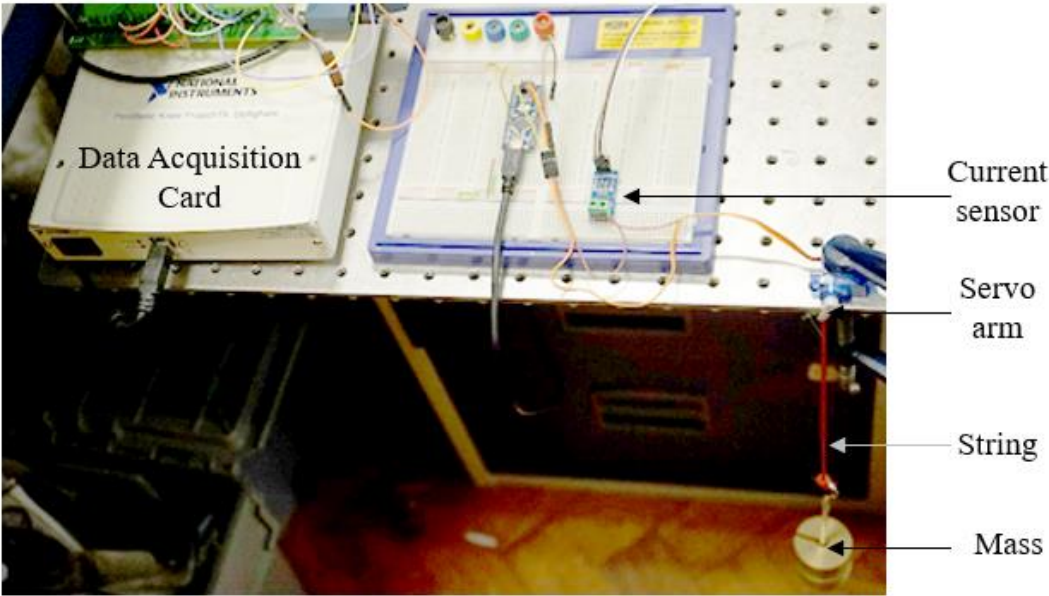


**Figure 3.23 Experimental setup for measuring current-torque relationship**

**Analysis** The force acting on the arm can be described as the product of the load and gravitational force as shown in Figure 3.24.

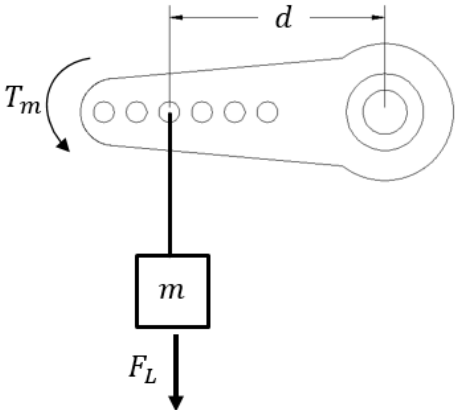


**Figure 3.24 Torque and force acting on the servo arm**

Therefore, force caused by the load,

$$F_L = 9.81m \tag{3.11}$$

Where m is the mass in kg. The torque applied,  $T_m$  can then be calculated as

$$T_m = F_L d \tag{3.12}$$

The torque vs current graph was plotted, and a best fit linear line was fitted using Matlab software to define the torque-current relationship.

**Results** Figure 3.25 shows the relationship between torque and current when different load were applied to the motor.

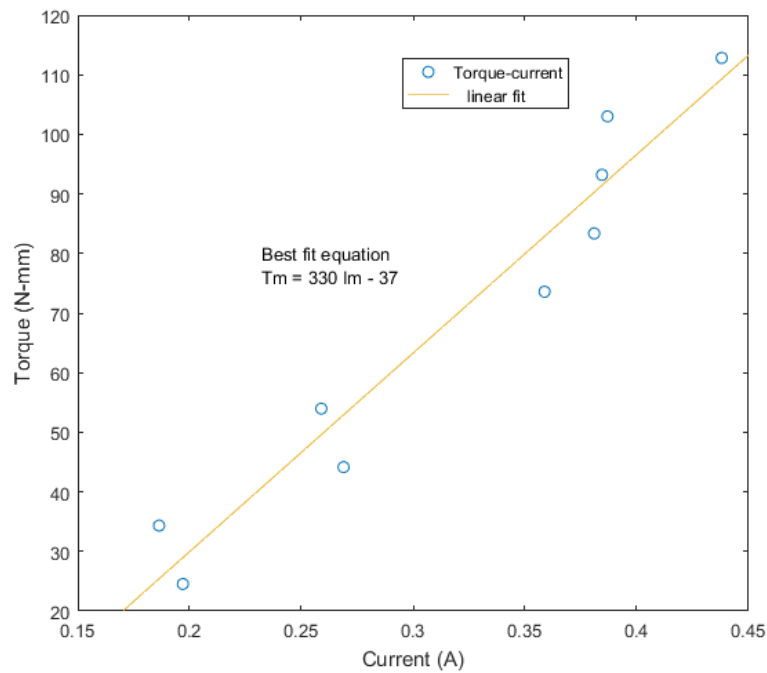


**Figure 3.25 Torque vs current graph for various loads**

The best fit line which defines the relationship was found to be

$$T_m = 330I_m - 37 \quad (3.13)$$

### 3.5 Revised Design

This section presents a revised design of the haptic module based on the feedback from the experimental work described in the first half of chapter 5. It's worth noting that this revised design does not include any changes in drive mechanism or actuation method, but was rather focused on the footprint and the drive electronics. The main objective of the design was to minimize the number of parts in the design assembly as well as reducing its overall size and weight. In addition, a more modular approach was attempted with the revised design to allow its placement on virtually any part of the body, rather than only on the upper leg.

#### 3.5.1 Design Justification

The requirement to redesign the haptic module was based on the following justifications:

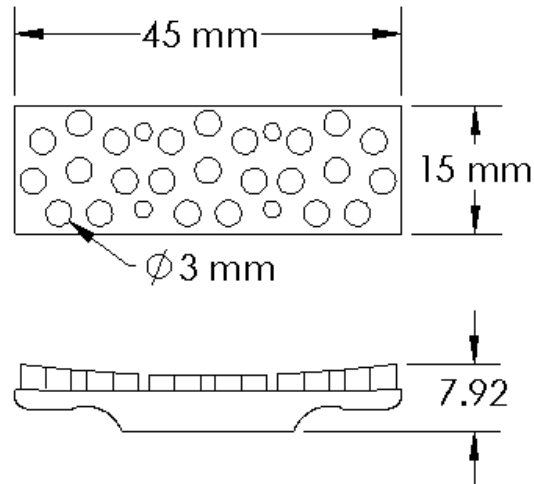
1. Placement – As described in Chapter 5, the placement of the feedback module on the leg has some drawbacks in the dynamic mode, including the masking

of the stimuli as well as the force exerted to the haptic module during toe off events. In turn, it is possible for the module to shift its position throughout the walking activity. Moreover, for transfemoral amputee, it was necessary to be able to place the module on other parts of the body since the placement on the thigh of the amputated leg might not be possible due to the socket covering the stump up to the hip joint. However, placement of the module in its existing form on other places of the limb was not achievable due to its size and shape.

2. Footprint – The size of the overall module was predominantly determined by the size of the haptic plate and the required stretch distance. The existing design considered maximizing the area in which the haptic module makes contact, and therefore was chosen to be one-fourth of the average size of adult human thigh (allowing up to four modules to be fitted around the thigh). The distance in which the module can travel (i.e the effective length of the rack-pinion assembly) was also chosen to be large to allow testing different possible stretch length. However, since the stretch stimulus could be perceived even in smaller magnitude (~4 mm), the effective length of the pinion-rack assembly can be drastically reduced.
3. Centralized control – Existing control unit for the haptic module was not designed to handle multiple haptic modules, making it a less modular control system. As the communication and data transfer to the computer is done wirelessly, it was necessary to reduce the number of transmitters to reduce complexity of the communication design and reduce interference between the signals.

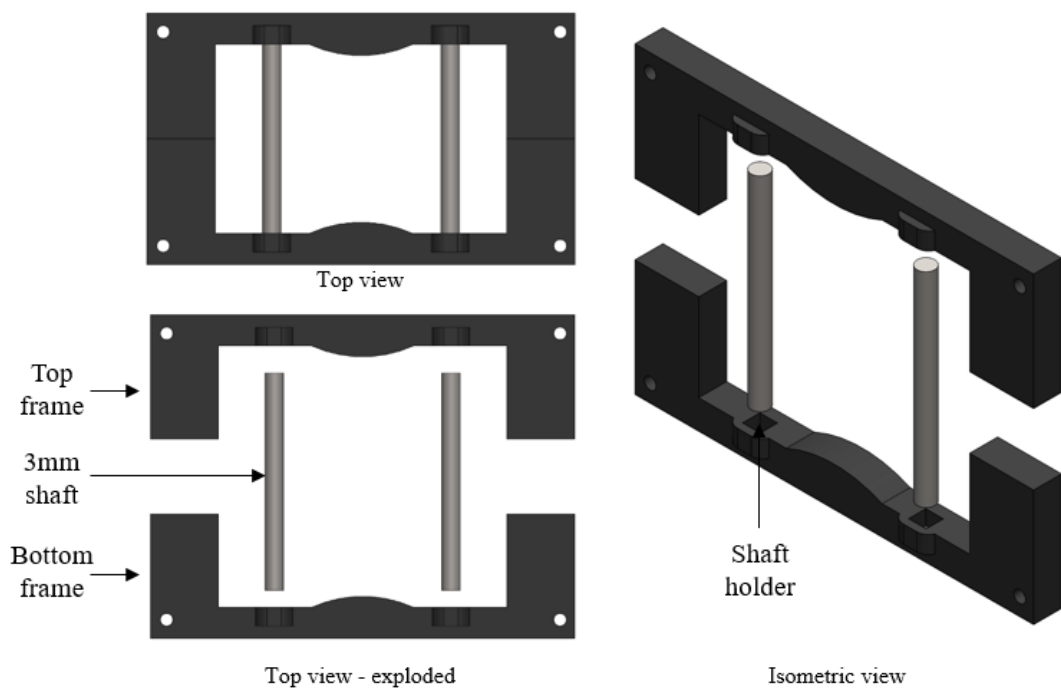
### 3.5.2 CAD Design and Prototyping

In this prototype, full 3D printing parts were used for the module assembly, apart from the off the shelf drive parts (motors, bushing, and shaft). The haptic plate retains similar multiple points stimuli configuration. As depicted in Figure 3.26, the revised haptic plate design has 15 mm × 45 mm footprint, compared to 15 mm × 97 mm in the previous design.



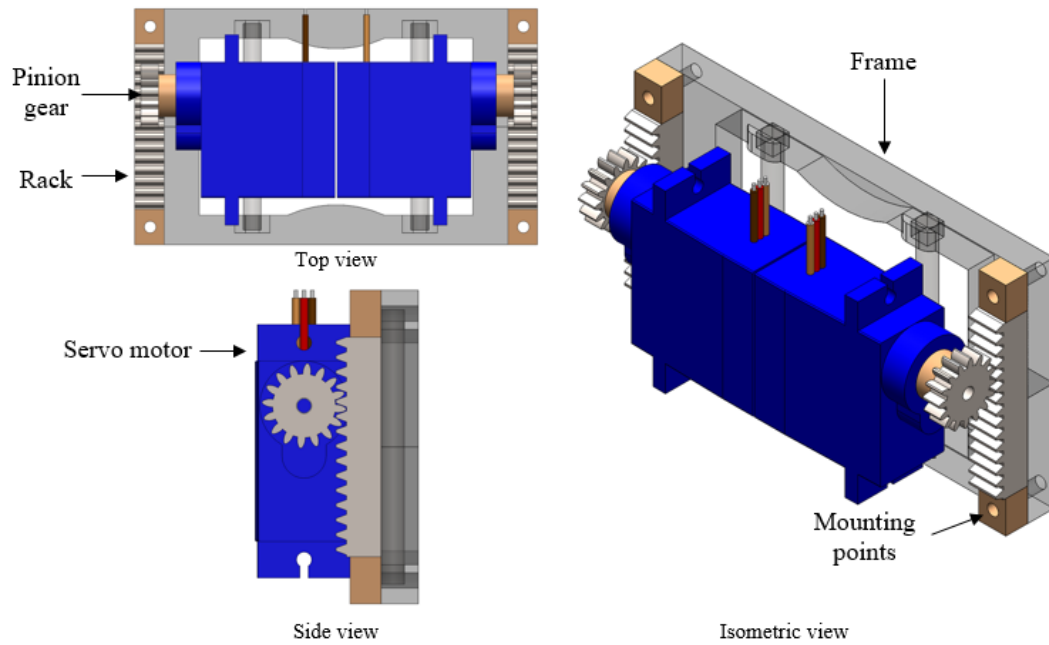
**Figure 3.26 Configuration of the new haptic plate**

The haptic frame as shown in Figure 3.27 consists of extruded rectangular frame split into top and bottom sections. A hollow exists on the inside part of both sections to allow the shaft to be positioned within the frame.



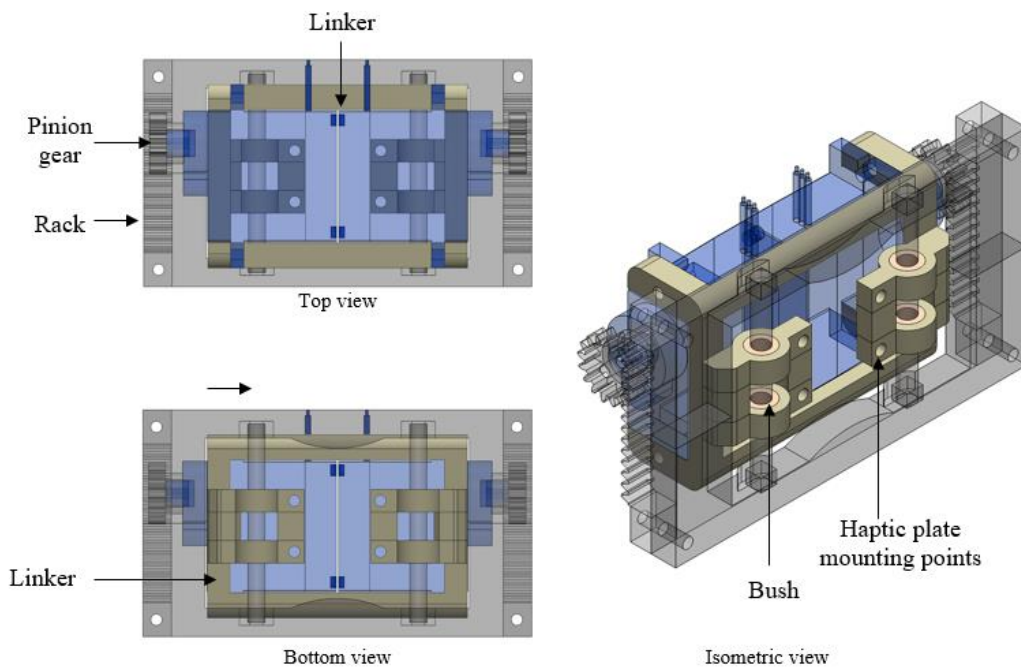
**Figure 3.27 Haptic frame assembly**

The drive assembly was also reduced in size albeit retaining the same mechanism, placement and orientation. The rack has mounting holes on its ends which was aligned to the hole on the frame. When bolted, this arrangement keeps the split frame in position (Figure 3.28).



**Figure 3.28 Drive assembly**

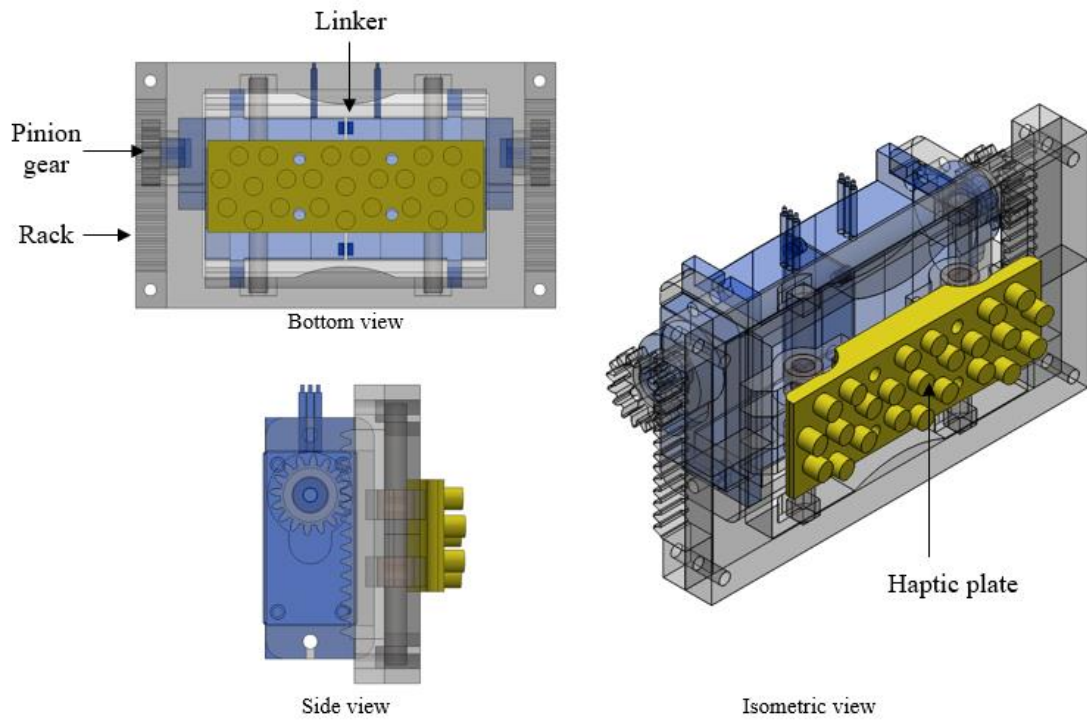
The linker frame spans in both directions in the revised design. On the upper part of the frame, the linker holds the servo motors (Figure 3.29).



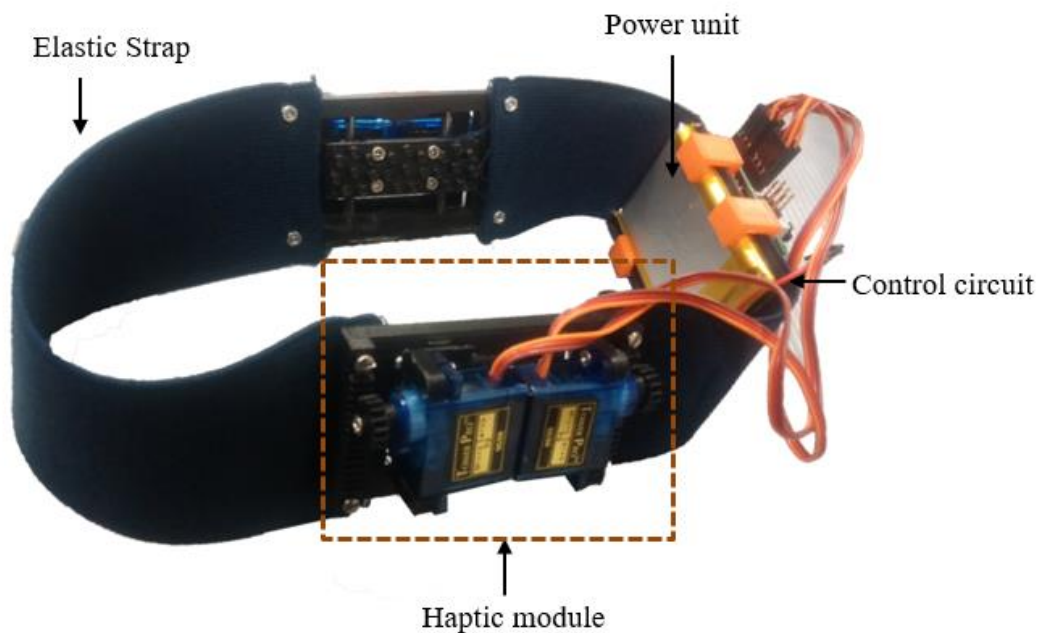
**Figure 3.29 Linker frame**

On the lower part, the linker frame has the mounting points for the haptic plate. Essentially, rather than placing the haptic plate on top of the motors, it was moved to

the bottom part of the frame (Figure 3.30). This way, the depth of the whole assembly is minimized. Figure 3.31 shows the assembled haptic feedback modules.



**Figure 3.30 The haptic plate**

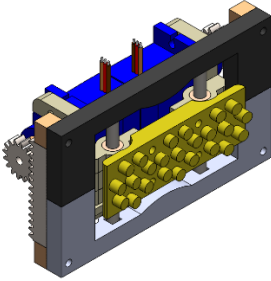
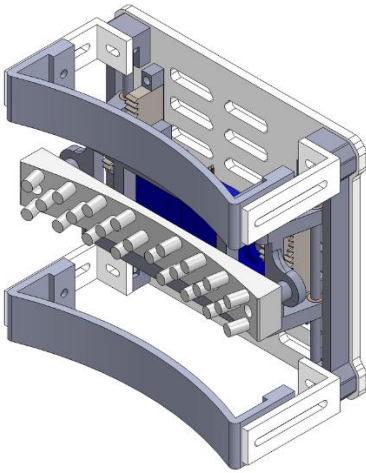


**Figure 3.31 Assembled haptic module**

Because of the significantly smaller footprint, the limb contact holder was not required for this design. Table 3.8 shows the comparison between the previous and the revised design.



**Table 3.8 Comparison of design parameters**

	Revised Version	Previous version
		
Weight	50 g	160 g
Dimension	69 mm (W) 40 mm (L) 28 mm (H)	98 mm (W) 90 mm (L) 50 mm (H)
Control Unit	Seperated	Attached on haptic module
Power Unit	Seperated	Attached on haptic module

### 3.6 Control and Power Unit

The design of electronics satisfied several significant functions to the haptic module:

- Providing control of the motor movement including setting the speed, travel distance and direction.
- Wireless communication between the module and the control computer, allowing instructions to be sent untethered.
- Regulating the voltage from the power unit, to allow using input from multiple power unit types.
- Providing necessary attachment socket for the user response switch which was used during experimental work.

The main component of the control circuitry is the microcontroller. A tiny (33mm × 23mm) wireless microcontroller (Moteino, Low Power Lab) was selected as the driver for the control circuitry. Moteino (Figure 3.32) was based on the widely-used open source microcontroller kit Arduino, with the advantage of having miniature package size and equipped with on board Radio Frequency (RF) transceiver, allowing two-way communications. In addition, embedding this microcontroller in the circuitry

meant that multiple sensors and actuators can be connected to its analog and digital pins for data acquisition and control purposes. A control program could be written and uploaded onto the microcontroller, eliminating the need for tethered operation.

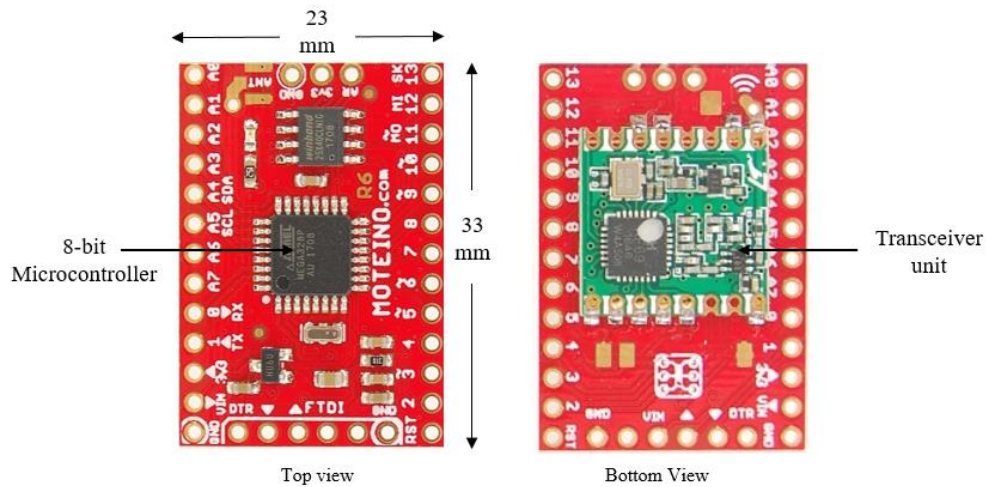


**Figure 3.32 Moteino microcontroller**

To allow portability, a power unit must be considered for the design circuitry and actuators. A rechargeable battery was the most sensible option, given that it can be used repeatedly and could hold decent amount of charge. A 3.7V Lithium-Polymer (Li-Po) battery was selected as the power unit. The battery has 2000 mAh capacity with built in overcharge and under-voltage protection. The most important feature of this battery was its small footprint- measuring just 60 mm x 42 mm, with the thickness of 6 mm and weight of 16g. Since the actuators and the microcontroller can both be powered with 5V voltage, it was necessary to add a voltage regulator into the circuit design to allow constant 5V DC voltage to be supplied throughout the operation. Figure 3.33 shows both units selected for the control unit.



**Figure 3.33 Left: battery unit. right: voltage regulator**

To allow user to give response acknowledging receiving the stimuli during experimental work (details in Chapter 5), handheld response switch shown in Figure 3.34 was designed and connected to the circuit board. Similarly, two versions of circuit boards were designed, each for the first iterative module and the revised module. The early version circuit board, shown in Figure 3.35(a) had additional motor driver boards to allow testing multiple actuators during actuator selection period. The revised circuit board (Figure 3.35(b)) focused on accommodating only the servo motors and had a modular ‘plug and play’ design to allow easy interface of actuators, power unit and the response switch.

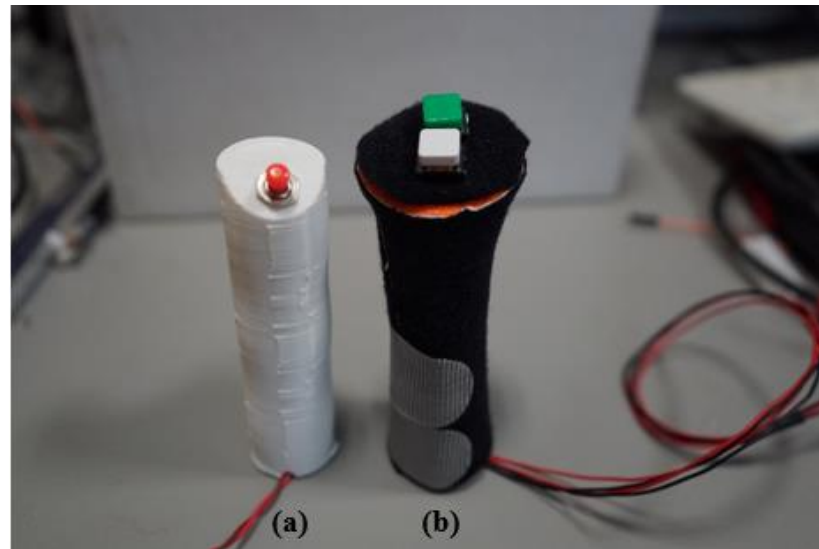


**Figure 3.34** Handheld response switch used in (a) first design (b) revised design

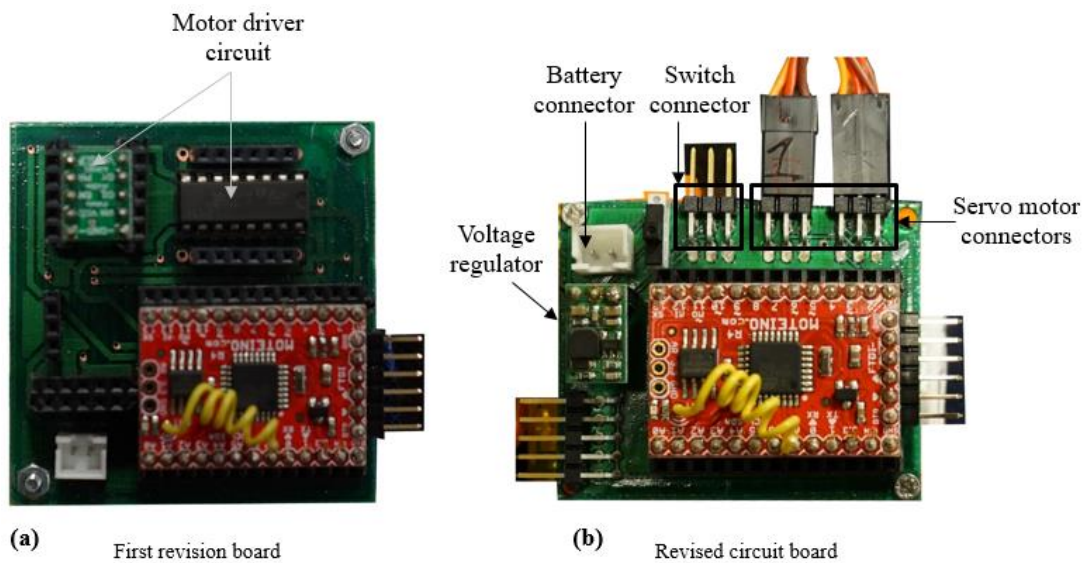


**Figure 3.35** Revisions of circuit board

Figure 3.36 shows the summary of the control scheme. The data recording was made on a PC running the Graphical User Interface to set required parameters for the haptic module. The data is then wirelessly sent to the haptic module via a Moteino transceiver. The handheld switch was connected to the control circuit and any response indicated by the user are sent back to the PC via the Moteino transceiver on the control unit. This scheme allows two-way communication and are also employed in the gait detection and analysis modules.

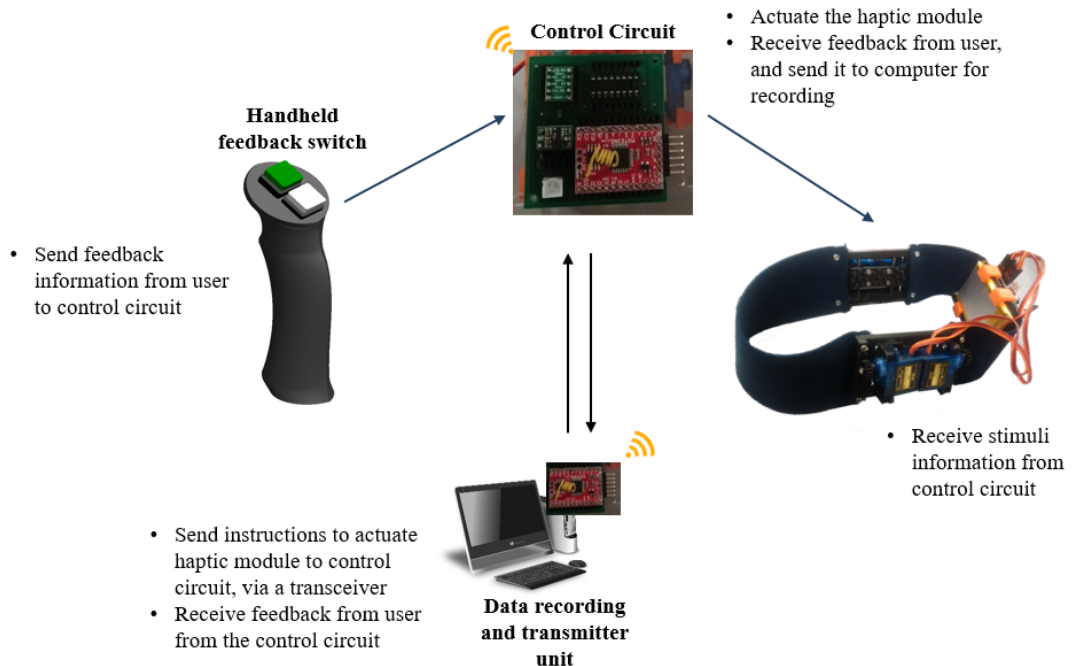


**Figure 3.36 Control unit scheme**

### 3.7 Summary

This chapter presented the design and development of the haptic module. An elementary design for skin-stretch was first introduced and evaluated and the results from the experimental work and observation aided in design of the subsequent modules. A skin-stretch method based on rack-and pinion mechanism was designed for the haptic module. The characterization of the design parameters was carried out to obtain the suitable stretch range that could be delivered by the module and to confirm that the module could deliver stimuli within reasonable duration. The next section will discuss the gait event detection module and complete integration of the haptic feedback system. In addition, development of gait measurement and analysis tool for experimental work will also be presented.

## **CHAPTER 4:**

# **Gait Event Detection and Analysis Modules**

### **4.1 Introduction**

This chapter reports the integration of gait event detection module into the haptic feedback system. As explained earlier in the thesis, the haptic feedback system consists of two main elements, namely the haptic module which delivers the feedback to the skin, and the event detection module which identifies the events during walking gait and sets the corresponding haptic module to be activated. The inertial measurement unit (IMU) based event module presented in the section has been developed in a previous work, however, improvement was made to the design and additional experimental validation and algorithm are presented. The second part of this chapter will discuss the development of an insole-based vertical ground reaction force (GRF) measurement system, for analysing vertical GRF data during the experimental work. The last part of the chapter will present the haptic feedback system integration, detailing the interface between various hardware and the graphical user interface designed for data acquisition and analysis.

### **4.2 Gait Event Detection**

Before proceeding further, it is worth reproducing the extract described in the beginning of the thesis regarding the framework of the haptic feedback system. The intended feedback scheme is shown in Figure 4.1. Two gait events, namely the Initial Contact (IC) and Toe-off (TO) were the events of interest to this scheme. Initial contact marks the beginning of stance phase, transitioning from swing phase. Successful IC depends on the ability to control both knee and ankle [135]. The TO, marks the beginning of the swing phase, when the foot is lifted off the ground and the whole limb is moved forward (limb advancement). Therefore, both the IC and TO gives indication of the positioning of the foot with respect to the ground, whether it is

in contact (stance) or not (swing). Delivering haptic stimuli which corresponds to these two events were the main objective of the haptic feedback system.

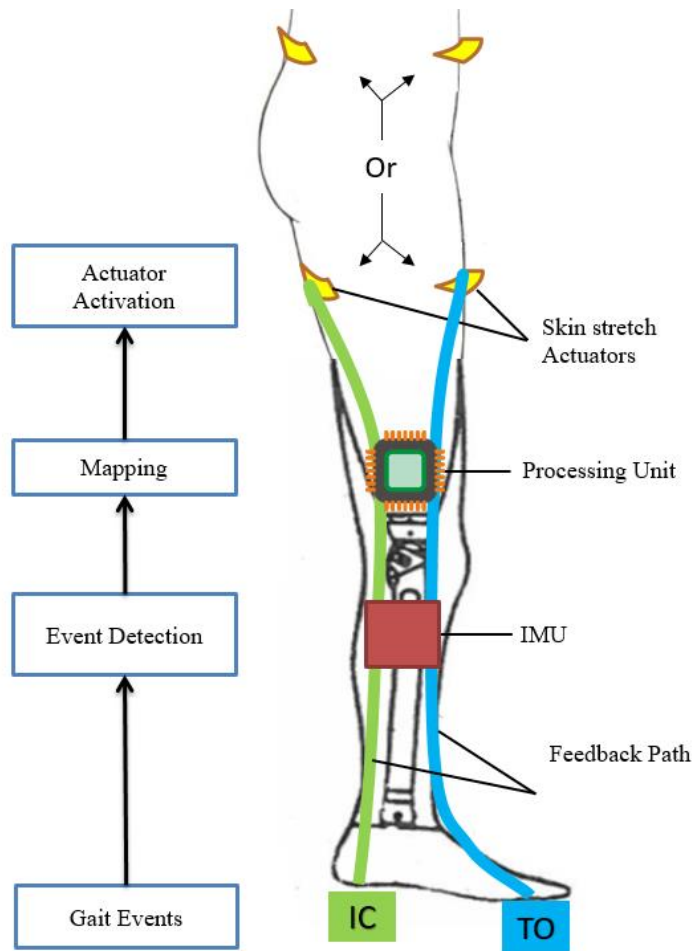


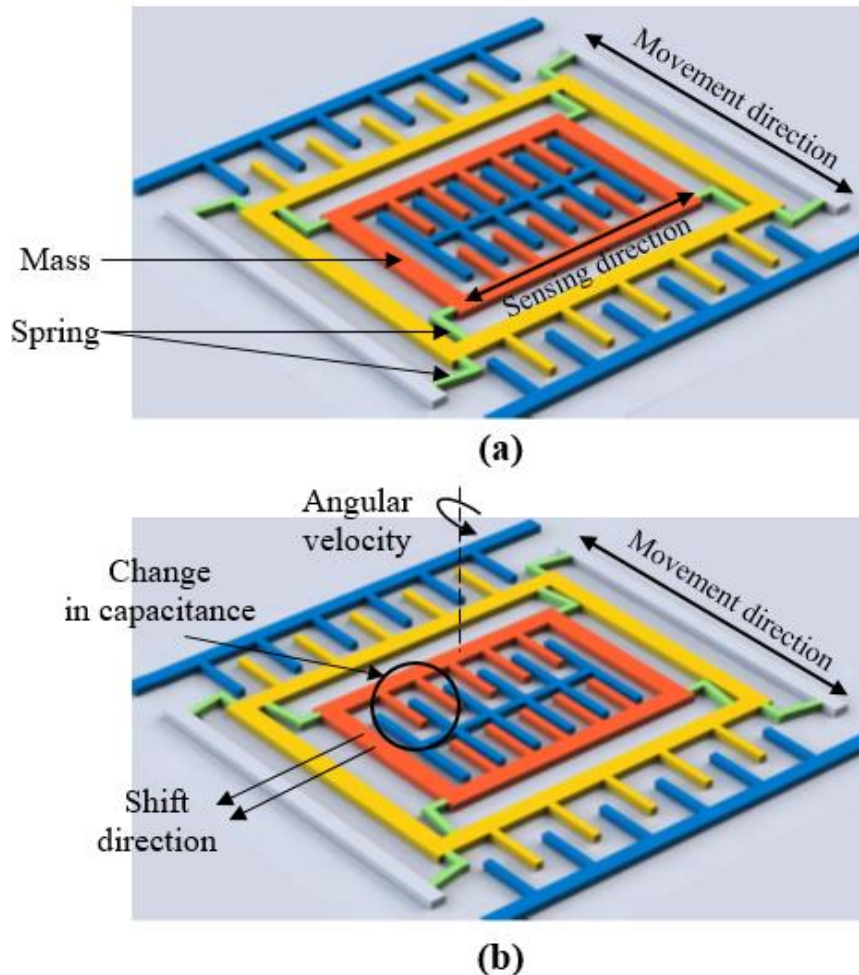
**Figure 4.1 Proposed scheme for haptic feedback system**

#### 4.2.1 Background

The event detection module presented in this section was initially designed in previous work [49, 136]. The system was based on a single gyroscope signal from an Inertial Measurement Unit (IMU) attached at shank. IMU is a generic term often used to describe the combination of different sensors such as gyroscope, accelerometer, and magnetometer into a single package. The focus of the following discussion is on the gyroscope sensor, whose output was utilised to quantify and classify gait event.

Gyroscope is a device that can measure the rate of change in angular movement (angular velocity). Consider the structure of a typical Microelectromechanical system (MEMS) based gyroscope shown in Figure 4.2(a). A mass attached to spring is constantly oscillating in the direction shown with the capacitance of the sensing elements determined by the distance between the mass and

capacitance comb structure (shown as the orange and blue comb). When an angular velocity is applied to the gyroscope unit, the mass is shifted perpendicular to its movement direction (also known as the Coriolis Effect), causing change in the capacitance of the sensing elements (Figure 4.2(b)). This change in capacitance is recorded and translated as the magnitude of the angular velocity applied.



#### 4.2.2 Hardware setup

A MEMS based IMU MPU-6050 chip (InvenSense, CA) was selected in the setup for the gait event detection module. MPU-6050 has 3-axis accelerometer and 3-axis gyroscope in a single chip. A breakout board of the MPU-6050, GY-521 board (Figure 4.3 (b)) was used to allow easy interfacing to the microcontroller and design of the circuit board. Since the footprint of the IMU board was small (21 mm × 16 mm), it can be virtually mounted anywhere in the body or embedded in devices and measurement tools. In this study, the IMU was mounted on the lateral side of the shank, with the z-axis of the IMU aligned with the tibia. The gyroscope signal of

interest for gait event detection was identified as the angular velocity of the shank along the medio-lateral axis which corresponds to the X-axis of the IMU when mounted at the shank as shown in Figure 4.3(b).

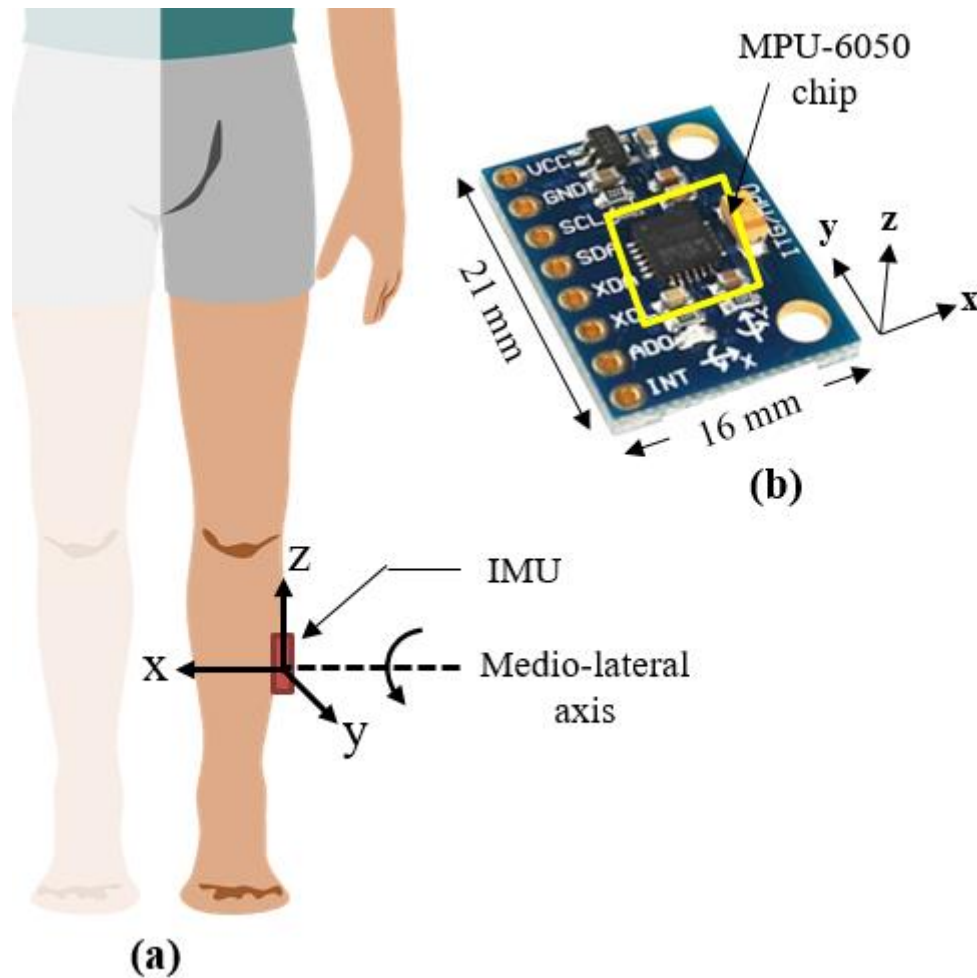


**Figure 4.3 (a) IMU attachment for obtaining gait event information (b) GY-521 IMU breakout board.**

The IMU uses the I<sup>2</sup>C protocol to transfer data and communicate with a microcontroller. Like the electronics unit for the haptic module, the IMU was interfaced to a wireless microcontroller (Moteino R4, LowPowerLab). A 5V voltage regulator was added to regulate the voltage from the battery for powering the microcontroller, while the IMU unit was run on 3.3V obtained from the microcontroller 3.3V output pin. For collecting full gait cycle parameters during experiments, it was necessary to have IMU fitted on each leg, therefore the circuit was designed to allow attachment of 2 IMUs. Since single Moteino microcontroller can accommodate two I<sup>2</sup>C devices on its I<sup>2</sup>C bus, there was no need for an additional microcontroller or circuitry for receiving data from 2 IMUs. This was achieved by



setting the ADO pin on the one IMU board to low (GND), and the other one to high (3.3V) while sharing the same I<sup>2</sup>C line. Figure 4.4 shows the schematics of the connection. It can be noted that both IMUs had similar connection to the microcontroller except for the logic level assigned to pin ADO, which allowed the microcontroller to identify two IMU device addresses.

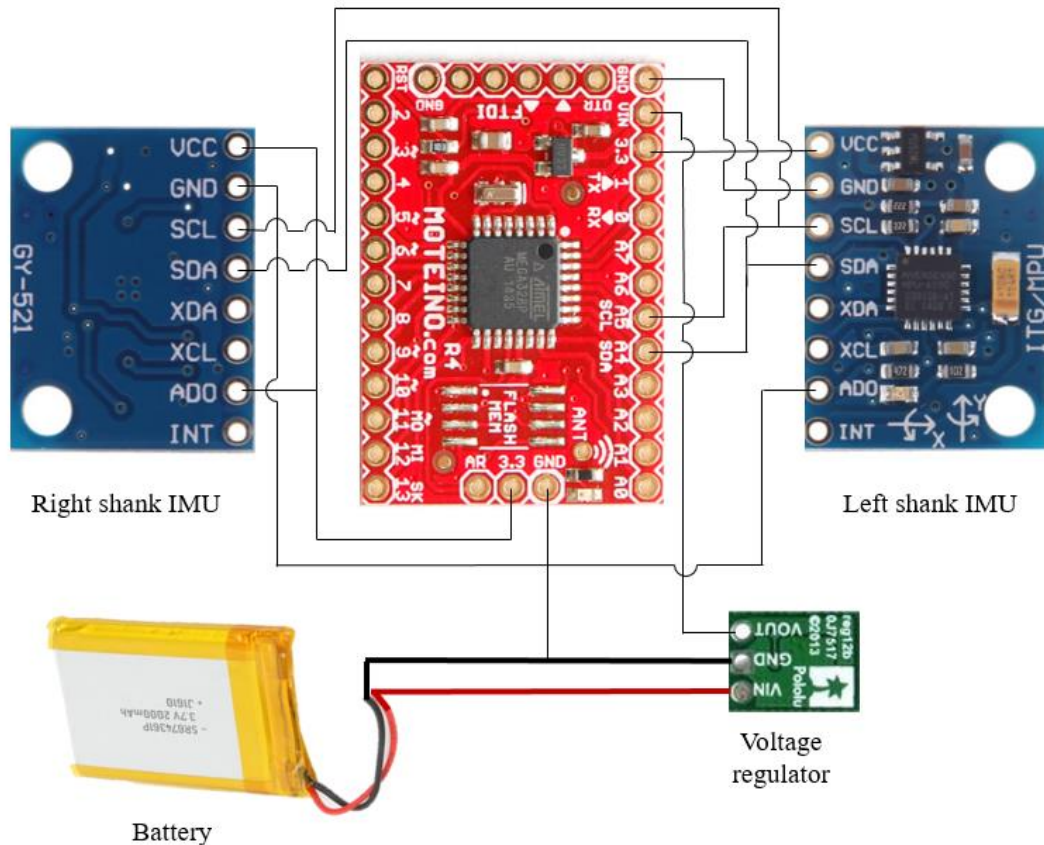


**Figure 4.4 Connection schematics.**

The initial design of the module from the previous work consisted of two attachments on the leg, the first one was the IMU holder, and the other one the circuitry and power unit (Figure 4.5(a)). The module has since been redesigned to a single attachment around the shank using a flexible strap that accommodates both the IMU holder and the power unit and circuitry (Figure 4.5(b)). The new setup reduced the weight and footprint of the gait event detection in the following ways:

- The use of 3D printed IMU holder in the new design as opposed to solid acrylic IMU holder in the previous design.
- Switching from using 2 AA battery to using rechargeable Lithium-Polymer battery reduced the weight and eliminated the need for battery holder, which further reduces the assembly size.

- Using single flexible strap to place both the IMU holder and the circuitry and power unit eliminated extra attachment for the module.

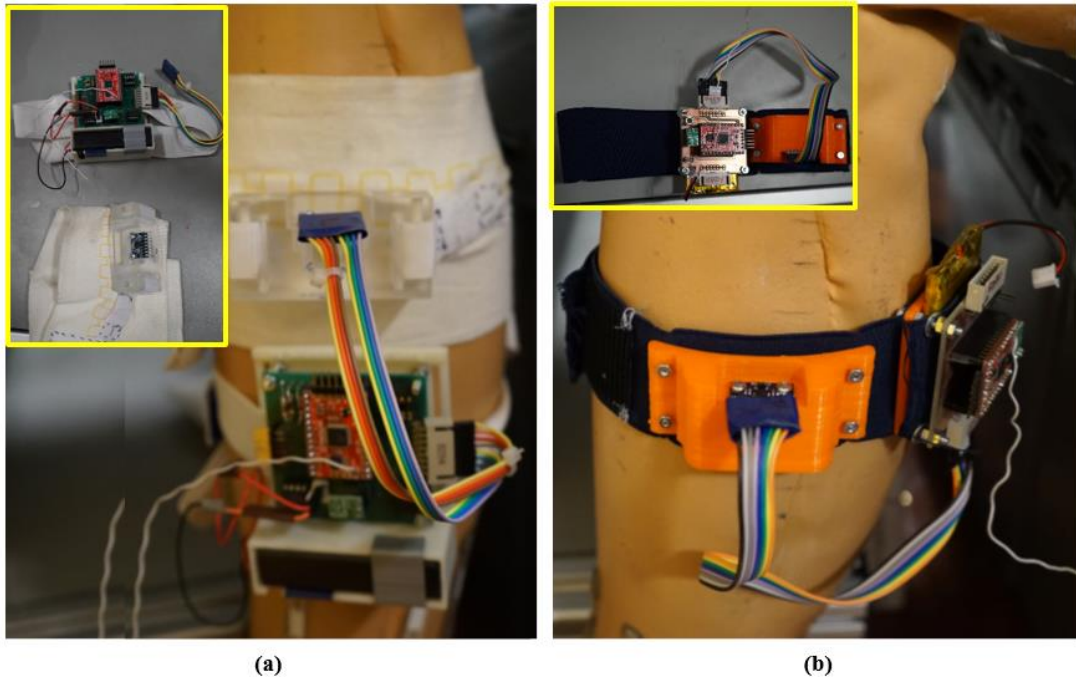


**Figure 4.5 Event detection modules (a) old modules with two attachments. (b) revised module single attachment and reduced footprint**

### 4.2.3 Detection Method

The method for event detection relied on the cyclic nature of the angular velocity pattern of the shank along the sagittal plane during walking. The findings and proposed algorithm are summarized here. Figure 4.6 shows a sample of the gyroscope signal characteristics obtained from walking activity described in Section 4.2.5. For each gait cycle, two negative peaks (minima) followed by a positive peak (maxima) can be observed in the shank angular velocity pattern. The first negative peak corresponds to the TO event, while the second negative peak corresponds to the IC. The positive peak following the second negative peak corresponds to the Mid-Swing (MSW) event. It can be observed that the magnitude of the positive peaks changes in between gait cycle (~60 deg/s difference). The advantage of having event detection using shank angular velocity signal, however, was that the characteristics of the signal (i.e the peaks) determines the event, rather than the magnitude of the signal. Therefore, given an appropriate threshold based algorithm, the method can

accommodate slight changes in the magnitude of the peaks without compromising the detection of the events.

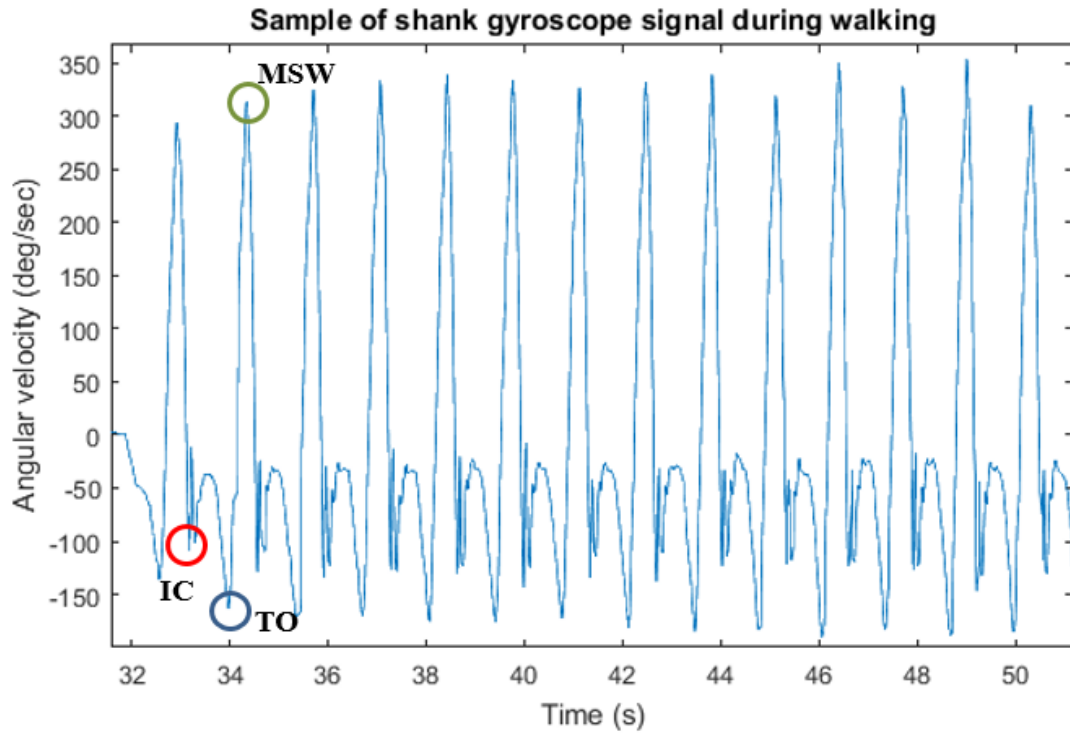


**Figure 4.6 Sample of shank angular velocity during walking**

A threshold based algorithm was proposed [136] to identify these events in real-time, by modifying the wavelet analysis method initially proposed by Aminian et al. [137]. The advantage of threshold based algorithm was that it allows the detection algorithm to be applied online which makes it suitable for controlling the haptic feedback module in real-time. In real-time data acquisition, the algorithm analysed the signal sample by sample by considering the following parameters:

$w_n$  = current angular velocity sample

$w_{n-1}$  = previous angular velocity sample

$D_n = w_n - w_{n-1}$  = difference between current and previous sample

$D_{n-1}$  = previous difference of angular velocity samples

The algorithm then determines whether an event would be identified using one or a combination of the following:

1. The magnitude of the  $w_n$
2. The sign of  $D_n$  and  $D_{n-1}$  whether it was positive or negative

3. A counter to skip/wait for N number of samples

The threshold value was determined experimentally from previous work [49, 136] and the algorithm is summarized as follows:

**MSW** The algorithm begins with the detection of MSW. Since there are two positive maxima in the signal, a maximum found when the angular velocity is greater than 80 degree/s threshold was defined as the MSW event. The conditions for this can be written as:

$$w_n > 80 \text{ degree/sec}$$

Which is the threshold of the angular velocity, and,

$$D_n < 0 \text{ and } D_{n-1} > 0$$

Which indicates a change of slope from positive to negative (a maxima)

**IC** After detection of the MSW, the IC event was identified as the first minima following the MSW. The following conditions must then be satisfied:

$$w_n < 0 \text{ degree/sec}$$

Because angular velocity during IC is in the negative region, and,

$$D_n > 0 \text{ and } D_{n-1} < 0$$

Which indicates a change from negative to a positive slope (a minima)

**TO** TO event was identified as the minima found after IC, and when the angular velocity is less than a threshold of -20 degree/s. Because of the presence of jitters that can contribute to false detection of the TO, a counter was activated in which the algorithm waits for 300 ms before marking the position of the TO. The conditions can be written as

$$w_n < -20 \text{ degree/sec}$$

Where -20 degree/sec was the TO threshold value, and,

$$D_n > 0 \text{ and } D_{n-1} < 0$$

Which indicates a change from negative to a positive slope (a minima), and,

$$Count = 300ms$$

Where 300 ms has elapsed since the detection of the IC.

#### 4.2.4 Experimental Validation

To validate the proposed algorithm and investigate the reliability of the signal acquired through the IMU, an experimental work was carried out.

**Method** Two healthy male subjects (S1 - age: 30 years old; height: 172 cm; weight: 67 kg and S2 - age: 25 years old; height: 173 cm; weight: 68 kg) with no apparent gait abnormalities participated in the study. The event detection module was fitted on the lateral side of the shank on both legs and subjects were asked to walk on a treadmill at self-selected slow, normal and fast walk. For each walking mode, the treadmill speed was adjusted until the subjects indicated comfortable ambulation on the specified speed. At least 15 complete gait cycles were obtained from each walking mode for each subject. Two active infrared markers were fitted using Velcro tape along the lateral side of the left shank, one on lateral calcaneus and one on the great toe. A motion tracking system (Visualeyez III, Phoenix Technologies Inc., Canada) captured the marker position at 60 Hz frame rate. The marker and IMU placement for the setup is shown in Figure 4.7.

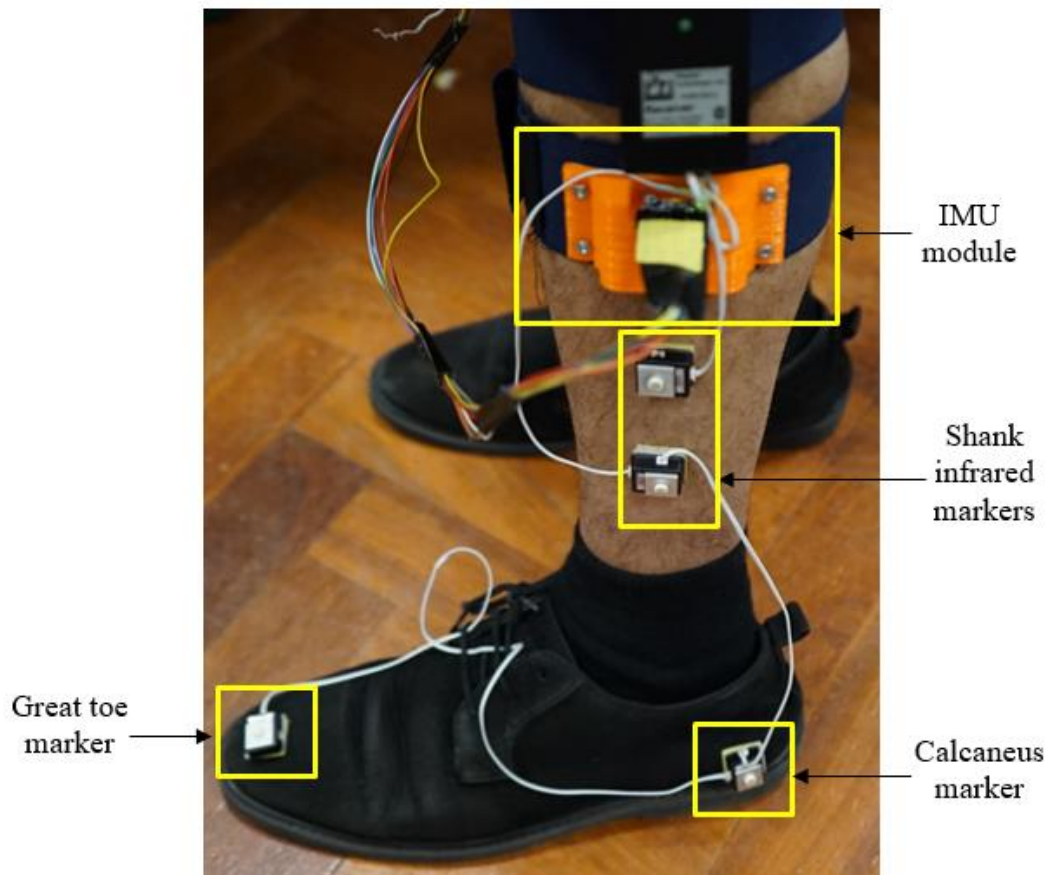


**Figure 4.7** Placement of IMU and motion capture markers on shank and foot

**Analysis** Both IMU and motion capture data were filtered with 2<sup>nd</sup> order Butterworth filter with 10 Hz cut-off frequency. Identification of gait events using motion capture system was carried out using protocol mentioned in [138] in which the IC was defined as the first instance where the calcaneus markers stopped moving forward while TO was defined as the first instance where the great toe marker starts to move forward. Figure 4.8 shows a sample of position plot for both markers in the anterior-posterior direction. (x-axis of the motion capture system reference frame). Forward movement of the markers was indicated as the negative slope (markers approaching origin) and reverse movement as the positive slope. Therefore, in the position vs time plot, IC was defined as the minimum point of the calcaneus marker plot and TO was defined as the maximum point in the great toe marker plot.

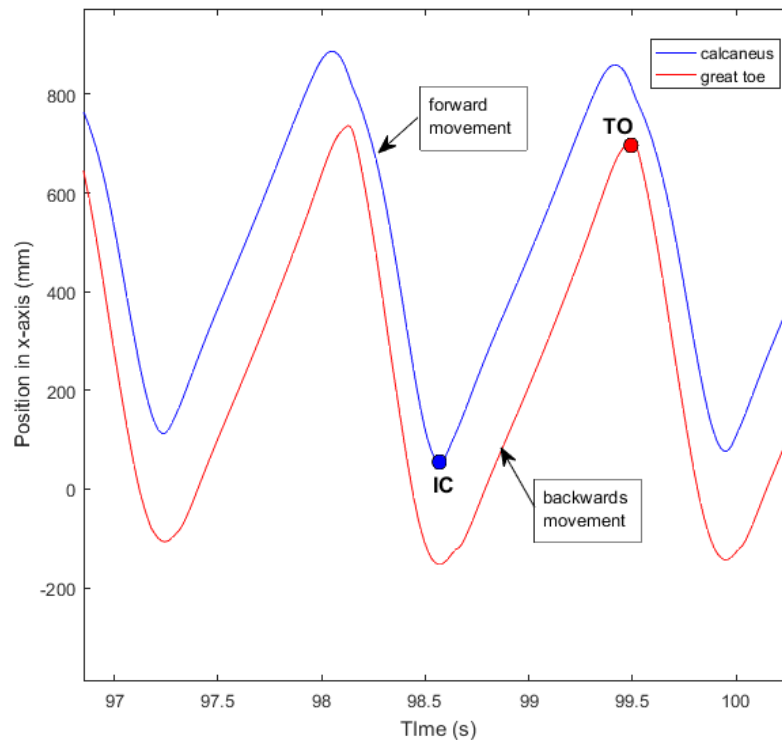


**Figure 4.8 Calcaneus and toe marker positions in anterior-posterior direction**

The markers at the shank were used to calculate the angular velocity of the shank and compared to the angular velocity data gathered from the IMU. Given a top marker with coordinate of  $(x_1, y_1)$  and a bottom marker with coordinate of  $(x_2, y_2)$  as depicted in Figure 4.9, the shank angle  $\theta_s$  at any time  $t$  can be calculated as:

$$\theta_s(\text{rad}) = \tan^{-1} \frac{y_1 - y_2}{x_1 - x_2} \quad (4.1)$$

Where

$$\theta_s(\text{degree}) = \begin{cases} \theta_s(\text{rad}) \frac{180^\circ}{\pi} & \theta_s(\text{rad}) > 0 \\ \theta_s(\text{rad}) \frac{180^\circ}{\pi} + 180^\circ & \theta_s(\text{rad}) < 0 \end{cases} \quad (4.2)$$

Subsequently the angular velocity of the shank can be obtained by differentiating the angular velocity over time:

$$\omega_s = \frac{d\theta_s}{dt} \quad (4.3)$$

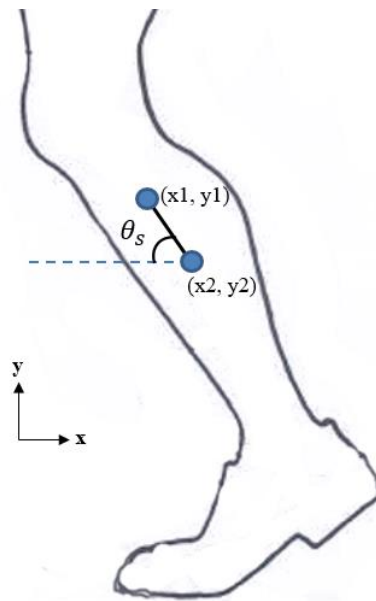


**Figure 4.9 Marker placement on the x-y coordinate system**

Identification of gait events using IMU was carried out using the algorithm presented in section 4.2.3. Correlation coefficient between the two angular velocity signals were calculated. Average timing difference between IC and TO detected by both systems were calculated for 15 events.

**Results and discussion** The self-selected speed for slow, normal and fast walk for both subjects are indicated in Table 4.1. Figure 4.10 and Figure 4.11 show the comparison between angular velocity data acquired using motion capture system and the IMU for both subjects for 15 gait cycles.

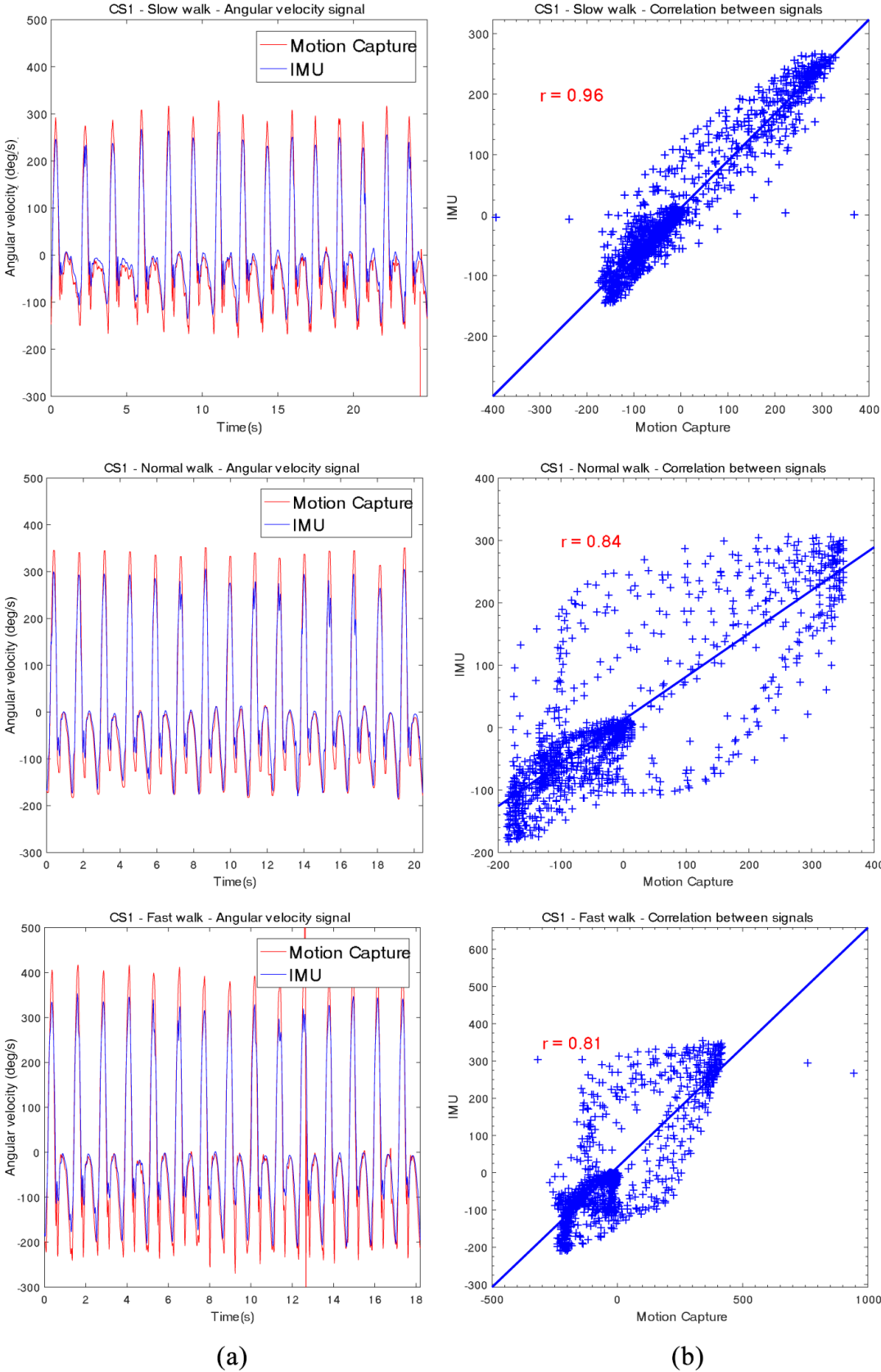


**Figure 4.10 (a) Shank angular velocity from motion capture data and IMU from CS1. (b) Correlation plot between the signals.**



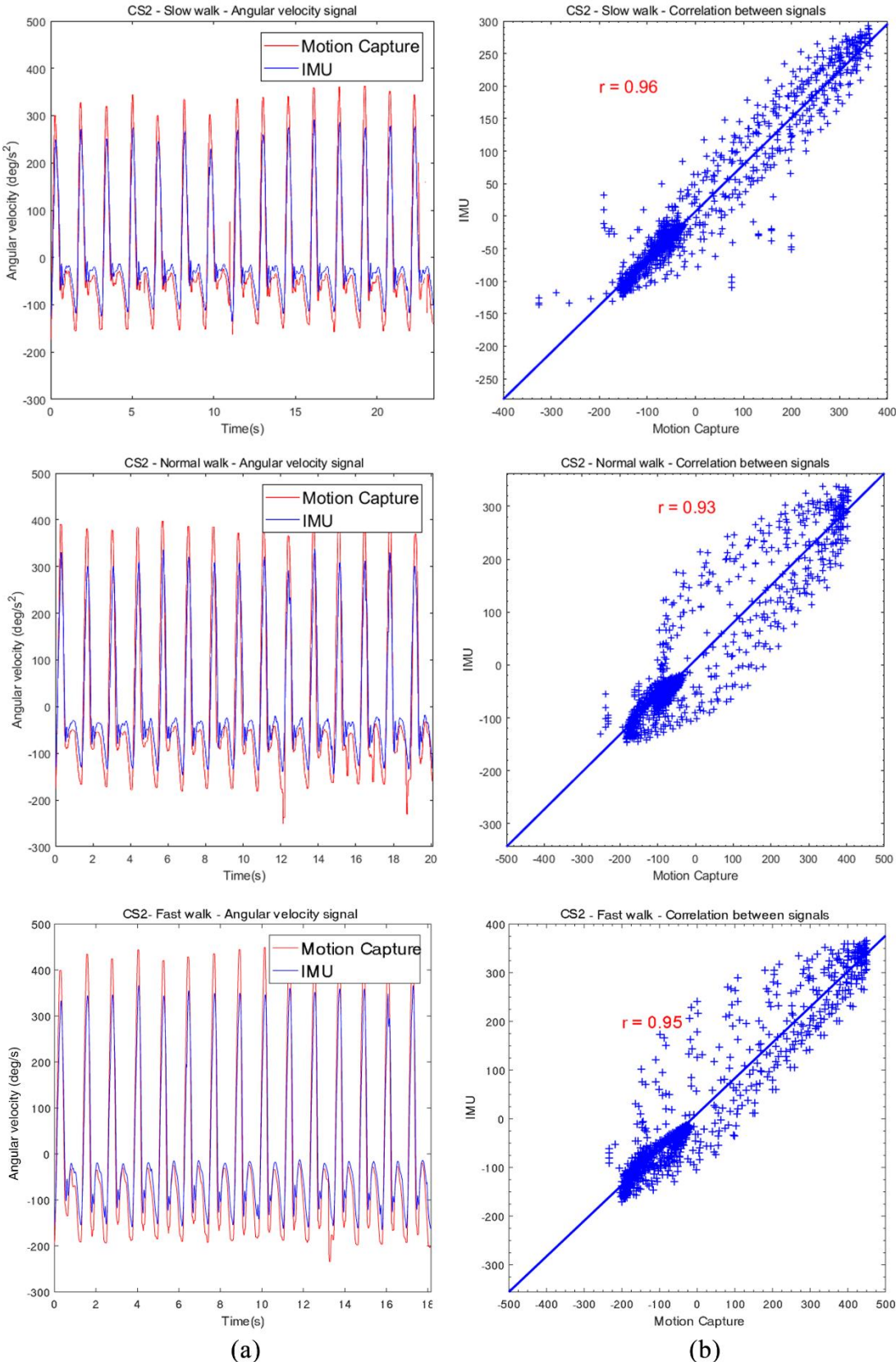


**Figure 4.11 (a) Shank angular velocity from motion capture data and IMU from CS2. (b) Correlation plot between the signals.**

The angular velocity data from both IMU and motion capture can be observed to show similar pattern, confirming to those described in [137]. However, the magnitude of the peak during MSW can be observed to be higher in motion capture data. High correlation coefficient ( $r > 0.81$  for CS1 and  $r > 0.93$  for CS2) was found for the signals, indicating the validity of using the shank signal for event detection purpose. Figure 4.12 shows a sample of detected events in slow walk for S1. It can be observed that the presented IMU algorithm was capable of detecting all IC and TO events throughout the gait cycles. Similar observation was noted with all the signal samples collected from both subjects. In addition, the algorithm detected IC slightly delayed in comparison to the detection performed using the motion capture system, while the TO was detected earlier. Both observations were in agreement with a previous work [49] in which foot-switch was used to investigate the timing accuracy of the gait events.

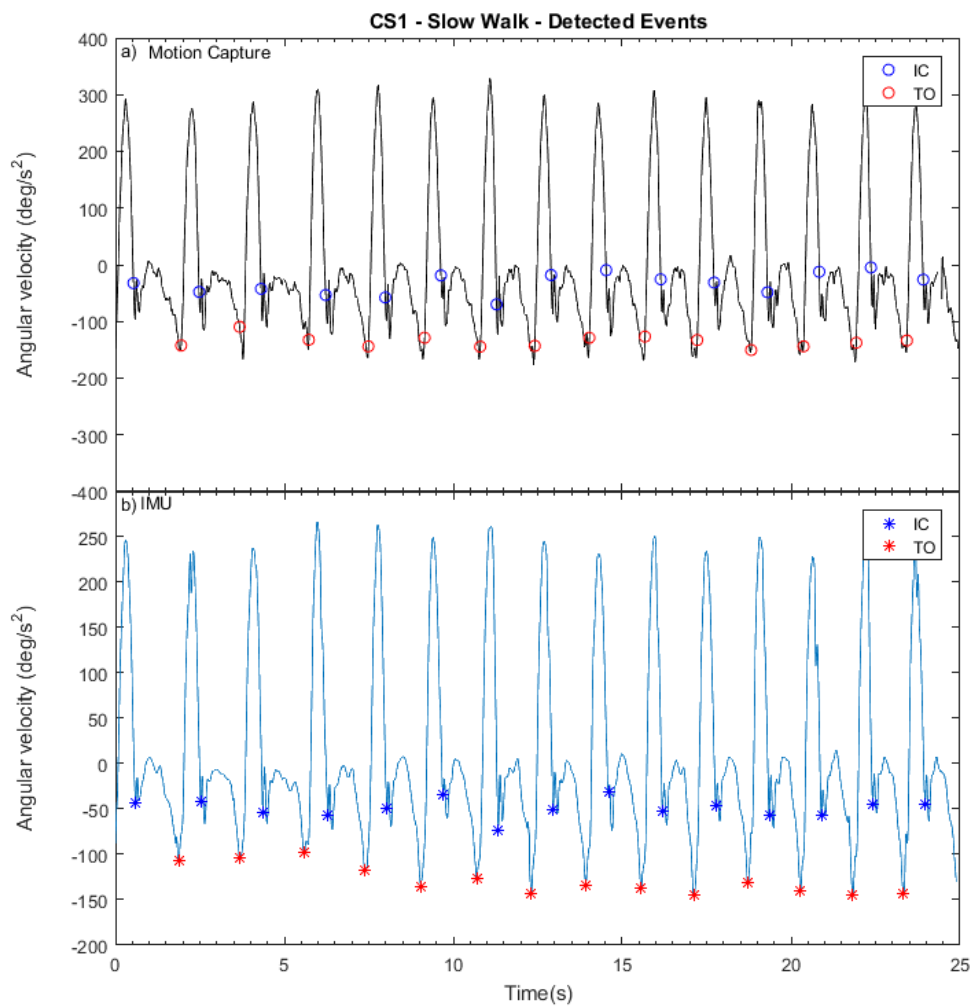


**Figure 4.12** Sample of detected events from (a) motion capture and (b) IMU.

However, the average timing difference of TO and IC events between the motion capture system and the IMU was found to lie within  $\pm 100$  ms as shown in Table 4.1. This value is higher than the timing difference between IMU events and foot switch system from [49] which was determined to be within  $\pm 50$  ms range for control subjects. This was most likely because the markers on the calcaneus and great toe (the two markers used as reference data for motion capture event detection) were positioned on the subject's shoe and therefore were prone to shifting in position during walking. This can also be observed from Figure 4.12 where detection of events using IMU algorithm showed a more consistent behaviour in comparison to the motion capture algorithm.

**Table 4.1 Mean  $\pm$  SD difference in timing of detected events using the IMU algorithm in comparison to motion capture data. Positive value indicates delayed detection while negative values indicates early detection.**

		Timing difference (ms)			
		IC		TO	
		CS1	CS2	CS1	CS2
Walking speed	<b>Slow</b> S1: 2.3 km/h S2: 2.0 km/h	59 $\pm$ 9	90 $\pm$ 9	-92 $\pm$ 36	-49 $\pm$ 8
	<b>Normal</b> S1: 3.2 km/h S2: 3.1 km/h	76 $\pm$ 8	64 $\pm$ 8	-77 $\pm$ 10	-30 $\pm$ 103
	<b>Fast</b> S1: 4.0 km/h S2: 3.9 km/h	53 $\pm$ 25	67 $\pm$ 9	-85 $\pm$ 11	-29 $\pm$ 12

The data collected by the IMU was not free from noise and artefact, most likely due to vibrations produced during walking (especially during IC) and the slight movement of the IMU sensor due to intense muscle contraction. Since the algorithm presented utilizes peak detection method (maxima and minima), the presence of these noise can create inaccuracies in the algorithm, where presence of additional peaks in between the expected signal characteristics can create false identification of the events. Filtering the signal in real-time, however, will introduce delay to the system. The amount of delays depends on the filter order and the cut-off frequency chosen for the signal. The angular velocity signal throughout the experimental work described in this thesis was filtered with a 2<sup>nd</sup> order Butterworth filter with cut-off frequency of 10 Hz, which was determined to be the most suitable for the system [49].

#### 4.2.5 Predictive Algorithm for Feedback

In real-time application, the presented detection algorithm was successful in identifying IC and TO around the time the event happens ( $\pm 50$  ms according to [49]). For control application however, it might be necessary to deliver the feedback earlier or later than the detected IC and TO event. One advantage of this was that the timing of the feedback can be adjusted according to the walking pattern, thus accommodating wide range of gait patterns. Also, since the haptic feedback was intended to create awareness of the foot placement with respect to the ground while walking, it was deemed sensible to allow flexibility around the timing of the delivery of the feedback.

To allow this functionality, a predictive algorithm was introduced in conjunction with the detection algorithm. The framework of the predictive algorithm alters the conventional feedback method where feedback was given based on the detected events. Rather, the algorithm ‘learns’ the timing information from the initial few IC and TO events and delivers the stimuli based on the timing information. Specifically, the algorithm works by calculating in real-time the average time difference between specified number of previous consecutive IC or TO events. Consider the following parameters:

$N$	=	number of selected events
$ICt$	=	Time index of previous IC event
$TOt$	=	Time index of previous TO event
$IC_A$	=	Average time difference between consecutive IC events
$TO_A$	=	Average time difference between consecutive TO events
$ICp$	=	Time index of predicted IC event
$TOp$	=	Time index of predicted TO event
$ICm$	=	Time index of manipulated IC event
$TOm$	=	Time index of manipulated TO event
$T_M$	=	Time constant for feedback manipulation

The predictive algorithm can be implemented in the following steps:

1. Specify  $N$ . The value of  $N$  determines the number of events that are used to average the time difference. Selecting larger number of  $N$  can reduce the error

in calculating the average time difference, however it also means that the system is less sensitive to change because more number of events (which means longer time) are required to initiate the computation.

2. For a selected number of the  $N$ ,  $IC_A$  can be calculated as follows:

$$IC_A = \frac{(\sum_{n=1}^{N-1} ICt_{n+1} - ICt_n)}{N} \quad (4.4)$$

Similarly,  $TO_A$  can be calculated as:

$$TO_A = \frac{(\sum_{n=1}^{N-1} TOt_{n+1} - TOt_n)}{N} \quad (4.5)$$

3. Since  $IC_A$  and  $TO_A$  have been obtained, the predicted future IC and TO can be estimated as follows:

$$ICp_i = ICt_{N+i-1} + IC_A \quad (4.6)$$

and

$$TOp_i = TOt_{N+i-1} + TO_A \quad (4.7)$$

4. Manipulation to the timing of the feedback delivery can be made by introducing the time constant  $T_M$  to the predicted IC and TO time.

$$ICm_i = ICp_i + T_M \quad (4.8)$$

and

$$TOM_i = TOP_i + T_M \quad (4.9)$$

The delivered feedback could be delayed if  $T_M$  is positive and could be advanced if  $T_M$  is negative.

The predictive algorithm might be useful when combined with targeted feedback delivery. For example, rather than delivering the feedback exactly when IC and TO events happen, the feedback could be delivered in other gait phases by manipulating the timing of  $T_M$ .

### 4.3 Plantar Force Insole

Measuring plantar (foot) data while walking can give a lot of insight into the walking pattern. This section describes a foot plantar insole designed to measure the vertical ground reaction force (vGRF) during experimental work with amputee described in Appendix A. Although it does not constitute as a part of the final haptic feedback system, a portable plantar measurement system is desirable for data gathering outside gait laboratory environment. In addition, wearable plantar sensor can provide continuous monitoring of foot-ground data rather than a single-step data obtained

from force platform measurements. Specifically, two vGRF parameters, the loading rate and the push off rate, which depend on the timing of the peaks generally observed in vGRF signals are to be obtained during the experimental work.

The placement of the sensors on the foot is first discussed, followed by the description of a sensorized force insole design. Calibration of the sensor and the validation against the force platform data were carried out to assess the usability of the design.

### 4.3.1 Sensor Placement

Work in literatures shows variability in location of pressure sensor placement at the foot, as summarized in Table 4.2. Among the early works was by Soames [139] who suggested a placement of sensors in 15 weight-bearing locations to measure foot pressure patterns during gait using strain gauges, as depicted in Figure 4.13(a). The author divided the area into medial and lateral heel, (1-3), the midfoot region (4, 5), the fifth to first metatarsal head (6-10) and the fifth to first toe (11-15).

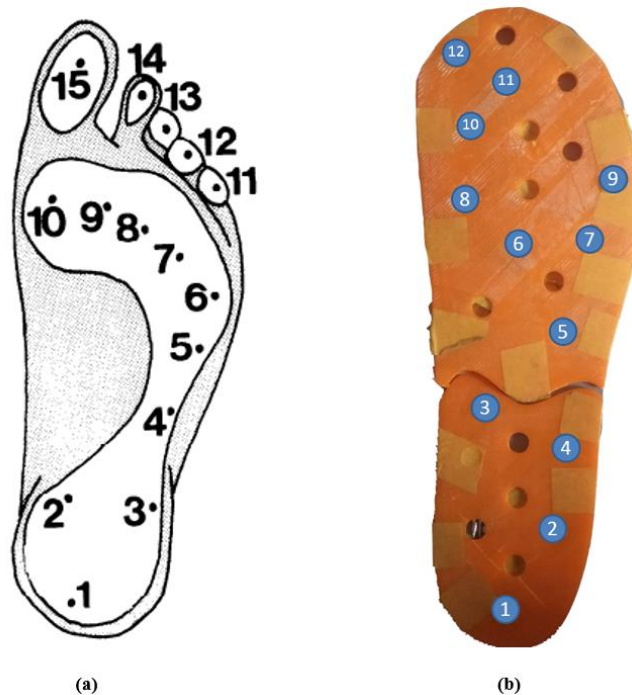


**Figure 4.13 (a) Sensor attachment sites suggested by Soames [139] and (b) sensor placement location adopted in the insole design.**

Fan et al. [16] noted that significant weight bearing area for locomotion are consistently the hallux, the central heel and the first, second and fifth metatarsal heads. Rajala et al. [140] in a review on plantar shear stress measurements also indicated that

the hallux, fifth metatarsal and heel as being the most common location of sensor placement recorded in the literatures. Shu et al. [141], while presenting an in-shoe pressure measurement system using fabric textile pressure sensing suggested that six sensors across the heel and metatarsal position are adequate for sports and fitness assessments. Table 4.2 shows various foot plantar sensing design presented in literatures, with the numbers of sensors used and their respective placement locations.

**Table 4.2 Force sensing methods and sensor locations described in literatures.  
Adapted from [142]**

No. of Sensors	Sensor Locations	Reference
5	Heel, 1 <sup>st</sup> , 2 <sup>nd</sup> , 5 <sup>th</sup> metatarsal head, great toe	[143]
8	Hallux, midfoot, medial heel and lateral heel and 4 on the forefoot	[144]
6	Center, lateral and medial heel, 1 <sup>st</sup> 2 <sup>nd</sup> , and 5 <sup>th</sup> metatarsal head	[141]
5	Heel, great toe, 1 <sup>st</sup> 2 <sup>nd</sup> , and 5 <sup>th</sup> metatarsal head, lateral forefoot	[145]
5	Great toe, metatarsal heads, medial and lateral heel	[146]
3	Heel, 1 <sup>st</sup> and 5 <sup>th</sup> metatarsal head	[147]
7	Heel, lateral midfoot, great toe, head of the first metatarsal, center midfoot, lateral forefoot and center forefoot	[148]
64	All over the foot	[50]
4	1 <sup>st</sup> metatarsal head, between 4 <sup>th</sup> and 5 <sup>th</sup> metatarsal heads, heel	[149]
8	Heel, along arch of foot, big toe	[150]

Based on the placement suggested by Soames [139] and the sensor placement studied from the review, an insole with 12 force sensors was designed for obtaining plantar force data during walking. The sensors are placed across the heel, lateral midfoot, metatarsal heads and great toe region (Figure 4.13(b)). The number of sensors selected was enough to cover significant weight-bearing area on the foot, and are reasonable for fabrication and embedding into a 3D printed insole.

### **4.3.2 Hardware**

This section will describe the fabrication of the insole, starting with the selection of the force sensors, followed by insole design and the underlying electronics circuit for untethered operation.

#### **4.3.2.1 Sensor**

A flexible piezoresistive based sensor was used to fabricate the instrumented insole. FlexiForce A201 (Tekscan Inc.) 100lb sensor is a thin (0.008 in.) flexible printed circuit consisting of a conductive material (silver) and a pressure sensitive ink layer bonded together. In the absence of load, the sensor has a very high resistance ( $> 5 \text{ M}\Omega$ ) and when force is applied, the resistance of the sensor decreases. A relationship can be established between the applied force and the sensor output by passing current through the sensor and measuring the change in voltage value across varied force loading. A linear relationship between force applied and the output voltage is expected.

#### **4.3.2.2 Insole Fabrication**

The insole for attaching the force sensors was designed in 3D CAD program and fabricated using a 3D printer. The insole was designed based on a standard foot shape so that it can be easily inserted into shoes. Figure 4.14 shows the design of the force insole. To ensure fitting into different shoe sizes, the insole was split into two parts, along the belly of mid-foot region, since this region has least weight bearing function during locomotion. Two 1 mm thick layers of insole were printed with multiple holes for marking the sensor placement sites. FlexiForce sensors were placed in between the layers on the specified placement location, and on top of each force insole, a puck was placed to allow concentrating the force into the sensing area as recommended by the manufacturer [151]. The thickness of the insole layer was chosen such that it allowed the insole to be easily trimmed if needed and allowed it to be flexed while inside the shoe. To protect the 3D printed sensor housing from breaking and to avoid damage to the sensors, vinyl tape was used to cover the insole during experimental work.



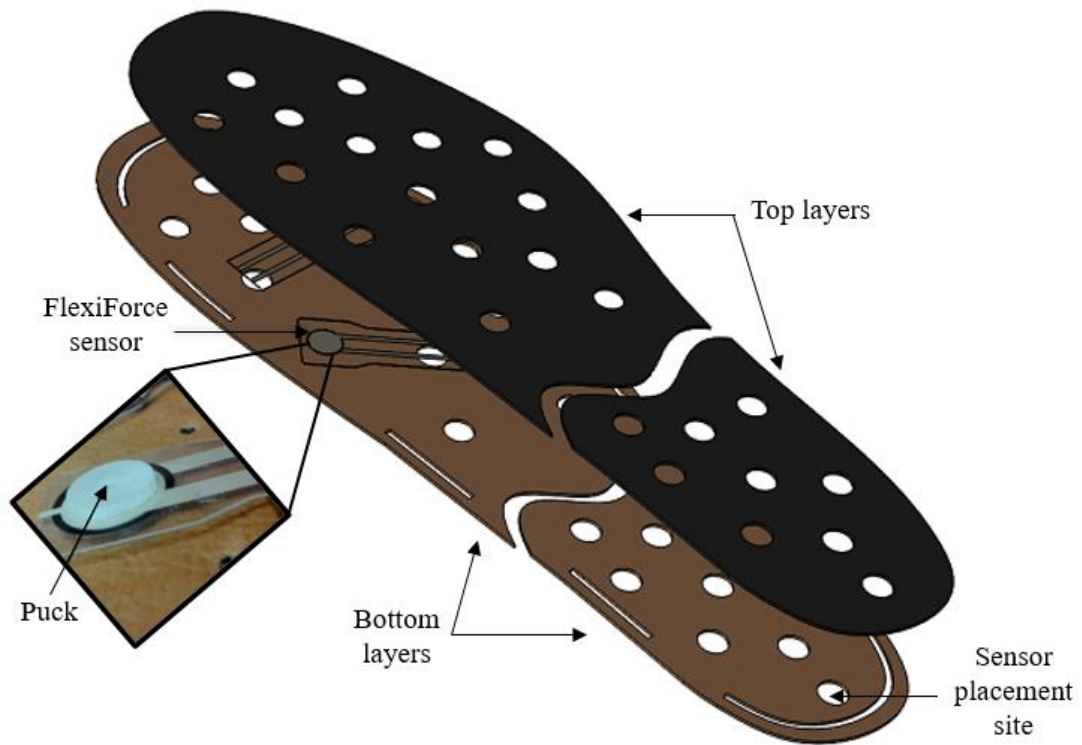


**Figure 4.14 Design of the 3D printed insole**

#### 4.3.2.3 Electronics

**Signal Conditioning** Figure 4.15 shows the manufacturer's recommended conditioning circuit for interfacing the force sensors. This circuit uses an operational linear amplifier (op-amp) MCP6004 (Microchip Technology Inc.) to provide a linear voltage output in the range of 0-5V.

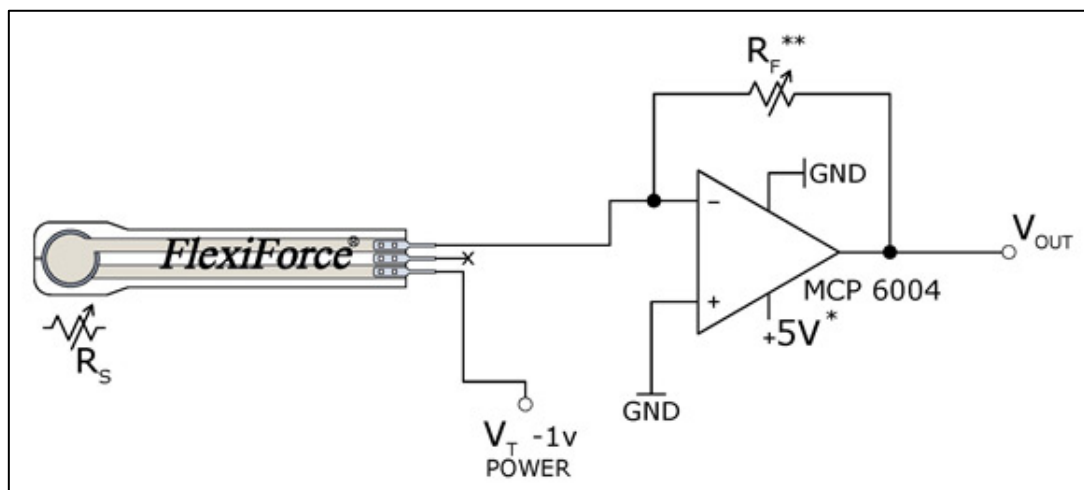


**Figure 4.15 FlexiForce recommended circuit from [151]**

Assuming ideal characteristics of op-amp, the circuit output equation can be described as follows:

$$V_{OUT} = -V_T \frac{R_F}{R_S} \quad (4.10)$$

As previously described, in no-load condition, the value of  $R_S$  is very large ( $> 5 \text{ M}\Omega$ ), Thus

$$\frac{R_F}{R_S} \approx 0, \quad V_{OUT} = -V_T (0) \quad (4.11)$$

therefore,

$$V_{OUT} \approx 0$$

Since  $R_F$  was selected to be the resistance value of the force sensor when it is subjected to full load, upon applying the load,  $R_S$  value drops and at full load,

$$R_S \approx R_F ,$$

so

that

$$V_{OUT} \approx -V_T (1) \quad (4.12)$$

and since  $V_T$  is a negative voltage,

$$V_{OUT} \approx V_T$$

This configuration gives the output swing of  $0 - V_T$  for no load to full load condition of the force sensors. By replacing the resistor  $R_F$  shown in Figure 4.15 with a variable resistor, the range and sensitivity of the force sensor can be adjusted during calibration of the insole. Since the default sensing range of the force sensor was only 100lbs, necessary adjustment was made to the signal conditioning circuit circuit, which will allow for increase in its dynamic range. As recommended by the manufacturer, the dynamic range can be increased by either decreasing the  $V_T$  value or increasing the  $R_F$ . In this design, a positive to negative voltage convertor was used to supply -5V as the FlexiForce input  $V_T$ . By driving the  $V_T$  at this low value, the dynamic range of the FlexiForce sensor can be increased to the range suitable for foot plantar sensing application.

**Data Acquisition** A separate electronic circuit was designed to acquire and transmit the force data wirelessly. Since the number of force sensors (12 sensors)

exceed the number of analog inputs available on the Moteino microcontroller (8 pins), a 16 channel analog multiplexer (CD74HC4067, Sparkfun) was interfaced to the microcontroller. The schematics is shown in Figure 4.16.

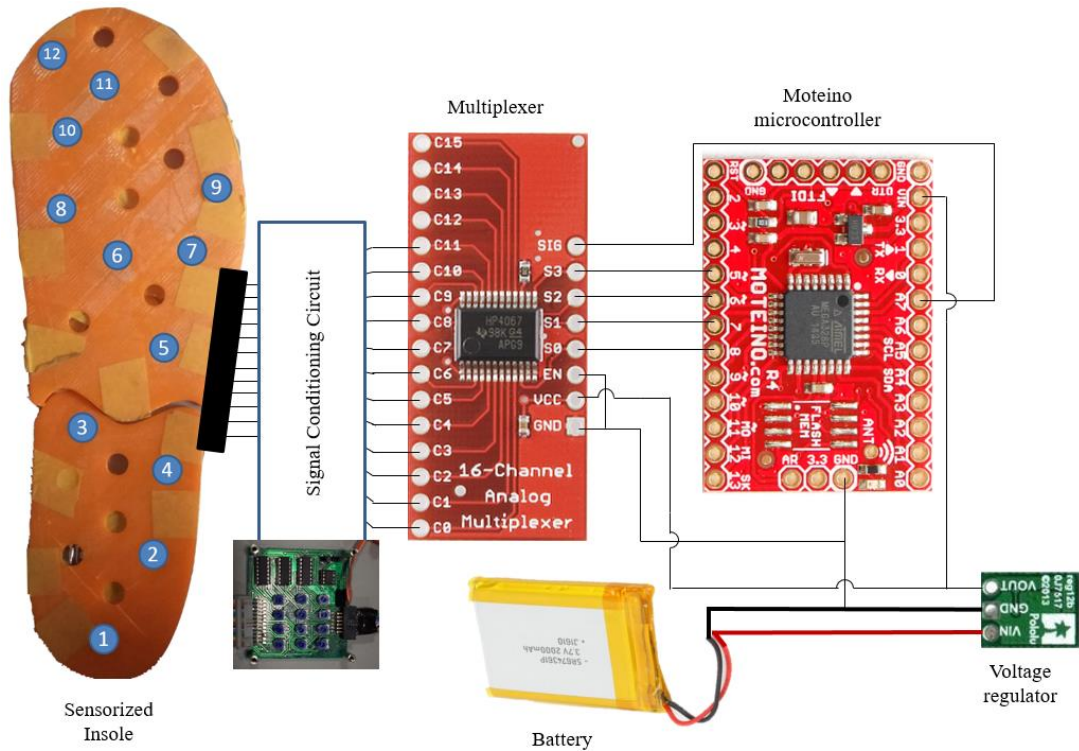


**Figure 4.16** data acquisition schematics for the force insole

The analog multiplexer added 16 analog inputs to the microcontroller, making it possible to read data from all 12 sensors.

### 4.3.3 Calibration

The calibration of the force sensors was necessary to find the relationship between the exerted force and the output voltage. A maximum force of 400 N per sensor was deemed appropriate because during ambulation, the exerted force is distributed among multiple sensors.

**Method** A load testing machine (Instron 5985, Instron) equipped with a 5 kN load cell was used to calibrate the force sensors. The force insole was fixed on a test bed and the testing probe was positioned roughly near above a force sensor. The test probe was then moved with fine adjustments using the machine's built in control pendant such that when the testing probe was barely touching the sensor, the recorded force on the pendant showed 0 N. Next, a force of 400 N was exerted on the sensor, and the potentiometer on the signal conditioning circuit (Figure 4.17 (inset)) was

adjusted such that the output voltage showed approximately 4.5 V. This procedure was done to set the force sensing range of the FlexiForce sensor before calibration. The sensor was then unloaded and force in the range of 0 – 400 N was exerted onto the force sensor incrementally and the output voltage from the signal conditioning circuit was recorded. 9 measurement points were obtained for each FlexiForce sensor.

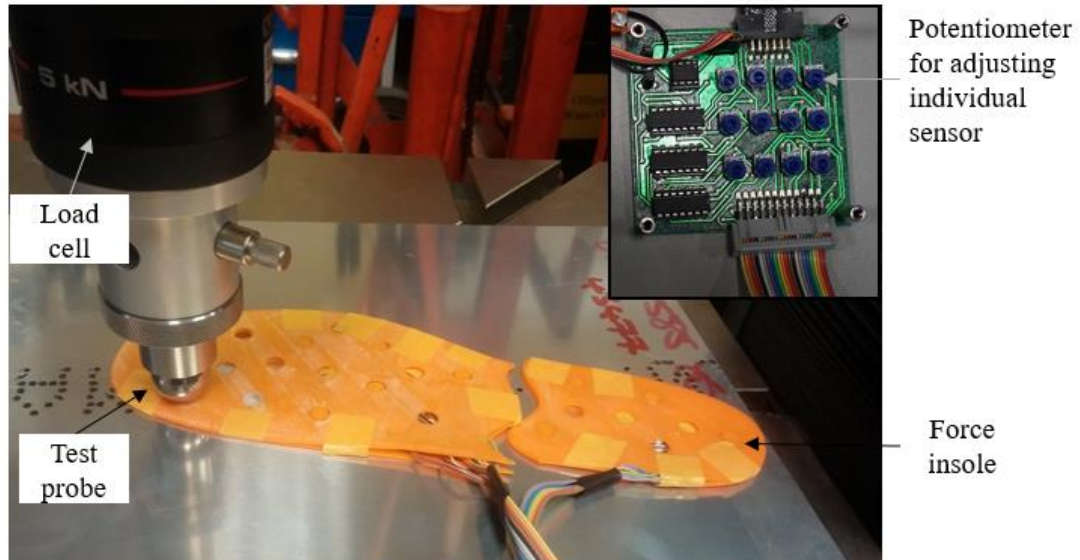


**Figure 4.17** The setup for force sensor calibration. (inset) Signal conditioning circuit

**Analysis** A force vs voltage graph was plotted for each sensor. A best fit line that describes the linear relationship between force and voltage was obtained for each sensor. The equation of the linear relationship can be described as:

$$F = mV + C \quad (4.13)$$

Where

$F$  = Force

$V$  = Voltage

$m$  = slope of the best fit linear line

$C$  = the y-intercept of the best fit linear line

**Results** Figure 4.18 shows the calibration data for the force insole. A linear relationship was found between the force and the voltage for all sensors. The linear fit line equation displayed on each plot is used to approximate the force value for each sensor.

#### 4.3.4 Experimental Validation

To investigate the vertical GRF profile generated by the insole, a comparison was carried out using force platform data as a reference.

**Method** 3 healthy subjects (CS1 - age: 30 years old; height: 172 cm; weight: 67 kg, CS2 - age: 37 years old; height: 172 cm; weight: 60.5 kg and CS3 - age: 33 years old; height: 170 cm; weight: 56.7 kg) wore comfortable sport shoes embedded with the force insole in one of the shoe. All subjects chose to wear to insole on the right shoe. Subjects were instructed to walk around the laboratory before beginning of the trial to familiarize with the setup. A force plate (AMTI, Watertown, MA) was used as a reference. Subjects were instructed to walk normally without targeting the feet position on the force plate, to ensure no distortion of the data. Each subject walked such that the foot with force insole landed completely on one force platform. Trials in which the foot exceeded the force platform area or where incomplete recorded were discarded from analysis. Data were collected simultaneously between the force insole and the force plate for comparison. Figure 4.19 shows the experimental setup.

**Analysis** Force data from the force plate were sampled at 400 Hz. The signal was filtered using 4<sup>th</sup> order Butterworth filter with cut-off frequency of 5 Hz. The force insole was sampled at 120 Hz and passed through a 2<sup>nd</sup> order Butterworth filter with 10 Hz cut-off frequency. Corresponding signal from the force insole and force plate were synchronized and equalized in Matlab (MathWorks Inc.) software. Pearson's correlation was calculated for every force profile pairs to find qualitative correlation between the two systems. The vertical ground reaction force data was obtained using the following equation:

$$F_{vGRF} = \sum_{n=1}^{12} F_n \quad (4.14)$$

where  $F_n$  is the vertical ground reaction force obtained from the individual FlexiForce sensor.

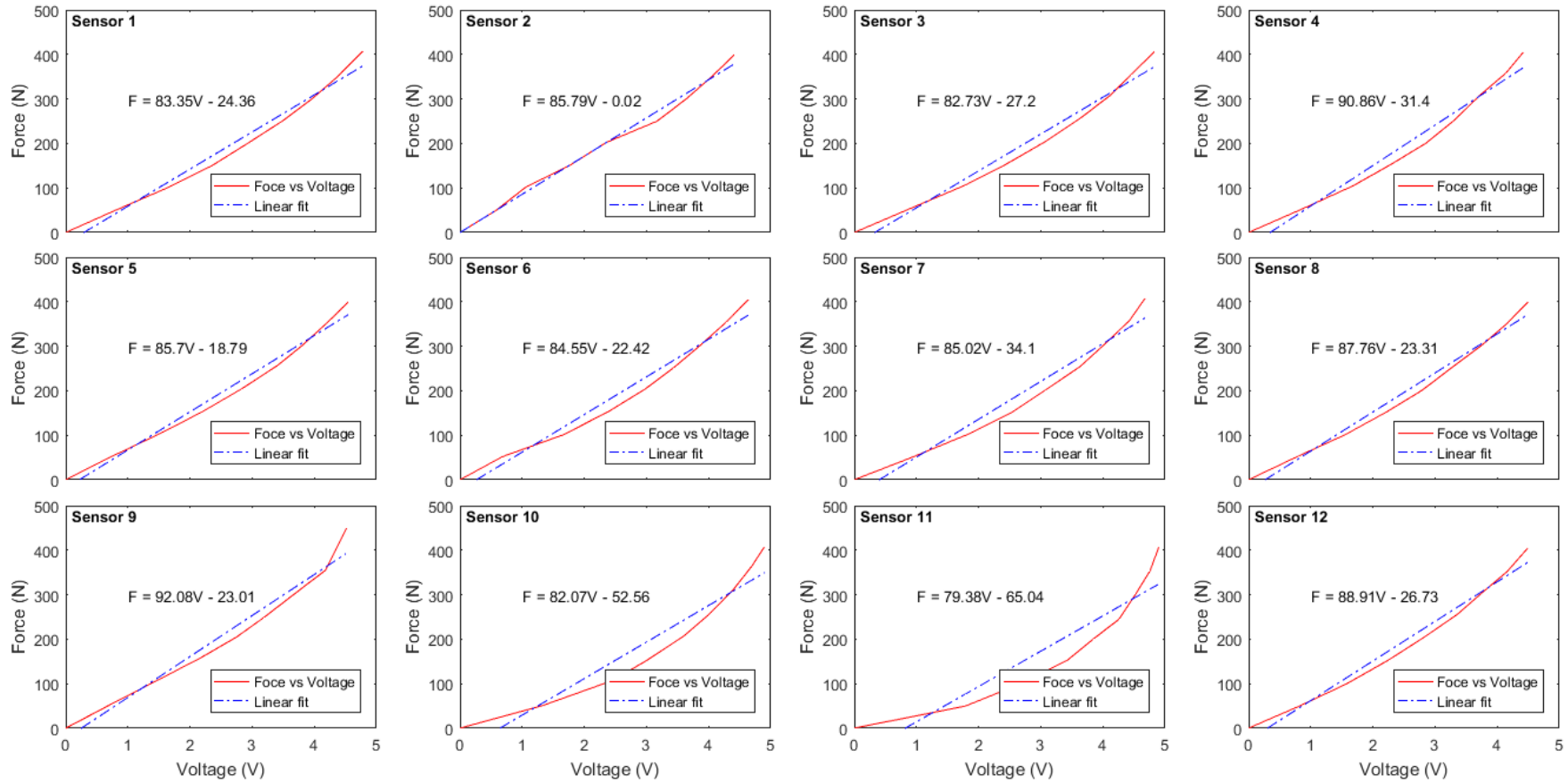
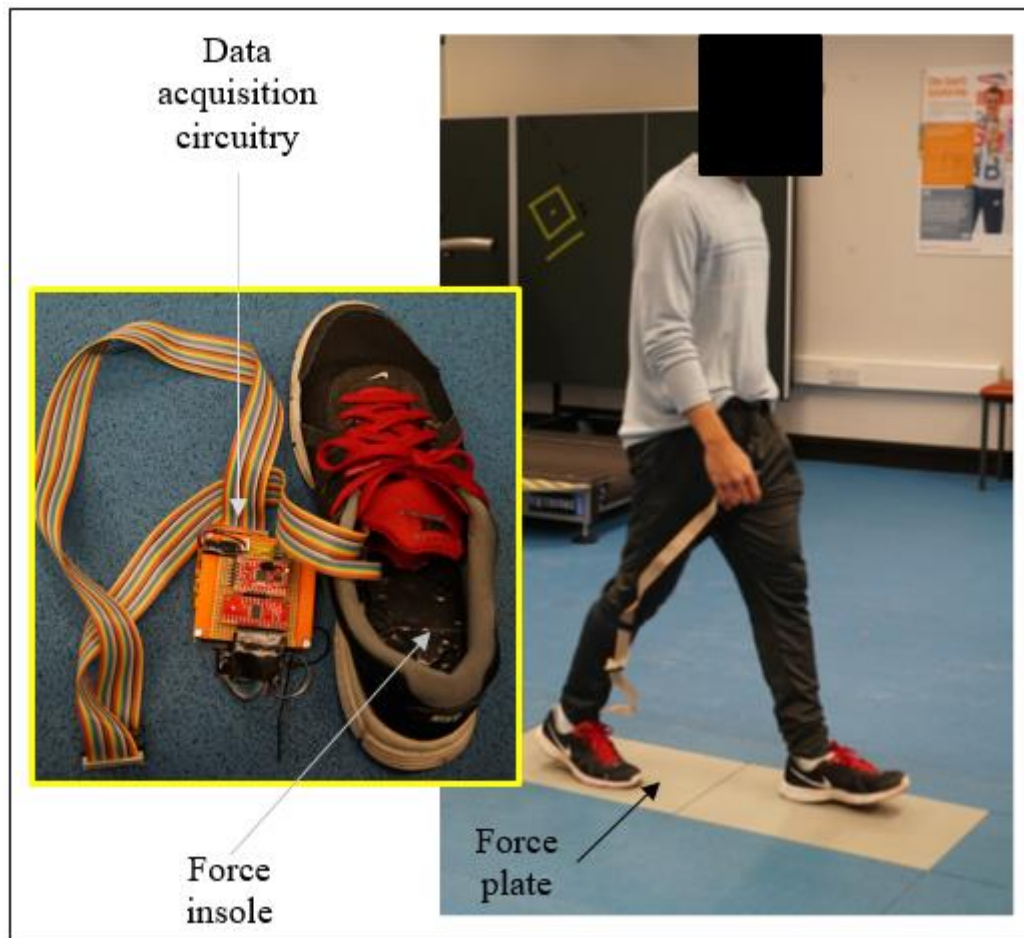


Figure 4.18 Calibration plot for individual FlexiForce sensors



**Figure 4.19** Experimental setup for investigation of force profile generated by the insole

**Results and Discussion** Figure 4.20 shows the resulting GRF data collected from the insole. For each step, corresponding data from force plate is plotted. The Pearson's correlation coefficient between the signal from the insole and the force plate for all the samples from each subject is shown in Table 4.3. It can be observed that the magnitude of the force obtained from the insole were much lower than the reference force obtained from the force plate.

**Table 4.3** Pearson's correlation coefficient for signal samples shown in Figure 4.20

Subject	Pearson's correlation coefficient		
	CS1	CS2	CS3
Step 1	0.90	0.80	0.90
Step 2	0.94	0.81	0.92
Step 3	0.90	0.81	0.94

There are two potential reasons for this observation. Firstly, the calibration of the force sensors was done against a rigid bed, however, most shoe insole will have soft padding that might dampen the effect of the foot contact with the force insole, thus resulting in lower force value. Secondly, the assumption made about the maximum possible force on each sensor (400N) during the insole calibration turned out to be lower than the true maximum force exerted on individual sensor during walking, resulting in lower values for the summation of the force. Crea et al. [50] while presenting their custom made light-based sensorized insole consisting of 64 sensor arrays also noted similar findings, in which the value of the force magnitude was lower in comparison to those of the force platform. One of the possible reasons mentioned by the authors was that the calibration technique might have contributed to the lower final values of the force estimated by the insole.

However, it can be noted from Table 4.3 that the correlation coefficient calculated from each signal pair indicated good agreement ( $r \geq 0.8$  for CS2 and  $r \geq 0.9$  for CS1 and CS3), especially on the onset of the first and second peak, indicating good qualitative agreement between the force insole and the force platform signal. It was thus concluded that while the force insole is not suitable for representing the true absolute magnitude of the vGRF, it is suitable for analysing temporal events in a subject specific application.



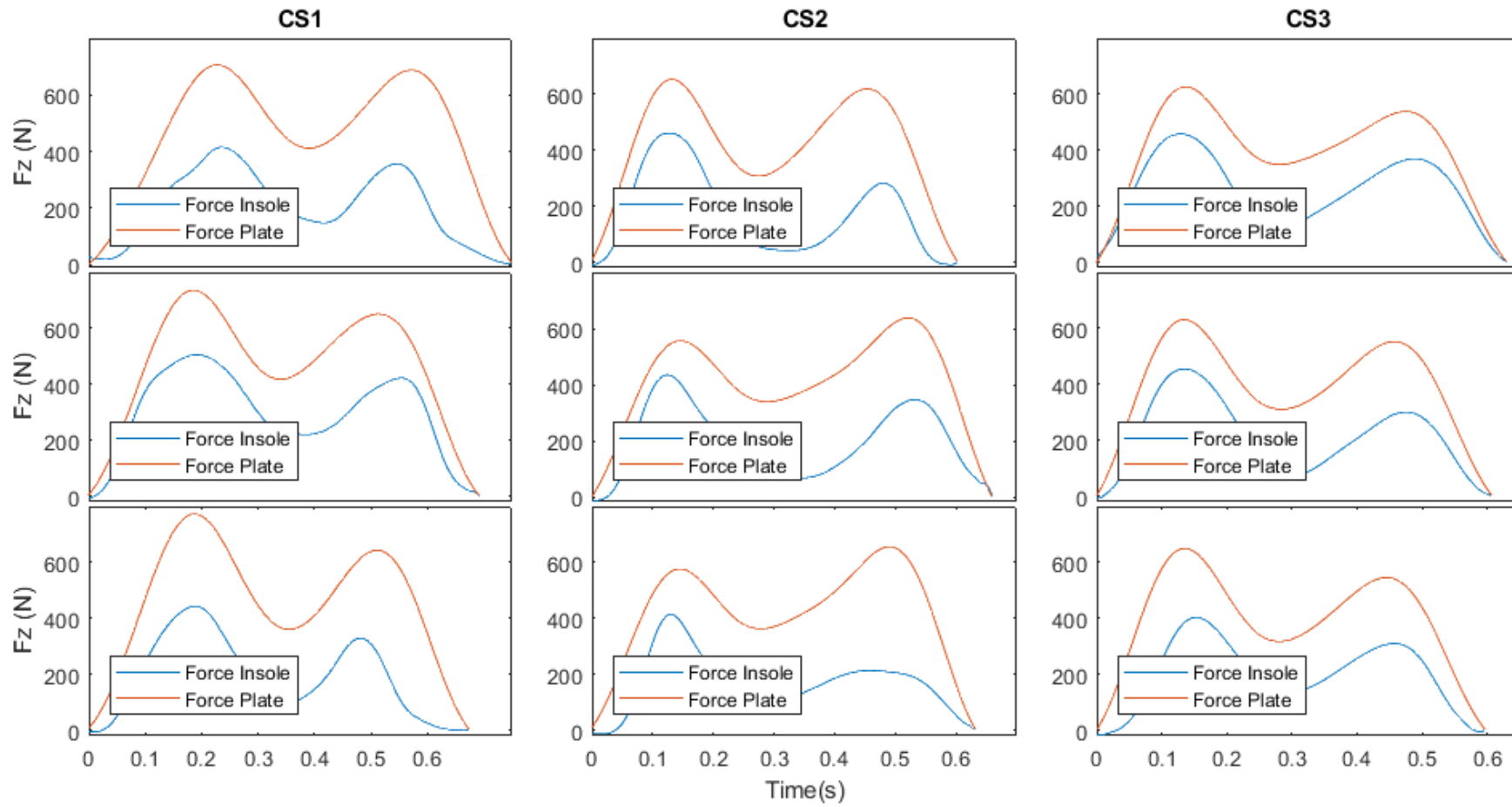


**Figure 4.20** GRF data generated from the insole compared against the force plate for all three subjects. Three samples are shown for each subjects.

## 4.4 System Integration

This thesis has so far covered the description of the individual modules in terms of its mechanical and electronic design. The functionality of the haptic feedback system however, depends on the ability to combine these individual modules into an integrated workflow that can perform seamless data acquisition, communication and control. It is therefore necessary to describe the Graphical User Interface (GUI) design used throughout the work.

### 4.4.1 Graphical User Interface

The GUI designed for the haptic feedback system served the following purposes:

- Provides a database system for recording subject's information and experimental parameters.
- Connecting to the hardware modules and monitor sending and receiving of data through the wireless communication.
- Recording experimental data into files readable from analysis software.
- Automating experimental design.
- Displaying information regarding change in modules' parameters or change in experimental parameters
- Troubleshooting and testing the hardware modules
- Acts as an interface to other software for data analysis

The GUI was designed in C#.NET programming language using Microsoft Visual Studio as the visual Integrated Development Environment (IDE). Figure 4.21 shows the hardware-GUI workflow. A personal computer (PC) hosts the GUI and is interfaced with Moteino wireless microcontrollers via USB connection. Each hardware module (haptic, event detection and force insole) has an independent Moteino microcontroller that will communicate wirelessly with the Moteino interfaced at the PC. The GUI communicates (send and receive) with the hardware using serial communication. From within the GUI, serial port connections can be established and any data sent to these ports are transmitted wirelessly to the hardware modules. Similarly, data from hardware modules are transmitted wirelessly to the Moteino on the PC and passed to the GUI via serial communication. This bi-

directional feature allows simultaneous control of the hardware modules and recording of data during experimental work.

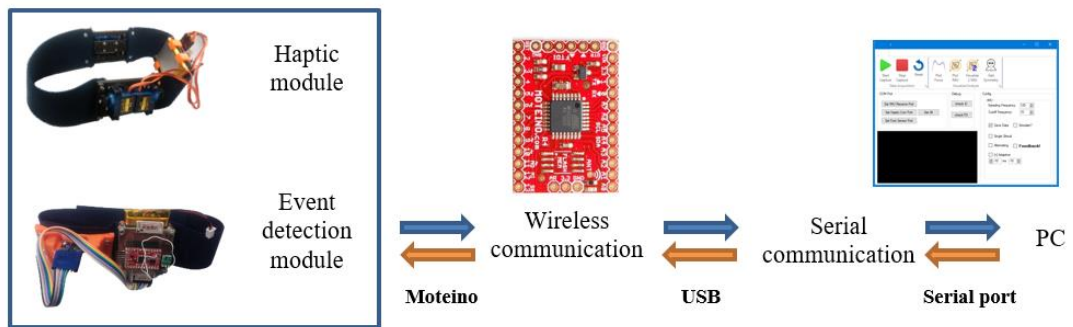


**Figure 4.21** Workflow of the integrated system

Figure 4.22 shows the main GUI windows designed for the hardware-GUI interaction. The use of descriptive labels and intuitive menus made it possible for the GUI to be used by a novice user, and allow easy modification to the design. Clicking any of the menu might open a child window which allows a specific function to be executed. An example is shown in Figure 4.23, where a database window opens to show subject's information.

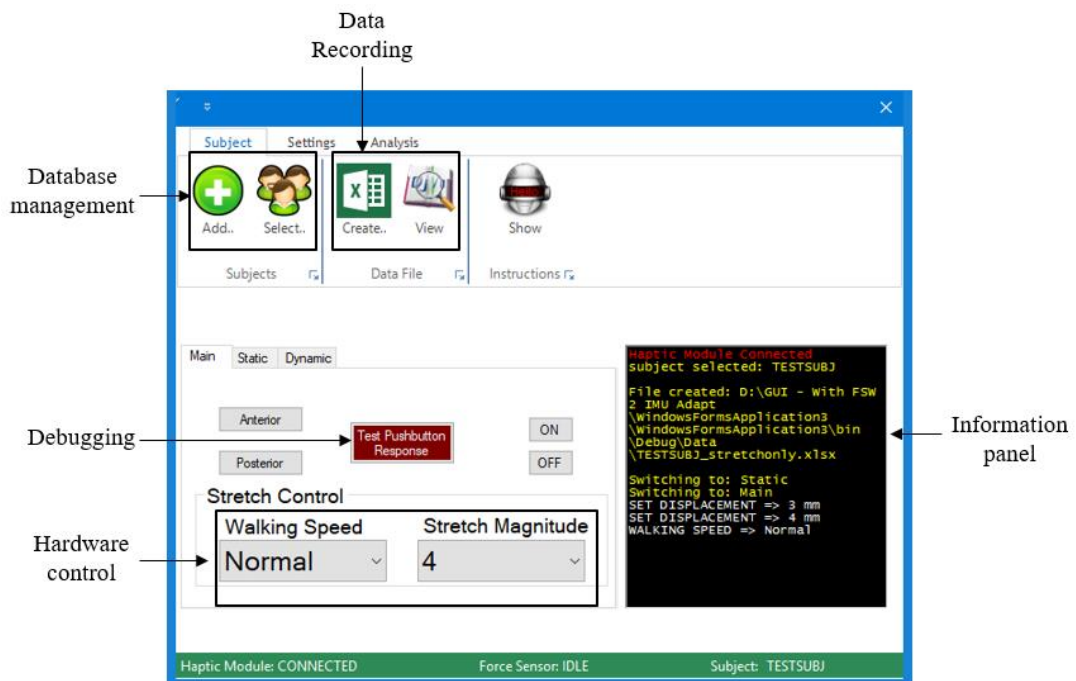


**Figure 4.22** Example of the GUI window, with description of the functions

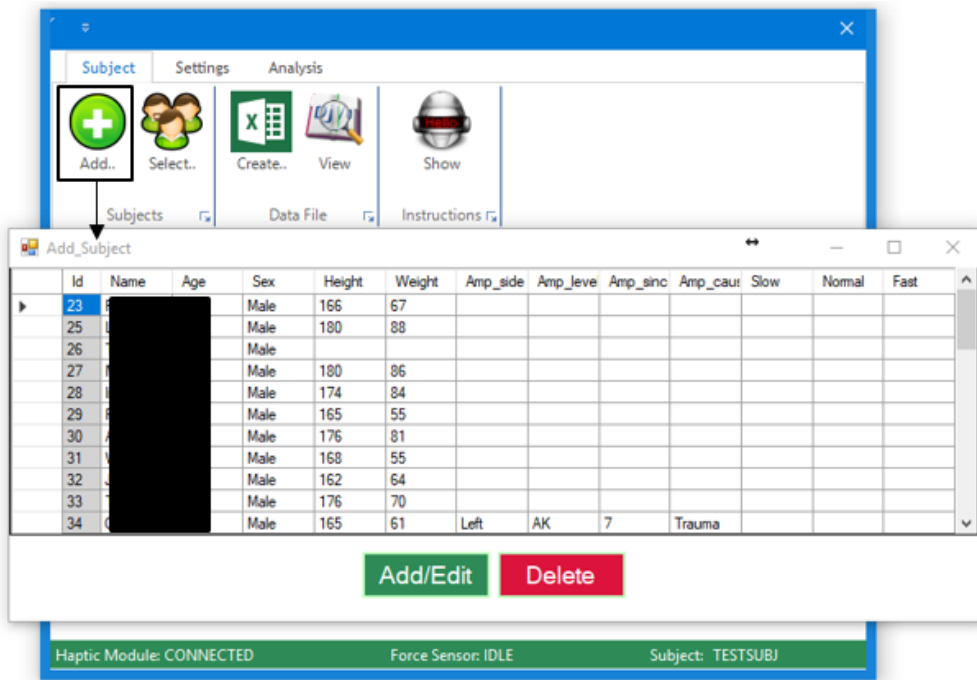


**Figure 4.23 Database management child window**

Figure 4.24 shows another GUI window for experiment control and data analysis.

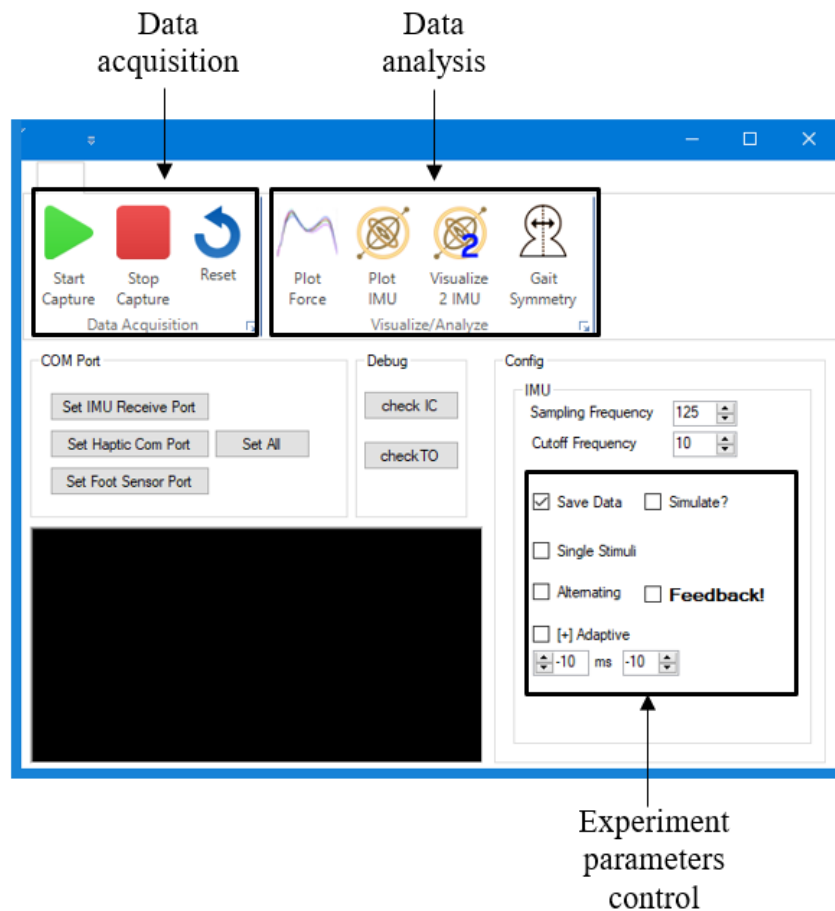


**Figure 4.24 Experiment control and data analysis window**

## 4.5 Summary

This chapter presented the description of a gait event detection using inertial measurement unit attached at shank. The angular velocity signal produced in the sagittal plane during walking was verified against a motion capture system and was found to be suitable for event detection purpose. A threshold based algorithm was described for detecting IC and TO events during gait by identifying the maxima and minima point in the angular velocity signal based on empirically determined thresholds. The IC and TO events were successfully detected using the algorithm during walking in different speed, making it a suitable method for controlling the activation of the haptic modules. For analysis of the gait parameters in future experimental work, the design of a custom insole embedded with 12 force sensors was described. The vertical GRF output from the insole was found to exhibit similar signal pattern when compared to the force plate output, albeit with a lower force magnitude. The last part of this chapter presented the integration workflow for the haptic feedback system, detailing the design of a GUI and its integration with the hardware modules. The next chapter will describe the experimental work carried out to assess the haptic modules described in Chapter 3 and the gait event detection modules described in this chapter. The use of force insole as a measurement tool in combination with the haptic feedback system are described in Appendix A.

## **CHAPTER 5:**

# **Haptic Feedback: Static and Dynamic Evaluation**

### **5.1 Introduction**

This chapter describes the setup and experimental works carried out to assess the perceptibility (the perception of the stimuli) and the feasibility of the haptic feedback system. The experimental environment consisted of a variable speed motorised treadmill and a fall arrest safety rig. The experiments were carried out in two particularly distinctive modes, namely the static (standing) and dynamic (walking) to obtain an insight into the differences in the participant's perception to the stimuli delivered during these two modes.

In the first part of this chapter, static and dynamic perceptibility is investigated using single haptic module introduced in section 3.4 of this thesis. In the experiments, the haptic module was attached on the upper leg around the mid-thigh region and the effect of stretch magnitude to the subject's perception of the feedback was investigated.

The second part of the chapter describes the experimental work carried out with haptic modules integrated with event detection module. Two haptic modules, which design was presented in Section 3.5 of this thesis were attached on the lower trunk and perceptibility and subject's response time to various feedback strategies corresponding to IC and TO events were investigated. This section serves as a foundation to the evaluation of the haptic feedback system with a lower limb amputee described in Appendix A.

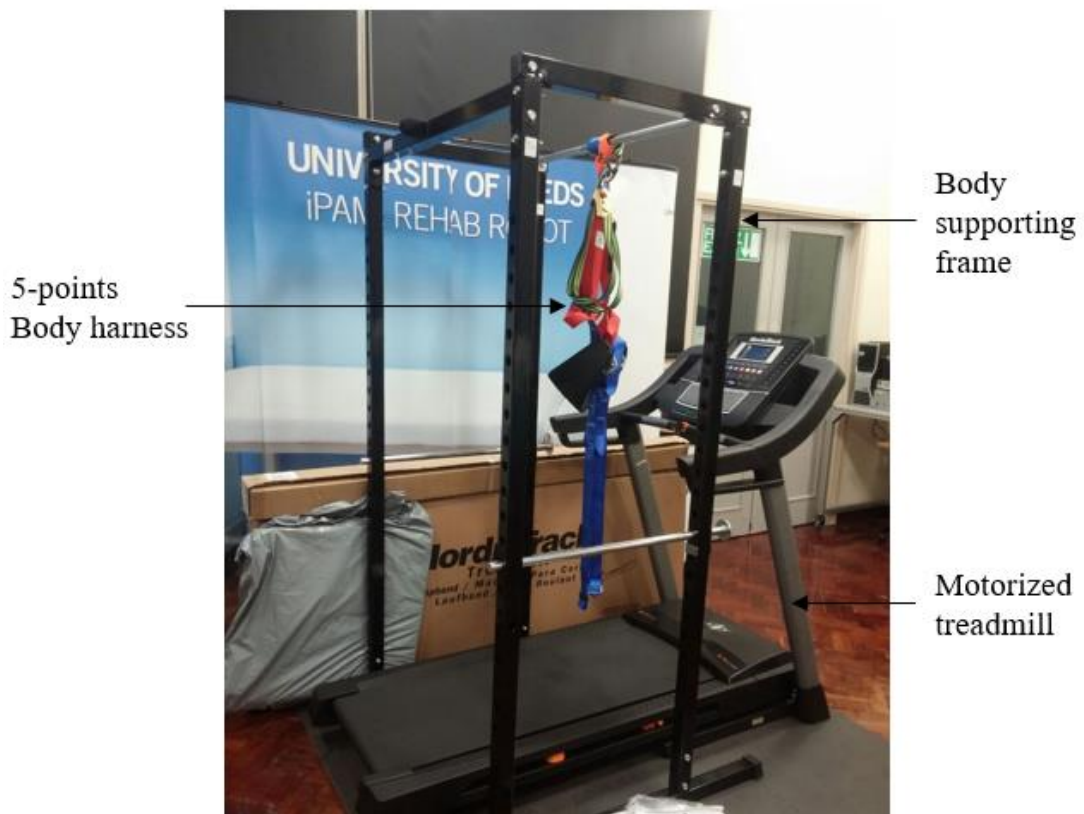
For all experimental work described, the participants were briefed and consented to taking part in the research. In addition, participants also consented to photographic and video records taken throughout the experiments. The experimental protocol received an approval from the University of Leeds Ethical Review Board (MEEC 14-012 – Appendix D).

## 5.2 Experimental Setup

Before running the experimental work, two preliminary works were undertaken. The first was determining a suitable platform for dynamic activities that would allow data collection for uninterrupted lengthy walking sessions. The second work was identifying the normal force to be asserted on the skin by the haptic system such that slip does not occur and the skin-stretch can be delivered effectively.

### 5.2.1 Walking Platform

To collect larger sets of data from walking mode, either a large space that allows walking to take place for longer duration or repeated short walking trials are required. However, treadmill walking provides smaller footprint for experimental purpose, while allowing recording larger number of gait cycles. Therefore, a treadmill setup was designed for the data collection purpose carried out in this section.



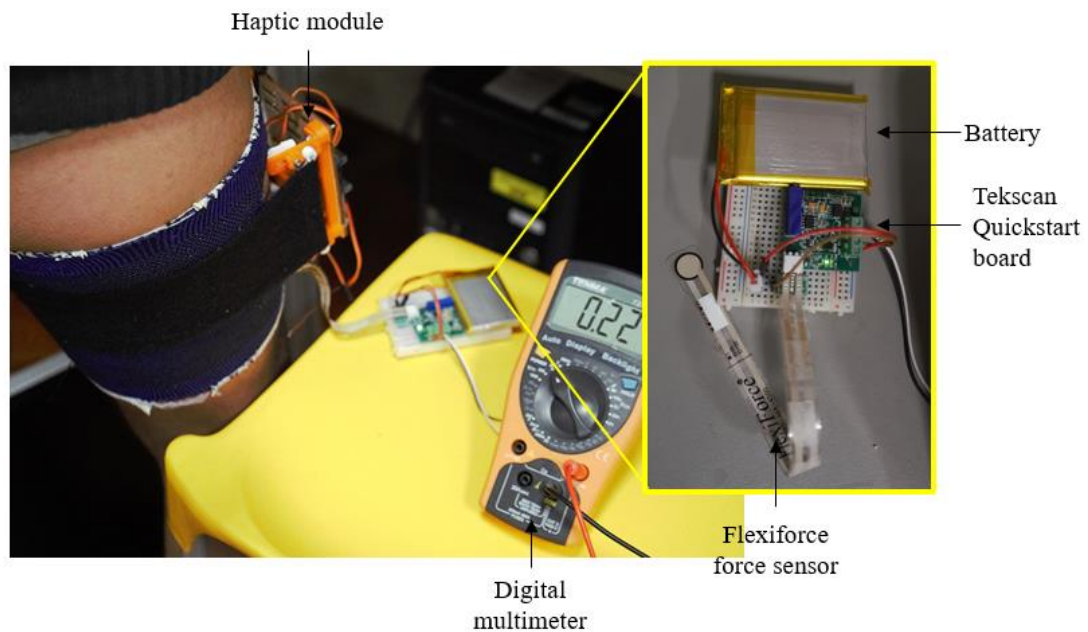
**Figure 5.1 Treadmill setup, with fall safe rigid frame**

Figure 5.1 shows the proposed experimental rig setup. The treadmill allows speed adjustment from 0-20 km/h with 0.1 km/h increment. The fall arrest system consists of a fitness power rack with a pull-up steel bar that can take up to 300 kg weight. A

5-point body harness were attached to the pull-up bar to catch the body if fall occurs during the walking experiment. This feature is especially important for amputee participants because of the reduction in their dynamic stability. The fall arrest system does not provide any body weight support (0% body weight support) so as not to alter the kinetics and kinematics of a regular walking gait.

### 5.2.2 Determining Normal Force

The haptic-skin interface requires force to be exerted on the skin to allow the plate to stretch the skin without slipping. The normal force exerted by the haptic plate depends on how tight the module is wrapped around the limb. To investigate the appropriate range of normal force such that the haptic module works appropriately, an experimental test was carried out.



**Figure 5.2 Setup for determining force range for haptic-skin interface**

**Method** As shown in Figure 5.2 (inset), a FlexiForce A201 (Tekscan, USA) sensor was used to measure the force between the haptic plate and the skin. The sensor was connected to a commercial FlexiForce Quickstart board (FLX-QSB, Tekscan, USA) which allows easy calibration of a single sensor. Initially, the calibration of the FlexiForce sensor was carried out to find the voltage-force relationship. This was achieved by loading the sensor with dead weights in the range 0-700 g, with 100 g increments (allowing calibration in the range of ~1-7 N). The output voltage obtained



from the Flexiforce Quickstart board was recorded. The haptic module was adjusted by tightening the fabric cuff around the thigh such that slip does not occur when the module was activated. The calibrated force sensor was then placed between the haptic plate and the skin. A digital multimeter was used to read the voltage value output from the Quickstart board. The equivalent normal force was then determined by using force-voltage relationship obtained from the calibration.

**Result and Discussion** From the calibration using dead weights, the relationship between the sensor output voltage (V) and force (F) was determined to be:

$$F = 1.665 (V) + 0.1729$$

The force value when the haptic plate did not slip was found to be in the range of  $0.51 \pm 0.04$  N. This value was higher than the one reported by Chen et al. [33] and Gleeson et al. [152] in which normal force of around 0.25 N was needed to prevent the feedback interface from slipping and not causing discomfort on the limb. It is worth noting that Chen et al. glued the haptic interface onto the skin to minimize slip. The use of glue was considered unsuitable for a wearable feedback module; therefore, it might explain the higher normal force needed for this haptic module. Throughout the experimental work discussed in this thesis, the value of normal force was maintained approximately at this range and was not subjected to manipulation.

### 5.3 Single Module-Perceptibility Test

The purpose of this experimental work was to assess whether the feedback delivered can be perceived by the subjects during static standing and while walking. In both modes, the stretch magnitude was varied to identify the relationship between stretch parameters and perceptibility. In this experiment, the perceptibility test was carried out without any control from event detection modules. In both static and dynamic modes, the haptic module was activated randomly, and the subjects were asked to indicate if the stretch feedback can be felt or perceived. The details are presented as follows.

### 5.3.1 Methods

5 healthy subjects and one above-knee amputee participated in this experiment. The subjects' details are indicated in Table 5.1 and Table 5.2.

**Table 5.1 Demographic data of Control Subjets (CS)**

Subject	Gender	Age (Year)	Height (cm)	Weight (Kg)	Preferred side (L/R)
<b>CS1</b>	Male	24	173	66	R
<b>CS2</b>	Male	29	172	68	R
<b>CS3</b>	Male	22	166	86	R
<b>CS4</b>	Male	31	174	85	R
<b>CS5</b>	Male	32	165	66	R

**Table 5.2 Details on the Above-knee (AK)**

Subject	Gender	Age (Year)	Height (cm)	Weight (Kg)	Intact side (L/R)
<b>AK1</b>	Male	54	165	61	R

Figure 5.3 depicts flowchart of the feedback scheme. A random sequence of 10 binary digits (0 and 1) was generated by the computer. A binary digit 1 indicates activation of the haptic module, while binary digit 0 indicates non-activation. Each sequence contained 8 activations and 2 non-activations (e.g. 1101110111). The function of the non-activation condition was to eliminate the possibility of the participants guessing the stimuli pattern. The binary sequence was then fed into the Graphical User Interface (GUI) that controlled the experimental flow, which then iterated over this binary sequence. If an activation digit (1) was identified, the haptic module was activated, and the system waited for a push button feedback from a subject within a period of 2 seconds. If the subject pressed the push button indicating feeling the feedback, this was recorded as 1 (perceived) in the spreadsheet. Otherwise the response is recorded as 0 (missed).

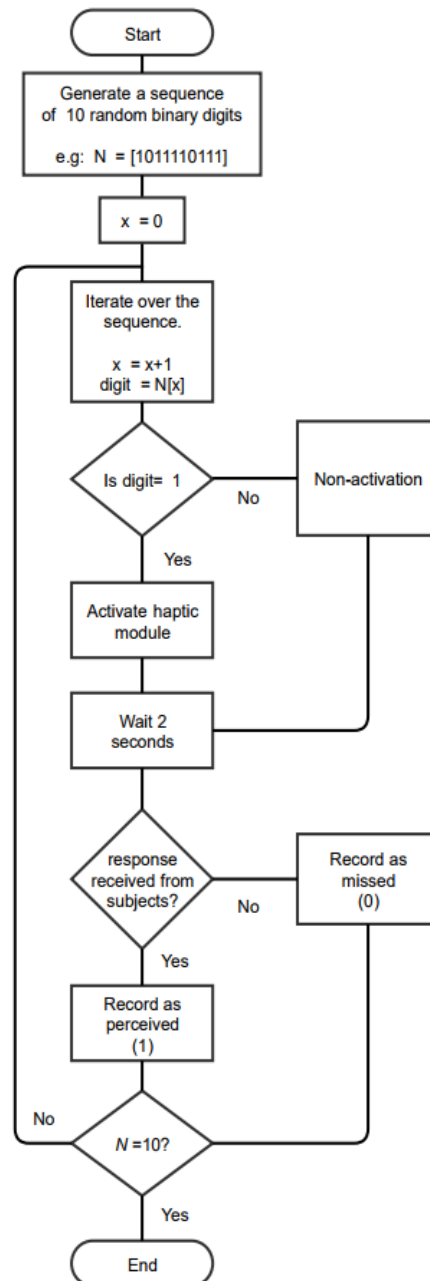


**Figure 5.3 Feedback scheme for the perceptibility experimental work**

#### **a) Static Perceptibility**

The haptic module was strapped on the anterior mid-thigh on the preferred leg, approximately 10 cm above the knee joint while the subject was standing. The haptic plate was adjusted such that it was rested firmly on the skin. For the above knee amputee, the device was fitted on the intact leg for this assessment. Participants held the handheld switch with one hand to indicate perceived stimuli. Participants also wore a headphone playing white noise to mask the sound coming from the haptic device, thus eliminating the chance of guessing the stimuli via auditory means. The

subjects were allowed to familiarize with the system and briefed on the experimental procedure.

Sequences of stretch stimuli as shown in Figure 5.3 were delivered to the skin with the skin-stretch magnitude of 1 mm. A single stimulus is completed when the actuator moved from baseline position to the intended displacement value and return. Participants were instructed to push the handheld switch upon perceiving the stretch stimuli. A pause of 2 seconds was given in between each stimulus to allow sufficient time for the participants to respond. The procedure was repeated two times (3 sequences altogether for a single stretch magnitude). The experiment was then repeated with skin-stretch magnitude of 2 mm, 3 mm and 4 mm.

### **b) Dynamic Perceptibility**

To assess perceptibility of the device in dynamic mode, the participants performed the walking activity on a treadmill. As a safety measure, participants were required to wear safety harness attached to a rigid frame to prevent falling, in case of tripping or missteps. The treadmill was started at an arbitrary low speed (~2 km/h) to allow the participants to do a 2-minute warming up session. Subsequently, the participants were asked to adjust the treadmill speed in 0.1 km/h increment until it reached the speed which they considered matching their normal walking speed overground. When the participants achieved steady walking pattern, similar experimental routine protocol as described in the static perceptibility was carried out. Figure 5.4 shows the haptic modules setup on the amputee subject, with similar setup used in the healthy subjects.

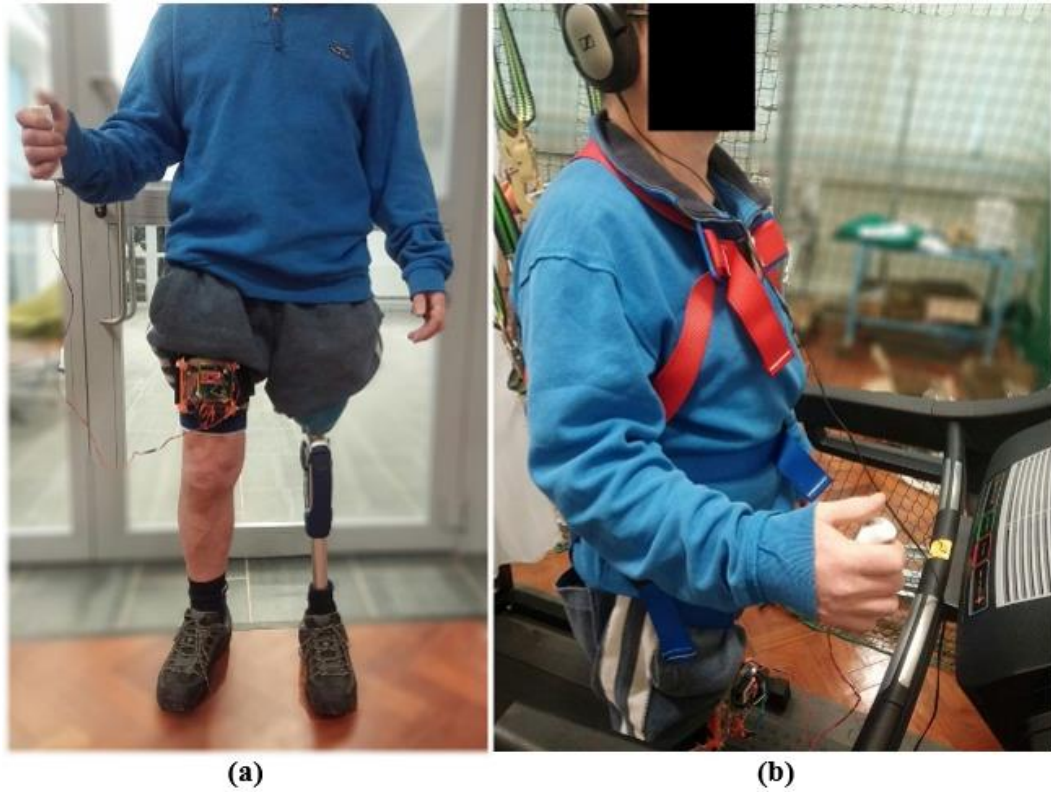


**Figure 5.4** Experimental setup, showing placement of haptic module on the amputee for (a) static and (b) dynamic experiment.

### 5.3.2 Data Collection and Analysis

A total of 96 skin-stretch stimuli in the range of 1 mm – 4 mm were delivered to each participant in each activity mode (8 stimuli  $\times$  4 stretch levels  $\times$  3 trials). A button press was recorded as an indication that the participants perceived a stimulus.

The response received from the participants were sent wirelessly to a computer which stored the data into a spreadsheet. The percentage of correctly identified stimuli were used as a measure of the perceptibility.

$$\text{Perceptibility (\%)} = \frac{\text{Number of stimuli identified}}{\text{number of stimuli delivered}} \times 100 \quad (5.1)$$

Participant's responses were also analysed for any false perceptions (participants indicating stimuli when there was not one).

### 5.3.3 Results and Discussion

Figure 5.5 shows the perceptibility of the skin-stretch feedback recorded for healthy subjects and the AK amputee and Table 5.3 summarizes the perceptibility value for each stretch magnitude and walking mode.

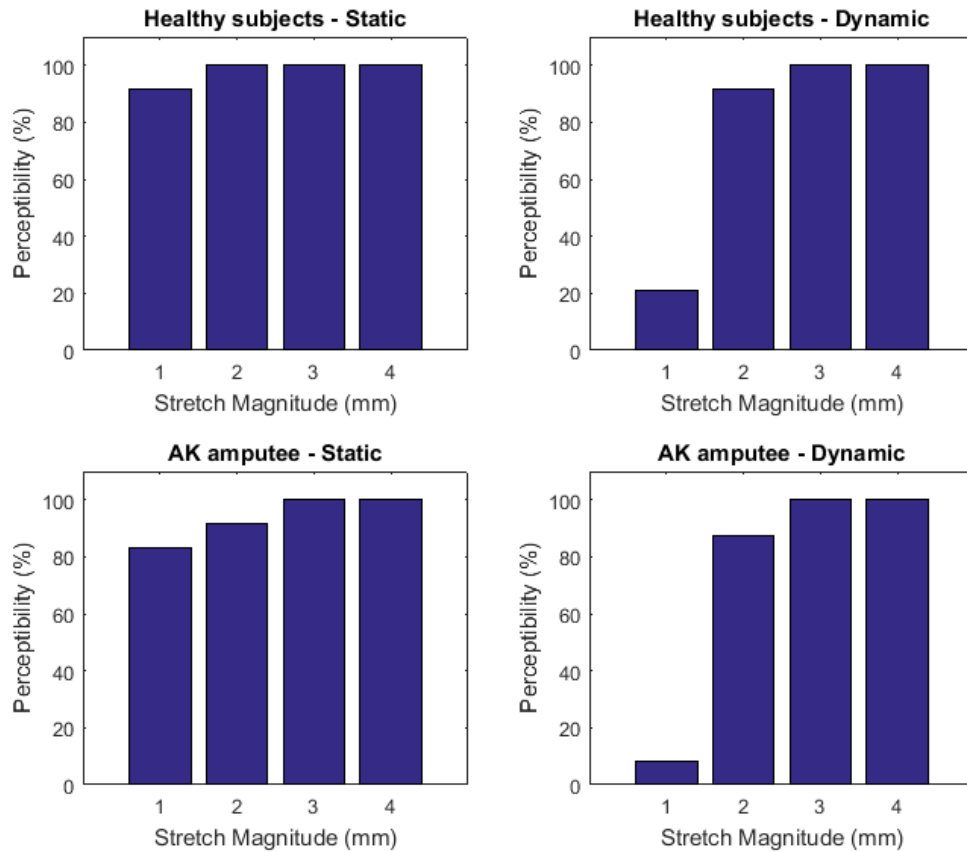


**Figure 5.5** Result of the subjects' perception to the stimuli in both static and dynamic mode.

**Table 5.3** Summary of perceptibility (%). Darker shades indicate higher perceptibility.

Stretch level	Healthy subjects		Amputee	
	<i>Standing</i>	<i>Walking</i>	<i>Standing</i>	<i>Walking</i>
1mm	91.7	20.8	83.3	8.3
2mm	100	91.7	91.7	87.5
3mm	100	100	100	100
4mm	100	100	100	100

The results for both healthy subjects and the amputee showed similar pattern of increasing perceptibility with increase in stretch magnitude. While 3 mm and 4 mm stretch remained highly perceived throughout the experiment in static and dynamic modes, the perception of 1 mm stretch dropped to virtually non-existing (< 21%) for

both groups during dynamic mode. Similar reduction in perception can be observed with 2 mm stretch during dynamic mode, although the perceptibility remained higher (> 90%) in comparison to 1 mm stretch. This observation and others are discussed as follows.

The stretch duration of the stimuli provided throughout the experimental work was fixed to 150 ms, which denotes the time taken to complete the movement of the haptic plate from baseline position to target position. As presented in section 3.4.3.1, 150 ms was found to be the most optimal stretch duration to deliver skin-stretch in the range of 1 – 4 mm. Some studies were conducted to study the factors contributing to the perception of lateral skin-stretch. Chen et al. [33] and Gleeson et al. [152] found that the perception of skin-stretch increase with speed as well as the stretch magnitude. The study by Gleeson et al however was conducted on the glabrous skin of fingertip which is more sensitive to feedback and therefore concluded that stretch as small as 0.2 mm can be perceived with high accuracy (more than 95%) at 1 mm/s stretch speed. Chen et al. studied the perception of skin-stretch on the skin of lower leg and found out that the direction of 0.2 mm stretch can be correctly perceived (> 97% accuracy) when the speed was at least 4 mm/s. In both studies, however, it was worth noting that the authors investigated the directional accuracy of the applied skin-stretch, rather than just the perception of the stretch sensation itself. In other words, in those studies, response from the subjects were considered accurate if the subjects managed to correctly identify the direction in which the stretch was applied. In this research, however, the perception of the stretch alone was investigated, without requiring the subjects to correctly identify the direction of the stimuli. Therefore, a direct comparison to the previous studies will not be appropriate since the approach of the study is different. Nevertheless, similar trend was observed in this study and that of Chen's, in which the increase in the stretch magnitude contributed to higher perception of the stimuli. However, the perception of 1 mm stretch in this study was lower than those presented by Chen (91.7% vs 100%). An explanation to this could be that the upper leg, especially the thigh area is less sensitive to skin-stretch stimuli in comparison to lower leg. Although no skin-stretch data from previous studies can be found to support this suggestion directly, similar finding was suggested Karuei et al. [153] where vibration feedback across the body locations was investigated and the thigh was found to be one of the least sensitive areas apart from the foot. It was also

found that walking caused the perception of the skin-stretch, especially the lower magnitude stimuli to be reduced even further. Milne et al. [154] and Chapman et al. [155] in both their studies have shown that the movement induced by limbs effectively masks the cutaneous stimuli provided on the skin, except when the stimuli was intense enough to be perceived. Based on the experimental results, it can be concluded that a minimum of 3 mm stretch can be perceived during both static and dynamic condition for normal walking speed. The instances of false perception as shown in Table 5.4 occurred randomly, albeit rarely, throughout the walking experiments.

**Table 5.4 Instances of false perceptions (indicating stimuli when none was given)**

Stretch level	Able-bodied		Amputee	
	<i>Standing</i>	<i>Walking</i>	<i>Standing</i>	<i>Walking</i>
1mm	0	1	0	0
2mm	0	1	0	1
3mm	0	0	0	1
4mm	0	1	0	1

This might be attributed to the movement of the haptic module caused by vibrations during walking (especially during the loading phase) which eventually cause the subjects to perceive it as a form of stimuli.

The previously described dynamic experiment was carried out on a treadmill rather than over ground to allow controlled and uninterrupted walking sessions, and eliminating the effect of changing environment on the subject's ability to perceive the delivered stimuli. The studies on comparison of treadmill and over ground walking presented unequivocal findings. Riley et al. [156] studied the kinetics and kinematics parameters of 33 healthy subjects walking on the treadmill concluded that they are qualitatively and quantitatively similar to walking over ground. Some studies like the one conducted by Hollman et al. [157] however, argued that the treadmill walking are not similar to over ground walking in terms of stride-to-stride variability and is therefore not suitable for translating clinical rehabilitation effects. As the experiments conducted in this section were concerned on the perception of stimuli throughout continuous walking gait, the choice of treadmill was deemed advantageous and suitable for the task involved.



Although perceptibility of the feedback was satisfactory and was found to be useful for delivering feedback, the previous experimental work provided some insights on several limitations of the currently employed feedback scheme. These limitations are detailed as follows:

- a) *Hardware* – The haptic module had a rather large footprint; 98 mm (W) × 90 mm (L) × 50 mm (D). As presented in chapter 3, the design of the module was initially intended to deliver the haptic feedback on the thigh region. However, this design inevitably presented two disadvantages. Firstly, the overall weight of the module proved to be larger than ideal, mostly notable during dynamic mode, as indicated by some participants as feeling a ‘bulk of material’ attached to the limb. Secondly, the large depth of module in combination with the weight, created an additional torque that pulled the device down during the walking task.
- b) *Anatomical factor* – Although the placement location of the module in the current scheme was thought to be the most ideal, it needs revisiting for the following reasons: Firstly, the conical shape of the thigh made it very easy for the modules to slide down during walking. Intense muscle contraction and extension during walking also contributed to this problem. Secondly, for above knee amputees, the socket will most probably cover the whole remaining stump, making it impossible to deliver the feedback on the amputated side, since there is virtually no space to embed the haptic module.
- c) *Effects on feedback strategy* – The current choice of placing the haptic module on the thigh will also affect the feedback strategy designed for the haptic module system. As shown in Figure 5.6, the thigh muscles on the posterior side are highly active during the IC phase of the gait. Conversely, during TO, the muscles on the anterior side of the thigh are relatively active. As the initial feedback strategy relies on placing the feedback modules on both locations (refer to Figure 4.1) during IC and TO, the skin-stretch feedback will coincide with the contraction and extension of the muscle groups in these locations.

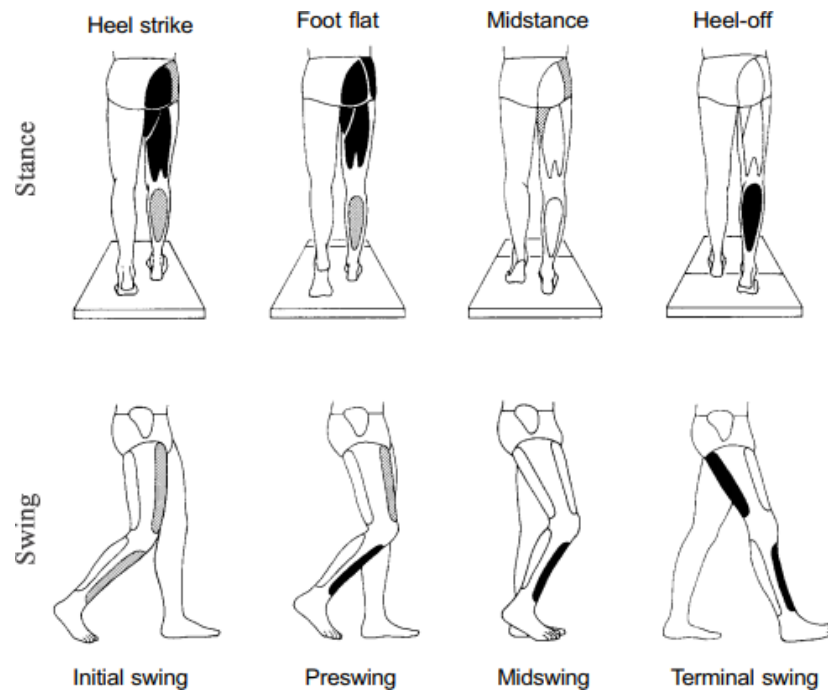


**Figure 5.6 Muscle activities during gait. Darker shade indicates more intense activity. Adapted from [158]**

To address the first issue, the design of the haptic modules was revised and presented in Section 3.5 of this thesis. The reduced footprint and weight of the revised module was expected to minimize the effect of gravity on the haptic modules when fitted on the subjects. The last two issues call for exploring a new placement location for the feedback device for investigation of the integrated haptic feedback system. The alternative location for placing the haptic modules must preferably:

- a) Allow attribution of sides, i.e the “left” and “right” sides of the placement site can be identified. This is so that idea behind the initial feedback strategy, in which the feedback is given on the same side as the leg that bears the event detection module, can be retained.
- b) Has close proximity to the leg.
- c) Has minimal movement during walking, so that the delivered feedback will not coincide with intense muscle movements during IC and TO events.
- d) Has anatomical shape that minimizes slip and movement of the haptic modules during walking.
- e) Equal or better in terms of sensitivity towards cutaneous stimuli.

Based on the criteria a-e, an analysis of possible alternative for placing the haptic modules was carried out. Table 5.5 shows the details of the findings.

**Table 5.5 Evaluation of alternative placement for haptic feedback module**

		Criteria					Remarks
		a	b	c	d	e	
<b>Location</b>	Head	•		•		•	Limited space for placement
	Upper trunk	•				•	Bony area around chest
	Upper arm	•			•	•	
	Wrist	•	•		•	•	Pronation and supination creates change in orientation
	Lower trunk	•	•	•	•	•	
	Foot	•	•				Not useful for amputee

The lower trunk stands out as a viable alternative for the haptic module placement site. Since lower trunk is directly connected to the lower limb at hip joint, it has the most merit in terms of proximity. Unlike lower limb though, the movement of the trunk during gait is minimal and is mostly around the anterior-posterior axis.

#### 5.4 Gait-Event-Based Feedback

This section will describe an experimental work to further assess the perceptibility and feasibility of the haptic feedback system during ambulation. Recall that while previous experiment showed the relationship between stretch magnitude and the perceptibility of the feedback, there was no association between gait events and the feedback given. The purpose of the experimental work described in this section is therefore to:

- a) Assess subjects' ability to perceive and identify skin-stretch feedback in two locations, in response to the IC and TO events.
- b) Investigate different feedback modes for delivering the skin-stretch feedback during ambulation.
- c) Investigate the subjects' response time to such feedback across various walking speed (2.0 km/h – 5.0 km/h).
- d) Investigate indication of learning and adaptation to the haptic feedback system throughout ambulation.

### 5.4.1 Feedback Strategy

Figure 5.7 shows the feedback strategy employed for the haptic feedback system. Two feedback modules are placed on the lower trunk, around the abdominal area along the same side of the leg which holds the event detection module. The feedback modules were placed such that they match the spatial location in which the IC and TO events take place. Specifically, one module was placed on the posterior (back) side of the abdomen to match the IC event which happens when the posterior side of the foot (heel) makes contact with the ground. In similar pattern, the other module was placed on the anterior (front) side of the abdomen to match the event during TO where the anterior side of the foot (toe) leaves the ground.

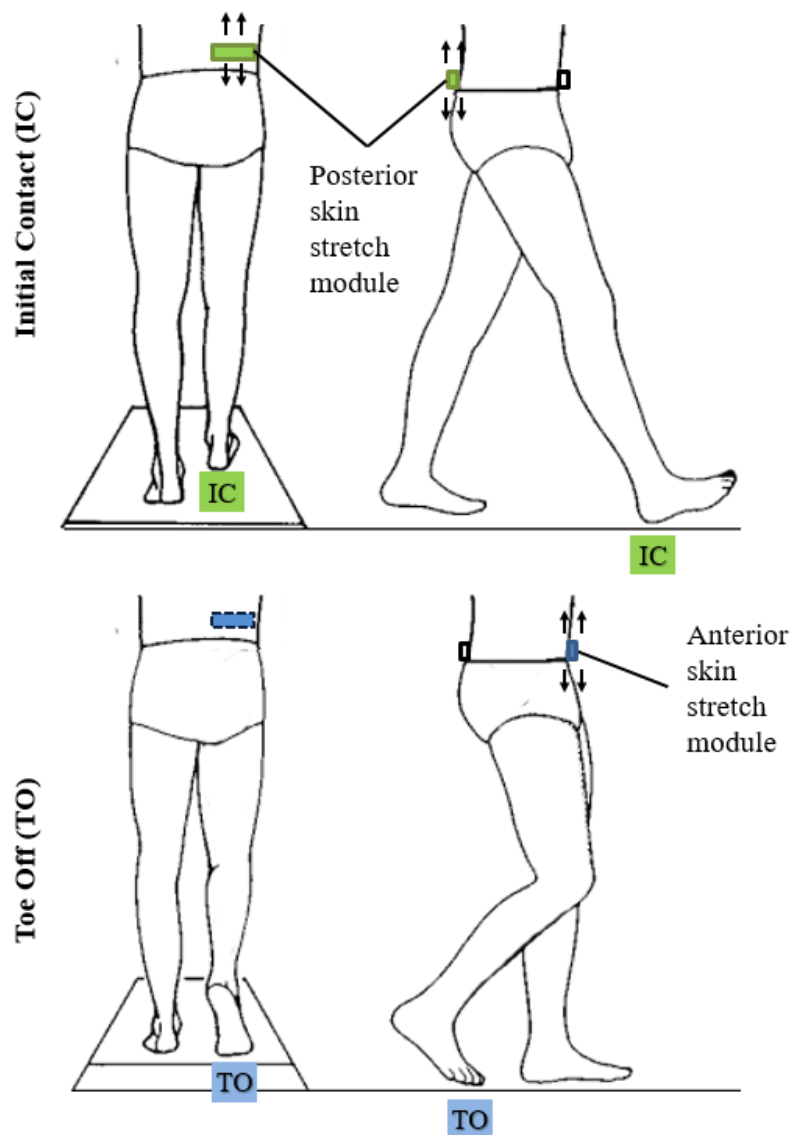


**Figure 5.7** Haptic feedback strategy, showing the placement of corresponding feedback modules. Images modified from [158]

An IMU attached at the lateral shank continuously records the shank angular velocity and transmits the data wirelessly to a PC. The event detection algorithm was carried out in real-time and upon detection of events, activation instructions were sent to respective feedback modules placed on the trunk.

#### 5.4.2 Feedback mode

Based on the detection of IC and TO events during walking, three different feedback modes are investigated. The purpose of varying the feedback mode was to investigate whether subjects perform better in terms of perceptibility and response time when subjected to different frequency of stimuli throughout the walking gait. The explanation for each feedback mode is accompanied by a figure showing the occurrence of the feedback with respect to the angular velocity signal at the shank during the gait cycle.

##### a) *Sparsely distributed (SD) feedback*

In the SD feedback, only a maximum of one haptic module was activated in a single gait cycle, with no two activations happening sequentially. As shown in Figure 5.8, the activation of posterior feedback module is not followed by activation of the anterior module and vice versa. This feedback mode denotes the most discrete form of feedback, and should exert the least cognitive loads on the subjects because the occurrence of the feedbacks is very sparse throughout the gait.

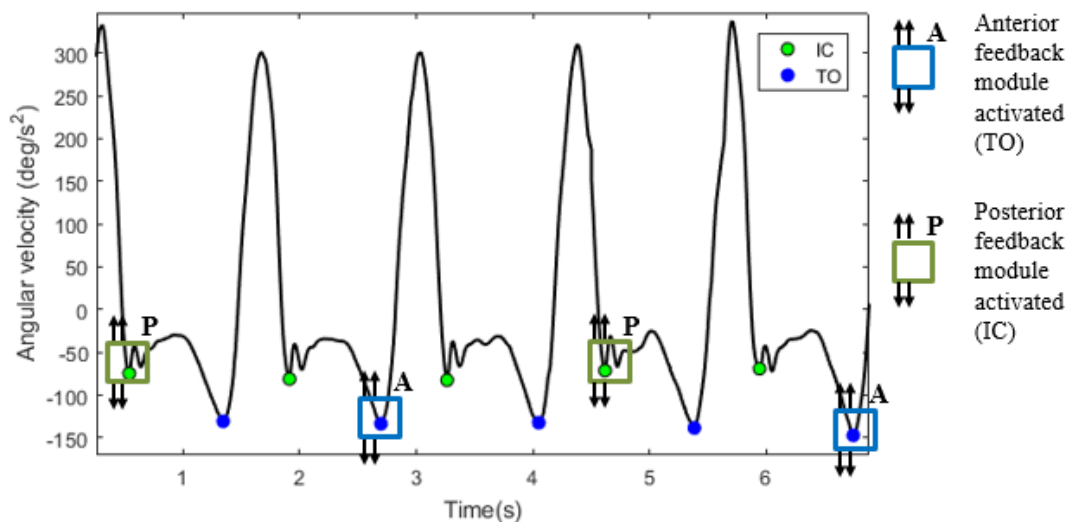


**Figure 5.8 SD feedback mode**

b) *Sequential-alternating (SA) feedback*

In the SA feedback, both IC and TO events trigger activation of the respective haptic feedback module in a complete gait cycle. However, the feedback will only be delivered on every other gait cycle (alternating pattern - Figure 5.9). The SA feedback is in between the SD and the continuous feedback in terms of the frequency of stimuli delivered throughout the gait.

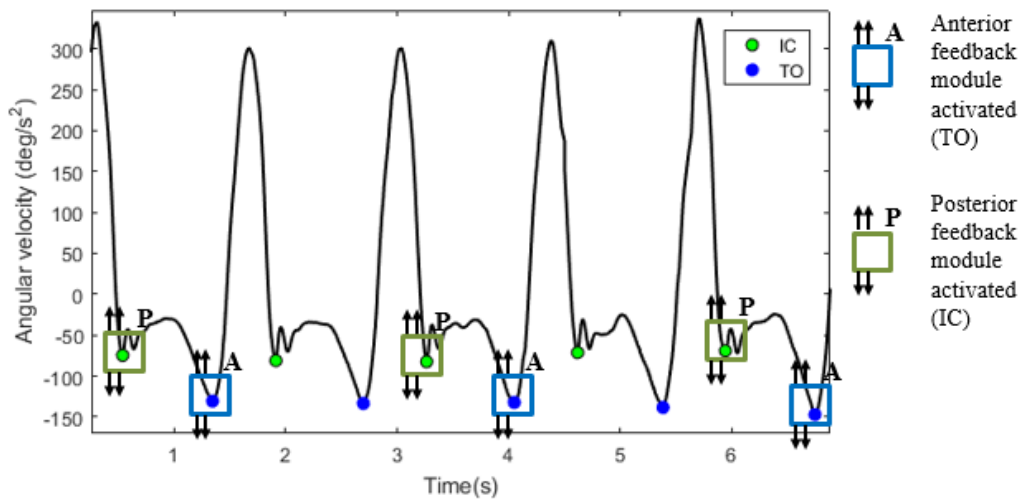


**Figure 5.9 SA feedback mode**

c) *Sequential-continuous (SC) feedback*

In the SC feedback mode, the haptic modules were activated on every IC and TO detected throughout the ambulation as shown in Figure 5.10. This feedback is expected to exert most cognitive demand to the subjects, especially during faster walking speed as the feedback is delivered continuously for every gait cycle.

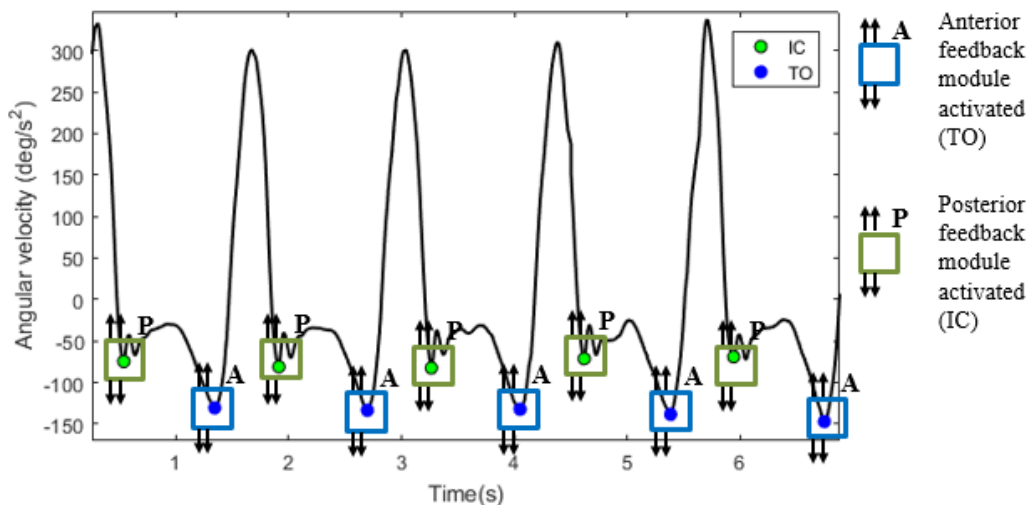


**Figure 5.10 SC feedback mode**

### 5.4.3 Experimental Setup

Six healthy male participants (age:  $29.7 \pm 4.8$  years; height:  $175.3 \pm 5.2$  cm; weight:  $74.6 \pm 7.7$  kg) without any known gait abnormalities participated in this study. Consents were obtained from the participants and the activities performed were approved by the Ethical Review Board (MEEC 14-012 – Appendix D).

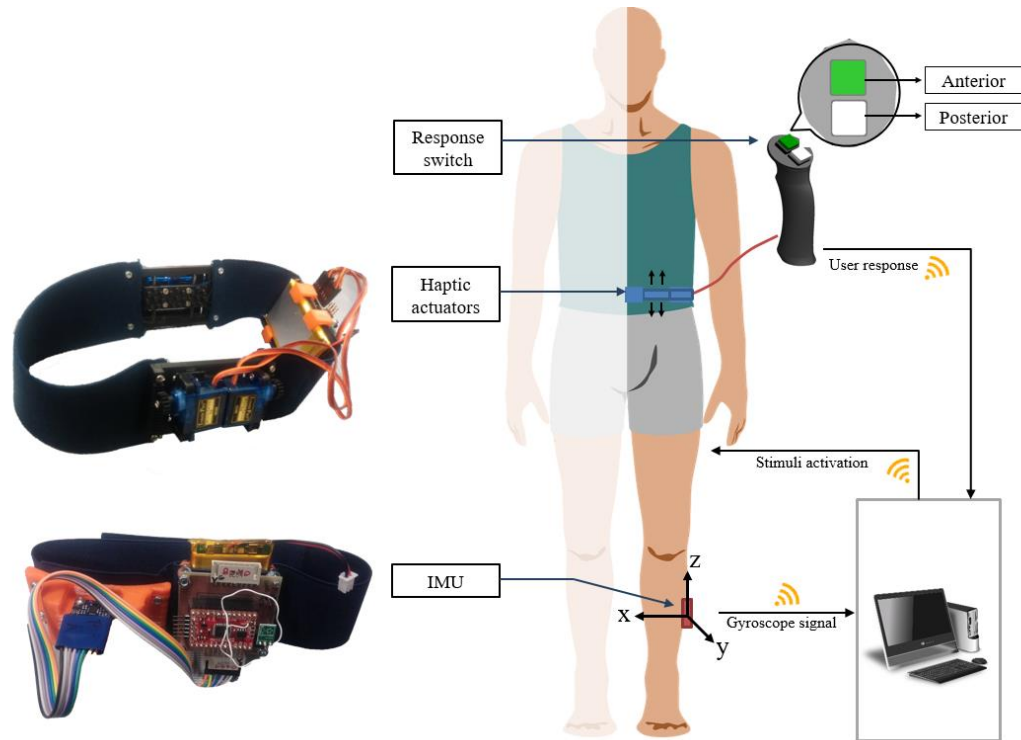


**Figure 5.11 Experimental apparatus**

Figure 5.11 shows the experimental apparatus. An event detection module consisting of an IMU and processing unit was fitted on the lateral side of the right shank. The haptic feedback modules were fitted on the right side of the lower trunk, around the abdominal area of the body. The haptic modules were positioned on the anterior and posterior sides of the body, and held by an elastic fabric cuff. The haptic plate was positioned such that it touches the skin and enough force was exerted to prevent the actuator from slipping while delivering the skin-stretch stimuli. Subjects hold a handheld response switch on one hand throughout the walking experiment. The handheld switch has two color-coded pushbuttons, each one corresponds to the anterior and posterior feedback modules. Subjects were asked to familiarize with the system while walking on the treadmill for two minutes. The treadmill was then started at the speed of 2.0 km/h. Once stable walking has been achieved, one of the feedback

modes as described previously was selected. The angular velocity information from the IMU attached at shank was collected in real-time and passed through an event detection algorithm. Upon detection of the event, appropriate haptic modules were activated, based on the selected feedback modes. Subjects were asked to press the correct pushbutton as quickly as possible to indicate feeling the feedback either in anterior or posterior region of the lower trunk. The task was repeated until all three feedback modes (SD, SA, and SC) was carried out for that particular walking speed. The whole experiment was then repeated with walking speed of 2.5 km/h – 5 km/h, in 0.5 km/h increment.

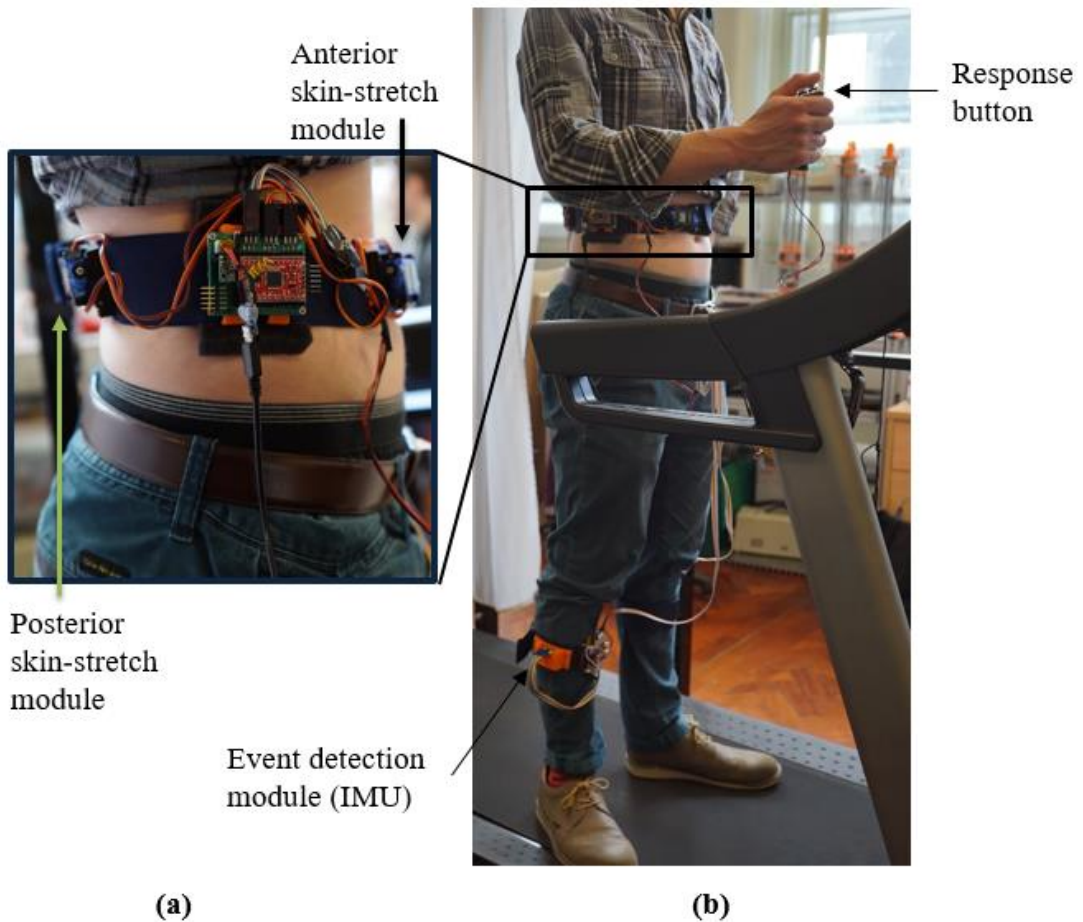


**Figure 5.12 Experimental setup, showing the placement of the (a) haptic module and (b) event detection modules and response button**



#### 5.4.4 Data Analysis

Figure 5.13 shows an example of the data collected as visualized in Matlab (R2016b, Mathworks Inc). The timing of stimuli and the response time from the subjects were super-imposed on the shank angular velocity plot to allow visual inspection of the data.

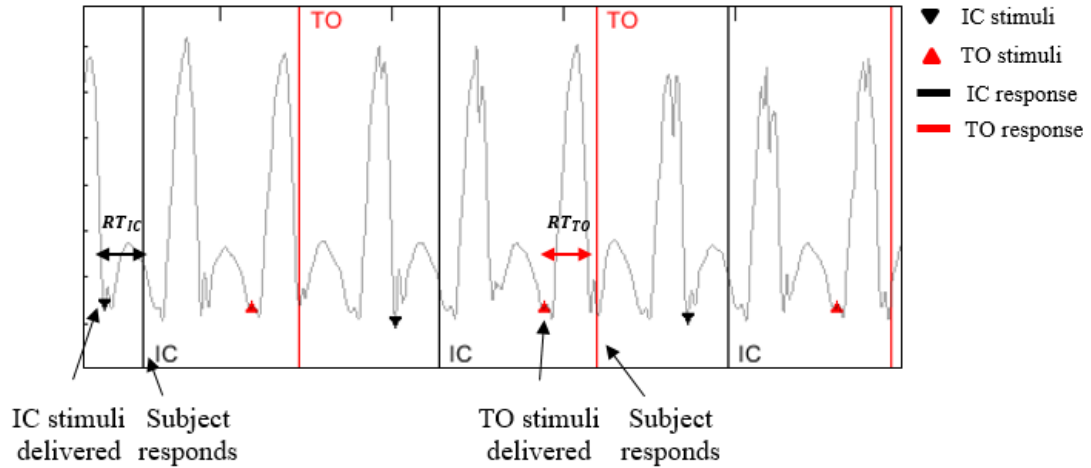


**Figure 5.13** An example of visualization of data analysis from the data collected during SD feedback mode.

A Matlab routine was then written to analyse the data and perform the following calculations.

##### a) Perceptibility

Since the haptic modules were placed in two locations, the perceptibility was calculated separately:

$$PE_{IC}(\%) = \frac{N_{IC}}{D_{IC}} \times 100 \quad (5.2)$$

Similarly,

$$PE_{TO}(\%) = \frac{N_{TO}}{D_{TO}} \times 100 \quad (5.3)$$

Where

$D_{IC}$  = Number of IC feedback delivered

$D_{TO}$  = Number of TO feedback delivered

$N_{IC}$  = Number of IC feedback identified

$N_{TO}$  = Number of TO feedback identified

*b) Response time*

The response time is defined as the time taken for the subjects to register response indicating the stimuli delivered is perceived. Let

$T_f$  = time index of the delivered feedback

$T_r$  = time index of subjects' response

$RT$  = response time

The response time for any identified feedback can be found as:

$$RT = T_f - T_r \quad (5.4)$$

The average response time for identified IC and TO events can be calculated as:

$$RT_{IC} (ms) = \frac{\sum_{i=1}^{N_{IC}} (T_{fi} - T_{ri})}{N_{IC}} \quad (5.5)$$

and,

$$RT_{TO} (ms) = \frac{\sum_{i=1}^{N_{TO}} (T_{fi} - T_{ri})}{N_{IC}} \quad (5.6)$$

While calculation using automated method using Matlab yielded systematic output for data analysis, it was possible that the algorithm was not robust enough to identify irregularities in the acquired data. A visual inspection was therefore carried out with all the data to validate the analysis method. The results from manual inspection showed two possible scenarios that could affect the PE and RT calculations. Figure 5.14(a) depicts the first irregularity in which subjects mistakenly pressed the pushbutton twice in short time. This can contribute to over-estimation of the number of feedback received and therefore affect the PE calculation. In this case, before proceeding with the analysis, the occurrence of the second feedback was removed from the data. The second irregularity was rather interesting. As shown in Figure 5.14(b), the subject pressed the response button just before the feedback was delivered, instead of after receiving the feedback. This observation is further discussed at the end of this section. The response by the subjects in this case was considered invalid and was considered as unsuccessful detection of the feedback.

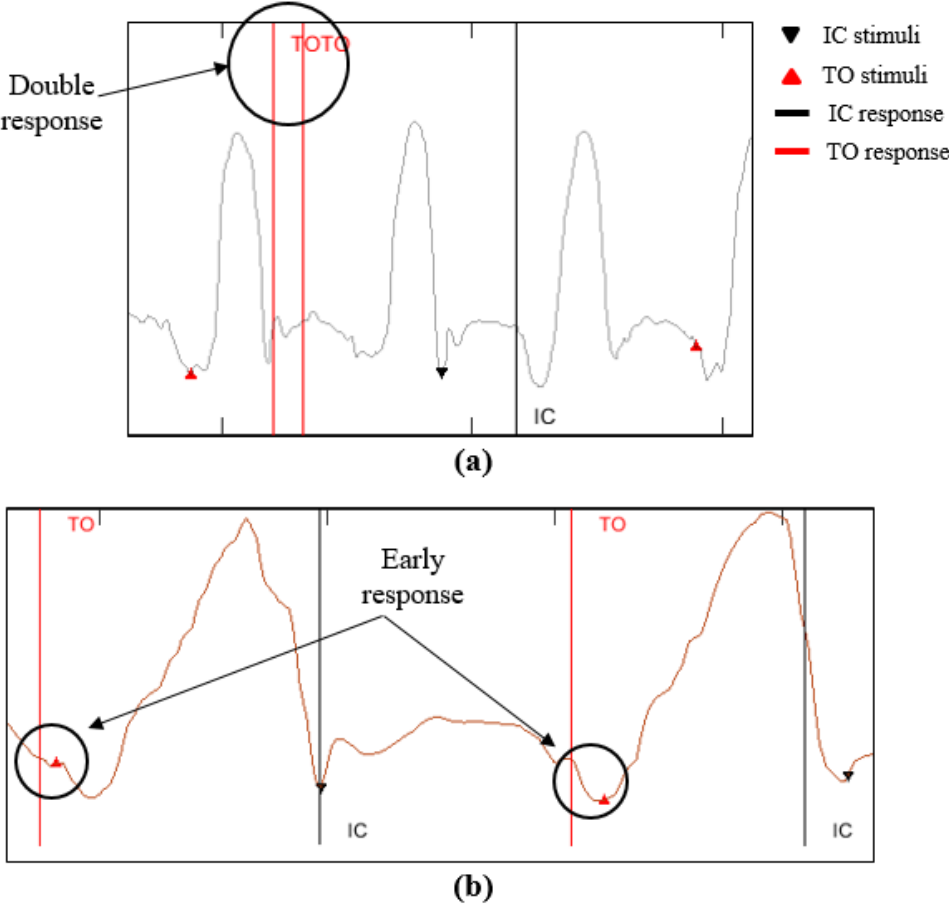
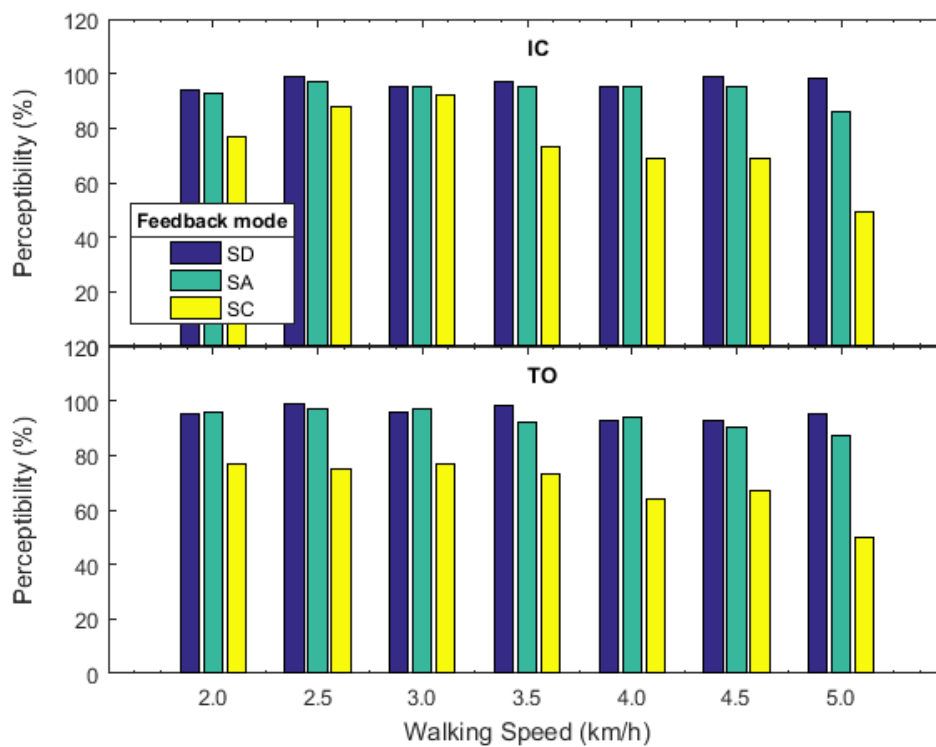


Figure 5.14 Possible irregular data scenarios (a) double response and (b) early response.

## 5.4.5 Results

### 5.4.5.1 Perceptibility (PE)

An overview of PE was found by plotting the subjects' PE for the stimuli in both location (posterior – IC, anterior – TO) across the feedback mode and walking speed as shown in Figure 5.15. A noticeable trend can be observed for PE across the feedback mode. SD feedback mode has the highest PE at all walking speed, and lowest during SC. SA feedback was always more perceptible than SC but does not differ in comparison to SD.



**Figure 5.15 PE across walking speed**

Table 5.6 shows the tabulated value of PE across both walking speed and feedback mode. It can be noted that an average PE > 96% was achieved by the subjects for SD feedback, > 95 % for SA and > 85% for SC. In addition, it can be observed that higher walking speed of 4.0 – 5.0 km/h contributed to decrease in the PE for the subjects. This is especially true in the case of SC feedback mode, in which the PE reduces to almost only 50% for walking speed of 5.0 km/h.

**Table 5.6 Perceptibility distribution across experimental parameters**

		IC							
		Walking Speed							
Feedback Mode		2.0	2.5	3.0	3.5	4.0	4.5	5.0	Mean $\pm$ SD
	SD	94.2	99.3	94.6	97.0	95.1	98.7	97.9	96.7 $\pm$ 3.3
	SA	92.6	97.2	95.4	94.8	96.2	95.0	85.6	93.8 $\pm$ 14.4
	SC	76.8	87.9	92.4	73.0	68.8	69.0	49.3	73.9 $\pm$ 14.2
		TO							
		Walking Speed							
Feedback Mode		2.0	2.5	3.0	3.5	4.0	4.5	5.0	Mean $\pm$ SD
	SD	95.3	98.8	96.4	97.8	92.6	93.0	95.1	95.6 $\pm$ 3.4
	SA	96.3	96.8	97.2	91.8	97.6	89.9	87.2	93.8 $\pm$ 14.8
	SC	76.7	74.5	76.7	72.7	63.5	67.5	49.9	68.8 $\pm$ 9.6

	$PE > 95\%$
	$85\% \leq PE < 95\%$
	$PE < 85\%$

### 5.4.5.2 Response Time (RT)

#### 1. Individual RT

Figure 5.16 shows the overall response time for across the subjects for all walking speed and feedback modes. It can be observed that there exists a variability in response time between the subjects. However, with the exception of S3, the difference between RT for IC stimuli and TO stimuli is not significant ( $< 50$  ms), albeit  $RT_{IC}$  being slightly higher than  $RT_{TO}$  for some subjects. The result suggests that the placement of the haptic module in the anterior and posterior region of the lower trunk did not affect the response time. In other words, both regions seem to be similar in sensitivity to the skin-stretch feedback. It is worth noting, however, the data in Figure 5.16 averages all the RT for IC and TO across different feedback mode and therefore did not give the specific detail of the variation in RT for different experimental conditions. However, the standard deviation value, denoted as the error bar in Figure 5.16 indicated that the RT varies greatly between different experimental conditions.

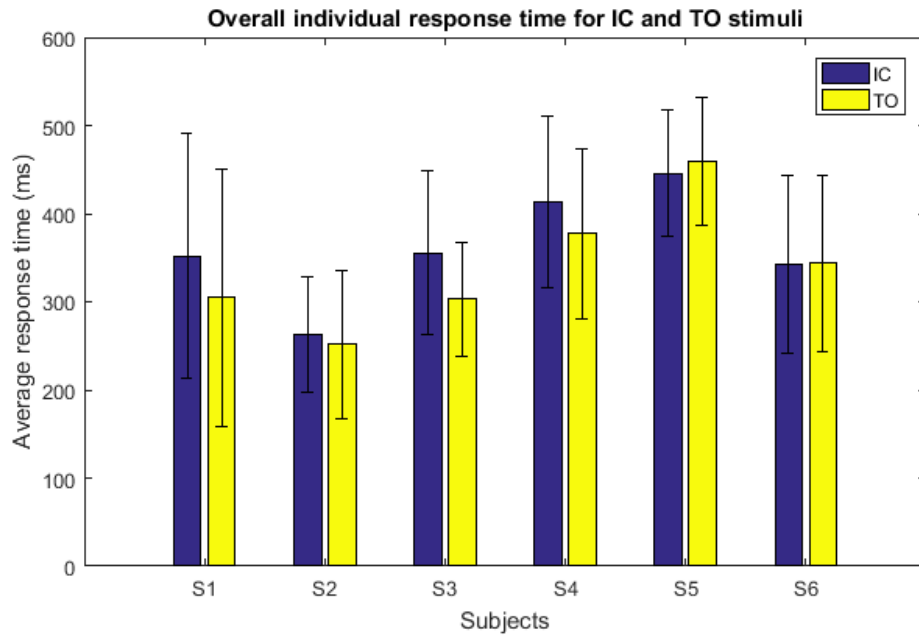


**Figure 5.16**  $RT_{IC}$  and  $RT_{TO}$  for all subjects. Error bar shows the standard deviation value

To examine the effects of walking speeds and feedback modes on the response time, further analysis was carried out as follows:

## 2. *RT across feedback mode*

Figure 5.17 shows the distribution of the  $RT_{IC}$  and  $RT_{TO}$  across the feedback mode, for each walking speed. It can be observed that subjects' RT exhibits a particular trend. Firstly, both IC and TO RT decreases steadily (with the exception of SD feedback mode) from 2.0 km/h to 3.5 km/h walking speed. Secondly, it can be noted that from 4.0 km/h to 5.0 km/h, subjects' RT remains more or less steady, and settles at a value lower than RT at 2.0 km/h. The trend was particularly clear with the SA and SC feedback modes. These observations can be explained as follows:

1. The decrease in RT was most possibly caused by the increase in the frequency of the feedback delivered to the subjects. As the walking speed increases, the frequency of gait cycle increases, and therefore the subjects were more vigilant in pressing the pushbutton throughout the experiment. This is also evident in Figure 5.17 where the SA and SC feedback mode have lower average RT since the stimuli frequency in these modes are higher.
2. The RT settles towards the higher walking speed, and the value of RT was not higher than it was when subjects were walking at the lowest speed (2.0 km/h).

This observation suggested that the subjects adapted to the change in stimuli frequency throughout the experiment and reacted more quickly when subjected to more frequent stimuli.

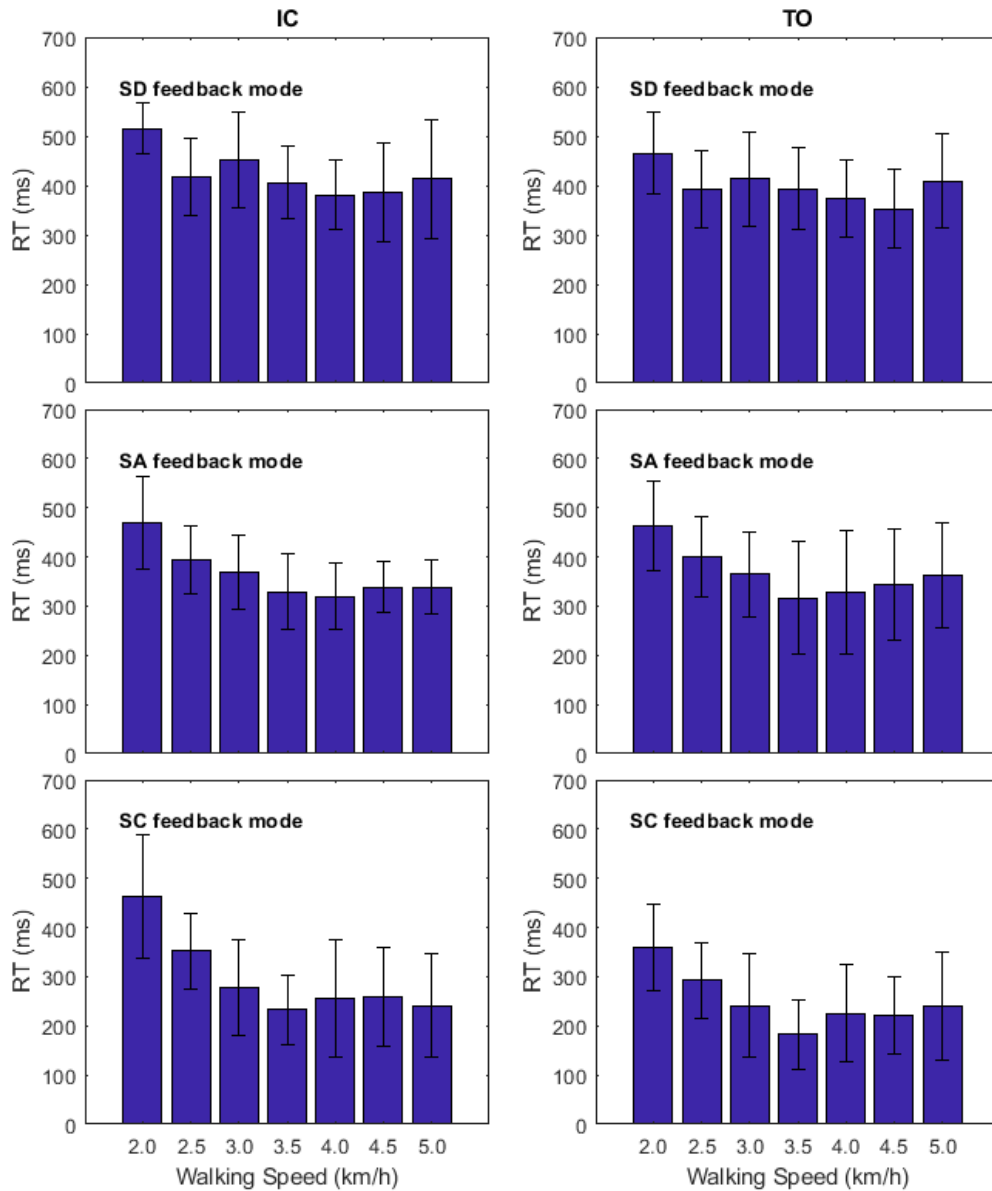
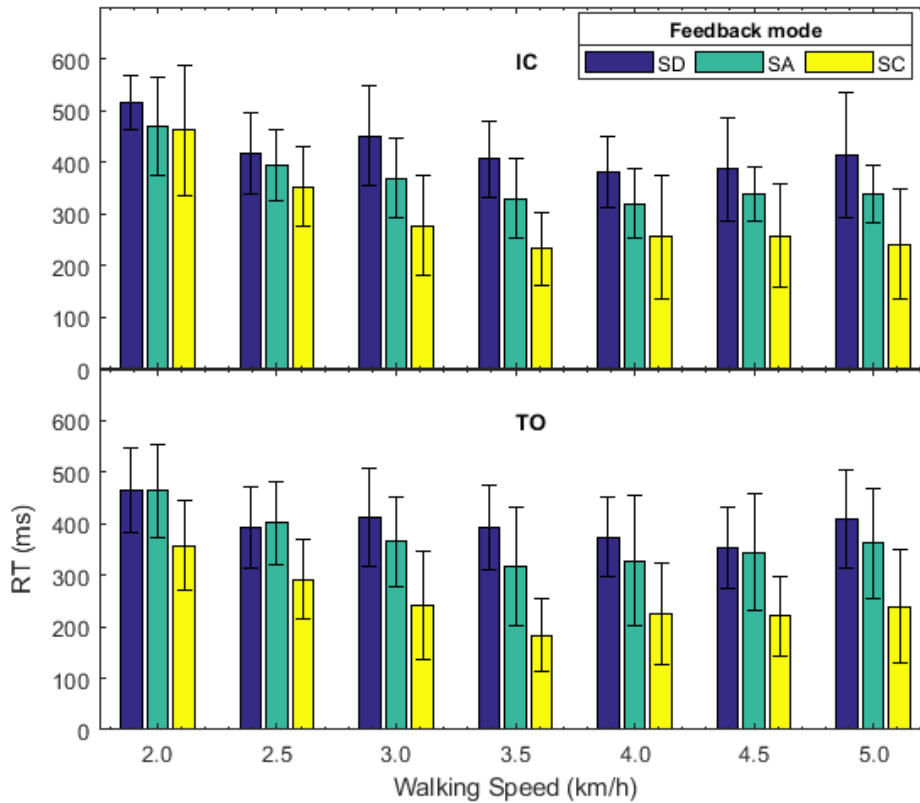


Figure 5.17  $RT_{IC}$  and  $RT_{TO}$  across different feedback modes

### 3. RT across walking speeds

The RT across walking speeds are shown in Figure 5.18. Subjects response for both IC and TO stimuli showed a clear trend; RT was highest during SD feedback mode, followed by SA and SC feedback modes.



**Figure 5.18** RT<sub>IC</sub> and RT<sub>TO</sub> across different walking speeds

To verify this result, a two-way repeated measures ANOVA was run to determine the effect of different feedback modes over various walking speeds on subjects' response time. There were no outliers, as assessed by examination of studentized residuals for values greater than  $\pm 3$  and Shapiro-Wilk's test of normality on the studentized residuals ( $p > .05$ ) indicated that the RT was normally distributed. There was no statistically significant two-way interaction between feedback modes and walking speeds. The main effect of feedback mode showed a statistically significant difference in RT between trials (IC -  $F(2, 10) = 19.754, p < .001$  and TO -  $F(2, 10) = 29.569, p < .001$ ). Table 5.7 shows the result of post hoc tests using the Bonferroni correction carried out on both feedback modes to find out if there was any significant difference in RT between feedback modes. It can be observed for both IC and TO stimuli, there



was a significant reduction in the RT between SD feedback mode and SC feedback mode (140.07 ms and 148.33 ms) respectively. No statistically significant effect of walking speed was found to conclude that subjects' response time were affected by the change in walking speed. Table 5.8 summarizes the distribution of RT across feedback mode and walking speed.

**Table 5.7 Mean difference in RT (ms) between SA, SD and SC mode**

Feedback mode	IC			TO		
	SD	SA	SC	SD	SA	SC
SD	-	<b>71.95*</b>	<b>140.07*</b>	-	31.07	<b>148.33*</b>
SA		-	68.12		-	<b>117.62*</b>
SC			-			-

\*indicates statistically significant difference at  $p < .05$

**Table 5.8 Response time distribution across experimental parameters**

		IC							
		Walking Speed							Mean $\pm$ SD
Feedback Mode	Feedback Mode	2.0	2.5	3.0	3.5	4.0	4.5	5.0	
		SD	515	416	451	406	381	387	413
	SA	470	393	369	329	336	338	338	367.5 $\pm$ 46.6
	SC	462	353	278	233	256	258	241	297.1 $\pm$ 76.5
		TO							
		Walking Speed							Mean $\pm$ SD
Feedback Mode	Feedback Mode	2.0	2.5	3.0	3.5	4.0	4.5	5.0	
		SD	465	392	413	393	374	353	409
	SA	464	401	365	317	359	344	362	373.2 $\pm$ 43.8
	SC	358	292	241	183	226	221	239	251.4 $\pm$ 52.7

	$RT > 450$ ms
	$350 \text{ ms} \leq RT < 450$ ms
	$RT < 350$ ms

#### 5.4.6 Discussion and Key Findings

- a) The purpose of investigating different feedback modes was to identify the possibility of reducing the frequency of stimuli delivered to skin throughout

walking without compromising the perceptibility. Unlike continuous feedback such as demonstrated by Fan et al. [26], this haptic feedback system was intended for providing event-based information, and therefore does not require continuous activation of the haptic modules. This type of feedback has been suggested to allow its user to learn the feedback pattern without needing to pay attention continuously to the stimuli [25]. The results from this experiment suggested that the degree in which the subjects were able to perceive the skin-stretch feedback depended on both the feedback mode and the walking speed, while response time was mostly dependent on the feedback mode.

- b) Subjects demonstrated highest PE in the SD mode. This was consistent with the results obtained from previous experiment described in Section 5.3, in which stimuli was delivered with reduced timing constraint throughout the walking experiment. The subjects were able to perceive the stimuli with more than 95% perception accuracy. However, this particular feedback mode was not practical for real-time application since the subjects' *RT* for this feedback mode was very high ( $> 400$  ms).
- c) In contrast, the SC feedback, in which stimuli was delivered for each IC and TO event, caused the subjects' *RT* to decrease significantly to an average of 297.1 ms for IC and 251.4 ms for TO. However, the subjects' PE in this mode was lower (around 71%). This is partly caused by a pattern mentioned in Section 5.4.4, in which the subjects pressed the response button before the actual activation of the haptic module. This behaviour was observed in the SC feedback mode, especially during faster walking speed (4.0 – 5.0 km/h). Analysis of the data showed that this happened around  $< 50$  ms before the actual stimuli was delivered. A possible explanation for this was that because of the high frequency of stimuli during faster walking speed, the subjects tend to learn the pattern of the stimuli, and therefore tried to achieve the quickest response time by anticipating the subsequent stimuli. This scenario is not entirely discouraging, because it indicated that the subjects could actually learn the event based feedback pattern and translate this into mechanical action. Rather than a disadvantage, this could benefit the amputees by

allowing them to learn the feedback pattern over time, reducing the cognitive loading exerted by trying to feel the stimuli during each gait cycle.

- d) The SA feedback mode appears to present the most optimal results in terms of PE (95%) and RT (370 ms). The delivery of skin-stretch in sequential manner (IC followed by TO) caused participants to react quickly to the stimuli. At the same time, skipping a gait cycle reduces the chance of confusing consecutive stimuli, especially at the higher speed as observed in SC feedback mode. Crea et al. [25] studied subjects' PE to vibrotactile stimuli triggered by gait phase change during treadmill walking, in similar pattern described in SA feedback mode. The authors found that at the speed of 2.0 km/h the subjects were able to identify missing stimuli around 85% of the time, which is lower than the subjects' PE in this experiment at the same speed (~96%). In fact, an average PE of 95% was achieved by subjects throughout the walking speed, indicating high perceptibility of the stimuli during the SA feedback.

## 5.5 System Evaluation with Amputee

Appendix A presents an evaluation of the haptic feedback system with an above-knee amputee. To investigate the effect of the haptic feedback system on the amputee gait, changes to spatio-temporal parameters as well as vertical ground reaction force parameters during baseline and feedback walking condition are recorded and analysed. The experimental work described focuses on the engineering aspect of the haptic feedback system rather than a clinically designed trial. Further details of the work and the discussion of the findings can be found in Appendix A.

## 5.6 Summary

This chapter presented two experimental works to assess the design presented in the previous two chapters. The first experiment was carried out to assess the perceptibility of the haptic module during static and dynamic conditions. It was found that stretch as small as 3 mm was enough to be perceived during dynamic trials. The findings from the first experiment prompted a redesigning of the haptic device to reduce the footprint and allow more modular design that can be placed around other parts of the body. A review of placement location for the haptic modules was carried out and the lower trunk was decided as the best alternative for placement of two haptic modules.

The second experiment utilised the revised haptic module and evaluated the complete haptic feedback system which consist of the skin-stretch haptic modules and the event detection module based on IMU. Three feedback modes were investigated during dynamic condition, across various walking speeds. Subjects' perceptibility towards the skin-stretch feedback and their response time indicated feasibility for using the system in real time during ambulation. The next chapter summarizes the work presented in this thesis, as well as outlining potential future works to improve the system presented in this study.

## **CHAPTER 6:**

### **Summary, Conclusion, and Future Works**

#### **6.1 Summary and Assessment of the Research Aim and Objectives**

This section describes the assessment of research objectives outlined in Section 1.3.2. The aim of this study is to design a skin-stretch feedback system to create awareness of limb placement during walking for lower limb amputee. This was achieved by fulfilling the following objectives:

- To carry out an iterative design of a skin-stretch module that can be worn around the lower limb or on the body.

Chapter 3 describes the development and design iterations of the proposed skin-stretch feedback module. In Section 3.2, a preliminary design to assess skin-stretch as a haptic modality was presented. The findings from the preliminary trials facilitated the development of a novel skin-stretch mechanism which is intended for delivering event-based information. The description of mechanism and fabrication of this module were described in Section 3.4. Further revision of the design, which reduces its footprint and allows modularity and flexibility of attachment was described in Section 3.5.

- To characterize the skin-stretch module to obtain its performance and working parameters.

The characterization carried out to assess the skin-stretch device parameters was described in Section 3.4.3 in chapter 3. The movement profile and the force profile were obtained to evaluate the design parameters. Skin-stretch period of 150 ms was found to be the most effective, with high accuracy of stretch magnitude in the range of 1 mm – 4 mm.

- To evaluate users' perception to the skin-stretch module in static and dynamic conditions.

An experimental work carried out to evaluate subjects' perceptibility of the skin-stretch device was reported in Section 5.2 of Chapter 5. The trials with healthy subjects and an above-knee amputee were carried out to assess the effect of stretch magnitude towards perception of the stimuli during static (standing) and dynamic (walking) condition. It was found that stretch magnitude of at least 3 mm delivered in duration of 150 ms was enough to be perceived by subjects during walking.

- To integrate an event detection module for controlling the activation of the skin-stretch device during gait.

To form a complete haptic feedback system, an integration of an event detection module is described in Section 4.2 of Chapter 4. The module was based on an IMU placed at shank to obtain the angular velocity data during walking. A distinctive characteristic of the signal in sagittal plane allowed a threshold based algorithm to be utilized to detect IC and TO events. Section 4.2.4 describe the experiment carried out to assess the existing algorithm for event detection. A predictive algorithm was proposed in Section 4.2.5 to expand the capability of the event detection system when used as a control mechanism for the skin-stretch haptic device.

- To assess users' perception and performance of the complete haptic feedback system.

The evaluation of the complete haptic feedback system was carried out and described in Section 5.4 where detection of IC and TO events were utilised to control the activation of the skin-stretch module across various feedback modes and different walking speeds. The subjects' perceptibility and response time were evaluated. The results showed that subjects can identify the skin-stretch stimuli across walking speed of 2.0 km/h – 4.0 km/h with high accuracy (> 90%) within an average of 350 ms in SA and SC feedback modes, indicating feasibility of the system for use in real-time

gait feedback. Response time to stimuli was found to be dependent on feedback mode, without significant effects from the varying walking speed

- To evaluate the system on lower limb amputee and assess its effects on the gait parameters.

Appendix A describes an experimental work carried out to assess the haptic feedback system with an above-knee amputee. Spatio-temporal and kinematic data were collected using wearable IMU sensors and force insole described in Chapter 4. Two walking environments, namely the treadmill and overground walk were assessed. Although no significant effects of the feedback can be concluded based on the results from the experimental work, during feedback condition, especially the SC feedback mode, an increase in prosthetic leg stance duration was recorded for walking speed lower than 4.0 km/h. Although the increase was not significant, the decrease in timing to first peak as analysed from the ground reaction force data supports the possibility of increased confidence in prosthetic leg placement during feedback condition.

## 6.2 Conclusions

This research work presented a novel wearable skin-stretch device capable of conveying gait information to its wearer during gait activity. The work is concluded as follows:

1. Literature review revealed common challenges faced by amputee due to sensory deficit, which is the loss of awareness of limb placement during walking. However, very limited work can be found that describes providing haptic feedback to lower limb amputees.
2. Skin-stretch haptic modality was selected as the focus of this study as it presented certain advantages over commonly used feedback modality such as vibration, but no available literature described skin-stretch feedback for conveying gait event information.
3. The proposed haptic feedback system consists of two main elements; the skin-stretch device for providing feedback and a gait event detection module for identifying IC and TO events during walking.

4. Three designs of the haptic feedback modules were presented. The initial design used a grooved belt to simulate multiple contact points to provide stretch sensation using a DC motor. The design indicated feasible application of stretch stimuli for providing feedback, however was limited in terms of its capability and control.
5. A second design which retains the idea of multiple contact points for stimuli, but using a different mechanism was presented. The skin-stretch was delivered using a haptic plate attached to two servo motors in a rack-and-pinion arrangement. The feedback module was fabricated using 3D printed components. Characterization of the haptic device was carried out to assess the design parameters such as the movement and the force profile.
6. An integration of event detection module based on angular velocity signal at shank was described. Validation of the angular velocity signal with motion capture system indicated successful identification of all IC and TO events throughout walking at different speeds and similarity to angular velocity profile generated by the motion capture system. An additional predictive algorithm was proposed for the event detection system to increase its usability in future control application.
7. Design of a force insole was described, for obtaining vertical ground reaction force (vGRF) parameters during evaluation of the haptic feedback system with an above-knee amputee. The insole design allowed monitoring the vGRF continuously during experimental work outside gait laboratory environment.
8. An experimental work was carried out with healthy subjects and an amputee to assess subjects' perception towards the delivered stimuli using the second haptic module design. Results indicated good perceptibility in static and dynamic mode for stretch magnitude of at least 3 mm delivered in the period of 150 ms. However, the experimental work revealed some limitations in delivering the haptic feedback on thigh, and highlighted some limitations of the existing design.
9. A suitable alternative placement location was investigated, and a revised haptic module design which has reduced footprint and allows modular placement on the body was used for the subsequent experimental work.



10. The revised design was used in conjunction with the gait event detection module to form a complete haptic feedback system. Three feedback strategies were described, and evaluation of the system was carried out with healthy subjects to identify feasibility of the proposed system in providing real-time feedback during gait activity.
11. An evaluation was carried out with one above-knee amputee to assess the effect of the feedback during real-time walking, as presented in Appendix A. Overground and treadmill walking session was carried out, in which the subject walked in baseline (no feedback) and with feedback condition. Two IMUs were fitted on the intact and prosthetic sides to record the temporal parameters while force insole on the prosthetic side was used to collect the vertical GRF data. The results showed possible effect of the haptic feedback on gait symmetry where the above-knee subject showed increased stance duration of the prosthetic leg during SC feedback condition, specifically during lower walking speed ( $< 4.0$  km/h). In some instances, analysis of timing to first peak force of the vertical GRF also indicates preference on shifting the weight towards the prosthetic side during feedback condition. However, no conclusive evidence was found to indicate that the delivery of the haptic feedback had a significant immediate effect on the gait parameters during short-term intervention.
12. The proposed haptic feedback could be beneficial in the following applications:
  - Gait retraining, for persons with lower limb amputation and people who exhibit walking impairment but still retain sensitivity to tactile stimuli.
  - As a warning system for preventing falls among amputee community in response to detection of irregular characteristics of gait during walking.
  - Intervention in early stage gait rehabilitation post-amputation, as subjects are more likely to adapt to feedback during gait retraining stage.

### 6.3 Future Works

As the design provides a preliminary investigation into using skin-stretch feedback as a mechanism for delivering gait event information, the following are suggested to extend the research in the future:

1. The existing design focuses on delivering skin-stretch by manipulating the stretch magnitude rather than the stretch force. Therefore, an approximately constant range of normal force, i.e. the force between the haptic plate and the skin was applied throughout the experimental work. Since the normal force will also affect the intensity of the skin-stretch stimuli, future work will extend existing design into a dual action skin-stretch device, in which not only the stretch can be delivered in lateral direction, but can also be manipulated in the normal direction.
2. In all designs proposed in this work, rigid actuators such as DC motors and servo motors were used. However, in general, human limb tend to have curves and compliance structure which responds better to compliance actuation. Investigating the use of soft actuator such as artificial muscle providing skin-stretch feedback would be an interesting direction for future work.
3. One clear limitation of the study is the evaluation of the system with only a single amputee. Although it is known that amputees exhibit high variabilities in the gait and therefore between-subject comparison can often be difficult to make, an increased pool of amputee participants can provide a better idea of the performance of the haptic feedback system in improving common gait problems such as gait symmetries. Future work will also consider both below knee and above knee participants and investigate the effects of such feedback in both groups.
4. The final design of the haptic module was placed on the lower trunk and feedback was delivered to the skin in response to detected IC and TO events. This is especially practical for above knee amputees since the prosthetic socket usually covers the stump entirely. Future work should investigate methods for embedding the skin-stretch device within the sockets, for example by designing a custom-made socket which allows access to the stump skin surface for placing the skin-stretch device.

5. The current work only investigated the performance of the haptic device during level ground walking. Future work shall include assessment of the practicality and usefulness of such device in different walking environment such as inclined surface, stairs, and uneven walking terrain.
6. The current work was focused on investigating changes in gait parameters over a short period of time/session. While gait retraining and change is possible, such observation might not be possible within limited experimental sessions. One improvement that can be proposed for future work is investigating the haptic feedback effect on instantaneous postural adjustment such as balance during perturbation or simulated dynamic disturbances. Such work could benefit from the use of an adjustable platform coupled with virtual reality environment to provide realistic real-time perturbation to the subject. In this way, a more instantaneous gait adaptation can be forced and the effect of the haptic feedback in delivering awareness of limb position can be better understood. In addition, experimental work should also be carried out with novice prosthetic leg users, such as those at the beginning of the rehabilitation stage, to observe effect of such intervention at the stage where walking strategies post-amputation are still being developed.

## References

1. Zhang, X.R., et al., *On Design and Implementation of Neural-Machine Interface for Artificial Legs*. Ieee Transactions on Industrial Informatics, 2012. 8(2): p. 418-429.
2. Ahmad, N., et al., *The prevalence of major lower limb amputation in the diabetic and non-diabetic population of England 2003-2013*. Diab Vasc Dis Res, 2016. 13(5): p. 348-53.
3. HQIP *Lower limb amputation report*. 2014.
4. Sabzi Sarvestani, A. and A. Taheri Azam, *Amputation: a ten-year survey*. Trauma Mon, 2013. 18(3): p. 126-9.
5. Kishner, S.L., J. M. *Gait Analysis After Amputation*. 2015 [7-Oct-2017]; Available from: <http://emedicine.medscape.com/article/1237638-overview>.
6. Gailey, R., et al., *Review of secondary physical conditions associated with lower-limb amputation and long-term prosthesis use*. Journal of Rehabilitation Research and Development, 2008. 45(1): p. 15-29.
7. Nikolajsen, L. and T.S. Jensen, *Phantom limb pain*. Current Pain and Headache Reports, 2000. 4(2): p. 166-170.
8. Rusaw, D., et al., *Bilateral electromyogram response latency following platform perturbation in unilateral transtibial prosthesis users: Influence of weight distribution and limb position*. Journal of rehabilitation research and development, 2013. 50(4): p. 531-544.
9. Miller, W.C., M. Speechley, and A.B. Deathe, *Balance confidence among people with lower-limb amputations*. Physical therapy, 2002. 82(9): p. 856-865.
10. Miller, W.C., et al., *The influence of falling, fear of falling, and balance confidence on prosthetic mobility and social activity among individuals with a lower extremity amputation*. Archives of Physical Medicine and Rehabilitation, 2001. 82(9): p. 1238-1244.
11. Miller, W.C., M. Speechley, and B. Deathe, *The prevalence and risk factors of falling and fear of falling among lower extremity amputees*. Archives of physical medicine and rehabilitation, 2001. 82(8): p. 1031-1037.
12. Schmalz, T., S. Blumentritt, and R. Jarasch, *Energy expenditure and biomechanical characteristics of lower limb amputee gait: The influence of prosthetic alignment and different prosthetic components*. Gait & Posture, 2002. 16(3): p. 255-263.
13. Johansson, J.L., et al., *A clinical comparison of variable-damping and mechanically passive prosthetic knee devices*. American Journal of Physical Medicine & Rehabilitation, 2005. 84(8): p. 563-575.
14. Seymour, R., et al., *Comparison between the C-leg (R) microprocessor-controlled prosthetic knee and non-microprocessor control prosthetic knees: A preliminary study of energy expenditure, obstacle course performance, and*

- quality of life survey*. Prosthetics and Orthotics International, 2007. 31(1): p. 51-61.
15. Clippinger, F.W., et al., *Afferent Sensory Feedback for Lower-Extremity Prosthesis*. Clinical Orthopaedics and Related Research, 1982(169): p. 202-206.
  16. Fan, R.E., et al., *A haptic feedback system for lower-limb prostheses*. Neural Systems and Rehabilitation Engineering, IEEE Transactions on, 2008. 16(3): p. 270-277.
  17. Walker, J.M., et al. *Tactile feedback of object slip improves performance in a grasp and hold task*. in *Haptics Symposium (HAPTICS), 2014 IEEE*. 2014. IEEE.
  18. Kim, K. and J.E. Colgate, *Haptic Feedback Enhances Grip Force Control of sEMG-Controlled Prosthetic Hands in Targeted Reinnervation Amputees*. Ieee Transactions on Neural Systems and Rehabilitation Engineering, 2012. 20(6): p. 798-805.
  19. Shull, P.B. and D.D. Damian, *Haptic wearables as sensory replacement, sensory augmentation and trainer - a review*. Journal of Neuroengineering and Rehabilitation, 2015. 12.
  20. Sabolich, J.A. and G.M. Ortega, *Sense of Feel for Lower-Limb Amputees: A Phase-One Study*. JPO: Journal of Prosthetics and Orthotics, 1994. 6(2): p. 36-41.
  21. Lee, M.-Y., C.-F. Lin, and K.-S. Soon, *Balance control enhancement using sub-sensory stimulation and visual-auditory biofeedback strategies for amputee subjects*. Prosthetics and orthotics international, 2007. 31(4): p. 342-352.
  22. Rusaw, D., et al., *Can vibratory feedback be used to improve postural stability in persons with transtibial limb loss?* Journal of rehabilitation research and development, 2012. 49(8): p. 1239-1254.
  23. Plauché, A., D. Villarreal, and R.D. Gregg, *A haptic feedback system for phase-based sensory restoration in above-knee prosthetic leg users*. IEEE transactions on haptics, 2016. 9(3): p. 421-426.
  24. Marayong, P., et al., *Vibrotactile Device for Rehabilitative Training of Persons with Lower-limb Amputation*. 2014 IEEE Healthcare Innovation Conference (HIC), 2014: p. 157-160.
  25. Crea, S., et al., *Providing Time-Discrete Gait Information by Wearable Feedback Apparatus for Lower-Limb Amputees: Usability and Functional Validation*. Ieee Transactions on Neural Systems and Rehabilitation Engineering, 2015. 23(2): p. 250-257.
  26. Fan, R.E., et al. *Pilot testing of a haptic feedback rehabilitation system on a lower-limb amputee*. in *Complex Medical Engineering, 2009. CME. ICME International Conference on*. 2009. IEEE.
  27. Kaczmarek, K.A., et al., *Electrotactile and vibrotactile displays for sensory substitution systems*. IEEE Trans Biomed Eng, 1991. 38(1): p. 1-16.
  28. Bark, K., et al., *Comparison of skin-stretch and vibrotactile stimulation for feedback of proprioceptive information*. Symposium on Haptics Interfaces for Virtual Environment and Teleoperator Systems 2008, Proceedings, 2008: p. 71-78.
  29. Wheeler, J., et al., *Investigation of rotational skin-stretch for proprioceptive feedback with application to myoelectric systems*. Neural Systems and Rehabilitation Engineering, IEEE Transactions on, 2010. 18(1): p. 58-66.

30. Bark, K., et al., *Rotational Skin-stretch Feedback: A Wearable Haptic Display for Motion*. Ieee Transactions on Haptics, 2010. 3(3): p. 166-176.
31. Caswell, N.A., et al. *Design of a forearm-mounted directional skin-stretch device*. in *Haptics Symposium (HAPTICS), 2012 IEEE*. 2012. IEEE.
32. Guinan, A.L., et al., *Back-to-Back Skin-stretch Feedback for Communicating Five Degree-of-Freedom Direction Cues*. 2013 World Haptics Conference (Whc), 2013: p. 13-18.
33. Chen, D.K.Y., et al., *Lower Extremity Lateral Skin-stretch Perception for Haptic Feedback*. Ieee Transactions on Haptics, 2016. 9(1): p. 62-68.
34. Ion, A., E.J. Wang, and P. Baudisch. *Skin drag displays: Dragging a physical tactor across the user's skin produces a stronger tactile stimulus than vibrotactile*. in *Proceedings of the 33rd Annual ACM Conference on Human Factors in Computing Systems*. 2015. ACM.
35. Abernethy, B., *Biophysical foundations of human movement*. 3rd ed. 2013, Champaign, IL: Human Kinetics. xiii, 394 p.
36. Healthline.com. *Leg Anatomy, Pictures & Model | Body Maps*. 2014; Available from: <http://www.healthline.com/human-body-maps/leg#seoBlock>.
37. Whittle, M.W., *Gait analysis : an introduction*. 4th ed. 2007, Edinburgh: Butterworth-Heinemann. 255 p.
38. Perry, J., *Gait analysis : normal and pathological function*. 1992, Thorofare, NJ: SLACK. xxxii, 524 p.
39. Linthorne, N.P., *Analysis of standing vertical jumps using a force platform*. American Journal of Physics, 2001. 69(11): p. 1198-1204.
40. Marasović, T., M. Cecić, and V. Zanchi, *Analysis and interpretation of ground reaction forces in normal gait*. WSEAS transactions on systems, 2009. 8(9): p. 1105-14.
41. DeLisa, J.A., *Gait analysis in the science of rehabilitation*. Vol. 2. 2000: Diane Publishing.
42. Barre, A. and S. Armand, *Biomechanical ToolKit: Open-source framework to visualize and process biomechanical data*. Computer Methods and Programs in Biomedicine, 2014. 114(1).
43. Mayagoitia, R.E., A.V. Nene, and P.H. Veltink, *Accelerometer and rate gyroscope measurement of kinematics: an inexpensive alternative to optical motion analysis systems*. Journal of Biomechanics, 2002. 35(4): p. 537-542.
44. Kavanagh, J.J. and H.B. Menz, *Accelerometry: A technique for quantifying movement patterns during walking*. Gait & Posture, 2008. 28(1): p. 1-15.
45. Tao, W., et al., *Gait analysis using wearable sensors*. Sensors, 2012. 12(2): p. 2255-2283.
46. Bamberg, S.J.M., et al., *Gait analysis using a shoe-integrated wireless sensor system*. Ieee Transactions on Information Technology in Biomedicine, 2008. 12(4): p. 413-423.
47. Liu, T., Y. Inoue, and K. Shibata, *Development of a wearable sensor system for quantitative gait analysis*. Measurement, 2009. 42(7): p. 978-988.
48. Catalfamo, P., S. Ghousayni, and D. Ewins, *Gait Event Detection on Level Ground and Incline Walking Using a Rate Gyroscope*. Sensors, 2010. 10(6): p. 5683-5702.
49. Maqbool, H.F., et al., *A Real-Time Gait Event Detection for Lower Limb Prosthesis Control and Evaluation*. Ieee Transactions on Neural Systems and Rehabilitation Engineering, 2017. 25(9): p. 1500-1509.

50. Crea, S., et al., *A wireless flexible sensorized insole for gait analysis*. *Sensors*, 2014. 14(1): p. 1073-1093.
51. Veltink, P.H., et al., *Ambulatory measurement of ground reaction forces*. *IEEE Trans Neural Syst Rehabil Eng*, 2005. 13(3): p. 423-7.
52. Bilro, L., et al., *A reliable low-cost wireless and wearable gait monitoring system based on a plastic optical fibre sensor*. *Measurement Science and Technology*, 2011. 22(4): p. 045801.
53. Stupar, D.Z., et al., *Wearable Low-Cost System for Human Joint Movements Monitoring Based on Fiber-Optic Curvature Sensor*. *Ieee Sensors Journal*, 2012. 12(12): p. 3424-3431.
54. Menguc, Y., et al., *Wearable soft sensing suit for human gait measurement*. *International Journal of Robotics Research*, 2014. 33(14): p. 1748-1764.
55. Mohamed, A.A., et al., *Comparison of Strain-Gage and Fiber-Optic Goniometry for Measuring Knee Kinematics During Activities of Daily Living and Exercise*. *Journal of Biomechanical Engineering-Transactions of the Asme*, 2012. 134(8).
56. Aminian, K., et al., *Evaluation of an ambulatory system for gait analysis in hip osteoarthritis and after total hip replacement*. *Gait & posture*, 2004. 20(1): p. 102-107.
57. Bugane, F., et al., *Estimation of spatial-temporal gait parameters in level walking based on a single accelerometer: Validation on normal subjects by standard gait analysis*. *Computer Methods and Programs in Biomedicine*, 2012. 108(1): p. 129-137.
58. Jasiewicz, J.M., et al., *Gait event detection using linear accelerometers or angular velocity transducers in able-bodied and spinal-cord injured individuals*. *Gait & posture*, 2006. 24(4): p. 502-509.
59. Kotiadis, D., H.J. Hermens, and P.H. Veltink, *Inertial Gait Phase Detection for control of a drop foot stimulator Inertial sensing for gait phase detection*. *Med Eng Phys*, 2010. 32(4): p. 287-97.
60. Pappas, I.P., et al., *A reliable gait phase detection system*. *IEEE Trans Neural Syst Rehabil Eng*, 2001. 9(2): p. 113-25.
61. Selles, R.W., et al., *Automated estimation of initial and terminal contact timing using accelerometers; Development and validation in transtibial amputees and controls*. *Ieee Transactions on Neural Systems and Rehabilitation Engineering*, 2005. 13(1): p. 81-88.
62. Suh, Y.S. and S. Park, *Pedestrian Inertial Navigation with Gait Phase Detection Assisted Zero Velocity Updating*. *Proceedings of the Fourth International Conference on Autonomous Robots and Agents*, 2009: p. 505-510.
63. Williamson, R. and B.J. Andrews, *Gait event detection for FES using accelerometers and supervised machine learning*. *Ieee Transactions on Rehabilitation Engineering*, 2000. 8(3): p. 312-319.
64. Kirkwood, C.A., B.J. Andrews, and P. Mowforth, *Automatic Detection of Gait Events - a Case-Study Using Inductive Learning Techniques*. *Journal of Biomedical Engineering*, 1989. 11(6): p. 511-516.
65. Kong, K. and M. Tomizuka, *Smooth and continuous human gait phase detection based on foot pressure patterns*. *2008 Ieee International Conference on Robotics and Automation, Vols 1-9*, 2008: p. 3678-3683.

66. Roerdink, M., et al., *Online gait event detection using a large force platform embedded in a treadmill*. Journal of Biomechanics, 2008. 41(12): p. 2628-2632.
67. Skelly, M.M. and H.J. Chizeck, *Real-time gait event detection for paraplegic FES walking*. IEEE Transactions on neural systems and rehabilitation engineering, 2001. 9(1): p. 59-68.
68. Lauer, R.T., B.T. Smith, and R.R. Betz, *Application of a neuro-fuzzy network for gait event detection using electromyography in the child with cerebral palsy*. Ieee Transactions on Biomedical Engineering, 2005. 52(9): p. 1532-1540.
69. Qi, Y.B., et al., *Assessment of Foot Trajectory for Human Gait Phase Detection Using Wireless Ultrasonic Sensor Network*. Ieee Transactions on Neural Systems and Rehabilitation Engineering, 2016. 24(1): p. 88-97.
70. Kurichi, J.E.B., B. E.;Stineman, M.G *Amputation*. International Encyclopedia of Rehabilitation 2010.
71. Pitkin, M.R., *Biomechanics of lower limb prosthetics*. 2010, Heidelberg ; New York: Springer. xvii, 141 p.
72. Ertl, J.P. *Lower Limb Amputations*. 12-Sep-2014]; Available from: <http://emedicine.medscape.com/article/317358-overview>.
73. Christian, J. *MIT lab recasting prosthetics via 3-D printing*. 2015 7-Oct-2017]; Available from: <https://www.bostonglobe.com/business/2015/09/08/mit-lab-develops-next-generation-prosthetics-for-amputees/pOwbmPFThlP8Z9RfW1zPnO/story.html>.
74. Laing, S., P.V. Lee, and J. Goh, *Engineering a trans-tibial prosthetic socket for the lower limb amputee*. Ann Acad Med Singapore, 2011. 40(5): p. 252-9.
75. Yigiter, K., G. Sener, and K. Bayar, *Comparison of the effects of patellar tendon bearing and total surface bearing sockets on prosthetic fitting and rehabilitation*. Prosthet Orthot Int, 2002. 26(3): p. 206-12.
76. Ottobock. *Ottobock - Modular Knee Joints*. 2015 12-Jan-2015]; Available from: [http://professionals.ottobockus.com/cps/rde/xchg/ob\\_us\\_en/hs.xsl/605.html](http://professionals.ottobockus.com/cps/rde/xchg/ob_us_en/hs.xsl/605.html).
77. Nielsen, D.H., et al., *Comparison of Energy-Cost and Gait Efficiency during Ambulation in Below-Knee Amputees Using Different Prosthetic Feet - a Preliminary-Report*. Journal of Prosthetics and Orthotics, 1988. 1(1): p. 24-31.
78. Highsmith, M.J., et al., *Differences in the spatiotemporal parameters of transtibial and transfemoral amputee gait*. JPO: Journal of Prosthetics and Orthotics, 2010. 22(1): p. 26-30.
79. Berger, N., *Analysis of Amputee Gait*, in *Atlas of Limb Prosthetics: Surgical, Prosthetic, and Rehabilitation Principles*. 2002, American Academy of Orthopedic Surgeons.
80. Jaegers, S.M., J.H. Arendzen, and H.J. de Jongh, *Prosthetic gait of unilateral transfemoral amputees: a kinematic study*. Archives of physical medicine and rehabilitation, 1995. 76(8): p. 736-743.
81. Waters, R.L. and S. Mulroy, *The energy expenditure of normal and pathologic gait*. Gait & Posture, 1999. 9(3): p. 207-231.
82. Genin, J.J., et al., *Effect of speed on the energy cost of walking in unilateral traumatic lower limb amputees*. Eur J Appl Physiol, 2008. 103(6): p. 655-63.



83. Waters, R.L., et al., *Energy cost of walking of amputees: the influence of level of amputation*. J Bone Joint Surg Am, 1976. 58(1): p. 42-6.
84. Schmalz, T., S. Blumentritt, and R. Jarasch, *Energy expenditure and biomechanical characteristics of lower limb amputee gait: The influence of prosthetic alignment and different prosthetic components*. Gait & posture, 2002. 16(3): p. 255-263.
85. Taylor, M.B., et al., *A comparison of energy expenditure by a high level transfemoral amputee using the Intelligent Prosthesis and conventionally damped prosthetic limbs*. Prosthetics and Orthotics International, 1996. 20(2): p. 116-121.
86. Flor, H., *Phantom-limb pain: characteristics, causes, and treatment*. Lancet Neurology, 2002. 1(3): p. 182-189.
87. Ehde, D.M., et al., *Chronic phantom sensations, phantom pain, residual limb pain, and other regional pain after lower limb amputation*. Archives of Physical Medicine and Rehabilitation, 2000. 81(8): p. 1039-1044.
88. van der Schans, C.P., et al., *Phantom pain and health-related quality of life in lower limb amputees*. Journal of Pain and Symptom Management, 2002. 24(4): p. 429-436.
89. Kavounoudias, A., et al., *Bilateral changes in somatosensory sensibility after unilateral below-knee amputation*. Archives of Physical Medicine and Rehabilitation, 2005. 86(4): p. 633-640.
90. Isakov, E., et al., *Standing Sway and Weight-Bearing Distribution in People with Below-Knee Amputations*. Archives of Physical Medicine and Rehabilitation, 1992. 73(2): p. 174-178.
91. Vrieling, A.H., et al., *Balance control on a moving platform in unilateral lower limb amputees*. Gait & Posture, 2008. 28(2): p. 222-228.
92. Shull, P.B., et al., *Training multi-parameter gaits to reduce the knee adduction moment with data-driven models and haptic feedback*. Journal of Biomechanics, 2011. 44(8): p. 1605-1609.
93. Barnett, C.T., N. Vanicek, and R.C.J. Polman, *Postural responses during volitional and perturbed dynamic balance tasks in new lower limb amputees: A longitudinal study*. Gait & Posture, 2013. 37(3): p. 319-325.
94. Fernie, G.R., P. Eng, and P.J. Holliday, *Postural Sway in Amputees and Normal Subjects*. Journal of Bone and Joint Surgery-American Volume, 1978. 60(7): p. 895-898.
95. Highsmith, M.J., et al., *Short and mid-distance walking and posturography with a novel microprocessor knee*. Technology & Innovation, 2014. 15(4): p. 359-368.
96. Kannenberg, A., et al., *Activities of daily living: Genium bionic prosthetic knee compared with C-Leg*. JPO: Journal of Prosthetics and Orthotics, 2013. 25(3): p. 110-117.
97. Lee, S.C., Sophia, *Rehabilitation of Vascular Amputee*, in *Vascular surgery: principles and practice*. 2017, CRC Press.
98. Hargrove, L.J., et al., *Robotic leg control with EMG decoding in an amputee with nerve transfers*. N Engl J Med, 2013. 369(13): p. 1237-42.
99. Ku, P.X., N.A. Abu Osman, and W.A.W. Abas, *Balance control in lower extremity amputees during quiet standing: A systematic review*. Gait & Posture, 2014. 39(2): p. 672-682.

100. Marasco, P.D., et al., *Robotic touch shifts perception of embodiment to a prosthesis in targeted reinnervation amputees*. *Brain*, 2011. 134(3): p. 747-758.
101. Yadav, S. and R. Krishnaiah, *Haptic science and technology*. arXiv preprint arXiv:1309.0185, 2013.
102. Lederman, S.J. and R.L. Klatzky, *Haptic perception: A tutorial*. *Attention Perception & Psychophysics*, 2009. 71(7): p. 1439-1459.
103. Washington, U.o., *The somatosensory system*. 2006.
104. Haslwanter, T., *Sensory receptors in the human skin*, S. proprioception.svg, Editor. 2011.
105. Purves, D.E., et al., *Neuroscience*. 1997: Sunderland, MA, US: Sinauer Associates.
106. Lopes, P. and P. Baudisch. *Muscle-propelled force feedback: bringing force feedback to mobile devices*. in *Proceedings of the SIGCHI Conference on Human Factors in Computing Systems*. 2013. ACM.
107. King, C.H., et al., *Tactile Feedback Induces Reduced Grasping Force in Robot-Assisted Surgery*. *IEEE Trans Haptics*, 2009. 2(2): p. 103-110.
108. Wagner, C.R., N. Stylopoulos, and R.D. Howe, *The role of force feedback in surgery: Analysis of blunt dissection*. 10th Symposium on Haptic Interfaces for Virtual Environment and Teleoperator Systems, Proceedings, 2002: p. 73-79.
109. Altinsoy, M.E. and S. Merchel, *Electrotactile Feedback for Handheld Devices with Touch Screen and Simulation of Roughness*. *IEEE Trans Haptics*, 2012. 5(1): p. 6-13.
110. Rogers, C.H., *Choice of stimulator frequency for tactile arrays*. *IEEE Transactions on Man-Machine Systems*, 1970. 11(1): p. 5-11.
111. Honegger, F., et al., *The effect of prosthetic feedback on the strategies and synergies used by vestibular loss subjects to control stance*. *Journal of neuroengineering and rehabilitation*, 2013. 10(1): p. 115.
112. Ajoudani, A., et al., *Exploring teleimpedance and tactile feedback for intuitive control of the Pisa/IIT SoftHand*. *IEEE Trans Haptics*, 2014. 7(2): p. 203-15.
113. Brown, J.D., et al., *Understanding the Role of Haptic Feedback in a Teleoperated/Prosthetic Grasp and Lift Task*. 2013 World Haptics Conference (Whc), 2013: p. 271-276.
114. Chelette, A.M. and C.S. Layne. *Effects of low frequency continuous muscle vibration on learning and transfer of a knee joint positioning task*. in *Haptics Symposium (HAPTICS), 2014 IEEE*. 2014. IEEE.
115. Pasquero, J. and V. Hayward. *STReSS: A practical tactile display system with one millimeter spatial resolution and 700 Hz refresh rate*. in *Proc. Eurohaptics*. 2003.
116. Provancher, W.R. and N.D. Sylvester, *Fingerpad skin-stretch increases the perception of virtual friction*. *IEEE Transactions on Haptics*, 2009. 2(4): p. 212-223.
117. Nakatani, M., et al., *Tactile illusion caused by tangential skin strain and analysis in terms of skin deformation*. *Haptics: perception, devices and scenarios*, 2008: p. 229-237.
118. Gleeson, B.T., S.K. Horschel, and W.R. Provancher. *Communication of direction through lateral skin-stretch at the fingertip*. in *EuroHaptics conference, 2009 and Symposium on Haptic Interfaces for Virtual*

- Environment and Teleoperator Systems. World Haptics 2009. Third Joint. 2009. IEEE.*
119. Bau, O., et al. *TeslaTouch: electrovibration for touch surfaces*. in *Proceedings of the 23rd annual ACM symposium on User interface software and technology*. 2010. ACM.
  120. D'Alonzo, M., et al., *HyVE-Hybrid Vibro-Electrotactile Stimulation-Is an Efficient Approach to Multi-Channel Sensory Feedback*. *Ieee Transactions on Haptics*, 2014. 7(2): p. 181-190.
  121. D'Alonzo, M., et al., *HyVE: Hybrid Vibro-Electrotactile Stimulation for Sensory Feedback and Substitution in Rehabilitation*. *Ieee Transactions on Neural Systems and Rehabilitation Engineering*, 2014. 22(2): p. 290-301.
  122. Gwilliam, L.T., A.J. Doxon, and W.R. Provancher, *Haptic Matching of Directional Force and Skin-stretch Feedback Cues*. 2013 World Haptics Conference (Whc), 2013: p. 19-24.
  123. D'Alonzo, M., et al., *HyVE: hybrid vibro-electrotactile stimulation for sensory feedback and substitution in rehabilitation*. *Neural Systems and Rehabilitation Engineering, IEEE Transactions on*, 2014. 22(2): p. 290-301.
  124. Agnew, S.P., et al., *Targeted Reinnervation in the Transfemoral Amputee: A Preliminary Study of Surgical Technique*. *Plastic and Reconstructive Surgery*, 2012. 129(1): p. 187-194.
  125. Gopalai, A.A. and S.M.N.A. Senanayake, *A Wearable Real-Time Intelligent Posture Corrective System Using Vibrotactile Feedback*. *Ieee-Asme Transactions on Mechatronics*, 2011. 16(5): p. 827-834.
  126. Sienko, K.H., et al., *The effect of vibrotactile feedback on postural sway during locomotor activities*. *Journal of Neuroengineering and Rehabilitation*, 2013. 10.
  127. Horak, F.B., et al., *Vibrotactile Biofeedback Improves Tandem Gait in Patients with Unilateral Vestibular Loss*. *Basic and Clinical Aspects of Vertigo and Dizziness*, 2009. 1164: p. 279-281.
  128. McKinney, Z., et al., *Pilot Evaluation of Wearable Tactile Biofeedback System for Gait Rehabilitation in Peripheral Neuropathy*. 2014 *Ieee Haptics Symposium (Haptics)*, 2014: p. 135-140.
  129. Girone, M., et al., *A stewart platform-based system for ankle telerehabilitation*. *Autonomous Robots*, 2001. 10(2): p. 203-212.
  130. Culjat, M.O., R.E. Fan, and W.S. Grundfest. *Optimization of a tactile feedback system to aid the rehabilitation of lower-limb amputees*. in *Virtual Rehabilitation, 2008*. 2008. IEEE.
  131. Sharma, A., *Assessing the Use of Vibrotactile Feedback as a Means for Providing Sensory Information to the Upper Thigh*. University of Toronto, 2013.
  132. Biggs, J. and M.A. Srinivasan, *Tangential versus normal displacements of skin: Relative effectiveness for producing tactile sensations*. 10th Symposium on Haptic Interfaces for Virtual Environment and Teleoperator Systems, Proceedings, 2002: p. 121-128.
  133. Zeagler, C. *Where to wear it: functional, technical, and social considerations in on-body location for wearable technology 20 years of designing for wearability*. in *Proceedings of the 2017 ACM International Symposium on Wearable Computers*. 2017. ACM.
  134. Wentink, E.C., et al., *Vibrotactile stimulation of the upper leg: Effects of location, stimulation method and habituation*. 2011 Annual International

- Conference of the Ieee Engineering in Medicine and Biology Society (Embc), 2011: p. 1668-1671.
135. Perry, J. and J.R. Davids, *Gait analysis: normal and pathological function*. Journal of Pediatric Orthopaedics, 1992. 12(6): p. 815.
  136. Maqbool, H.F., et al., *Real-time gait event detection for lower limb amputees using a single wearable sensor*. 2016 38th Annual International Conference of the Ieee Engineering in Medicine and Biology Society (Embc), 2016: p. 5067-5070.
  137. Aminian, K., et al., *Spatio-temporal parameters of gait measured by an ambulatory system using miniature gyroscopes*. Journal of biomechanics, 2002. 35(5): p. 689-699.
  138. Johanson, M.A., et al., *Heel lifts and the stance phase of gait in subjects with limited ankle dorsiflexion*. J Athl Train, 2006. 41(2): p. 159-65.
  139. Soames, R., *Foot pressure patterns during gait*. Journal of biomedical engineering, 1985. 7(2): p. 120-126.
  140. Rajala, S. and J. Lekkala, *Plantar shear stress measurements - A review*. Clinical Biomechanics, 2014. 29(5): p. 475-483.
  141. Shu, L., et al., *In-Shoe Plantar Pressure Measurement and Analysis System Based on Fabric Pressure Sensing Array*. Ieee Transactions on Information Technology in Biomedicine, 2010. 14(3): p. 767-775.
  142. Razak, A.H., et al., *Foot plantar pressure measurement system: a review*. Sensors (Basel), 2012. 12(7): p. 9884-912.
  143. Cong, Y. and M. Zhang, *Measurement of In-Shoe Plantar Triaxial Stresses in High-Heeled Shoes*. 2010 3rd International Conference on Biomedical Engineering and Informatics (Bmei 2010), Vols 1-7, 2010: p. 1760-1763.
  144. Healy, A., et al., *Repeatability of WalkinSense® in shoe pressure measurement system: A preliminary study*. The Foot, 2012. 22(1): p. 35-39.
  145. Edgar, S.R., et al., *Wearable Shoe-Based Device for Rehabilitation of Stroke Patients*. 2010 Annual International Conference of the Ieee Engineering in Medicine and Biology Society (Embc), 2010: p. 3772-3775.
  146. Salpavaara, T., et al., *Wireless Insole Sensor System for Plantar Force Measurements during Sport Events*. Xix Imeko World Congress: Fundamental and Applied Metrology, Proceedings, 2009: p. 2118-2123.
  147. Holleccek, T., et al., *Textile Pressure Sensors for Sports Applications*. 2010 Ieee Sensors, 2010: p. 732-737.
  148. Saito, M., et al., *An in-shoe device to measure plantar pressure during daily human activity*. Medical Engineering & Physics, 2011. 33(5): p. 638-645.
  149. Chen, M., B. Huang, and Y.S. Xu, *Intelligent shoes for abnormal gait detection*. 2008 Ieee International Conference on Robotics and Automation, Vols 1-9, 2008: p. 2019-2024.
  150. Karkokli, R. and K.M.V. McConville, *Design and development of a cost effective plantar pressure distribution analysis system for the dynamically moving feet*. 2006 28th Annual International Conference of the Ieee Engineering in Medicine and Biology Society, Vols 1-15, 2006: p. 3114-+.
  151. Tekscan. *FlexiForce® User Manual*. 2017; Available from: <https://www.tekscan.com/resources/product-guide/flexiforce-user-manual>.
  152. Gleeson, B.T., S.K. Horschel, and W.R. Provancher, *Perception of Direction for Applied Tangential Skin Displacement: Effects of Speed, Displacement, and Repetition*. Ieee Transactions on Haptics, 2010. 3(3): p. 177-188.

153. Karuei, I., et al., *Detecting Vibrations Across the Body in Mobile Contexts*. 29th Annual Chi Conference on Human Factors in Computing Systems, 2011: p. 3267-3276.
154. Milne, R.J., et al., *Reduction in Perceived Intensity of Cutaneous Stimuli during Movement - a Quantitative Study*. Experimental Brain Research, 1988. 70(3): p. 569-576.
155. Chapman, C.E., et al., *Sensory Perception during Movement in Man*. Experimental Brain Research, 1987. 68(3): p. 516-524.
156. Riley, P.O., et al., *A kinematic and kinetic comparison of overground and treadmill walking in healthy subjects*. Gait & Posture, 2007. 26(1): p. 17-24.
157. Hollman, J.H., et al., *A comparison of variability in spatiotemporal gait parameters between treadmill and overground walking conditions*. Gait & Posture, 2016. 43: p. 204-209.
158. CL Vaughan, B.D., JC O'Connor, *Dynamics of Human Gait* 2nd ed. 1999, : Kiboho Publishers.
159. Gailey, R.S., et al., *The amputee mobility predictor: an instrument to assess determinants of the lower-limb amputee's ability to ambulate*. Arch Phys Med Rehabil, 2002. 83(5): p. 613-27.
160. Pohjolainen, T., H. Alaranta, and M. Karkkainen, *Prosthetic Use and Functional and Social Outcome Following Major Lower-Limb Amputation*. Prosthetics and Orthotics International, 1990. 14(2): p. 75-79.
161. Bilodeau, S., R. Hebert, and J. Desrosiers, *Lower limb prosthesis utilisation by elderly amputees*. Prosthetics and Orthotics International, 2000. 24(2): p. 126-132.
162. Godfrey, A., et al., *Instrumenting gait with an accelerometer: A system and algorithm examination*. Medical Engineering & Physics, 2015. 37(4): p. 400-407.
163. McCrory, J.L., S.C. White, and R.M. Lifeso, *Vertical ground reaction forces: objective measures of gait following hip arthroplasty*. Gait & posture, 2001. 14(2): p. 104-109.
164. Bhargava, P., P. Shrivastava, and S. Nagariya, *Assessment of changes in gait parameters and vertical ground reaction forces after total hip arthroplasty*. Indian J Orthop, 2007. 41(2): p. 158-62.
165. Nagano, H., et al., *A comparison of treadmill and overground walking effects on step cycle asymmetry in young and older individuals*. J Appl Biomech, 2013. 29(2): p. 188-93.
166. Malatesta, D., M. Canepa, and A. Menendez Fernandez, *The effect of treadmill and overground walking on preferred walking speed and gait kinematics in healthy, physically active older adults*. Eur J Appl Physiol, 2017.
167. Epomedicine.com. *Physical Examination: Gait | Epomedicine*. 2015; Available from: <http://epomedicine.com/clinical-medicine/physical-examination-gait/>.
168. Biomotionlabs.com. *Motion Capture Process | biomotionlabs.com*. 2014; Available from: <http://biomotionlabs.com/technology/understanding-3d-motionprint-technology/>.
169. Nedelkovski, D. *MEMS Accelerometer Gyroscope Magnetometer & Arduino. HowToMechatronics*. 2015; Available from: <https://howtomechatronics.com/how-it-works/electrical-engineering/mems-accelerometer-gyroscope-magnetometer-arduino/>.

**APPENDIX A:**  
**Evaluation of Haptic Feedback System Effects on**  
**Amputee Gait**

## **A.1 Introduction**

This section presents the evaluation of the haptic feedback system with an above-knee amputee. The evaluation was done on treadmill and overground walking to assess the effects of the skin-stretch feedback on the gait spatio-temporal parameters, gait symmetry and vertical ground reaction force (vGRF) during walking.

For all experimental work described, the subject was briefed and consented to taking part in the research. In addition, the subject also consented to photographic and video record taken throughout the experiments. The experimental protocol received an approval from the University of Leeds Ethical Review Board (MEEC 14-012-Appendix D)

### **A.1.1 Subject Background**

This section will present the background of the subject participated in the experimental work discussed in this chapter.

### **A.1.2 Amputation History**

The subject participated in this study is a 55 years old male unilateral above knee amputee (after this referred to as the AKS). Prior to amputation, he contracted an infection on the left knee joint which subsequently led to a knee replacement procedure in 2007. About 1.5 years after the procedure, the knee joint started to show more signs of infection, affecting the lower part of the limb. The above-knee amputation was finally carried out in April 2009 to save the remaining limb.

### **A.1.3 Mobility**

AKS is considered as a K-level 3 amputee according to the Medicare Functional Classification Levels, which classifies the activity levels for lower limb amputees. K3 is defined as an amputee having the “*ability or potential for ambulation with variable cadence – a typical community ambulator with the ability to traverse most environmental barriers and may have vocational, therapeutic, or exercise activity that demands prosthetic use beyond simple locomotion*” [159]. Apart from engaging in a full-time work, a verbal review of mobility history indicates that post-amputation, he maintained an active lifestyle and performed activities such trail-walking, hiking, and driving especially in the past five years.

#### **A.1.4 Prosthesis Use**

The AKS wears the prosthetic every day with more than 10 hours per day, higher than the average reported in [160] and [161] for the same age range. Over the course of rehabilitation and post-rehabilitation periods, he has used various different prosthetic components. For prosthetic knee, he was initially fitted with a passive mechanical knee, followed by 3R60 and then 3R80 hydraulic knee (Ottobock, Germany), and is currently using an Orion (Blatchford, UK) microprocessor knee. Following an increase in mobility activity, the prosthetic foot also changed from SACH rigid foot, to Kinterra hydraulic foot (Freedom Innovations, Canada) and he is currently using an Echelon (Blatchford, UK) hydraulic foot. In addition to that, he was involved in several trials and research related to prosthetic components and was therefore highly familiar with different technologies in lower limb prosthetic components.

#### **A.1.5 Gait Challenge**

The AKS reported numerous falls over the past three years, several of which required hospitalization. He reported that a simple misstep or losing focus while walking could trigger falls and that he was having more falls while using the mechanical knee in the earlier days following amputation. In terms of gait, the AKS exhibits vaulting behaviour during the swing phase which he attributed to the lack of proprioception and lack of haptic cue from the prosthetic socket during landing of the prosthetic feet, causing him to vault to maintain the ground clearance.



## A.2 Experimental Work

### A.2.1 Method

Table A.1 shows the details of the prosthetic components used while conducting the experimental work.

**Table A.1 Details of the AKS prosthetic components**

Components	Make	Type	Duration of Use
Knee	Orion	Microprocessor controlled knee	> 6 months
Foot	Echelon	Hydraulic ankle with independent control of plantar and dorsi-flexion	> 6 months

- System preparation

The AKS wore the haptic feedback module around the abdominal area, on the left lower trunk (aligned with the amputated leg-left). Two event detection modules consisting of two IMU's and a data acquisition circuitry were fitted on each leg; one on the lateral side of the shank of the intact leg, and the other one on the lateral side of the prosthetic knee cover, around the same height from ground as in the intact leg. The force insole was fitted inside the shoe on the prosthetic side, underneath the prosthetic feet. Two walking environments were included in this study, namely the treadmill and overground walking.

- Treadmill walking

The AKS was asked to familiarize with treadmill walking for 5 minutes across different speed (ranging from 2.0 km/h to 4.5 km/h). After the familiarization session, he was asked to adjust the treadmill in the increment of 0.1 km/h and identify the preferred slow, normal and fast walking speed. The experiment began with collecting the baseline (BL) data for slow walk. The AKS were asked to walk in no feedback condition and temporal gait data from the IMU and the vGRF data from the force insole were sent wirelessly and recorded into a PC. Next, he walked at the same selected slow speed, and skin-stretch stimuli were delivered to the subject in: (1) sequential-alternate (SA) feedback mode and (2) sequential-continuous (SC) feedback mode, in response to the IC and TO events detected by the IMU. The

mechanism of these feedback modes was previously described in Section 5.4.2. The same procedure was repeated with the self-selected normal and fast walking speed.

- Overground walking

A 20-m walkway was marked at the beginning and the end line. To familiarize with the walking environment, the AKS was asked to walk in self-selected slow, normal and fast walking speeds, starting from the beginning mark and stopping at the end mark. A digital stopwatch was used to record the time taken by the subjects to walk within the specified distance to calculate the walking speed, and video recordings were obtained for secondary reference. The experiment began with collecting the baseline data for slow walk. The AKS was asked to walk in baseline no-feedback condition across the walkway for three times. Next, he was instructed to maintain the same walking speed, and skin-stretch stimuli were delivered to the subject in: (1) SA feedback mode and (2) SC feedback mode. The whole procedure was repeated with self-selected normal and fast walk. Figure A.1 shows the experimental setup.

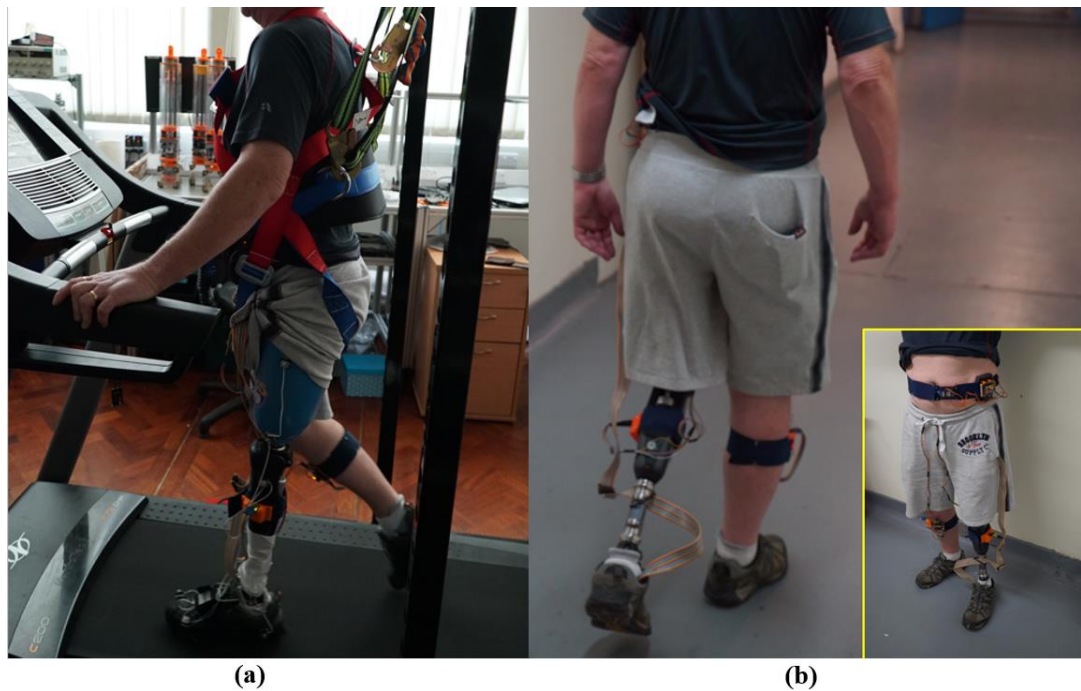


**Figure A.1** Experimental setup. (a) treadmill walk and (b) overground walk. (inset) placement of the haptic module on the lower trunk.

### A.2.2 Data Collection and Analysis

IMU data were sampled at 120 Hz and passed through a 2<sup>nd</sup> order Butterworth low pass filter with cut-off frequency of 10 Hz. The event detection for controlling the activation of the haptic feedback was carried out using signal obtained from the IMU on the prosthetic side. The force sensors in the insole were sampled at 120 Hz and passed through a 2<sup>nd</sup> order Butterworth filter with 10 Hz cut-off frequency. The spatio-temporal and vGRF parameters are described in Mean  $\pm$  Standard Deviation unless otherwise stated.

#### 1. Calculation of Gait Spatio-temporal Parameters

Figure A.2 shows a sample of angular velocity signals from both leg during several gait cycles. For clarity, the signal from the intact side (solid blue line) was shifted upwards along the y-axis. The timing of the IC and TO events are marked on the figure. Based on these timing information, the following gait parameters can be defined as follows [137, 162]:

The stance duration, ST is the time between consecutive IC and TO

$$ST_i = TO_i - IC_i \quad (6.1)$$

The swing duration, SD, is the time between TO and the next IC of the same leg

$$SW_i = IC_{i+1} - TO_i \quad (6.2)$$

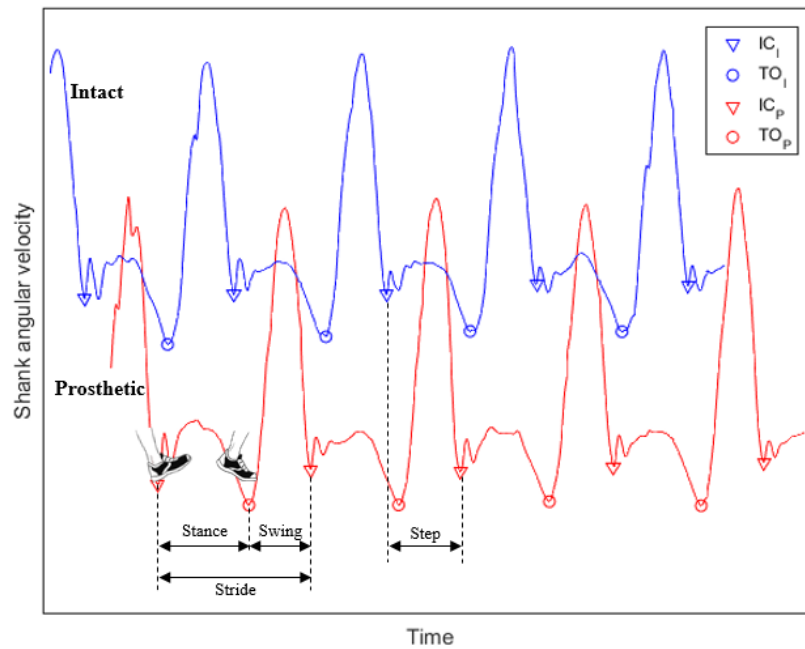


**Figure A.2 Calculation of temporal gait parameters from angular velocity signal. I= intact and P= prosthetic.**

The stride duration,  $SR$  can then be found as

$$SR = ST_i + TO_i \quad (6.3)$$

The step time,  $SPT$  of a leg can be found as the time between the heel strike of the contralateral leg to the heel strike of that leg.

For intact leg, the  $SPT_I$ , can be found as

$$SPT_I = IC_{Ii+1} - IC_{Pi} \quad (6.4)$$

And for prosthetic leg,  $SPT_P$  was defined as:

$$SPT_P = IC_P - IC_{Ii} \quad (6.5)$$

With the walking speed,  $V_w$  information, the step length,  $SPL$  was calculated as:

$$SPL = SPT \times V_w \quad (6.6)$$

Independent t-test was carried out using SPSS Statistics software (IBM) with the spatio-temporal data between the baseline group and the SC feedback and between the baseline and the SA feedback. Significant difference was indicated if p-value between the mean difference is less than 0.05.

## 2. Calculation of vGRF parameters

Figure A.3 shows a sample of vGRF obtained from the prosthetic side during walking trial.

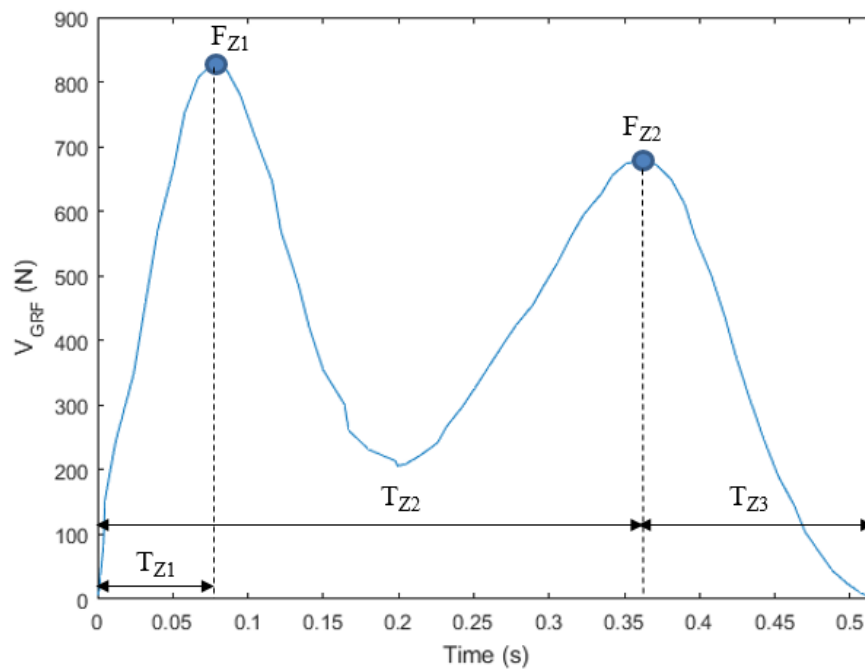


Figure A.3 Sample of a vertical GRF data, with important features marked

The following vGRF parameters can be found from the information shown in Figure A.3:

The  $F_{Z1}$  and  $F_{Z2}$  denotes the first peak force and second peak force observed during the loading and push-off phase of the stance.  $T_{Z1}$  denotes the time from starting of stance phase (IC) to first peak force while  $T_{Z2}$  indicates the time to second peak force. The  $T_{Z3}$  denotes the time taken from second peak force to the end of stance phase (TO). The  $T_{Z1}$  parameter can give indication of willingness to shift weight onto the prosthetic limb.  $T_{Z1}$  that occurs at later stage indicates that subject was not putting weight as quickly as one would, using an intact or healthy leg [163, 164].

The loading rate, LR is defined as the magnitude of the first peak divided by the time of its occurrence,

$$LR = \frac{F_{Z1}}{T_{Z1}} \quad (6.7)$$

The push-off rate, PR is defined as the magnitude of the second force peak divided by the time taken from the second peak force to the end of stance,

$$PR = \frac{F_{Z2}}{T_{Z3}} \quad (6.8)$$

### 3. Calculation of Gait Cycle Symmetry

The gait percentage in terms of stance and swing duration was also analysed to observe the change in gait cycle symmetry. For each intact and prosthesis side, the percentage of stance duration can be found as

$$Stance (\%) = \frac{ST}{ST + SW} \times 100 \quad (6.9)$$

Similarly,

$$Swing (\%) = \frac{SW}{ST + SW} \times 100 \quad (6.10)$$

### A.2.3 Results

#### 1. Walking speed

Table A.2 shows the self-selected walking speed during treadmill walking (TMW) and overground walking (OGW). It can be observed that the self-selected walking speed range was significantly different with the amputee selecting a much lower speed on the TMW in comparison to OGW.

**Table A.2 Walking speed across experimental conditions**

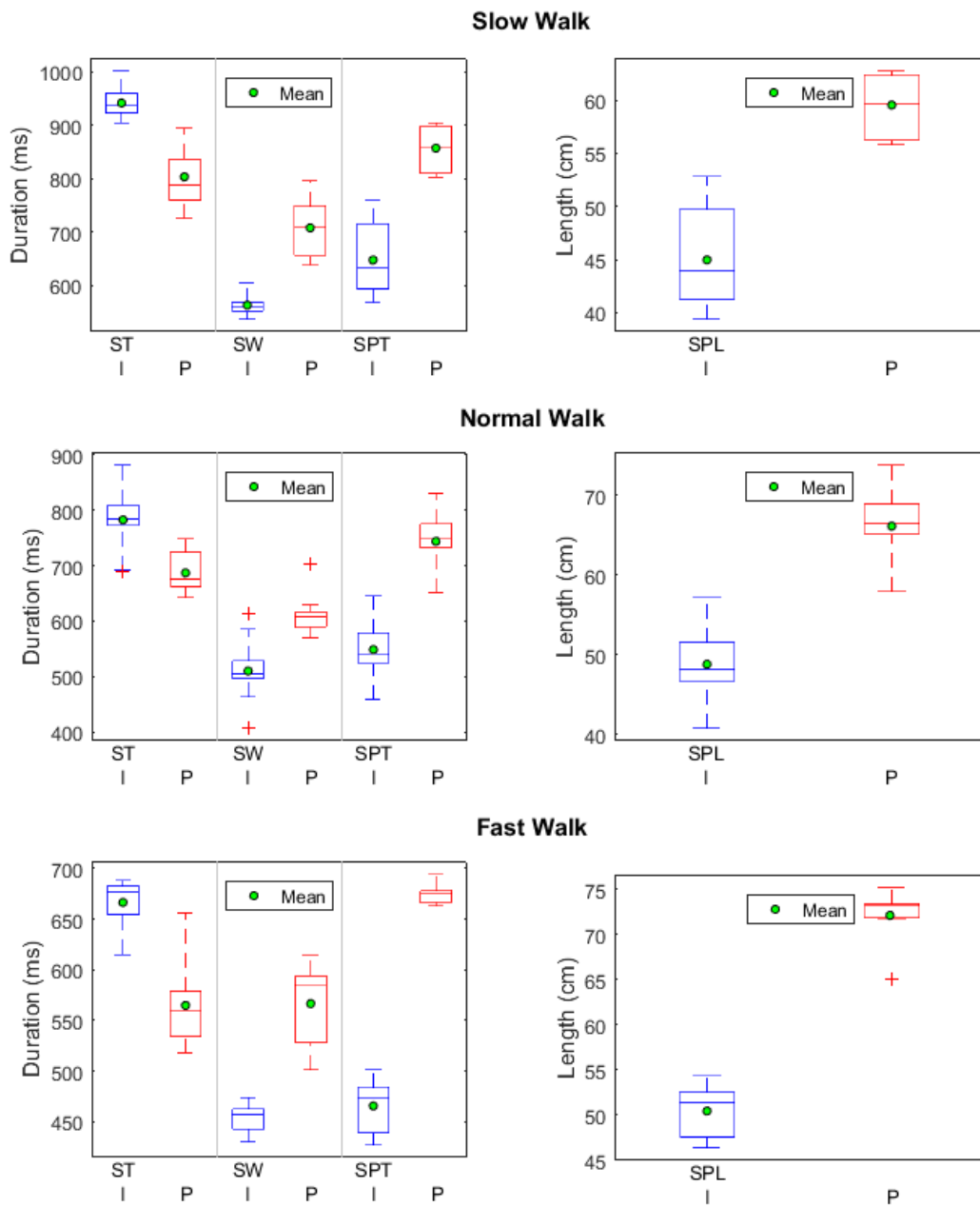
	Walking speed (km/h)								
	Slow			Normal			Fast		
	BL	SA	SC	BL	SA	SC	BL	SA	SC
Overground	3.6 ± 0.1	3.8 ± 0.1	3.5 ± 0.1	4.8 ± 0.1	5.0 ± 0.1	4.8 ± 0.1	5.8 ± 0.1	5.9 ± 0.1	6.1 ± 0.1
Treadmill	2.5			3.2			3.9		
BL: Baseline SA: Sequential-alternate feedback SC: Sequential-continuous feedback									

In fact, the fast walking speed on treadmill was almost equivalent to slow walking speed overground. This observation partially confirms to that of Nagano et al. [165], in which for older participants, the preferred speed for OGW was significantly lower (1.05 m/s vs 1.24 m/s) than that of TMW. Similarly, Malatesta et al. [166] found that the preferred OGW speed was significantly higher in both older subjects (1.45 m/s vs 1.31 m/s) and younger subjects (1.37 m/s vs 1.25 m/s) in comparison to TMW. The author suggested that the difference in speed could be attributed to the fact that walking on treadmill requires greater balance and therefore may lead to slower walking speed. In both studies, however, only the normal or self-selected preferred speed for healthy subjects was reported. The fact that the normal walking speed selected by the AKS in this study was much slower during TMW suggested lower balance confidence in the treadmill in comparison to OGW. Since the range of OGW and TMW speeds were not matched, the analysis of the feedback effect is considered separately.

#### 2. Treadmill walking

Figure A.4 shows the distribution of spatio-temporal parameters of the AKS during the BL walking across all walking speed. It can be observed that the variability in the temporal parameters was more pronounced during the slow and fast walk, most probably due to these walking speeds requiring more compensatory strategy than

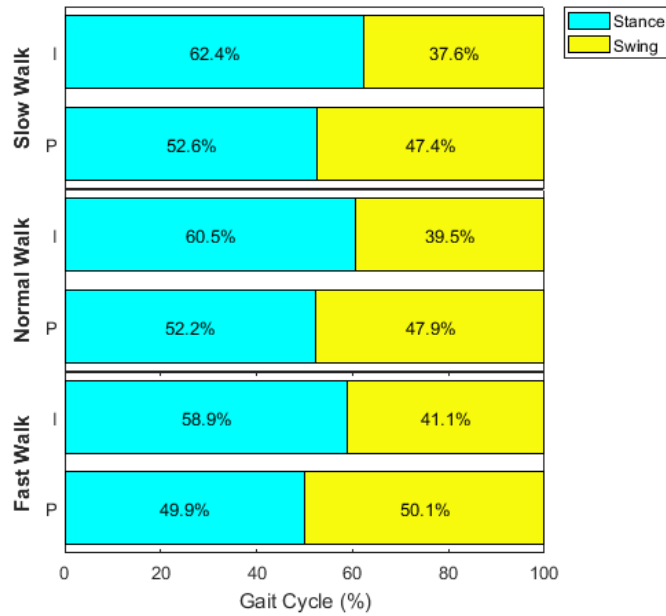
walking at the normal speed. In addition, it can also be noted that the average stance duration of the intact side is higher in all walking speeds in comparison to the prosthetic side.



**Figure A.4 Spatio-temporal parameters during TM baseline walking. I= Intact. P=Prosthetic**

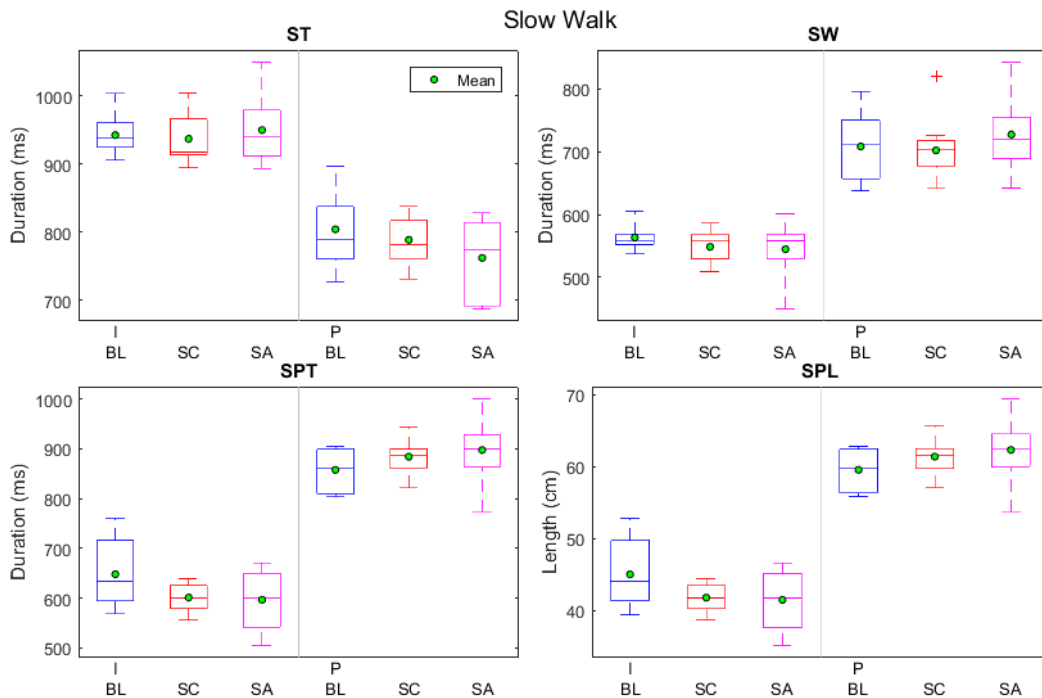
Conversely, the swing duration for the prosthetic side was much higher than the intact side. This can be confirmed in Figure A.5 which shows that for every walking speed, the AKS spent around 10% less time on the prosthetic leg during stance period. Furthermore, the percentage of stance for prosthetic side reduces as the walking speed increases (52.6%- slow, 52.2%-normal, 49.9%-fast). This pattern of favouring the

intact side during stance is a common gait pattern shown by lower limb amputee [6], and is the most likely explanation to the vaulting behaviour exhibited by the AKS during walking.



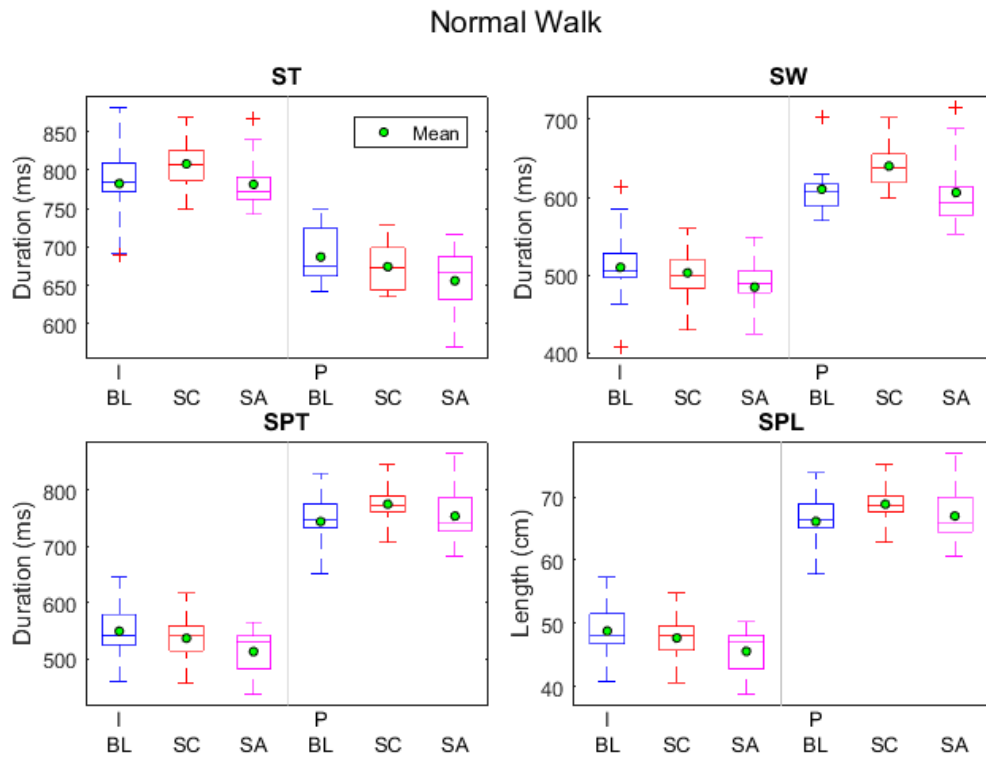
**Figure A.5 Stance and swing duration during baseline treadmill walk**

Figure A.6, Figure A.7 and Figure A.8 shows the comparison between the distribution of the spatiotemporal between the baseline (BL) and the feedback condition (SC and SA) for the slow, normal and fast walk respectively.



**Figure A.6 TMW Spatio-temporal parameters during BL, SA and SC condition-slow walk**





**Figure A.7 TMW Spatio-temporal parameters during BL vs SA and SC condition-normal walk**

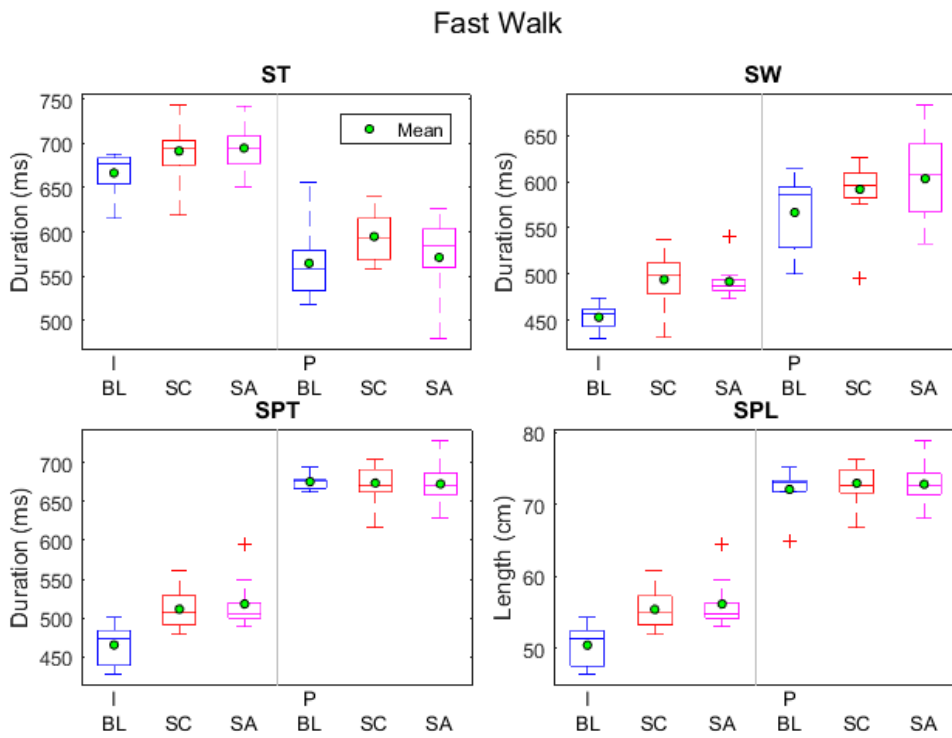


**Figure A.8 TMW Spatio-temporal parameters during BL, SA and SC condition-fast walk**

During slow and normal walking condition (2.5 km/h to 3.2 km/h), the SA feedback actually contributed to a slightly decreased stance duration on the prosthetic leg while SC feedback showed an increase. In addition, the variability between the stance duration was the smallest during the SC feedback condition. In fact, most spatio-temporal parameters showed the least variability during SC feedback, especially the step length (SPL). A different observation was made during fast walk (3.9 km/h). During feedback condition, every spatio-temporal parameter increased for the intact leg, while the average prosthetic stance duration increased during both SC condition. Figure A.9 summarizes the average gait cycle stance-swing distribution for all walking speed and feedback conditions.

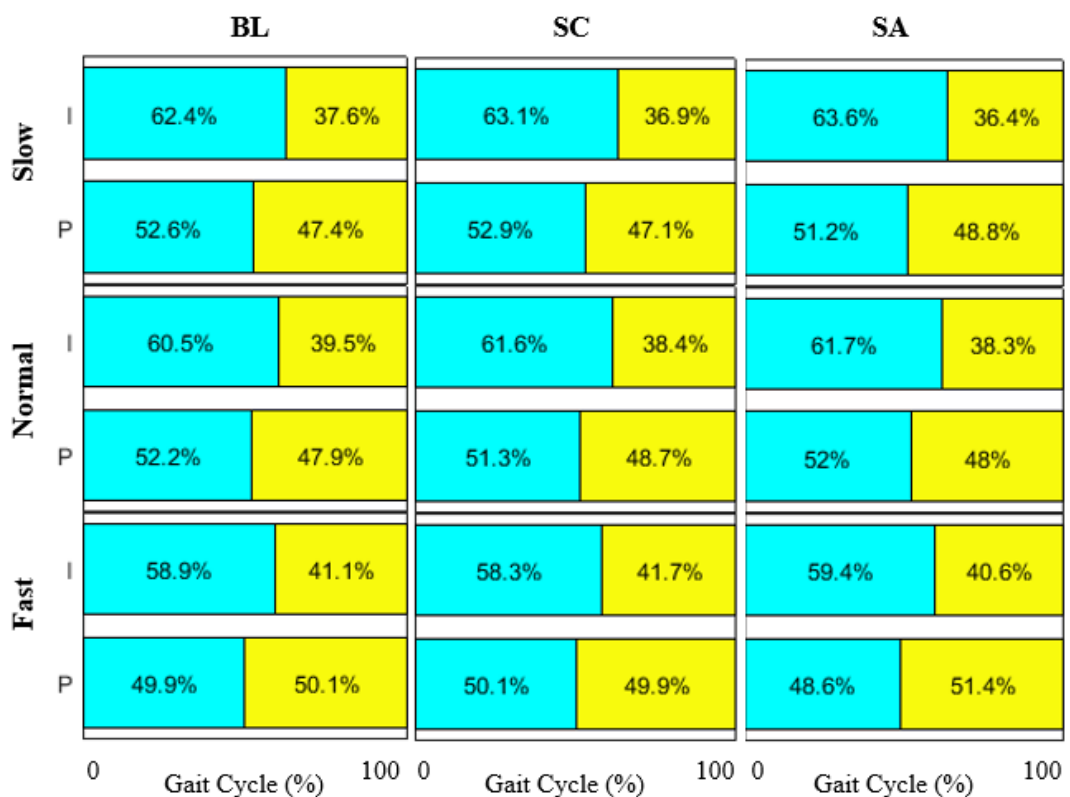


**Figure A.9 Average stance and swing percentage during all treadmill walking conditions**

To analyse whether any change in kinetic parameters occurs during the feedback condition, the loading parameters obtained from the force insole data on the prosthetic side is visualized in Figure A.10. The peak force FZ1 remained similar throughout the experimental condition. However, during slow and normal walks, the TZ1 during SC and SA feedback condition was less than that of baseline. The reduction in TZ1 suggested the AKS put the weight on the prosthetic limb quicker than he would during

baseline condition, an indication of increased shift in weight towards the prosthetic side [163, 164]. However, A t-test analysis showed no significant difference in these parameters between BL and feedback conditions during all walking speed.

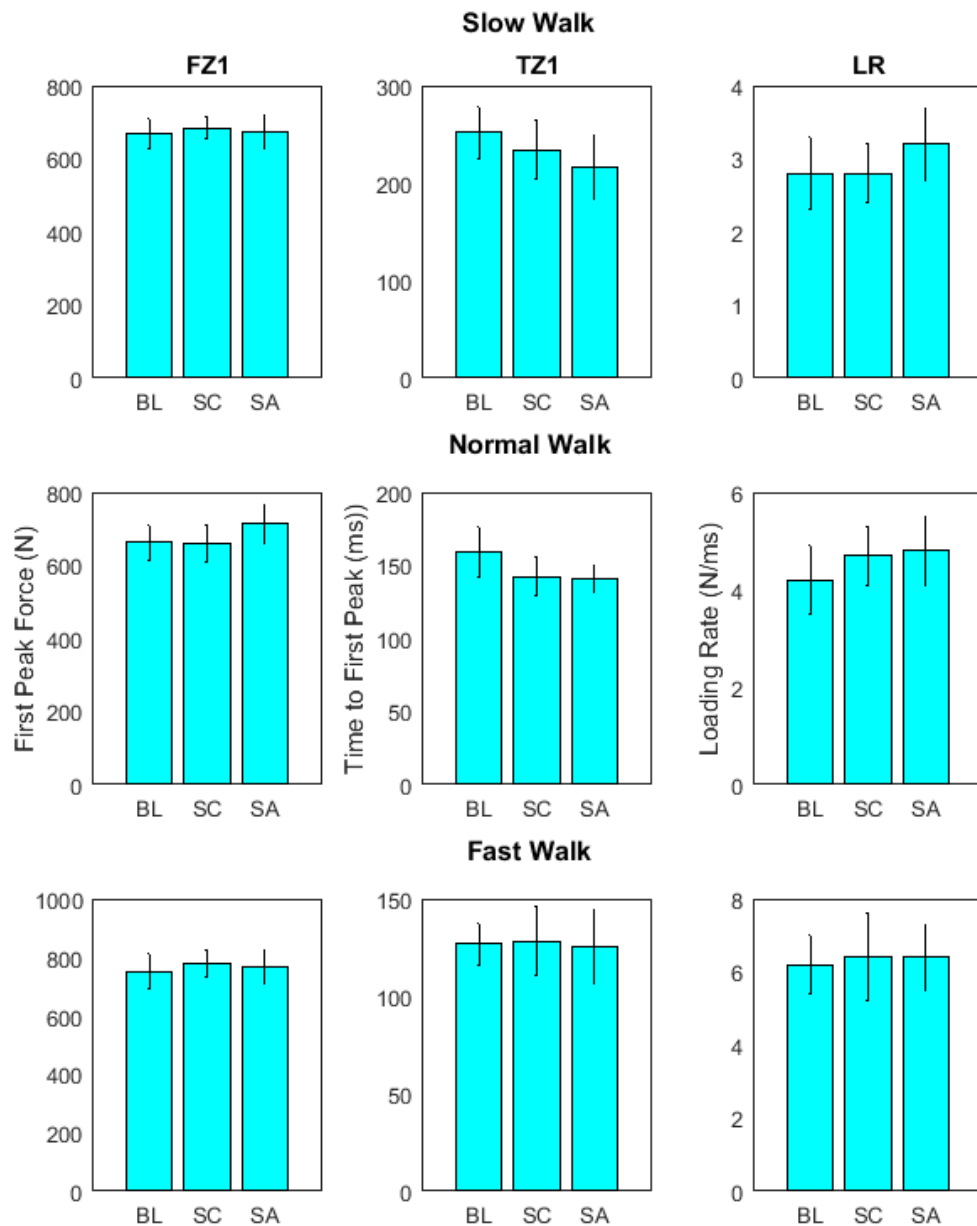


**Figure A.10 Mean FZ1, TZ1, and LR recorded on the prosthetic leg during all treadmill walking conditions. Error bar shows the standard deviation.**

### 3. Overground walking

As with TMW, the distribution of the spatio-temporal parameters across the walking speed are first visualized as shown in Figure A.11, Figure A.12 and Figure A.13. During slow walk (~3.7 km/h), an indication of increased stance duration of the prosthetic side in the SC feedback mode can be observed. This is reciprocated with the decrease in intact side ST duration and prosthetic side SW duration. The SA feedback mode exhibits almost similar trend to that of baseline as far as ST parameters are concerned. During normal walk (~4.9 km/h), the effect on prosthetic ST duration diminishes during SC feedback, however SA feedback showed slight increase in prosthetic ST duration. During fast walk (~5.9 km/h), both SC and SA feedback conditions showed slight increase in prosthetic side stance duration. This behaviour can be observed in summary of the gait cycle percentage as shown in Figure A.14.

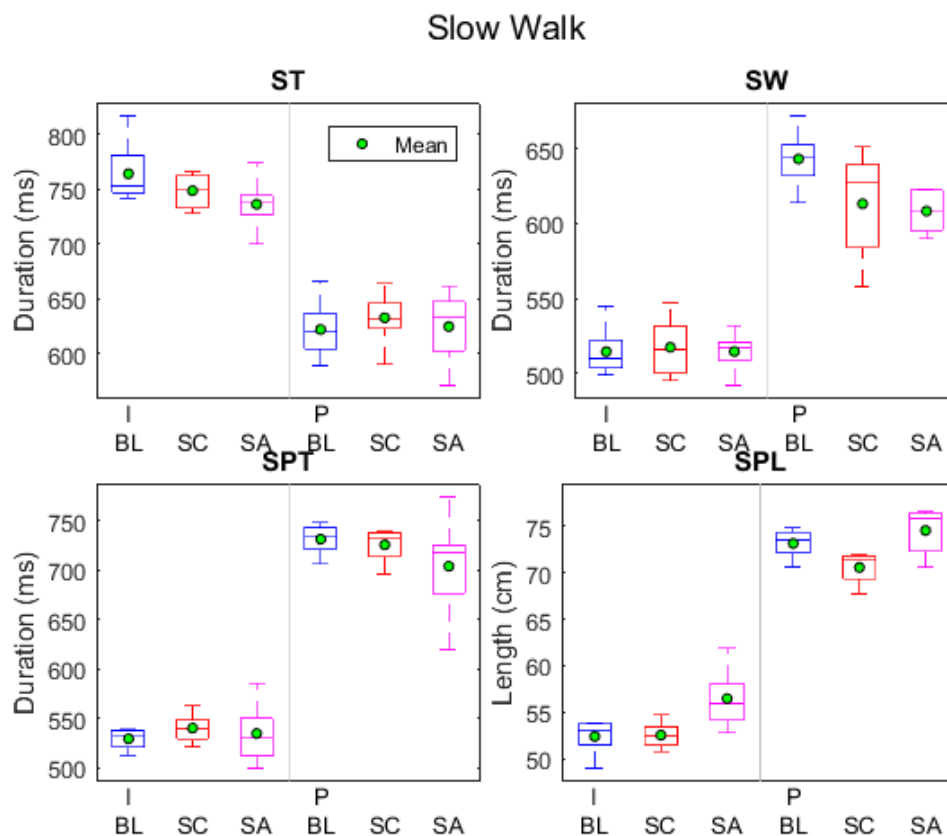


**Figure A.11 OGW Spatio-temporal parameters during BL, SA and SC condition-slow walk**

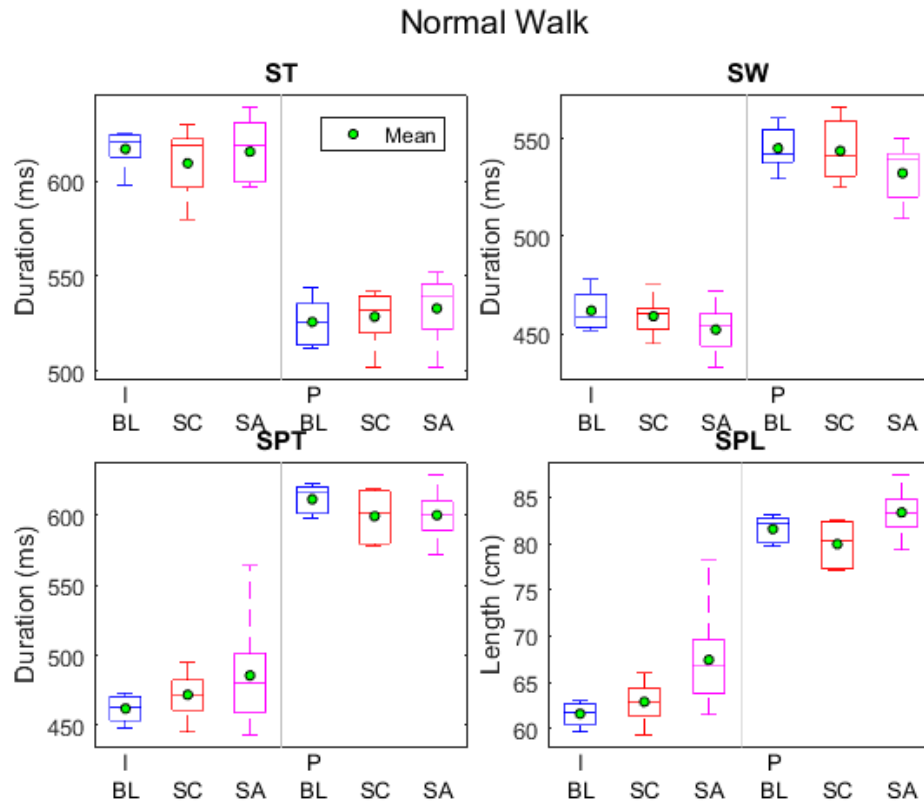


**Figure A.12** OGW Spatio-temporal parameters during BL, SA and SC condition-normal walk

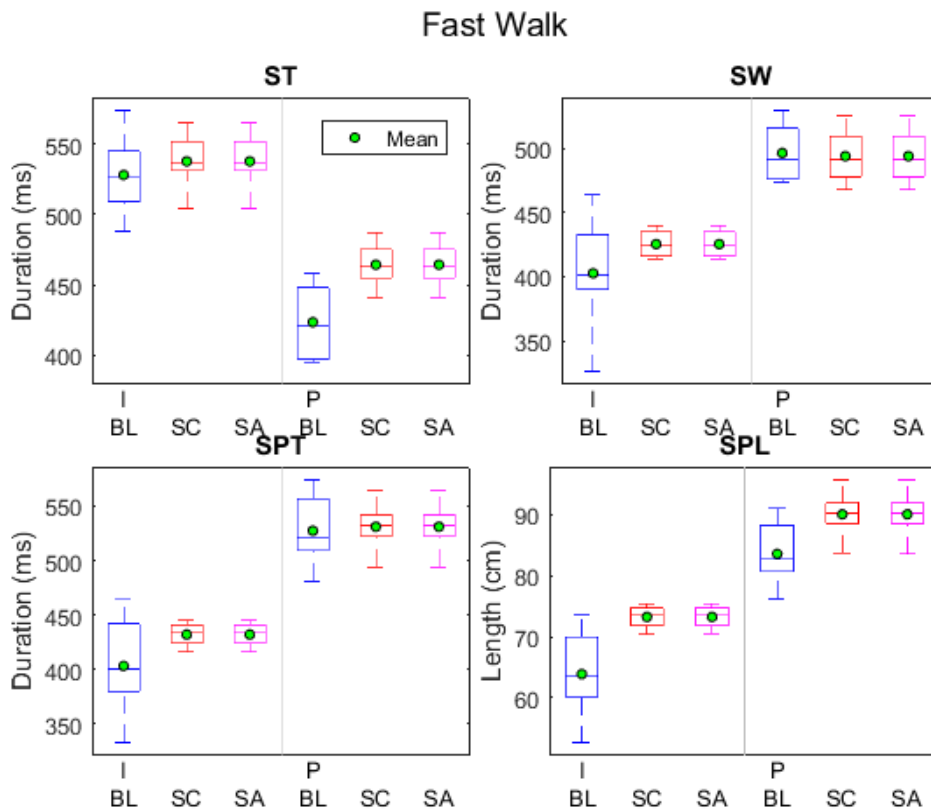


**Figure A.13** OGW Spatio-temporal parameters during BL, SA and SC condition-fast walk

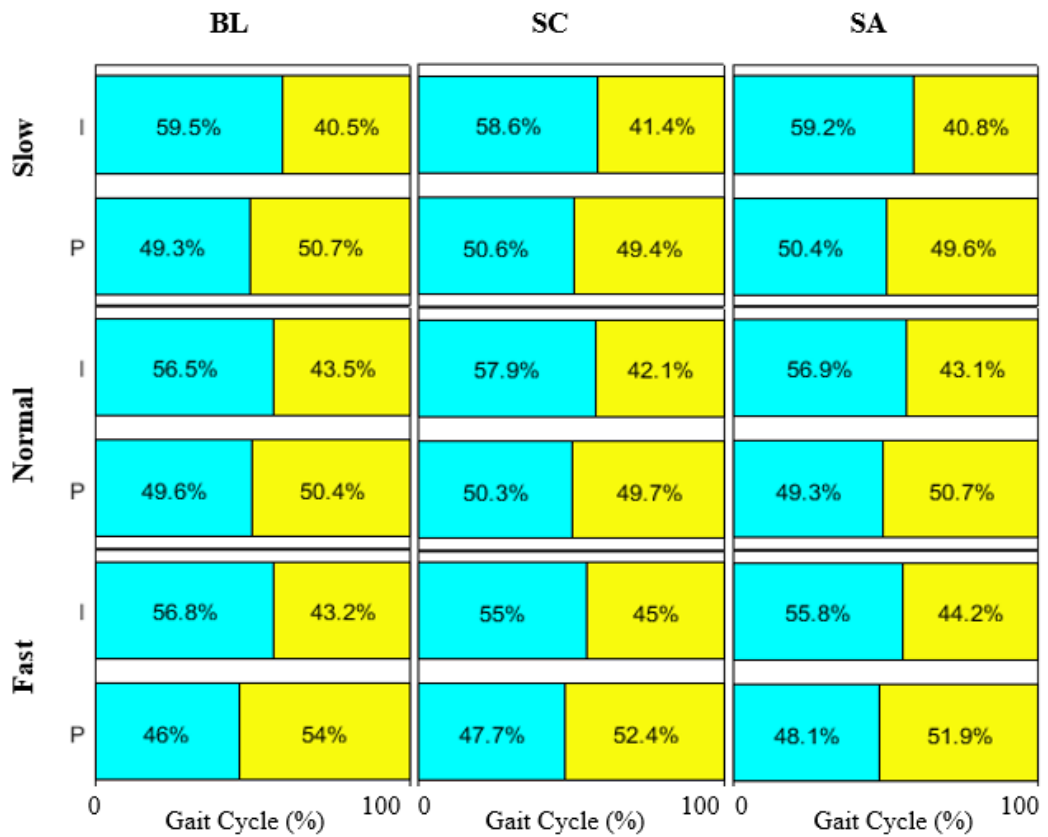


**Figure A.14 Gait cycle percentage throughout experimental conditions**

To investigate whether any significant difference exists between the temporal parameters during walking, an independent t-test was carried out between the BL and SC and between BL and SA feedback conditions. The result is summarized in Table A.3. The only instances where significant differences observed were the prosthetic SW for SC feedback condition during normal and slow walk. In addition, the prosthetic ST duration during normal walk for SA feedback showed significant difference ( $p < 0.05$ ) in comparison to the BL walk. No significant differences were found in any of the fast walk trials.

**Table A.3 p-value for comparison between BL and feedback condition. \* indicates significance difference**

	BL vs SC						BL vs SA					
	Slow		Normal		Fast		Slow		Normal		Fast	
	I	P	I	P	I	P	I	P	I	P	I	P
ST	0.13	0.38	<b>0.03*</b>	0.86	0.63	0.67	0.84	0.34	0.53	<b>0.01*</b>	0.40	0.30
SW	0.76	<b>0.04*</b>	0.98	<b>0.001*</b>	0.56	0.84	0.12	0.07	0.27	0.85	0.52	0.11
SPT	0.13	0.49	0.65	0.14	0.14	0.13	0.16	0.15	0.17	0.83	0.41	0.31

Figure A.15 shows the vGRF parameters of the prosthetic side across all experimental conditions. Similar to TMW, a reduction in TZ1 value can be observed for feedback condition, in comparison to BL during slow walk ( $\sim 3.7$  km/h). This trend, however, was not observed with either normal or fast walk.

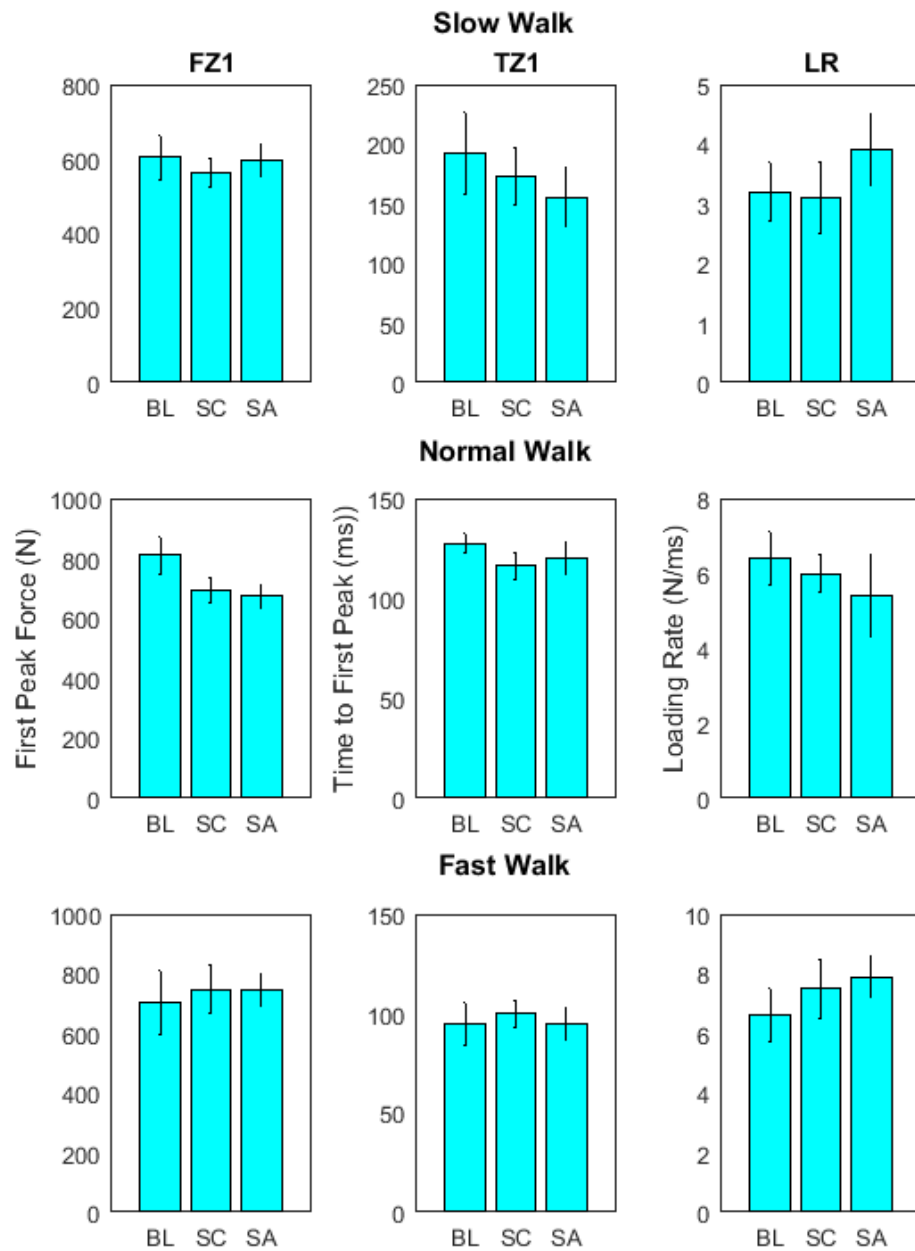


**Figure A.15 Mean FZ1, TZ1, and LR recorded on the prosthetic leg during all overground walking conditions. Error bar shows the standard deviation.**

### A.2.4 Discussion and Key Findings

1. In general, the temporal parameters during stance and swing indicated moderate variability as shown by the Coefficient of Variance (CoV) values in Table A.4.

**Table A.4 CoV (%) of temporal parameters during TMW and OGW**

	TM																	
	BL						SC						SA					
	Slow		Normal		Fast		Slow		Normal		Fast		Slow		Normal		Fast	
	I	P	I	P	I	P	I	P	I	P	I	P	I	P	I	P	I	P
ST	3.1	7.2	6.2	5	3.7	7.8	3.8	4.2	4.1	4.5	4.1	4.3	5.4	7.7	4.6	7	3.8	7.8
SW	3.5	7.5	9.6	5.3	3.2	7.4	4.7	6.4	6.9	4.8	5.3	5.2	8.3	9	6.7	7.9	4	7.5
SPT	10.5	4.7	8.3	6	5.9	1.5	4.6	3.8	7.1	4.1	4.6	3.4	10.5	7.9	8.5	6.7	6.4	3.9
	OG																	
	BL						SC						SA					
	Slow		Normal		Fast		Slow		Normal		Fast		Slow		Normal		Fast	
	I	P	I	P	I	P	I	P	I	P	I	P	I	P	I	P	I	P
ST	3.3	4	1.6	2.4	5.6	7	1.9	3.5	2.9	2.6	3.9	3.5	2.9	5.2	2.6	3.1	3.9	3.5
SW	3	2.8	2.1	2	11.6	4.5	3.8	5.5	2	2.8	2.4	4.4	2.4	2.5	2.8	2.8	2.4	4.4
SPT	2	2.1	2.1	1.7	11.6	6.4	2.6	2.2	3.3	2.9	2.5	4.3	5	6.2	7.7	2.9	2.5	4.3

The variability in the data presents a challenge in analysing specific effect of the manipulated condition towards the studied parameters. Step variability can occur between one walking session and another, especially in OGW where regulating the walking speed is virtually impossible.

2. Since the AKS exhibits a rather clear pattern of gait asymmetry, in which the stance duration of the prosthetic leg was inherently shorter (~50%) than a normal gait stance duration (~60%), it would be of interest to see the effects of the haptic feedback in improving the degree of symmetry. Moreover, since the AKS associated preferring the intact limb over prosthetic limb with, among others, insecurity while placing the limb on the ground, the haptic feedback would be expected to enable more use of the prosthetic limb throughout ambulation. However, apart from several instances, no consistent effects of the feedback could be seen based on the collected data. This could be explained in a few ways:
  - a) The change in dynamic gait is more challenging than postural control during static condition. Lee et al. [21] described a subsensory electrical stimulation delivered to lower extremity amputees. Improvement in static balance indexes



were reported with the stimuli condition, however the effect of such stimuli in dynamic condition was yet to be investigated.

- b) As detailed in Section 5.4.5, the perceptibility reduces with increasing walking speed. In the OGW trials, the self-selected walking speed was significantly higher than the range of walking speed investigated in Section 5.4.5. Thus, it is appropriate to associate the diminishing effect of the haptic feedback with the increasing speed selected during the trials. In fact, during both TMW and OGW trials, the instances of increased stance duration of the prosthetic leg and reduction in TZ1 duration were observed for walking speed less than 4.0 km/h (slow, normal and fast in TMW and slow in OGW). In addition, higher walking speed requires greater coordination and perceived effort to maintain stable dynamic posture. Plauche et al. [23] reported improvement in gait stability of healthy subjects wearing simulated prosthetic leg and subjected to vibrotactile feedback during treadmill walking. However, the authors did not report the average walking speed of the participants, although mentioning that all subjects were regarded as novice prosthetic user.
  - c) The acclimation to prosthetic device might also reduce visibility of the effects of haptic feedback in short-term intervention. The AKS has been wearing the prosthetic device for about 8 years, where rehabilitation stage has long passed and a specific gait strategy might have already been established. In contrast, the subjects in [23] were healthy subjects fitted with a transfemoral leg, which walking condition would be equivalent to that of novice prosthetic users. Similarly, Sabolich and Giovani [20], who reported an improvement in gait parameters for above and below knee amputees subjected to transcutaneous electrical stimulation, recruited participants from amputee population who were still in the rehabilitation stage. Moreover, the subjects were subjected to familiarization period of five to six hours, which is much longer than the one conducted in this study.
3. The different feedback mode did not play significant role in influencing the gait pattern for short term trials. The SA mode, which showed best performance as reported in Section 5.4, did not stand out as having better effects in influencing change in gait parameters. In fact, the SC mode, which has higher stimuli frequency (skin-stretch applied at every IC and TO event) was shown to have greater effect on the prosthetic stance duration, especially during TMW where

---

average walking speeds were lower. This shows that applying stimuli at every IC and TO event is appropriate for robust walking task and that the information can be readily perceived by the user during walking.

### **A.3 Summary**

This section described an investigation into the effects of the haptic feedback on instantaneous gait change of an above-knee amputee during walking. Indications of prolonged prosthetic duration in the stance phase for some feedback condition indicated that the amputee can benefit from such intervention during gait. However, since most changes were observed during slower walking speed, such feedback system might be most useful to the novice prosthetic leg users who would benefit more from gait rehabilitation or training. Overall, the haptic feedback system was successful in delivering the stimuli throughout the walking gait sessions, however, no evidence of significant effects of the feedback can be concluded based on the results from the experimental work. Future work with more amputee population, including novice prosthetic leg users would give a better idea on the usability and effects of such system in improving overall gait efficiency.

**APPENDIX B:**  
**Additional Literature Review**

## **B.1 Prosthetic Components**

### **1. Socket**

Prosthetic socket is the interface between residual limb and the prostheses. Not only the socket protects residual limb, it should also transmit necessary force during standing and locomotion. Post amputation, a temporary socket is prescribed and will require adjustments until the size of the stump stabilizes. Conventionally, sockets are created using plaster casting of the stump and manually adjusted for pressure points before fabricated into the final socket. A more recent advancement in this field however, attempted automating the procedure using sensors to replace a prosthetist's hand and 3D printers to replace casting. One such system was demonstrated by the Massachusetts Institute of technology (MIT) where mechanical indenters fitted with sensors were used to map and generate the profile of the stump and the generated CAD design were 3D printed into a socket using materials with different hardness for different pressure areas [73]. Patellar Tendon Bearing (PTB) socket, developed around 1950's, is the most commonly prescribed prosthetic socket for transtibial amputees. PTB socket is designed to employ total contact with the surface area of the residual limb by loading pressures at several pressure tolerant sites such as patellar tendon while relieving pressure from pressure intolerant sites such as the fibular the fibular head and distal anterior tibia. Alternative option to PTB socket is the Total Surface Bearing (TSB) socket which is made from cast of the original limb with little modification. In TSB socket, the weight is borne by the entire stump surface and used with inverted silicone liner rolled over the stump. The silicone interface protects and stabilizes the skin and tissue. On top of that, padding is fabricated over bony area during casting process [74]. A study by Yigiter et al. [75] showed that a TSB socket provides greater suspension and balance to the amputee, thus making it a more favourable option during rehabilitation. Figure B.1 shows an example of both sockets.

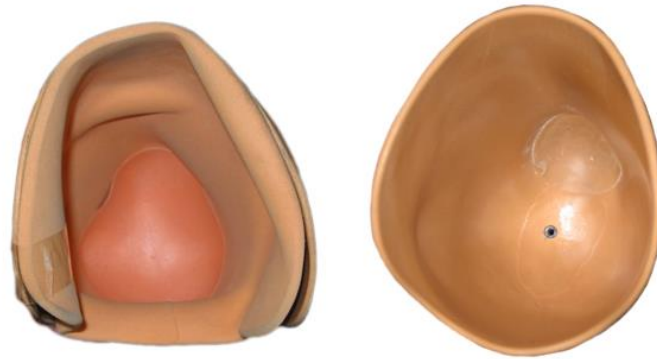


**Figure B.1 PTB socket (left) and TSB socket (right) for below knee amputee [76]**

## **2. Knee Joints**

Above knee or transfemoral amputee requires knee joint to establish normal walking gait. Knee joint functions to provide support during stance, allow unrestricted kneeling and sitting motion, and produce control during swing phase. Different types of knees have been developed and they are divided into two main categories, namely mechanical and microprocessor controlled knee. A manual locking knee (Figure B.2(a)) is the most basic and stable mechanical knee. The knee is locked during gait and released during sitting/kneeling. It results in awkward gait and is suitable for amputee with short residual limb or poor hip strength. Single axis constant friction knee (Figure B.2(b)) bends freely during walking, but requires strong voluntary muscle control. Thus, it provides no stance control and does not cater for variance in walking speed. An extension to single axis constant friction knee is the weight activated stance control knee (Figure B.2(c)). This type of knee incorporates a braking mechanism when weight is loaded on the knee, preventing it from buckling during stance phase. It is suitable for amputees who do not have enough control to bend the knee or hip control to stabilize. Polycentric knees (Figure B.2(d)) have multiple centre of rotation, allowing stability in both stance and swing gait phases. The four-bar linkage mechanism in polycentric knees shortens the shank during swing, allowing for better ground clearance. Long transfemoral amputee benefits from the cosmetic perspective while short transfemoral amputee benefits from the stability provided by polycentric knee type. However, due to nature of its mechanical built, polycentric knee is often bulkier and weigh more than single axis knee.



**Figure B.2 (a) Manual lock (b) single axis constant friction and (c) weight activated and (d) Polycentric prosthetic knee joints. All models from Ottobock [76]**

The latest technologically advanced knees are the microcontroller processed knees which have onboard microprocessors with real time gait evaluation and adjustment, aided by hydraulics, pneumatic and servomotors. They also make it possible to ambulate in uneven surfaces, stairs and slopes, apart from providing certain degree of fall control. The C-Leg (Ottobock, Germany) and Rheo Knee (Ossur, Iceland) are two examples of microprocessor knees available in the market.

### 3. Prosthetic Foot

A common component for both transtibial and transfemoral prosthetic devices is the prosthetic foot. A prosthetic foot ideally must be able to mimic the foot function during gait which is to absorb shock and provide stable surface for weight bearing. The prosthesis should also replace the lost muscle function, replicate the ankle joint as well as complement the whole prosthesis cosmetically. Prosthetic foot can be categorized into energy and non-energy storing. Single-axis and Solid Ankle Cushioning Heel (SACH) are the most common example of a non-energy returning foot family. The latter allows for plantar flexion and fixed with rigid keel to give sense of proprioception (awareness of limb position in space). However, this foot is not suitable for active users and for walking on uneven surfaces. The single axis foot extends SACH foot function by adding passive dorsiflexion, increasing stability during stance phase. Energy returning foot has flexible or elastic keel that compresses during stance and rebounds back during toe off. Nielsen et al. [77] found that the energy storing foot such as Flex-Foot increases the self-selected walking speed of amputee and reduces energy cost during faster walking speed (2.5 mph). As with other prosthetic components, level of activity and cost affordance are among the

determining factors for foot type selection. Figure B.3 shows an example of foot in both categories.



**Figure B.3 Example of commercially available non-energy storing foot (left) and energy storing foot (right)**

## **B.2 Advancements in Lower Limb Prosthetics**

### **1. Bionic Prosthesis Components**

The emergence of bionic prosthesis components which uses electro-mechanics to restore biological function to lower limb amputees has enabled close mimic of natural gait and robust usage for mobility activities. To achieve this, bionic prosthesis utilizes various sensors and actuating mechanisms in the prosthesis components. For example, commercialized products such as Genium® (OttoBock, Germany) is incorporated with six sensors including shank load sensors, knee and ankle load and moment sensors, and angle data from accelerometer and gyroscope [95]. A study by Kannenberg et al. [96] showed that in comparison to conventional knee, using the Genium knee improved the quality of life of the amputee specifically in terms of perceived safety and perceived difficulty during activities of daily livings. Apart from knee joint, bionic characteristics have also been developed for other prosthetic leg components such as the BiOM® ankle (BionX™ Medical Technologies Inc, USA) and the Proprio® foot (Ossur, Iceland). The former offers increased plantar flexion during push off and forward propulsion during toe-off causing reduction in the energy expenditure [97]. The latter, enhances foot clearance during swing phase by providing real-time adjustment of dorsiflexion and plantarflexion according to the walking terrain. As a result, risk of falls is minimized and gait quality and safety is improved [97].

### **2. Surgical Muscle Reinnervation and Robotic Legs**

Hargrove et al. [98] reported the success of a patient who underwent targeted muscle reinnervation post knee disarticulation in controlling robotic leg via EMG signals generated from the reinnervated muscles. During the surgery, tibial and fibular nerves were transferred to remaining limb and allowed to reinnervate the hamstring muscles (Figure B.4). After a few months, contractions could be seen at the innervated muscles when the subject attempted dorsiflexion or plantar flexion of his missing foot. The EMG signal patterns generated from the surgically innervated muscles were used to enhance the existing control strategy of a robotic prostheses. The author cited “robust and intuitive control of ambulation — with seamless transitions between walking on



level ground, stairs, and ramps — and of the ability to reposition the leg while the patient was seated.” [98]

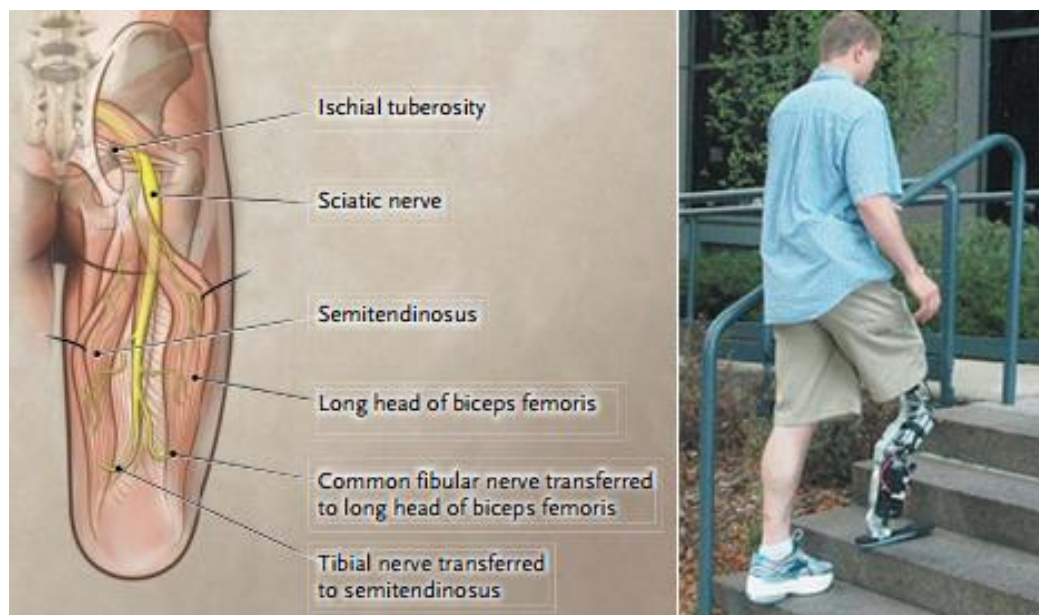


**Figure B.4 (left) Reinnervation strategy and (right) the patient ascending stairs [58]**

However, the effectiveness of this system remains as long as the EMG electrodes are in constant and full contact with the remaining limbs, which means that movement of the residual limb within the socket can create discomfort to the user for long-term use and also cause artefacts in the EMG signals [98].

**APPENDIX C:**  
**PCB Drawings**

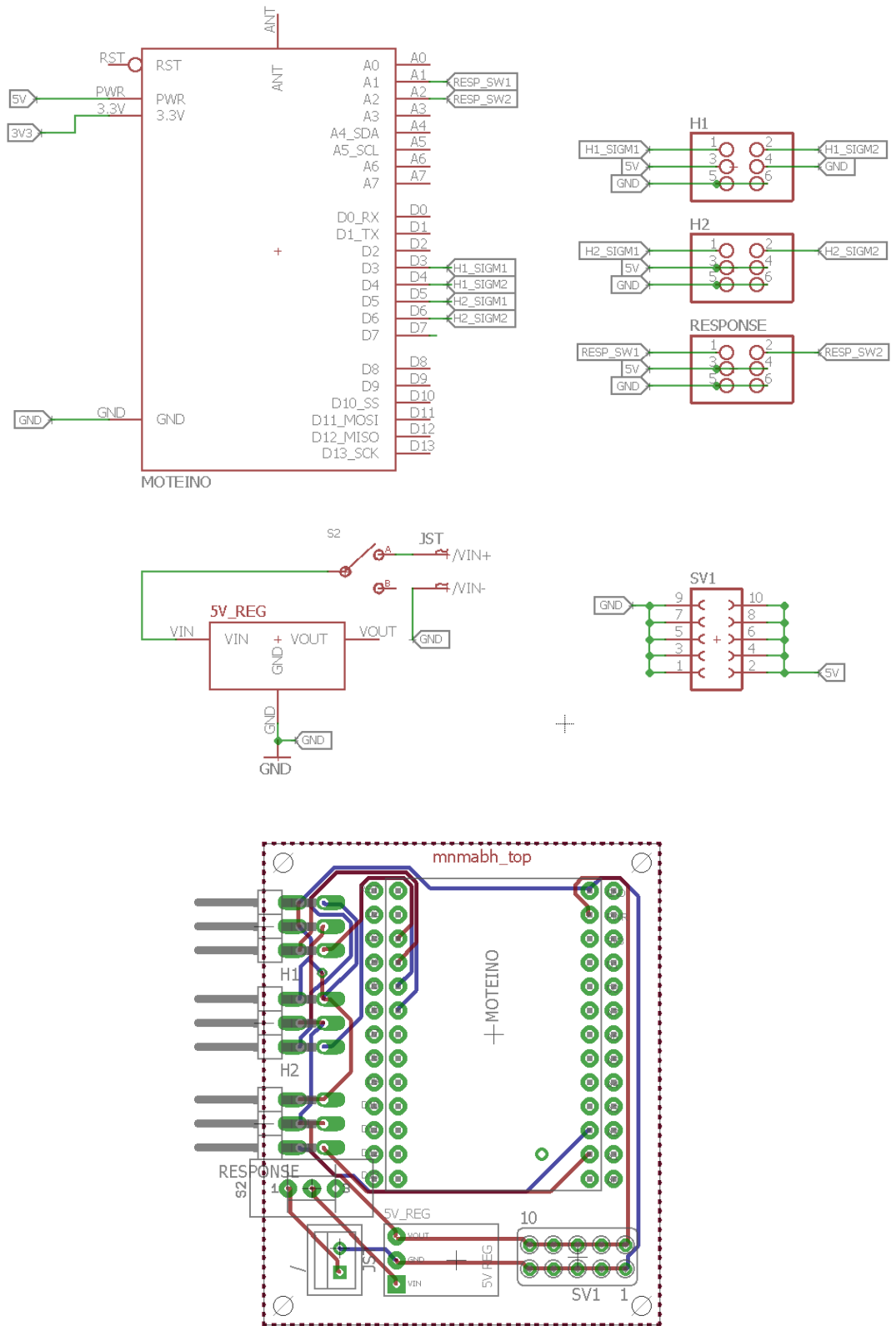


**Figure C.1 (top) schematics for final haptic feedback system. (bottom) PCB layout for board fabrication**

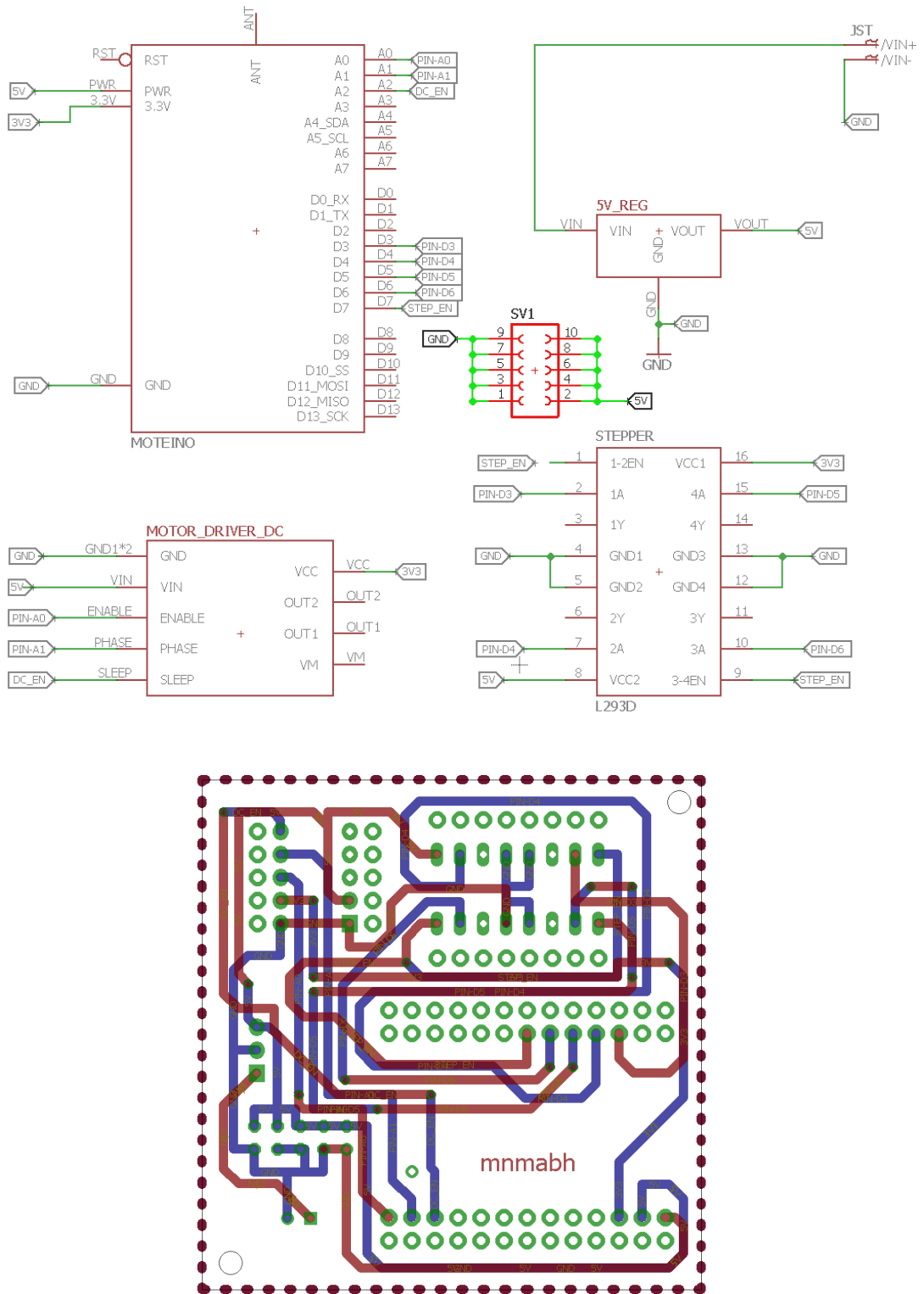


**Figure C.2 (top) schematics for earlier revision of the haptic feedback system, which allows testing different actuators. (bottom) PCB layout for board fabrication**

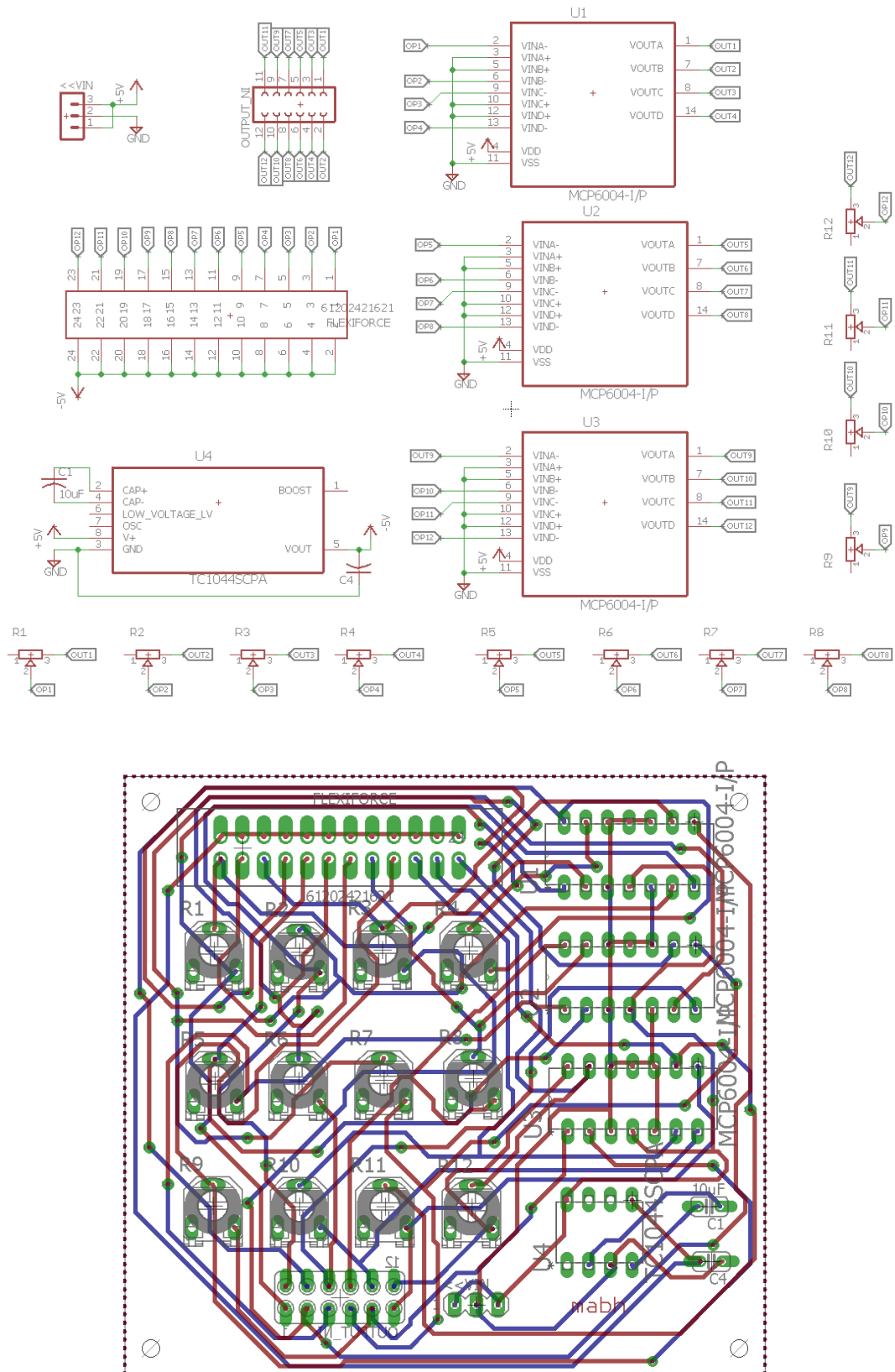


Figure C.3 (top) schematics the force insole. (bottom) PCB layout for board fabrication

**APPENDIX D:**  
**Ethical Approval**

Performance, Governance and Operations  
 Research & Innovation Service  
 Charles Thackrah Building  
 101 Clarendon Road  
 Leeds LS2 9LJ Tel: 0113 343 4873  
 Email: [ResearchEthics@leeds.ac.uk](mailto:ResearchEthics@leeds.ac.uk)



**UNIVERSITY OF LEEDS**

Muhammad Afif Bin Husman  
 Room 535b  
 School of Mechanical Engineering  
 University of Leeds  
 Leeds, LS2 9JT

**MaPS and Engineering joint Faculty Research Ethics Committee (MEEC FREC)  
 University of Leeds**

28 November 2014

Dear Muhammad

**Title of study**        **Haptic Feedback for Lower Limb Prosthesis**  
**Ethics reference**    **MEEC 14-012**

I am pleased to inform you that the application listed above has been reviewed by the MaPS and Engineering joint Faculty Research Ethics Committee (MEEC FREC) and following receipt of your response to the Committee's initial comments, I can confirm a favourable ethical opinion as of the date of this letter. The following documentation was considered:

<i>Document</i>	<i>Version</i>	<i>Date</i>
MEEC 14-012 Final version- Ethical Review- Haptic Feedback.pdf	1	28/10/14
MEEC 14-012_Response_Summary_final.docx	1	26/11/14
MEEC 14-012 Advertisement.docx	1	26/11/14

Please notify the committee if you intend to make any amendments to the original research as submitted at date of this approval, including changes to recruitment methodology. All changes must receive ethical approval prior to implementation. The amendment form is available at <http://ris.leeds.ac.uk/EthicsAmendment>.

Please note: You are expected to keep a record of all your approved documentation, as well as documents such as sample consent forms, and other documents relating to the study. This should be kept in your study file, which should be readily available for audit purposes. You will be given a two week notice period if your project is to be audited. There is a checklist listing examples of documents to be kept which is available at <http://ris.leeds.ac.uk/EthicsAudits>.

We welcome feedback on your experience of the ethical review process and suggestions for improvement. Please email any comments to [ResearchEthics@leeds.ac.uk](mailto:ResearchEthics@leeds.ac.uk).

Yours sincerely

Jennifer Blaikie  
 Senior Research Ethics Administrator, Research & Innovation Service  
 On behalf of Professor Gary Williamson, Chair, MEEC FREC  
 CC: Student's supervisor(s)